POLITECHNIKA LUBELSKA

Jerzy Józwik

Experimental methods of error identification in CNC machine tool operation

MONOGRAFIE

Lublin 2018

Experimental methods of error identification in CNC machine tool operation

Monografie – Politechnika Lubelska

Politechnika Lubelska
Wydział Mechaniczny
ul. Nadbystrzycka 36
20-618 LUBLIN

Jerzy Józwik

Experimental methods of error identification in CNC machine tool operation

Lublin University of Technology
Lublin 2018

Reviewers:
prof. dr hab. inż. Stanisław Legutko, Poznan University of Technology
prof. dr hab. inż. Józef Kuczmaszewski, Lublin University of Technology
dr hab. inż. Radosław Maruda, University of Zielona Gora

Edition and DTP:
dr Marcin Barszcz, Lublin University of Technology
dr inż. Krzysztof Dziedzic, Lublin University of Technology

Publication approved by the Rector of Lublin University of Technology

ISBN: 978-83-7947-312-0

Publisher: Lublin University of Technology
ul. Nadbystrzycka 38D, 20-618 Lublin, Poland
Realization: Lublin University of Technology Library
ul. Nadbystrzycka 36A, 20-618 Lublin, Poland
tel. (81) 538-46-59, email: wydawca@pollub.pl
www.biblioteka.pollub.pl
Printed by : TOP Agencja Reklamowa Agnieszka Łuczak
www.agencjatop.pl

The digital version is available at the Digital Library of Lublin University of Technology: www.bc.pollub.pl
Circulation: 100 copies

TABLE OF CONTENTS

ABSTRACT

The development of CNC machine tools is primarily aimed at creating new solutions as well as enhancing the existing ones. Despite the use of more and more precise machine tools, new drive units, spindles, transmissions, measurement-control systems, etc., the occurrence of errors in the production process has not been eliminated, resulting in the need to compensate for these errors, linear and angular alike [49, 51]. Errors resulting from a specific technical condition of machine tools are predominantly linear and angular positioning deviations, including their repeatability and clearance [30, 75, 96, 103, 113]. Their values depend on various internal and external factors. The most significant of these factors are geometric and kinematic factors associated with the machine tool, as well as thermal factors, drive errors, regulator and measurement system errors including those resulting from the machining process.

Errors occurring in machine tools can be divided into those occurring systematically and by chance (randomly) [30]. All systematic errors, irrespective of their type (geometric, kinematic, thermal), can be compensated, and the accuracy of their compensation depends on the accuracy of their identification and the rate of their change [74, 75]. Regular (predictable) errors with little dynamics can be compensated for with great accuracy if one knows the nature of their changes. It is difficult, however, to compensate for dynamic errors [113].

Machine tool errors are also caused by thermal action resulting from friction, compressive distortion, plastic deformation occurring in production processes (primarily as a result of force, inertial and kinematic interactions), etc. [13, 48, 53, 58, 66, 89–91, 95, 129]. Thermal changes in machine tools are mostly slowly varying processes with characteristics of the first-order inertial element, relatively simple to compensate [13, 90–91]. Obviously, a model describing these changes has to be developed and mathematically described. The capture of data necessary for building such model can be done experimentally or analytically. As far as analytical methods are concerned, they are easily implemented for single- or simple-geometry parts (e.g. ball screws) but – given the overall geometric complexity of machine tools – experimental methods are more precise and thus suitable for this purpose [13, 91, 129]. What they take into consideration is the actual machine structure and the real conditions of heat generation. A good example of changes resulting from heat fluctuations is the linear expansion of a ball screw, the change of guidebar dimensions or the change in a rotary axis position. The source of thermal interactions in machine tools are all types of heat-generating units such as bearings, motors, clutches, as well as gears, pumps, and the very physical machine tool process [53, 58]. In light of the above, if feasible, all heat-generating systems should be placed outside the machine tool to decrease the impact of heat changes on the machine tool body. All design and technological actions (the use of appropriate materials, correct operating parameters, etc.) are

aimed at reducing thermal deflections of the machine tool body and, consequently, at preventing changes in the position of shaft and spindle axes [91].

Another group of machine tool errors investigated in this study are stochastic errors. They result from the random impact of both external and internal factors such as vibrations transmitted by surface, vibrations generated during machine tool process, heat streams coming from the production area and external sunlight. This particular group of errors is more difficult to identify and compensate for due to the lack of functional relations describing their occurrence. Although there are some design methods by which – even at the design stage – designers try to limit the influence of random factors, e.g. by proper design and implementation of active vibration reduction systems, they are not sufficient and do not always bring the desired results. Some of these errors can be significantly reduced, but it is not possible to eliminate them altogether [1, 7, 8, 12, 15, 20, 27, 29, 33, 48, 62, 86, 92, 128].

Noise and its impact on the operator's and other people's hearing are a crucial problem with respect to the safety of machine tool operation. Noise generated during machine operation has a negative influence on the human body, contributing to difficult work conditions. It is therefore necessary to monitor and identify noise generated by machine tool components and the implemented process. Noise can also result from a deteriorating condition of the machine, and – for this reason – it can be a source of valuable information, e.g. about upcoming failures. This work also touches upon the problem of negative impact of noise on the human body [134, 147]. Acoustic maps for specific types of machine tools operating in different frequencies are produced by acoustic holography. Sources of noise in machine tools are identified and the levels of acoustic pressure generated by the machine tool are determined.

Programmed movements described in the set coordinate system are implemented in numerically controlled machine tools. The precision of realization of trajectories described in the programme depends on both the accuracy of movements in the numerically controlled axis and the influence of technological process factors. Spindle motion errors are also of crucial importance. This work describes methods for identifying spindle errors (synchronous, asynchronous and others). Finally, methods for rotary axis kinematic centre positioning in selected machine tools are discussed.

LIST OF ABBREVIATIONS AND SYMBOLS

NC	–	Numerical control
CNC	–	Computer numerical control
MHWT	–	Machine tool-handle-workpiece-tool system
X, Y, Z	–	Numerically controlled linear axes
A, B, C	–	Numerically controlled rotary axes
VE	–	Volumetric error
XTX, EXX	–	Position deviation in X-direction (for X-axis)
YTY, EYY	–	Position deviation in Y-direction (for Y-axis)
ZTZ, EZZ	–	Position deviation in Z-direction (for Z-axis)
YTX, EXY	–	Straightness deviation in X-direction (for Y-axis)
ZTX, EXZ	–	Straightness deviation in X-direction (for Z-axis)
XTY, EYX	–	Straightness deviation in Y direction (for X-axis)
ZTY, EYZ	–	Straightness deviation in Y-direction (for Z-axis)
XTZ, EZX	–	Straightness deviation in Z-direction (for X-axis)
YTZ, EZY	–	Straightness deviation in Z-direction(for Y-axis)
XRX, EAX	–	Roll around X-axis (for X-axis)
YRY, EBY	–	Roll around Y-axis (for Y-axis)
ZRZ, ECZ	–	Roll around Z-axis (for Z-axis)
YRX, EAY	–	Pitch around X-axis (for Y-axis)
XRY, EBX	–	Pitch around Y-axis (for X-axis)
ZRX, EAZ	–	Pitch around X-axis (for Z-axis)
XRZ, ECX	–	Yaw around Z-axis (for X-axis)
YRZ, ECY	–	Yaw around Z-axis (for Y-axis)
ZRY, EBZ	–	Yaw around Y-axis (for Z-axis)
XWY	–	Squareness error between X and Y axes
XWZ	–	Squareness error between X and Z axes
YWZ	–	Squareness error between Y and Z axes
TEM	–	Total error motion
TIR	–	Total indicated run-out
SE	–	Synchronous error motion
ASE	–	Asynchronous error motion
SEA	–	Precision spindle error analyser
X_{zm}	–	Measured value of coordinate X
Y_{zm}	–	Measured value of coordinate Y
X_{org}	–	Original set value of coordinate X
Y_{org}	–	Original set value of coordinate Y
P_i	–	Set position
P_{ij}	–	Actual position in the set position P_i
x_{ij}	–	Positioning deviations
$\bar{x}_i\uparrow$, $\bar{x}_i\downarrow$	–	Mean unidirectional positioning deviation in the position P_i
$\bar{x}_i$	–	Mean bidirectional positioning deviation in the position P_i
B_i	–	Returned value in the position P_i
B	–	Axis returned value

$\bar{B}$	–	Mean axis returned value
$R\uparrow, R\downarrow$	–	Unidirectional positioning repeatability
R	–	Bidirectional positioning repeatability
$E\uparrow, E\downarrow$	–	Unidirectional systematic axis positioning deviation
E	–	Bidirectional systematic axis positioning deviation
M	–	Mean bidirectional systematic axis positioning deviation
$A\uparrow, A\downarrow$	–	Unidirectional accuracy of axis positioning
A	–	Bidirectional accuracy of axis positioning
$s_i\uparrow$, $s_i\downarrow$	–	Estimator of unidirectional standard positioning uncertainty in a certain position P_i
CW	–	Clockwise rotation
CCW	–	Anti-clockwise rotation
t	–	Time
T	–	Temperature, time constant
s	–	Standard deviation
v_c	–	Cutting speed
v_f	–	Rate of feed
Δv_f	–	Relative percentage tolerance of feed rate
v_{fz}	–	Measured rate of feed
v_{fp}	–	Programmed rate of feed
n	–	Rotational speed
Δn	–	Relative tolerance of the rotational speed n
n_z	–	Measured rotational speed
n_p	–	Programmed rotational speed
u	–	Standard uncertainty
U	–	Extended uncertainty
k	–	Coverage factor, smoothing constant, system strengthening
G	–	Circularity hysteresis
y_i	–	Values of the measured variable y, “tolerance” in the considered period t
y^*_t	–	Forecast for the period t
y_{t-1}	–	Value of the measured variable y, “tolerance” in the period $t-1$
y_{t-k}	–	Value of the measured variable y, “tolerance” in the period $t-k$
w_i	–	Weights given to individual observations y
s*	–	Mean square error of ex-post forecast

INTRODUCTION

The problem of error identification in computer numerically controlled (CNC) machine tools is of vital importance for producers and users alike. Machine errors can effectively be assessed on the basis of successive measurements. Diagnostics and monitoring serve this purpose perfectly, providing valuable information about the technical condition of these objects [9, 10, 30, 31, 49, 51, 70, 91].

Given the range of applications for CNC machine tools as means of production as well as their design complexity (geometric and kinematic) and stringent quality requirements imposed on parts produced on these machines, it can undoubtedly be claimed that error identification via monitoring and diagnostics is the key to ensuring continual operational capacity of CNC machine tools [30–31, 75, 113].

Monitoring and diagnostics benefit from achievements in many fields of knowledge and cover many areas of the technical existence of CNC machine tools. Diagnostics is fundamental already at the stage of machine design and putting it into use, during machine operation, tests and acceptance testing after machine repairs and collisions, as well as during technical object organisation and management. In light of the above, the primary aim is to classify the machine with respect to specified technological tasks it can perform. The diagnostics of the technical condition of machine tool components and units is performed periodically or ad hoc in case of emergency failures [30, 31, 70, 90, 91]. Diagnostic testing of CNC machine tools is standardised and described in international standards confirmed by the Polish Committee for Standardization. Both international and Polish standards specify general regulations regarding machine tool testing as well as methods for determining specific deviations and tolerances describing their potential values [130–150].

Monitoring and diagnostics are nowadays key processes that consciously and effectively ensure the optimal use of means of production, while thanks to control processes their capacity to produce given classes of products is automatically controlled. This work undertakes an analysis of the sources of errors in CNC machine tools; it examines methods for identifying CNC machine tool inaccuracies and estimates their impact. A proper identification of error sources via monitoring and diagnostics is extremely crucial for optimising preventive measures in case of machine damage and eliminating damage from the production process. The work puts a particular emphasis on linear and rotary axis positioning errors and discusses other geometric, kinematic and thermal errors. The accuracy and repeatability of feed system positioning is a critical factor for the assessment of CNC machine tools and improvement of their accuracy. The subject matter of this work is researched by various centres in Poland [13, 16, 26, 37–61, 73–75, 91, 95, 112, 113] and internationally [1–3, 5–12, 14–24, 27–29, 33–36, 125–128].

The geometric inaccuracy of CNC machine tools can be classified according to various criteria, one of them being the source of error. By this criterion, machine tool errors result from the geometric imperfection of MHWT system components, changes in their operating temperature (due to external and internal friction) leading to thermal deformation of the MHWT system, elastic deformation of machine tools and their components due to machine overload during the cutting process, and the adjustment of control systems to a variable character of the feed drive behaviour. Machine tool errors can also be classified depending on the place of their occurrence. These include machine tool errors, process errors and the errors of auxiliary systems (adjustment, fixing, etc.). Errors resulting from geometric imperfection can be divided into the errors of spatial positioning of feed units and the kinematic and geometric errors [75, 92, 96, 103, 105, 112, 113, 124].

1. BASIC ISSUES

1.1. Errors of numerically controlled machine tools

There are many factors afecting the accuracy of computer numerically controlled (CNC) machine tool operation. These factors cause errors such as positioning deviations at every axis, angle deviations, timing over, tilting, deflection, squareness deviations between the axes, axial and radial clearances on every axis, shape deviations, reversal errors, and many more. Fig. 1 shows a graphic presentation of errors occurring in a computer numerically controlled machine tool axis [113, 170].

a) b)

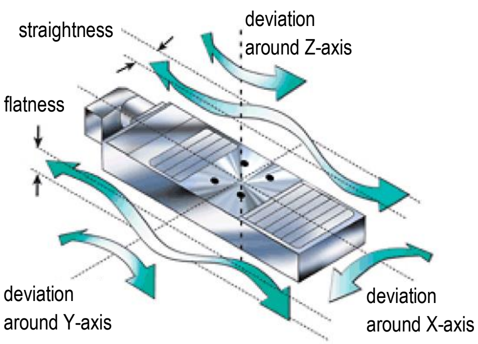

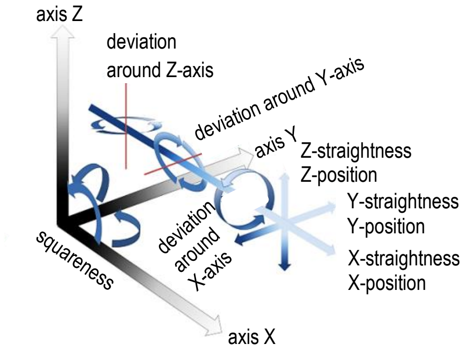

Fig. 1. Graphic presentation of errors occurring at one of the axes of a CNC machine tool: a) with respect to physical table, b) with respect to axis [103, 113, 121, 170]

An analysis of the geometric structure of the machine tool clearly demonstrates that every table position has six degrees of freedom: three linear degrees of freedom along the numerically controlled axes X, Y and Z and three rotary degrees of freedom A, B, C around the same axes. Therefore, there are 18 possible movements for the table moving in three axes (six at each axis), which yields as many as 18 deviations during relocation to other points during machine tool operation. Given the squareness deviations consisting in the angular deflection of the related perpendicular axes, this gives a possibility of the occurrence of 21 geometric errors in total [72–75, 113]. Hence, having considered three machine tool axes, the deviations of the numerically controlled axes may be presented as shown in Fig. 2 [152, 153].

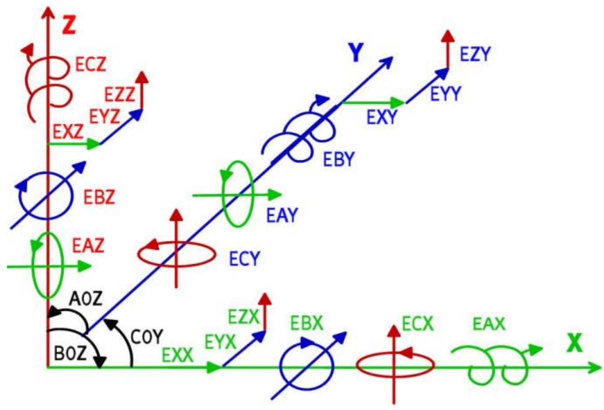

Fig. 2. CNC machine tool errors in three numerically controlled axes: X, Y, Z (indications in the text) [152, 153]

According to the VDI 2617 and ISO 230-1 standards and the results reported in [75, 130, 152, 153], the most important of the errors shown in Fig. 2 are:

a) Deviations of the X-axis
- position deviations in the X-direction (XTX, EXX),
- straightness deviation in the Y-direction (XTY, EYX),
- straightness deviation in the Z-direction (XTZ, EZX),
- roll around the X-axis (XRX, EAX),
- pitch around the Y-axis (XRY, EBX) – stroke,
- yaw around the Z-axis (XRZ, ECX) – getting out of course,

b) Deviations of the Y-axis
- position deviation in the Y-direction (YTY, EYY),
- straightness deviation in the X-direction (YTX, EXY),
- straightness deviation in the Z-direction (YTZ, EZY),
- roll around the Y-axis (YRY, EBY) – the barrel effect,
- pitch around the X-axis (YRX, EAY),
- yaw around the Z-axis (YRZ, ECY) – getting off the course,

c) Deviations of the Z-axis
- position deviation in the Z-direction (ZTZ, EZZ),
- straightness deviation in the X-direction (ZTX, EXZ),
- straightness deviation in the Y-direction (ZTY, EYZ),
- roll around the Z-axis (ZRZ, ECZ) – the barrel effect,
- pitch around the X-axis – stroke (ZRX, EAZ),
- yaw around the Y-axis (ZRY, EBZ) – getting off the course,

d) Squareness errors
- squareness error between the X and Y axes (XWY),
- squareness error between the X and Z axes (XWZ),
- squareness error between the Y and Z axes (YWZ).

According to Seng Khim, Tan and Chin Keong et al. [65], the errors specified in the standards can refer to both rectangle tables and machine tools rotary tables, as shown in Fig. 3. The error indications in Fig. 3 are the author's equivalents of the deviations defined by the standards, expressed as a function of displacement for specifies axes and angles.

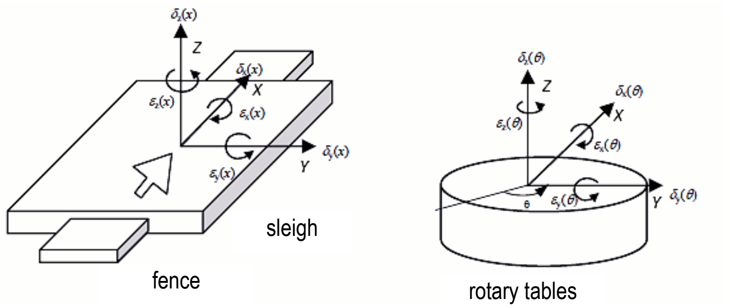

Fig. 3. Errors in the controlled axes: a) table with perpendicular linear axes, b) table with rotary axes [65, 166]

The errors shown in Figs. 1, 2 and 3 are inevitable and may occur in every machine. Experience shows that they usually occur during machine operation. Therefore, machine calibration and continuous (over a long period of time) diagnostics are crucial. Regular identification and calibration of CNC machines may significantly reduce the occurrence of errors.

From a statistical point of view, CNC machine tool errors can be classified into two groups:

- systematic errors,
- random errors.

Systematic error is a repetitive error of a single measurement, defined as the difference between the mean of an infinite number of measurements of one quantity taken in repeatable conditions and the true value of this quantity. A systematic error is either the same for each observation (hence it is repetitive) in given conditions or changes according to a specific pattern together with the change of the conditions [2, 5, 74, 75, 92].

Random error is an error of a single measurement, defined as the difference between the measurement result and the mean of an infinite number of measurements taken in repeatable conditions. A random error equal to the difference between the total error and the systematic error is usually different for single measurements and may take both positive and negative values. It is therefore modelled as a random variable [37, 38, 112].

Taking into consideration the design of a machine tool along with its supporting structures and kinematic systems, errors can be divided into:

- geometric,
- kinematic.

Geometric error of the machine tool results from machine design and is associated with machine shape and the mutual position of machine components and joints. Geometric errors include guidebar straightness error, flatness error, parallelism error, mutual position of axes error, etc. Geometric errors of machine tools occurring at a given stage of their operation strongly depend on the conditions of use and service, and, in particular, on the rate of wear processes. They also depend on thermal and compressive interactions. Geometric errors are defined at the stage of machine tool assembly and are subject to constant changes during machine operation. The PN-ISO 230-1 standard provides a detailed analysis of geometric errors of machine tools operated without load or in finishing machining conditions, as well as their testing methods [11, 24, 26, 40, 52–55, 73, 74, 92, 97, 130, 131, 133, 136–140].

Kinetic error is an error resulting from the kinematic motion of operational systems of a machine or devices. Kinematic errors occur during linear and rotary motion. They are caused by the overlapping of errors of kinematic joints of individual kinematic pairs (guidebar, screw, and gear pairs, etc.) in kinematic chains. They include errors of linear and angle positions and rotation errors. The gravity of these errors depends on the gravity of errors resulting from flawed kinematic pair design, assembly errors and the wear of mating components. The number of kinematic errors is the smaller, the fewer there are kinematic pairs in the kinematic chain. Kinematic errors can be observed and tested during the movement of machine tool units [12, 25, 28, 29, 43, 50, 52, 57, 104, 128, 136, 142].

Volumetric error (VE) is a total error resulting from the mutual position and orientation of the machine tool-workpiece system, defined in a multidimensional space. In the specialist literature, the volumetric error is also known as the error of spatial positioning of the machine tool axes. This error can only be determined with the use of specialist tracking diagnostic devices. These tools enable, among others, direct determination of *VE,* however they require a change of measurement base and measurement algorithms or the measurement of errors in the entire work space of the machine with the use of readily available diagnostic tools (e.g. laser interferometer or telescopic bar). In general, the volumetric error *VE* consists of kinematic and geometric errors resulting from machine tool design [22, 65, 72–75, 88]. A detailed comparison of the volumetric error measurement methods is given in [113].

Thermal error is an error associated with thermal deformations of the machine tool feed system occurring as a result of thermal interactions (heat generation, transfer and exchange) between frictional kinematic pairs of translational, rotational and translational-rotational nature, as well as variable environmental effects, engine heating and heat transfer in machining processes [13, 17, 53, 57, 87, 89, 90, 95, 129, 132, 146].

Error of rotary axis kinematic centre position is an error resulting from the machine tool kinematics due to a change in the position of the rotary axis coordinate system centre relative to which motion is observed. This system can be shifted, twisted or shifted and twisted at the same time. This usually takes place after a headstock collision between the machine tool and the table (in the case of a milling cutter) or between the tool head and the spindle (in the case of a lathe), or it can be caused by machine tool overload or decalibration. If this point is shifted, then the motion is performed relative to a system which is not specified in the control system kinematics table of the CNC machine tool. The identification of the rotary axis kinematic centre position error and its inclusion in the machine tool kinematics table enables the restoration of machine motion to the actual position of the system. This means that the motion is programmed relative to a specified point [25, 32, 35, 43, 48, 50, 52, 104, 116].

Yaw axis error (roll (R), pitch (P), yaw (Y)) is defined by RPY angles describing the momentary angular velocity of a rotating rigid body. Similarly to the Euler angles, they are strictly theoretical quantities. Fig. 4 shows the kinematic errors of axis rotation: roll (R), pitch (P) and yaw (Y).

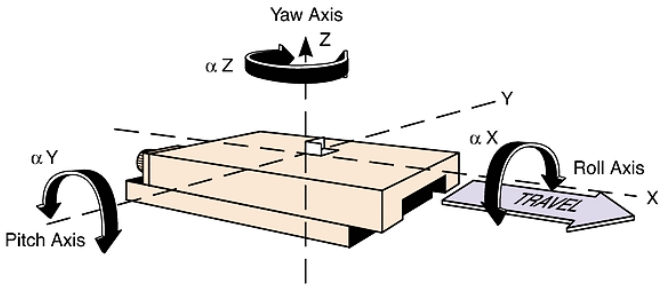

Fig. 4. Axis rotation kinematic errors: roll (R), pitch (P), yaw (Y) [170]

RPY rotations occur as a result of successive rotations relative to the base system, not the local system as is the case with the Euler angles. The rotation is successively performed in relation to the X, Y, Z axes. In contrast to the angle position errors, they are not associated with deviations of particular positions in relation to the programmed positions [65, 75, 130, 152, 153, 166, 170].

An important group of errors examined in the present study result from machine tool spindle motion. Taking into consideration their nature, they will be analysed in detail in Chapter 7.

1.2. Positioning repeatability and accuracy

According to the ISO 203 standard, positioning errors (deviations) can pertain to linear and angle positions. They constitute a separate group of machine tool errors associated with specified positions of machine tool systems in relation to the programmed motion. These deviations of machine tools are described in detail in PN-ISO 230-2, PN-ISO 10791-4 and PN-ISO 10791-5 standards.

The accuracy and repeatability of machine tool positioning can be affected by the following types of errors: geometric errors of machine units, kinematic errors, errors caused by extensive overload, thermal errors, dynamic errors, calibration errors, masurement errors. On the other hand, machine tool resolution depends on the accuracy of sensor and measuring instrument design, control system performance accuracy, dry friction (adhesion and slip), backlash and others. By measuring linear positioning deviations for linear tables and angular positioning deviations for rotary tables (alternatively, for tilting and rotary tables and lathe spindles) we can estimate the accuracy and repeatability of a particular machine tool in a particular axis.

According to the data specified in the standards [131, 140, 149, 150], particular deviations are defined as follows. **Linear positioning deviation** is defined as the difference between the set (programmed) linear position and the position observed on a given numerically controlled axis, specified in the rectangular coordinate system. **Angular positioning deviation** is the difference between the set (programmed) angular position and the position observed on a given numerically controlled axis. The axis is determined in the bi-polar coordinate system.

Analysing the positioning deviations related to linear and angular positions one may generally conclude that the **positioning deviation** $\boldsymbol{x_{ij}}$ (linear or angular positioning deviation) is the difference between the real position of the machine tool movable unit and the positon set in the control programme. **The set position** $\boldsymbol{P_i}$ (i=1÷m) is the position which the moving unit was programmed to reach. The index i indicates a specific position between other set positions along and around the axis. The real position $\boldsymbol{P_{ij}}$ (i=1÷m; j=1÷n) is the measured (observed) position achieved by the movable unit in the j-th run to i-th set position. **The positioning deviation** $\boldsymbol{x_{ij}}$ is best described by Equation (1):

$$x_{ij}=P_{ij}-P_i \tag{1}$$

After determining the positioning deviations in an n-series of unidirectional runs, one can determine **the mean directional positioning deviation in a position** $\bar{x}_i\uparrow$ or $\bar{x}_i\downarrow$. Unidirectional positioning deviations in a position are defined as the arithmetic mean of positioning deviations in an n-series of unidirectional runs to the position P_i. The deviations are described by Equations (2) and (3):

$$\bar{x}_i\uparrow=\frac{1}{n}\sum_{j=1}^{n}x_{ij}\uparrow \tag{2}$$

$$\bar{x}_i\downarrow=\frac{1}{n}\sum_{j=1}^{n}x_{ij}\downarrow \tag{3}$$

Unidirectional run refers to a series of measurements during which, to the set position P_i, the run is realized in this direction along or around the axis, and the symbol „↑" refers to a run towards the positive direction while „↓" from the negative direction, e.g. $x_{ji}\uparrow$ or $x_{ij}\downarrow$.

In the case of runs to the set position P_i from two directions, we can determine**a bidirectional positioning deviation in a position** $\bar{x}_i$. The bidirectional positioning deviation in the position $\bar{x}_i$ is defined as the arithmetic mean of average unidirectional positioning deviations ($\bar{x}_i\downarrow$, $\bar{x}_i\uparrow$), obtained in the run from two directions towards the Pi position, according to (4):

$$\bar{x}_i = \frac{\bar{x}_i\downarrow + \bar{x}_i\uparrow}{2} \tag{4}$$

The term "bidirectionality" refers to a series of measurements in which the runs towards the set position P_i are performed from two directions along (linear position assessment) or around (angular position assessment) the axis.

In CNC machine tool testing, valuable information is obtained from the **returned value** $\boldsymbol{B_i}$ in the position P_i. This value indicates the difference between mean unidirectional deviations achieved in the runs from two directions towards the position P_i. The returned value B_i is described with Equation (5):

$$B_i = \bar{x}_i \uparrow - \bar{x}_i \downarrow \tag{5}$$

The highest absolute returned value $|B_i|$ in all set positions P_i along and around the axis is referred to as an **axis returned value** and defined by Equation (6):

$$B = \max[|Bi|] \tag{6}$$

Mean axis returned value $\bar{B}$ is defined as an arithmetic mean of the returned value B_i, in all set positions P_i along or around the axis, based on Equation (7):

$$\bar{B} = \frac{1}{m}\sum_{i=1}^{m} B_i \tag{7}$$

The key parameters in accuracy and repeatability measurement are estimators. **The estimator of unidirectional standard positioning uncertainty in a given position $s_i\uparrow$ or $s_i\downarrow$** is the estimator of standard positioning deviation uncertainty in an n-series of unidirectional runs towards P_i, determined based on (8), (9):

$$s_i \uparrow = \sqrt{\frac{1}{n-1}\sum_{i=1}^{n}(x_{ij}\uparrow - \bar{x}_i\uparrow)^2} \tag{8}$$

$$s_i \downarrow = \sqrt{\frac{1}{n-1}\sum_{i=1}^{n}(x_{ij}\downarrow - \bar{x}_i\downarrow)^2} \tag{9}$$

Having a specificied value of unidirectional standard positioning uncertainty estimators in a given position (s_i↑, s_i↓), one can determine the unidirectional ($R_i \uparrow$ $R_i \downarrow$) and bidirectional R_i positioning repeatability in the set position P_i.

Repeatability is the degree of agreement between successive measurements taken at the same time and in similar measurement conditions. To assess it objectively, the following conditions must be satisfied: the measurement procedure is the same, the measurement is performed by the same diagnostician, the same measurement instrument is used, the measurement is performed under the same conditions and in the same place, the measurement is repeated in short time intervals. **Repeatability of linear position** refers to the degree of agreement between successive linear positioning measurement results in a rectangular coordinate system performed under the same conditions. In measurement practice, the repeatability of CNC machine tool service unit linear positioning is the ability to achieve the programmed target point (set point) in various repetitions performed in short intervals of time. **Repeatability of angular position** refers to the degree of agreement between successive measurement results of angular position in a polar coordinate system performed under the same conditions. In practice, the angular positioning repeatability of a CNC machine tool service unit is the ability to achieve the target point in many repetitions performed in short intervals of time.

Unidirectional positioning repeatability in a given position ($R_i \uparrow$, $R_i \downarrow$) refers to the range of extended uncertainty (s_i↑, s_i↓) of the unidirectional positioning deviation in the P_i position with a coverage ratio of 2, expressed by Equations (10) and (11):

$$R_i\uparrow = 4s_i\uparrow \tag{10}$$

$$R_i\downarrow = 4s_i\downarrow \tag{11}$$

Taking into consideration the estimated values of unidirectional standard positioning uncertainty in a given position (s_i↑, s_i↓) as well as the unidirectional positioning repeatability in the set position P_i ($R_i \uparrow, R_i \downarrow$) as well as the returned value B_i module in the P_i position, we can determine the bidirectional positioning repeatability R_i in a given position P_i.

Bidirectional positioning repeatability (R_i) in a given position P_i, is described by Equation (12):

$$R_i = \max[2s_i \uparrow + 2s_i \downarrow + |B_i|; R_i \uparrow; R_i \downarrow] \tag{12}$$

Unidirectional positioning repeatability ($R \uparrow$, $R \downarrow$) and bidirectional positioning repeatability (R) of an axis are the highest positioning repeatability values in a given position P_i along and around the axis, determined according to Equations (13), (14), (15):

$$R \uparrow = max[R_i \uparrow] \tag{13}$$

$$R \downarrow = max[R_i \downarrow] \quad (14)$$

$$R = max[R_i] \quad (15)$$

Unidirectional systematic axis positioning deviation ($E \uparrow, E \downarrow$) is defined as the difference between the highest and the lowest aerage values of unidirectional positioning deviations for the run from one direction to the set position P_i along and around the axis. The value of unidirectional systematic axis positioning deviations for a given direction of the run can be determined by the following equations (16) and (17):

$$E \uparrow = max[\bar{x}_i \uparrow] - min[\bar{x}_i \uparrow] \quad (16)$$

$$E \downarrow = max[\bar{x}_i \downarrow] - min[\bar{x}_i \downarrow] \quad (17)$$

Bidirectional systematic axis positioning deviation (E) is defined as the difference between the highest and the lowest average unidirectional positioning deviations for the run from both directions towards the set position P_i along and around the axis. Bidirectional systematic positioning deviation is described by the following equation (18):

$$E = max[\bar{x}_i \uparrow; \bar{x}_i \downarrow] - min[\bar{x}_i \uparrow; \bar{x}_i \downarrow] \quad (18)$$

Mean bidirectional systematic axis positioning deviation (M) is determined on the basis of average bidirectional positioning deviations in the set position P_i, determined along and around the axis. The mean bidirectional systematic axis positioning deviation is described by Equation (19) as the difference between the highest and the lowest average unidirectional positioning deviations.

$$M = max[\bar{x}_i] - min[\bar{x}_i] \quad (19)$$

Unidirectional axis positioning accuracy ($A \uparrow, A \downarrow$) is a combination of unidirectional systematic deviations and the estimator of standard uncertainty of unidirectional positioning with a coverage ratio of 2, according to Equations (20), (21):

$$A \uparrow = max[\bar{x}_i \uparrow + 2s_i \uparrow] - min[\bar{x}_i \uparrow + 2s_i \uparrow] \quad (20)$$

$$A \downarrow = max[\bar{x}_i \downarrow + 2s_i \downarrow] - min[\bar{x}_i \downarrow + 2s_i \downarrow] \quad (21)$$

Bidirectional axis positioning accuracy (A) is a combination of bidirectional systematic position deviations and the estimator of standard two-dimensional position uncertainty with a coverage ratio of 2. The bidirectional position accuracy of a numerically controlled axis A is described with the following equation (22):

$$A = ma\,x[\bar{x}_i \uparrow + 2s_i \uparrow;\ \bar{x}_i \downarrow + 2s_i \downarrow] - min[\bar{x}_i \uparrow - 2s_i \uparrow; \bar{x}_i \downarrow - 2s_i \downarrow] \quad (22)$$

1.3. Regulations regarding machine tool testing

As a result of more demanding requirements for the accuracy of produced parts, machine tools and machining systems must meet higher and higher geometric, kinematic, technological and efficiency-related expectations. A particular emphasis is primarily put on increasing machining efficiency and accuracy at the same time [49, 51, 70, 97]. To achieve and maintain the accuracy of a few micro metres, one should control and compensate for different types of errors. As indicated in 1.1, the regulations regarding machine tool testing are specified in international ISO standards developed by the International Committee for Standardization and in standards of individual countries (in Poland: PN-ISO, developed on the basis of translated versions of international ISO standards and replacing national PN standards). Therefore, accuracy tests for machine tools are standardised. Polish standards specify both general regulations regarding machine tool testing and detailed methods for determining deviations and tolerances limiting their permissible values [130–150]. PN-ISO standards primarily include specified regulations concerning the following aspects of machine tool testing:

- geometric accuracy of machines operating under no-load or finishing conditions,
- accuracy and repeatability of positioning numerically controlled machine axes,
- circular tests for numerically controlled machine tools,
- determination of the noise emission,
- geometric accuracy of machine tools with horizontal spindle (horizontal Z axis) and universal heads,
- geometric accuracy of machine tools with integral indexable or continuous universal heads (vertical Z axis),
- accuracy and repeatability of positioning of linear and rotary axes,
- accuracy of feeds,
- accuracy of speeds and interpolations,
- accuracy of a finished test piece.

The basic standards pertaining to the testing of machine tool accuracy include PN-ISO 230 (ISO 230) and PN-ISO 10791 (PN-ISO 10791). Each of the standards consists of a number of parts defining the terms and describing the rules, guidelines and the range of measurements, as well as specifying ways of reporting the results and describing the applied measuring instruments. The PN-ISO 230 (ISO 230) standard consists of 11 parts. Individual parts of PN-ISO 230 (ISO 230) are listed in Table 1.

PN-ISO 230 (ISO 230) describes the testing methods for power-driven machines which can be used for machining metal or wood, excluding portable power-driven portable tools. PN-ISO 230 (ISO 230) describes the regulations regarding machine tool testing for machine tools operating at no-load (idle run) or in finishing work conditions. PN-ISO 230 (ISO 230) mainly focuses on geometric accuracy testing, i.e., it does not cover the testing of machine tool operating variables, e.g. vibrations, stiffness, rotational speed, feed, etc. Such tests should be conducted prior to geometric accuracy testing. PN-ISO 230 (ISO 230) also covers thermal effects and noise emissions (machine acoustic emission pressure and sound power).

Tab. 1. List of PN-ISO 230 / ISO 230 standards for the machine tool testing and error identification

Standard number	The content of the standards/ title of the standard
PN-ISO 230 / ISO 230	
PN-ISO 230-1:1988	The regulations regarding machine tool testing. Part 1: Geometric accuracy of machine tools operating at no-load or in finishing work conditions.
ISO 230-1:1996	Test code for machine tools. Part 1: Geometric accuracy of machines operating under no-load or finishing conditions.
ISO 230-1:2012	Test code for machine tools. Part 1: Geometric accuracy of machines operating under no-load or quasi-static conditions.
PN-ISO 230-2:1999	The regulations regarding machine tools. Part 2: Designating accuracy and numerically controlled axis positioning repeatability.
ISO 230-2:2006	Test code for machine tools. Part 2: Determination of accuracy and repeatability of positioning numerically controlled machine axes.
ISO 230-2:2014	Test code for machine tools. Part 2: Determination of accuracy and repeatability of numerically controlled axes.
PN-ISO 230-3	Regulations regarding machine tools testing. Part 3: Designating heat effects.
ISO 230-3:2007	Test code for machine tools. Part 3: Determination of thermal effects.
PN-ISO 230-4:1999	Regulations regarding machine tools testing. Part 4: Testing roundness in in numerically controlled machine tools.
ISO 230-4:2005	Test code for machine tools. Part 4: Circular tests for numerically controlled machine tools.
PN-ISO 230-5:2002	Regulations regarding machine tools testing. Part 5: Designating noise emission.
ISO 230-5:2000	Test code for machine tool. Part 5: Determination of the noise emission.
ISO 230-6:2002	Test code for machine tools. Part 6: Determination of positioning accuracy on body and face diagonals. Diagonal displacement tests.
ISO 230-7:2015	Test code for machine tools. Part 7: Geometric accuracy of axes of rotation.
ISO/TR 230-8:2010	Test code for machine tools. Part 8: Vibrations.
ISO/TR 230-9:2005	Test code for machine tools. Part 9: Estimation of measurement uncertainty for machine tool tests according to series ISO 230, basic equations.
ISO 230-10:2011	Test code for machine tools. Part 10: Determination of the measuring performance of probing systems of numerically controlled machine tools.
ISO/FDIS 230-10	Test code for machine tools. Part 10: Determination of the measuring performance
ISO 230-10:2011	of probing systems of numerically controlled machine tools.
/Amd 1:2014	Measuring performance with scanning probes.
ISO/DTR 230-11	Test code for machine tools. Part 11: Measuring instruments suitable for machine tool geometry tests.

Another important standard for machine tool testing is PN-ISO 10791 (ISO 10791), which describes the testing conditions of processing centres (different groups of machine tools) and consists of 11 parts. Individual parts of this standard are listed in Tab. 2. PN-ISO 10791 is also a source of vital information concerning the possible testing of processing centres, with the possibility of their full of partial use in relation to numerically controlled boring mills and milling cutters with their configuration, motion and kinematics similar to those of processing centres. PN-ISO 10791 also specifies tolerance values or the highest permissible values of test results depending on the general need and the normal accuracy of processing centres. Other standards related to the testing conditions for CNC machine tools are listed in Tab. 3.

Tab. 2. List of PN-ISO 10791 / ISO 10791 standards for the testing and identification of machine tool errors

PN-ISO 10791 / ISO 10791	
PN-ISO 10791-1:2000	Testing conditions of processing centres. Part 1: Checking the geometric accuracy of machine tools with horizontal spindle (with horizontal axis Z) and with replaceable heads.
ISO 10791-1:2015	Test conditions for machining centres. Part 1: Geometric tests for machines with horizontal spindle (horizontal Z-axis).
ISO 10791-2: 2001	Test conditions for machining centres: Part 2: Geometric tests for machines with vertical spindle or universal heads with vertical primary rotary axis (vertical Z-axis).
PN-ISO 10791-3:2001	Testing conditions for machining centres. Part 3: Checking the geometric accuracy of machine tools with indexable spindle heads or positioned in a continuous way (with vertical Z-axis).
ISO 10791-3:1998	Test conditions for machining centres: Part 3: Geometric tests for machines with integral indexable or continuous universal heads (vertical Z-axis).
PN-ISO 10791-4:2001	Testing conditions for machining centres. Part 4: Accuracy and repeatability of positioning in linear and rotary axes.
ISO 10791-4:1998	Test conditions for machining centres: Part 4: Accuracy and repeatability of positioning of linear and rotary axes.
PN-ISO 10791-5:2000	Test conditions for machining centres. Part 5: Accuracy and repeatability of positioning of work-holding pallets.
ISO 10791-5:1998	Test conditions for machining centres: Part 5: Accuracy and repeatability of positioning of work-holding pallets.
PN-ISO 10791-6:2001	Test conditions for machining centres. Part 6: Accuracy of movements, spindle rotary speeds and interpolation.
ISO 10791-6:2014	Test conditions for machining centres. Part 6: Accuracy of speeds and interpolations.
PN-ISO 10791-7:2000	Test conditions for machining centres. Part 7: Accuracy of a finished test piece
ISO 10791-7:2014	Test conditions for machining centres. Part 7: Accuracy of a finished test piece.
ISO 10791-8:2001	Test conditions for machining centres. Part 8: Evaluation of the contouring performance in the three coordinate planes.
ISO 10791-9:2001	Test conditions for machining centres. Part 9: Evaluation of the operating times of tool change and pallet change.
ISO 10791-10:2007	Test conditions for machining centres. Part 10: Evaluation of the thermal distortions.
ISO 10791-11	Test conditions for machining centres. Part 11: Evaluation of the noise emission. Annex A of this part of ISO 10791 is for information only.

ISO and PN-ISO standards are used to comparatively assess the tested machine tools, both during their normal operation and during their periodical accuracy control and during the testing stage and trials by the producer or receiving party.

Tab. 3. List of additional standards for the testing and identification of machine tool errors	
ISO 8525:2008	Airborne noise emitted by machine tools. Operating conditions for metal-cutting machines.
PN-EN-01307: 1994	Noise. Permissible noise values in the workplace. Conditions regarding testing.
PN-EN ISO 4871:2010	Acoustics. Declaration and verification of noise emission values of machinery and equipment.
PN-EN ISO 11201:2012	Acoustics. Noise emitted by machines and devices. Testing acoustic pressure levels in the workplace and other places with conditions near to the essentially free field over a reflecting plane z with negligible environmental corrections.
PN-EN ISO 11202:2012	Acoustics. Noise emitted by machines and devices. Testing acoustic pressure levels in the workplace and other places using approximate environmental corrections.
PN-EN ISO 11203:2010	Acoustics. Noise emitted by machines and devices. Designating acoustic pressure levels in the workplace and other places on the basis of acoustic power levels.
PN-EN ISO 11204:2010	Acoustics. Noise emitted by machines and devices. Testing acoustic pressure emission levels in the workplace and other places using precise environmental corrections.
PN-EN ISO 11205:2010	Acoustics. Noise emitted by machines and devices. Technical method of designating acoustic pressure emission levels in in-situ conditions in the workplace and other places on the basis of sound intensity measurements.
PN-EN ISO 11689:2000 PN-EN ISO 11689:2000/AC:2009	Acoustics. Procedure for the comparison of noise-emission data for machinery and equipment. Acoustics. Procedure for the comparison of noise-emission data for machinery and equipment.
PN-EN ISO 9612:2011	Acoustics. Determination of occupational noise exposure. Technical method.
PN-N-01307:1994	Noise. Permissible noise parameters values in the workplace. Requirements concerning taking measurements.
PN-ISO 1999:2000	Acoustics. Determination of occupational noise exposure and estimating hearing damage due to noise.
PN-EN ISO 11690-2:2000	Acoustics. Recommended practice for the design of workplaces with limited noise, equipped in machines. Noise reduction measures.
PN-EN ISO 11690-3:2002	Acoustics. Recommended practice for the design of workplaces with limited noise, equipped in machines. Part 3: Propagation of noise and forecasting noise in the workplace.
PN-N-01307:1994	Noise. Permissible noise parameters values in the workplace. Requirements concerning taking measurements.

1.4. Machine tool measurement and diagnostic systems

The assessment of machine tool unit technical conditions is made via various methods for measuring machine tool geometric and kinematic accuracy [13, 83–93, 96, 103, 107, 108, 113, 120–124].

Fig. 5 presents the latest and, at the same time, the most popular systems, devices and methods for assessing the accuracy of CNC machine tools [152–157, 159, 165–177].

The most common machine tool control methods are those based on circular tests performed in accordance with ISO 230-4, e.g. with the use of QC10 Ballbar, QC20-W Ballbar, API Ballbar and DBB 110 Ballbar devices [40, 55, 56, 59, 69, 105, 169, 176]. Another group of systems are devices for measuring linear intervals. They include material standards, laser interferometers and measuring rules [2, 4, 11, 12, 14, 15, 20, 21, 36, 44–47, 67, 77, 68, 99]. The latest machine tool testing systems are volumetric (spatial) error testing systems. They include interferometric tracking systems such as LaserTRACER, LaserTRACER-MT and T3 LaserTRACKER dedicated to machine tools with high displacements [22, 65, 72–75, 88, 152, 153]. Fig. 5 shows modern machine tool accuracy testing devices. The aim of diagnostic testing is to determine the maximum deviation value of a particular error type.

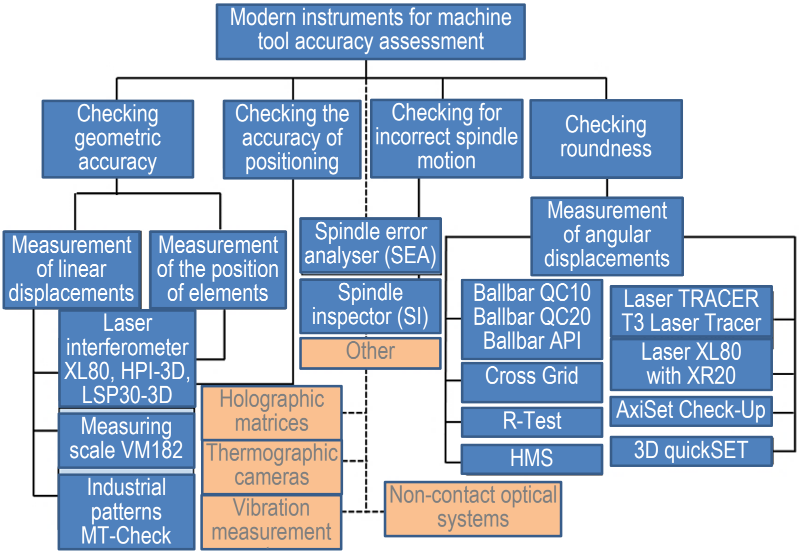

Fig. 5. Modern CNC machine tool accuracy testing devices [30, 45, 96, 103, 113, 123]

CNC machine tool diagnostic and calibration systems based on roundness testing enable the determination of key machine parameters. They also allow their monitoring (in time scale: months, quarters, years), which, in effect, leads to reduced risk of production shortages and losses. Using the newest diagnostic tools such as QC10 Ballbar, QC20-WBallbar [169], Cross Grind [18], R-test [25], HMS – Head Measuring System [159], the user can estimate within a few minutes whether the machine is suitable for realization of some technological tasks [25, 40, 55]. Fig. 6 shows selected CNC machine tool industrial diagnostic and calibration systems used in industrial practice. Thanks to diagnostic testing, all repairs and renovations can be planned beforehand. Until recently, there were no tools for automatic control and calibration of a machine rotary axis, especially in the case of axis collision or wear. In recent years however, together with a wider use of multi-axis machine tools, there have appeared many systems enabling the diagnostics, measurement and calibration of CNC machine tool rotary axis. They include the afore-mentioned laser systems and systems enabling the quick and precise assessment of machine kinematic joint position such as Renishaw's AxiSet™ Check-Up and DMG 3D quickSET (Figs. 6 h, l.)

A survey of the literature [1–129] reveals that the range of applications for some of the above-mentioned calibration systems (Renishaw's AxiSet™ Check-Up and DGM 3D quickSET) is relatively narrow. There is little information on the web pages [48, 156, 157, 168, 175] whereas the technical specification contains very little information on the subject [174].

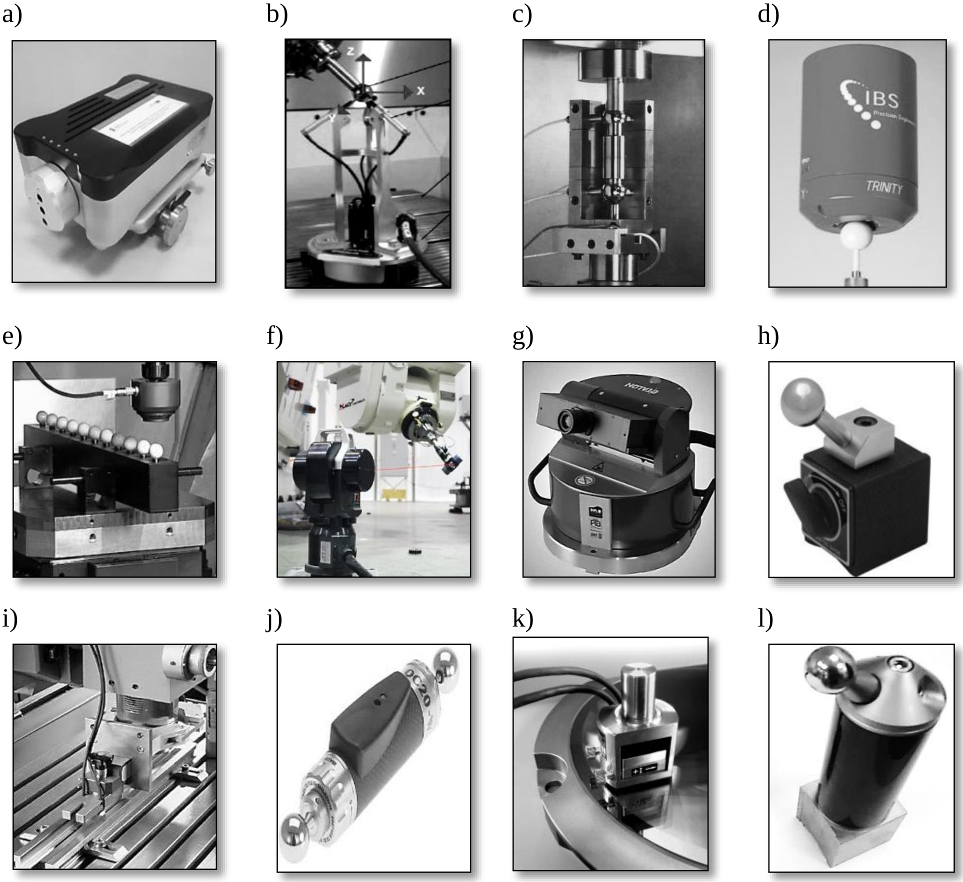

Fig. 6. Selected numerically controlled machine tool industrial diagnostics systems: a) laser interferometer XL80, b) five-axis machine tool calibrator Head Measuring System HMS), c) Spindle Error Analyser SEA, d) kinematic centre positioning calibration system R-Test System with TRINITY Probe, e) industrial design for Machine Tool Calibration MT-Check calibration, f) T3 Laser Tracker, g) TRACER, h) AxiSet™ Check-Up, i) VM 182 Comparator System, j) QC20-W Ballbar, k) Cross Grid (KGM), l) 3D quickSET [18, 25, 152, 153, 159, 164, 169]

2. AIM AND SCOPE OF THE WORK

CNC machine tool accuracy tests are performed to assess the technical condition of these machines, as this aspect is crucial for the accuracy of their movements. As regards cutting machine tools for metal, the accuracy of their movements affects the dimensional and shape accuracy of produced parts [2, 4, 11, 12, 14, 15, 20, 21, 36, 44–47, 67, 77, 68, 99]. Another aim of diagnostic testing is the possibility of compensating errors on the basis of collected diagnostic data (obtained from other sources) or undertaking the required action to restore the machine's operating capacity lost during operation or due to collision [1–3, 33, 37, 49, 55, 70, 97]. Such testing is run by the producer during machine assembly and installation in an industrial plant and during operation. The methods for measuring machine tool static and dynamic inaccuracies extensively described in the literature are relatively well-known and can be used irrespective of machine design features [30, 38, 45, 64, 83, 96, 108, 112, 113, 120, 122–125]. Nonetheless, the ISO standards classify measurement methods depending on the machine size and type [130, 131, 137]. It is worth emphasizing that accuracy tests are usually performed with only one, very often the simplest measurement method and the simplest diagnostic tools. Reported experiments demonstrate that the measurements are usually taken using material standards; more advanced diagnostic and calibration systems are far less frequently used [164]. In industrial practice direct measurement systems such as laser interferometers or electronic water levels are also used [45]. It turns out that direct measurements do not give a full and satisfactory answer with respect to machine tool spatial inaccuracy. A good example of it is the use of systems for 3D dynamic measurements such as the R-test [25, 32, 35, 43, 50, 52, 104, 116] or Spindle Error Analyser SEA [38, 39, 42, 57, 89, 112, 117, 127, 164] or machine tool inner measurement systems, AxisSet [175], 3D QuickSET [48] and others [123]. Machine tool spindle errors, especially spindle erroneous movements, are of crucial importance because they imbalance the tool path or change the position of rotary axis kinematic centres. Identification and analysis of errors becomes complicated when a large-size machine tool, e.g. a machine with a portal structure or a kinematically complex multi-axis machine tool, is to be diagnostically tested [75]. The increase in the number of numerically controlled machine tool axes considerably complicates the determination of their spatial inaccuracies [22, 65, 72–75, 88].

In addition, indirect assessment using e.g. a telescopic ballbar requires multiple bar changes on the machine tool table, using many different movement speeds and lengths of the measurement arms [7]. Like with material standards, also in this case the measurement requires discreet diagnostic tool positioning in the machine workspace. This method of spatial error assessment still has the features of discreet measurement although the whole workspace of the machine is tested. In this case, simple measurement methods are not enough. We must therefore reach for more complex and advanced diagnostic tools. The problem becomes more serious in a situation when we are forced to estimate the volumetric spatial error VE [22, 65, 72–75, 88]. On the basis of the knowledge of errors, one is required to ”map” a positioning error to determine the so-called volumetric error in the entire workspace of the machine. Should such situation be the case, the measurements become tiresome and take a lot of time, and in some cases even impossible (e.g. when there is no access to specialist measurement and diagnostic instruments). Frequently designed and well-known algorithms seem insufficient for the effective estimation of machine tool inaccuracy.

Very effective methods and tools for determining volumetric errors are presented in [72–75]. Nonetheless, these methods require that the measuring device be attached to the measurement machine table; at the same time, they enable the determination of spatial geometric and/or kinematic inaccuracy of the machine tool via one attachment [75]. Sometimes it is necessary to use many tools and methods to effectively determine machine tool inaccuracy. There is also a need for many diagnostic measurements but, above all, for many sources of information, including thermal, acoustic or vibroacoustic data to ensure the accuracy of diagnostic measurement. Sadly, companies do not usually possess many diagnostic tools, neither have they time for machine diagnoses. Machine diagnostics is therefore treated as something final, and on a number of occasions as a necessary evil. According to the practical experience gathered on the basis of cooperation with industry, such companies do not diagnose their machines unless this is forced upon them by the receiving party or general rules regulating a particular industry (e.g. aviation). As the author’s experience demonstrates, each and every machine tool should be tested systematically, not only at the design stage but especially during operation. The main objective of such action is to maintain their operating performance and accuracy in the long run. The lack of access to diagnostic tools or the knowledge of diagnostic methods in companies makes it necessary to develop for a specified group of machines effective models enabling the programming of their technical condition. This also inspired the author to undertake the subject matter of the present work.

The aim of this work is to present the applications of diagnostic methods and CNC machine tool diagnostic tools available on the market, as well as to create a relatively universal and simple diagnostic model for error prediction that can widely be used in companies. The work presents the author’s many-year experimental research on repeatability errors, positioning errors, and thermal and dynamic testing of machine tools (lathes and milling cutters). Error values obtained during measurements were used to create a diagnostic model. This, however, required systematic diagnostic measurements to create a history of machine tool geometric accuracy. The data captured in the form of time series enabled the creation of models, on the basis of which it is possible to formulate predictions concerning machine condition. This also gives a chance to transfer obtained results to other types of machine tools with similar kinematic and geometric properties used in industrial practice. The design of such models has produced measurable utilitarian results allowing the entrepreneur to foresee the machine condition and take the necessary steps towards systematic compensation and minimisation of existing errors.

The research involved the assessment of positioning errors (accuracy and positioning repeatability), rotary axis kinematic centre positioning, erroneous spindle movements, rotary speed variations, feed rate, and identification of the heat- and noise-generating sources. This research was conducted with the use of specialist diagnostic systems, including QC20-Ballbar, XL-80 laser interferometer with XR20 rotary axis calibrator and XC20 environmental station, R-Test, 3D quickSET, V20 thermographic camera, holographic matrix with dedicated software. Diagnostic tools used will be adequately characterised in subsequent chapters (Chapters 3÷9).

According to the literature [4, 49, 51, 70], the quality of parts depends, among other things, on numerically controlled axis positioning repeatability and accuracy, linear and angular movement accuracy, the position of the axes relative to each other during assembly, and clearances in the drive system during operation. Every, even the smallest inaccuracy of a machine tool affects the end quality of finished parts, which forces the user to perform systematic testing of machine tools [51].

3. LASER DIAGNOSTICS OF CNC MACHINE TOOLS

The use of multi-axis machine tools in the production processes has become very popular in recent years. This is due to the fact that these machines offer more possibilities to perform more and more complex movements and map more complex shapes. The greatest number of such machines can be found in the aviation and automotive industries where the use of five-axis machines enhances the production of complex-geometry parts, e.g., engine turbine blades, generators, complex-geometry car and aeroplane parts, etc. The performance of complex shaping movements requires machine tools with many numerically controlled axes, both linear and rotary. The most popular CNC machine tool rotary axes necessary for the machining of the above mentioned parts are rotary tables and tilting rotary tables that are often mounted as an addition to the linear axes. Ordinary axes are parallel to a selected linear axis of the machine, but there are machine tools in which the rotary axis is positioned at an angle of 45° to one of the linear axes of the machine. Rotary axes in machining centres can be mechanically attached to other elements besides the work table. There are design solutions of machine tools in which the spindle axis can perform angular movements irrespective of the rectangular table of the machine.

This chapter reports the results of research, including the analysis of accuracy and repeatability of linear and angular positioning of numerically controlled multi-axis CNC machine tools with different systems of numerical control. Machines for the research were selected depending on the criterion of kinematic and geometric similarity and grouped according to the type of test. The machines selected for the research included:

- DMC 635 ecoline 3-axis machining centre with Heidenhain TNC 620 control system,
- FV-580A 4-axis vertical machining centre with FANUC 0iMC control system,
- DMU 65 monoBLOCK 5-axis machining centre with numerically controlled Sinumerik 840D sl CNC Software 4.5 control system,
- numerically controlled CTX 310 ecoline lathe with drive tools and Heidenhain CNC PILOT 620 control system.

Errors were identified using a laser interferometer. A comparative analysis of tested machine tool errors is made and their sources are determined. Also, methods for minimising these errors are given. Possibilities of predicting the technical condition of machine tools on the basis of long-term observations and the capture of data necessary for machine condition prediction on the basis of time series are described.

3.1. Research object, methods and testing conditions

As mentioned in Chapter 3, the object of the present research are four numerically controlled CNC machine tools. All of them were tested with respect to linear positioning accuracy and repeatability. The assessment of rotary axis angular positioning accuracy and repeatability was also performed. This type of testing was carried out for the DMU 65 monoBLOCK rotary tilting machining centre and for the numerically controlled CTX 310 ecoline lathe. X, Y, Z axes positioning deviations were assessed, including bidirectional axis positioning accuracy A, unidirectional axis positioning accuracy (A↑ and A↓), unidirectional positioning repeatability (R↑ and R↓) and axis returned value B. Permissible values of the quantities in the linear axes for the tested machine tools are as follows: A=22μm, A↑=16μm, A↓=16μm, R↑=6μm, R↓=6μm, B=10μm. The research objects and employed research methods will be described in a subsequent part of this work.

Description of the DMC 635 3-axis vertical machining centre

Experimental tests of linear positioning accuracy and repeatability were run for the DMC 635 ecoline vertical machining centre with Heidenhein TNC 620 control (Fig. 7). A remote laser interferometer, XL-80, with dedicated software was used in the test. The essence of interferometer operation is the use of light of known wave length as the measure of length. Interferometer measurements rely on counting the length of light waves falling on the optical detector. This yields extremely accurate positioning results. According to the interferometer specifications provided by the producer, the accuracy of linear movement measurements, irrespective of adjustments, resulting from material heat expansion is MPE=±0.5ppm [156, 157].

Fig. 7. DMC 635 ecoline vertical machining centre

During the measurements, the compensation of laser light wave lengths due to temperature, pressure and humidity was applied, which helped to increase accuracy of the test. The employed research methodology included linear positioning measurements on the X, Y, Z axes. The research station consisted of a vertical machining centre, a laser head, a laser interferometer XL-80, linear lamps, a compensation station and a computer dedicated to the equipment requirements (Fig. 8).

An analysis of measurement uncertainty, taking into consideration the data provided by the producer in the machine technical specification, enables the estimation of its extended uncertainty of 6μm per one meter of axis length with a temperature difference of 5°C relative to the normal temperature (with coverage ratio k=2).

a) b)

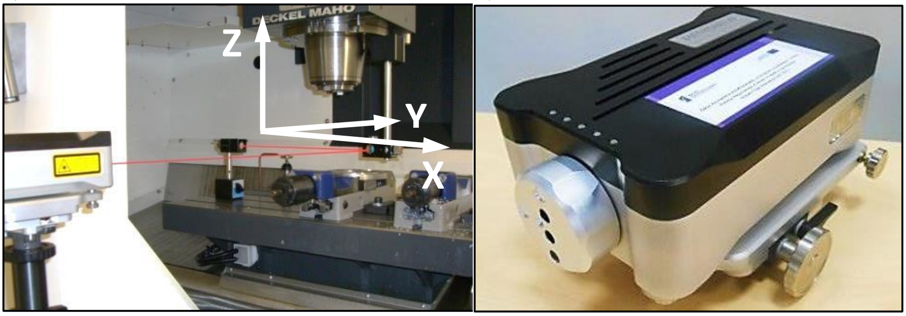

Fig. 8. Example of a device for measuring the positioning accuracy and repeatability of the DMC 635 ecoline milling centre: a) interferometer set-up, b) XL-80 laser interferometer

Optical systems were attached to the milling machine spindle and work table and synchronized with the XL-80 laser. The measurement was based on the work table movement from the zero point of the machine to the furthest possible point with a determined stroke (500mm), for the X axis within the range of 0÷600mm, for the Y axis within the range of 0÷500mm, for the Z axis within the range of 0÷450mm, respectively, and taking measurements in a given measurement point. The programmed feed movements for each axis are listed in Tab. 4.

Tab. 4. Programmed measurement points for each axis

Axis	Programmed measurement points, *Pi* [mm]												
X	0	50	100	150	200	250	300	350	400	450	500	550	600
Y	0	50	100	150	200	250	300	350	400	450	500	-	-
Z	0	50	100	150	200	250	300	350	400	450	-	-	-

The measurement was repeated three times for each of the axes. All tests were performed under no-load, following pre-heating of the machine. The velocity of movement for each test was maintained constant at v_f*=const.*

Fig. 9 a schematic set-up of the laser system during the measurements of the numerically controlled axes X, Y, Z. This set-up was used for every tested machine tool to identify positioning errors.

Description of the FV-580A 4-axis vertical machining centre

FV-580A 4-axis vertical machining centre is a machine tool with three numerically controlled linear axes (X, Y, Z) and one rotary axis C. The FV-580A centre can be used for machining parts with complex shapes. Its high drive power, a wide range of spindle rotary speeds and the rate of feed as well as high positioning precison make is suitable for performing economical and efficient trials with modern cutting tools. The centre can be used for machining complex-shape parts made of aluminium, steel and cast iron. Fig. 10 shows this machine tool with the LSP-30 measurement system from Lasertex during measurements.

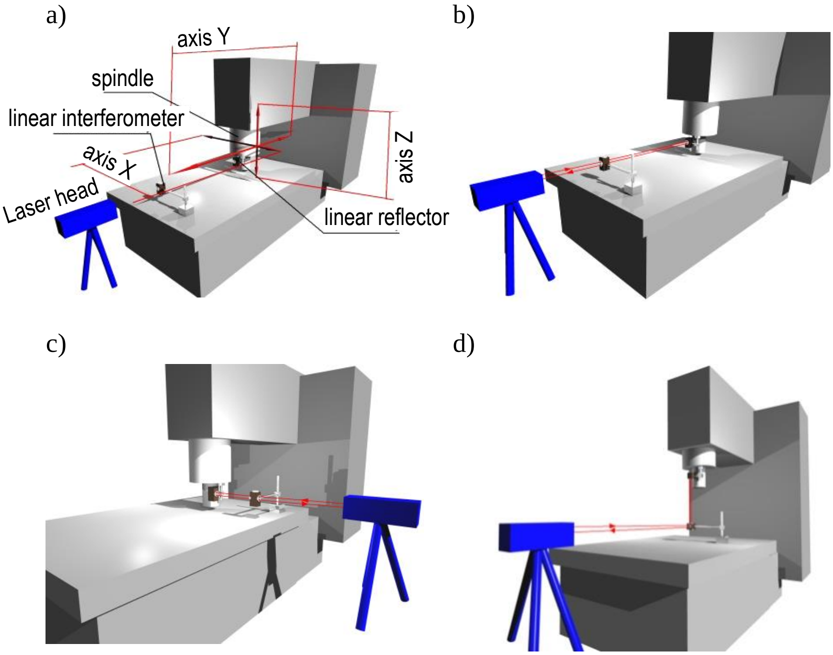

Fig. 9. Schematic design of the laser measurement system set-up during measurements on the numerically controlled axes: a) orientation of the axes and system components, b) measurement on X axis, c) measurement on Y axis, d) measurement on Z axis

The test stand consists of the FV-580A 4-axis vertical machining centre, a laser head, a laser interferometer, linear lamps, a meteo station with 3 temperature sensors, humidity and pressure sensors, magnetic handles and a computer as a system controller. A critical stage of the measurement was precise determination of basic testing conditions. Thermal conditions of the machine that must be met during measurement were provided by the producer. They specify the average required temperature in the room, maximum amplitude, frequency range for average temperature deviations and a gradient of the room temperature. For the measuring conditions to be optimal, the measurement instruments and the object must have the temperature of 20^{o}C. To satisfy this condition, the machine and measuring instruments as well as the testing equipment were controlled. The stabilisation of the measuring instruments and machine was realised by starting them up for a required period of time before proceeding with measurements. The machine was completely mounted, operational and properly levelled and aligned.

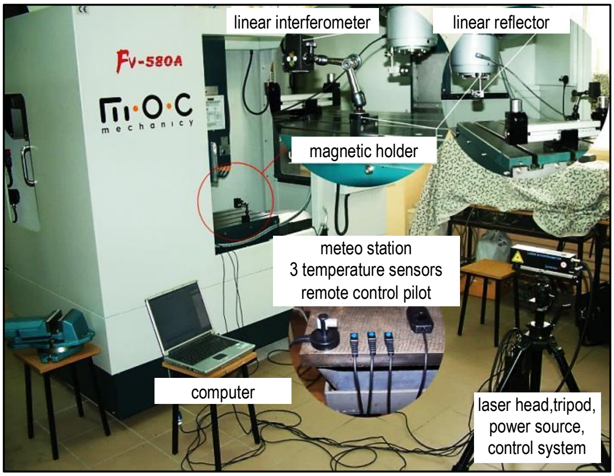

Fig. 10. CNC FV-580A vertical machining centre with installed measurement system LSP-30 from Lasertex

The tests were performed under no-load, after the machine had been preheated within the time specified by the producer. The measurements were conducted in such a way as to enable the registration of relative displacement between the region where the tool is attached and the region where the workpiece is attached in the direction of axis movement. When testing linear axes of up to 2000mm, six set positions per meter were assumed. According to the producer's recommendations, every measurement cycle can be repeated three times. The measurements were taken according to the standard testing cycle in the set positions. The positioning of the laser system for measurement on the X, Y, Z axes is presented in Fig. 9. The measurements were carried out for varying values of the feed rate v_f (50, 500, 2500, 5000, 10000, 24000mm/min). As a result of the measurements, the following variables were determined:

– unidirectional accuracy of positioning forward/backward A↑, A↓,
– bidirectional positioning accuracy A,
– unidirectional positioning repeatability forwards/ backwards R↑, R↓,
– bidirectional positioning repeatability *R*,
– axis returned value *B*,
– mean axis returned value $\overline{B}$.

Permissible values of individual parameters of the tested machine tool are listed in Tab. 5.

Tab. 5. Fragments of positioning tolerance board in the axes up to 800 mm [140]			
Name of ISO-specified quantity		Axis measurement path, [mm]	
		≤500	>500, ≤800
Bidirectional positioning accuracy	A[mm]	0,022	0.025
Unidirectional positioning accuracy	A↑[mm] A↓[mm]	0.016	0.020
Bidirectional positioning repeatability	R[mm]	0.012	0.015
Unidirectional positioning repeatability	R↑ [mm] R↓[mm]	0.006	0.008
Axis returned value	B[mm]	0.010	0.010
Mean axis returned value	$\bar{B}$ [mm]	0.006	0.006
Bidirectional systematic positioning deviation	E[mm]	0.015	0.018
Unidirectional systematic positioning deviation	E↑[mm] E↓[mm]	0.010	0.012
Mean bidirectional positioning deviation	M[mm]	0.010	0.012

The tests were performed in compliance with the bidirectional alternating strategy. The number of runs for the X and Z axes was set equal to 3, and for the Y axis – to 4. To diagnose the accuracy of the machine tool, a table of tolerances for machining centres of normal accuracy specified in PN-ISO 10791-4:2001 was used.

The testing characteristics of the numerically controlled CTX 310 ecoline lathe

Fig. 11 shows a numerically controlled CTX 310 ecoline lathe with Heidenhain CNC PILOT 620 control. The machine is equipped with drive tools and the C axis.

Fig. 11. Numerically controlled CTX 310 ecoline lathe with Heidenhain CNC PILOT 620 control

The tests of the numerically controlled CTX 310 ecoline lathe were run in laboratory conditions with the use of the XL-80 laser system with the XR20-W rotary axis calibrator (Fig. 12).

a)

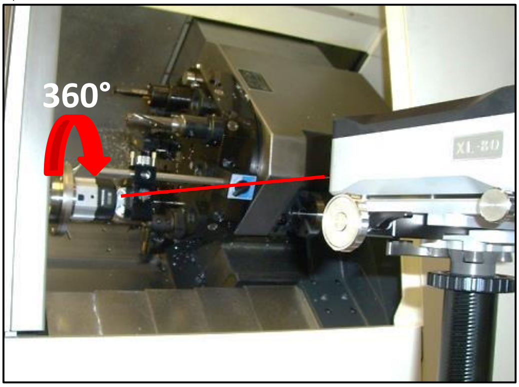

b)

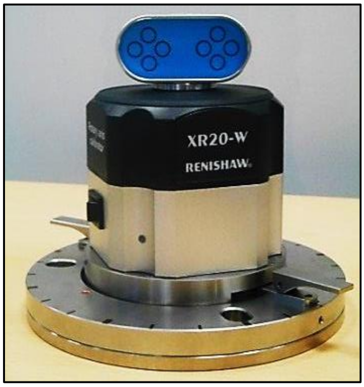

Fig. 12. Preparation and measurement of positioning deviations and angular positioning repeatability of numerically controlled CTX 310 ecoline lathe: a) XL-80 laser positioning, b) XR20-W rotary axis calibrator

Differently than in the case of lathes, here the methodology included angular positioning measurement of the machine tool. The rotary axis calibrator XR20-W was attached to the lathe handle and synchronized with the XL-80 laser. The tests were based on the rotation of the lathe handle in the range of 0÷360° with a step of every 20° and return to the initial position 0°. The time stoppage at every set position was 4 seconds. The tests were repeated three times. The XR20-W calibrator is equipped with an engine drive, and the capture of data is synchronized with displacement of the axis. The process of calibration via the XR20-W system is fully automated, which means that the process runs unattended during data capture. The use of the Renishaw laser system provides a touchless reference measurement of high integrity, remotely and with no contact from the tested numerically controlled axis. All tests were carried out under no-load, after machine pre-heating within the time specified by the producer. Additionally, measurements were taken in set positions according to the standard test cycle, i.e., at least twice in every direction according to the interferometer software.

Description and testing of the DMU 65 monoBLOCK machining centre

The aim of the test was to assess the positioning accuracy and repeatability of the rotary table axis C in the DMU 65 monoBLOCK vertical machining centre (Fig. 13).

The tests were conducted according to the PN-ISO 10791-4:2001 and PN-ISO 230-2 standards specifying the regulations for assessing the geometric accuracy of machining machine tools for metals. The XL-80 laser interferometer together with the XR20-W rotary axis calibrator were used to test the accuracy and repeatability of positioning (Fig. 13). The tests determined error values that have an essential influence on the accuracy of produced parts. The measurement methodology included an angular positioning measurement of the machine tool. The diagnostic and measurement process was preceded by a series of maintenance operations. The XR20-W calibrator was positioned precisely in the centre of the machine tool rotary table and configured with the XL-80 system (Fig. 13b).

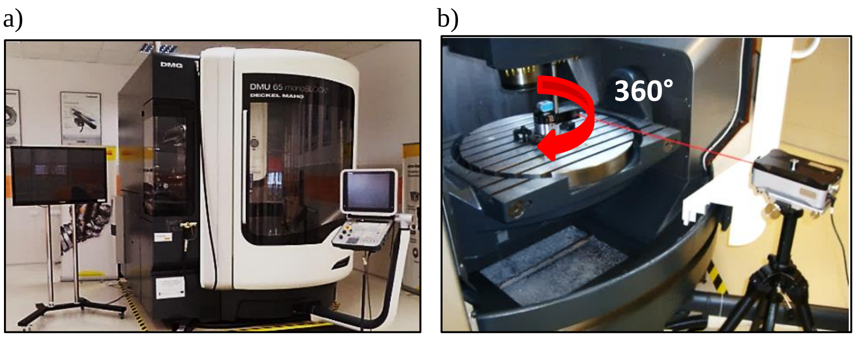

Fig. 13. Preparation and measurement of positioning deviations a) DMU 65 monoBLOCK 5-axis machining centre, b) interferometer positioning and measurement

Next, a mirror was properly attached and set with a magnetic handle. The XR20-W device was connected to the software with a cordless Bluetooth interface. The tests consisted in rotating the machine tool table in the range of 0°÷360° with a step of α=30°, and then returning it to the initial position 0°. The time of stoppage at every set measurement point was 4 seconds. Having completed the full rotation of 360°, the table turned in the opposite direction, until it reached the initial position, maintaining the same values of angular increment (α=30°) and time stoppage. The angular position was read and recorded. Three measurement cycles for each test were performed (clockwise and counter-clockwise).

3.2. Linear positioning repeatability test

Linear positioning accuracy and repeatability of the DMC 635ecoline vertical machining centre

The experimental tests provided information about linear positioning error values as a function of length of the measured axes (X, Y, Z, respectively). The test was performed for the feed motion from the positive (↑) and negative (↓) directions. Selected parameter values of the DMC 635 ecoline machine tool environment are listed in Tab. 6.

Taking into consideration the data captured by the environmental compensation unit for the DDMC 635 ecoline vertical machining centre, the following were determined: unidirectional and bidirectional positioning accuracy (A↑, A↓, A), unidirectional and bidirectional positioning repeatability (R↑, R↓, R), unidirectional and bidirectional systematic positioning deviations (E↑ E↓ E), mean bidirectional positioning deviation M as well as the axis returned value and its average value (B, $\overline{B}$).

Tab. 6. Compensation unit results describing the environmental conditions for testing the DMC 635 ecoline vertical machining centre						
	in X axis		**in Y axis**		**in Z axis**	
Data	**Beginning**	**End**	**Beginning**	**End**	**Beginning**	**End**
Air temperature [°C]	22.99	22.94	23.09	22.86	23.20	22.97
Pressure [hPa]	1004.80	1004.80	1004.40	1004.4	1004.20	1004.0
Humidity [%]	31.19	31.96	32.01	32.34	31.93	32.00
Surface temperature [°C]	21.11	21.14	21.20	21.22	21.34	21.32
Environmental factor 10^{-6}	316406.8	316406.7	316406.6	316406.4	316406.2	316406.2

Obtained results were processed in compliance with PN-ISO 10791-4:2001 using XCal-View 2.2. software [16]. Tab. 7 presents a comparison of all obtained accuracy parameters with a tolerance table specified in PN-ISO 10791-4:2001. The shaded fields in Table 7 indicate the exceeded tolerance values specified in the standard. For the X axis the tolerances are described for a measurement range from 501 to 800 mm, and for the Y and Z axes they are compared to the measurement path tolerances of up to 500mm. The unidirectional and bidirectional positioning accuracy in the Z axis exceeded the tolerances specified in PN-ISO10791-4:2001.

Tab. 7. Comparison of obtained accuracy parameters with the positioning accuracy tolerance table						
		Axis measurement path		**Measurement results** [*μm*]		
Tolerances	[*μm*]	≤500mm	>500. ≤800	X	Y	Z
Bidirectional positioning accuracy	A	22.0	25.0	10.5	4.6	23.7
Unidirectional Positioning accuracy	A↑ A↓	16.0	20.0	10.3	4.5	23.7
Bidirectional positioning repeatability	R	12.0	15.0	3.6	3.1	2.0
Unidirectional positioning repeatability	R↑ R↓	6.0	8.0	3.3	2.3	2.0
Axis returned value	B	10.0	10.0	0.4	0.9	0.5
Average axis returned value	$\bar{B}$	6.0	6.0	0.2	0.4	0.2
Bidirectional systematic positioning deviation	E	15.0	18.0	10.3	2.8	22.4
Unidirectional systematic positioning deviation	E↑ E↓	10.0	12.0	10.1	2.7	22.3
Average bidirectional positioning deviation	M	10.0	12.0	10.0	2.5	22.3

The subsequent figures (Figs. 14÷16) show the results of bidirectional positioning accuracy A for the X, Y, Z axes, respectively. The tests of bidirectional accuracy were repeated twice for each axis. Variations in the bidirectional positioning accuracy of the X axis of the DMU 635 ecoline 3-axis milling centre as a function of measuring point position are illustrated in Fig. 14. As shown in Fig. 14, the absolute value of bidirectional positioning deviation in the X axis is 10.5μm at the measuring point set to 500mm. The general trend of the X axis measurements is regressive and decreasing.

Fig. 15 shows results of the Y axis tests conducted according to PN-ISO 10791-4:2001. The highest bidirectional positioning accuracy of the Y axis is 4.6 μm.

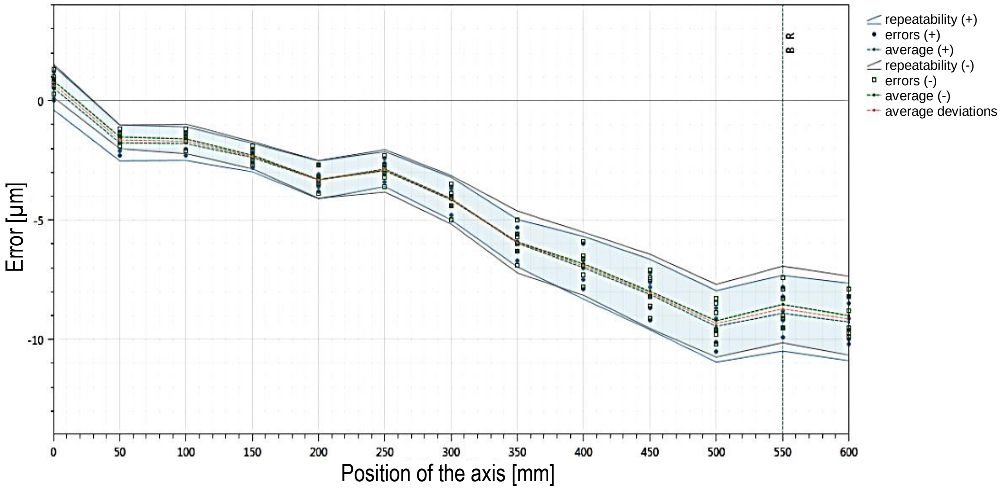

Fig. 14. Bidirectional positioning accuracy for X axis of DMU 635 ecoline 3-axis milling machine as a function of measurement point position

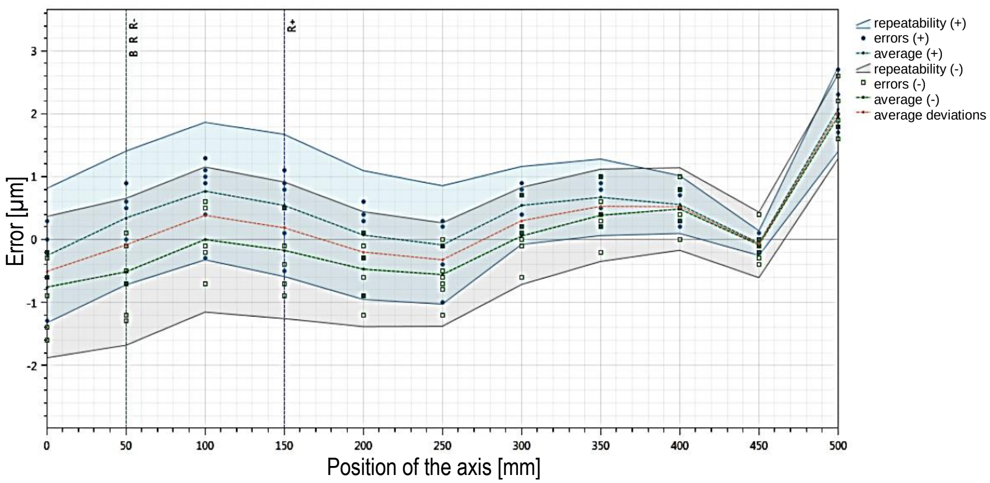

Fig. 15. Bidrectional positioning accuracy of the Y axis of the DMU 635 ecoline 3-axis milling machine as a function of measurement point position

Analysing the variations in the Y axis error values one can conclude that there is no increasing trend for this axis. The obtained data do not exceed the permissible limit values specified in the standard. Fig. 16 presents results of the Z axis tests. The highest obtained value of bidirectional positioning accuracy for the Z axis as a function of measurement point position is 23.7μm, which corresponds to its last position at 450mm. The results were assessed according to PN-ISO 10791-4:2001.

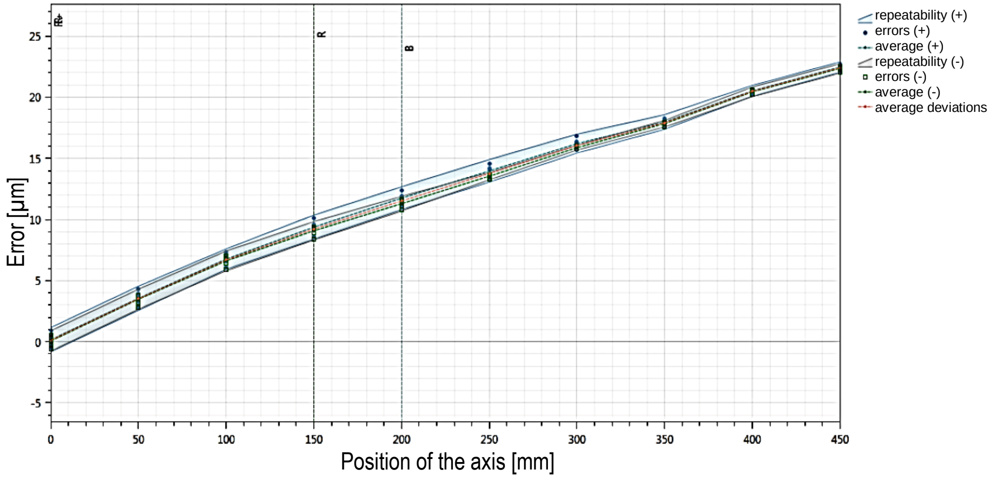

Fig. 16. Bidirectional positioning accuracy of the Z axis of the DMU 635 ecoline 3-axis milling cutter versus measurement point

As one may clearly notice from the comparison containing permissible values for this milling cutter, the obtained value of bidirectional positioning accuracy for the Z axis exceeds the premissible error tolerance. Fig. 17 compares the bidirectional positioning accuracy for all tested axes (X, Y, Z). As shown in the diagram, the lowest error values for bidirectional positioning accuracy were obtained in the Y axis while the highest – in the Z axis. The deviations of bidirectional positioning accuracy for the X and Y axes are in the range of permissible values according to PN-ISO10791-4:2001. Unidirectional and bidirectional systematic positioning deviations as well as the average bidirectional positioning deviation did not exceed the premissible tolerances.

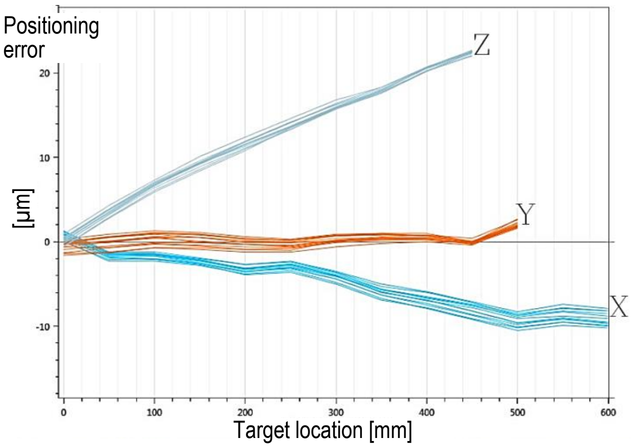

Fig. 17. Bidirectional positioning accuracy of the X, Y, Z axes of the DMU 635 ecoline 3-axis milling cutter versus measurement point position

On the basis of all obtained results, a comparison is made (Fig. 18) for average values of the highest positioning deviations: bidirectional positioning accuracy, average bidirectional positioning deviation and bidirectional positioning repeatability. As mentioned in the above paragraph, only the tolerances in the Z axis direction were exceeded, which is shown in the form of a bar graph (Fig. 18).

Regarding the Y axis, the lowest deviations were obtained for bidirectional positioning accuracy, mean bidirectional positioning deviation, and bidirectional positioning repeatability. Compared to the results obtained for the X axis, the bidirectional positioning accuracy and mean bidirectional positioning deviations are lower by 75%, and compared to the Z axis results – they are lower by as much as 94%. The bidirectional positioning repeatability deviations are similar for the three axes (X, Y, Z).

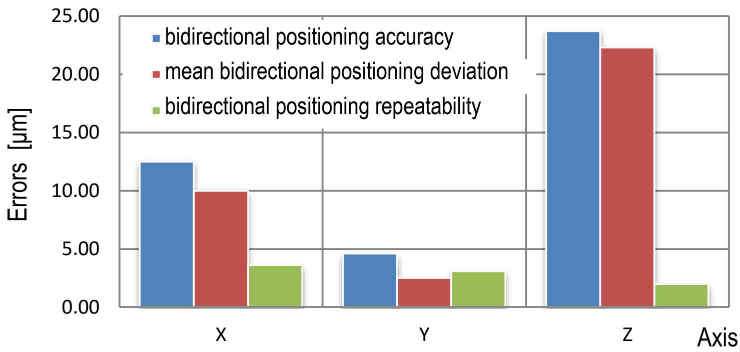

Fig. 18. Bidirectional positioning accuracy, mean bidirectional positioning deviation and bidirectional positioning repeatability

Tab. 8 lists error correction values which should be enetered in the DMU 635 eco milling machining centre in order to prevent the exceeding of tolerances in the Z axis. Table 8 was generated automatically by the XCal-View software on the basis of the results given in Fig. 17.

Tab. 8. Table of error compensation for Z axis

Indicator	Position [mm]	Correction [µm]
1	0	0
2	50	-3
3	100	-4
4	150	-2
5	200	-2
6	250	-3
7	300	-2
8	350	-2
9	400	-2
10	450	-2

The DMC 635 ecoline 3-axis vertical machining centre shows a high accuracy in the X and Y axes. The results for the X and Y axes show very high accuracy when compared to those listed in Tab. 3. The X axis shows a decreasing trend in positioning accuracy. The Z axis exceeds 5 out of 9 deviations included in the PN-ISO 10791-4:2001 standard, as marked by shadowed fields in Tab. 7.

Linear positioning accuracy and repeatability of the FV580A machining centre

The tests of linear positioning accuracy and repeatability were carried out for the FV580A machining centre as well. Tab. 9 shows results of all errors for the linear X axis. The results of bidirectional positioning accuracy A, bidirectional positioning repeatability R and axis returned value B for all axes (X, Y, Z) are shown graphically in Figs. 19–21. Fig. 19 gives the results of bidirectional positioning accuracy A, Fig. 20 presents the results of bidirectional positioning repeatability R, and Fig. 21 shows the results of axis returned value B. All the above quantities are shown as a function of feed rate for the numerically controlled axes of FV580A. During the positioning accuracy and repeatability measurements weather conditions were maintained stable within the range of permissible tolerance (Tab. 9). The greatest difficulty with interferometer measurements was to align the system to positioning measurement.

Tab. 9. Results of parameter measurements in X axis [11]

Machine: FV 580A Measurement system: LSP 30 Compact Laser interferometer from Lasertex		Axis X Number of measurement points: 6 Distance between the points: 80mm					
Tolerances		Feed rate v_f [mm/min]					
		50	500	2500	5000	10000	24000
Bidirectional positioning accuracy	A [mm]	0.0278	0.0248	0.0216	0.0232	0.0216	0.0212
Unidirectional positioning accuracy (forward/backward)	A↑ A↓ [mm]	0.0278 0.0268	0.0248 0.0224	0.0216 0.0193	0.0232 0.0188	0.0216 0.0195	0.0212 0.0179
Bidirectional positioning repeatability	R [mm]	0.0096	0.0094	0.0091	0.0090	0.0081	0.0086
Unidirectional positioning repeatability (forward/ backward)	R↑ R↓ [mm]	0.0057 0.0054	0.0032 0.0043	0.0034 0.0034	0.0029 0.0025	0.0039 0.0034	0.0026 0.0027
Axis returned value	B [mm]	0.0066	0.0068	0.0065	0.0068	0.0061	0.0064
Mean axis returned value	$\bar{B}$ [mm]	0.0038	0.0042	0.0039	0.0040	0.0037	0.0037
Air temperature	ºC	22.17	22.15	22.35	22.37	22.39	22.40
Surface temperature	ºC	22.28	22.25	22.53	22.56	22.57	22.58
Humidity	%	60	60	58	58	58	58
Pressure	hPa	993.2	993.3	992.6	992.6	992.6	992.6

The characteristics shown in Fig. 19 demonstrate that the Y axis parameters in the full velocity range are within a tolerance of 0.022mm (Tab. 5), whereas the parameters of the X axis are with the tolerance limit only for the following velocity values: 2500mm/min, 10000mm/min and 24000mm/min. The bidirectional positioning accuracy at the feed rate of 50mm/min exceeds the tolerance limit by 0.0058mm, at 500mm/min by 0.0028mm, and at 5000mm/min – the tolerance limit is exceeded by 0.0012mm.

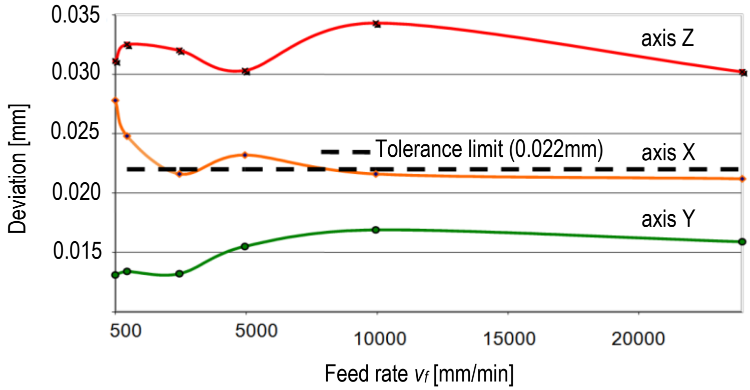

Fig. 19. Bidirectional positioning accuracy A of the X, Y and Z axes [11]

All parameters in the Z axis exceed their tolerance limits, respectively, for the velocity of 50mm/min by 0.0091mm, for 500mm/min by 0.0105mm, for 2500mm/min by 0.010mm, for 5000mm/min by 0.0083mm, for 10000mm/min by 0.0123mm and for 24000mm/min by 0.0082mm. The curve for the X axis in the initial phase differs significantly from the curves for the Y and Z axes that look similar.

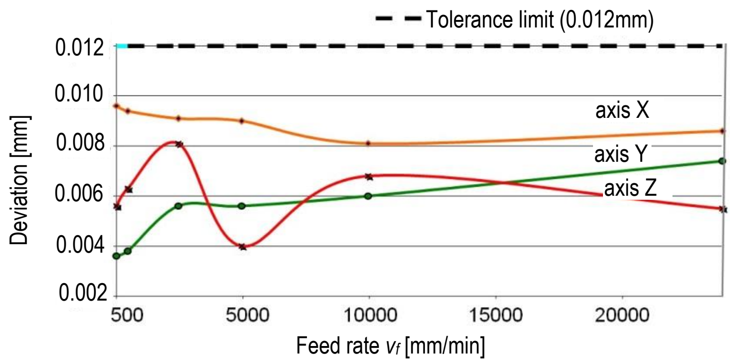

Fig. 20. Bidirectional positioning repeatability of the X, Y and Z axes [11]

As shown in Fig. 20, the results of bidirectional positioning repeatability *R* obtained for all axes do not exceed the permissible tolerance limit specified in the standard (0.012mm), irrespective of the applied feed rate. It can also be observed that the Z axis curve is strongly linear and significantly differs from other curves. It is characteristic of the Z axis curve that the variations in repeatability depend on the feed rate, especially in the operational range from 500mm/min to 10000mm/min. Fig. 21 shows variations in the axis returned value B for the X, Y and Z axes.

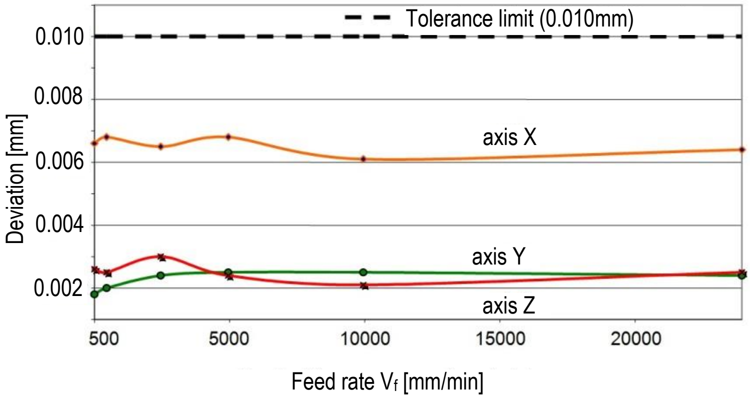

Fig. 21. Axis returned value B of the X, Y and Z axes [11]

The axis returned B value does not exceed the tolerance limit of any of the tested axes for all tested feed rates (Fig. 21). It was only observed that the axis returned value B of the X axis is significantly higher that obtained for the Z, Y axes. This may result from the considerable length of the X axis, the longest of the tested axes. The results demonstrate that the error values significantly change at low feed rates. It was observed that for the feed rates higher than 10000mm/min, the variations in error values are predictable (almost linear). As it turns out, the accuracy of the bidirectional positioning *R* primarily depends on the feed. In the Z axis for all the tested machine tools the positioning accuracy parameter values are the highest.

3.3. Angular positioning accuracy and repeatability assessment

Although linear axis accuracy is relatively easy to control and compensate for, rotary axes of machines may be effectively tested and their inaccuracies compensated for. This happens because of modern methods and diagnostics tools. Research methods related to rotary axis inaccuracy measurements in machining centres can be divided into two groups. One of them is the rotary axis positioning inaccuracy method. The second group contains axis rotation towards linear axis spatial orientation methods and determining real rotational axis together with the assessment of rotation centre positioning stability.

The most popular method of rotary axis positioning inaccuracy measurement is the use of a laser interferometer and rotary axis measurement attachment units. The authors of the works [38, 41, 44] used in their research diagnostic tools available on the market such as the XR-20 calibrator. The task of the interferometer attachment unit is to realise follow-up movements after the change of rotary axis angular positioning. The aim of the movement is to keep the laser beam in the angular measurement range. The measurement error is the difference between the set value and the realised value – real angular displacement of the tested machine axis, measured by the laser system. With this method it is possible to verify axis positioning accuracy, which is of key importance for the accuracy of the machined part. The works [25, 33–35, 42, 43, 48, 50, 52] used inner-machine tool diagnostic systems (inspection and object probes) as well as pins with model balls and specialist measurement macros (cycles) or automatic software. The methods are employed according to the ISO standards [138–140]. An analysis of the obtained errors also allows a verification of error sources (usually, a not-too-precise rotary angle transmitter or incorrect mounting [38]. The accuracy of the angular positioning interferometric method is ±0.5″ [14–16].

The assessment of the DMU 65 monoBLOCK milling centre technical condition

The measurement and analysis were performed using the dedicated software XCal-View 2.1. Obtained results are shown in tables and diagrams. The diagrams showing the measured deviations in a function of angle were generated by XCal-View 2.1, and their mean values in every repetition (three cycles) are shown in Figs. 22 and 23. Fig. 22 and Fig. 23 shows examples of graphic records of changes to the measurement values of unprocessed data, according to the ISO standards [131, 140].

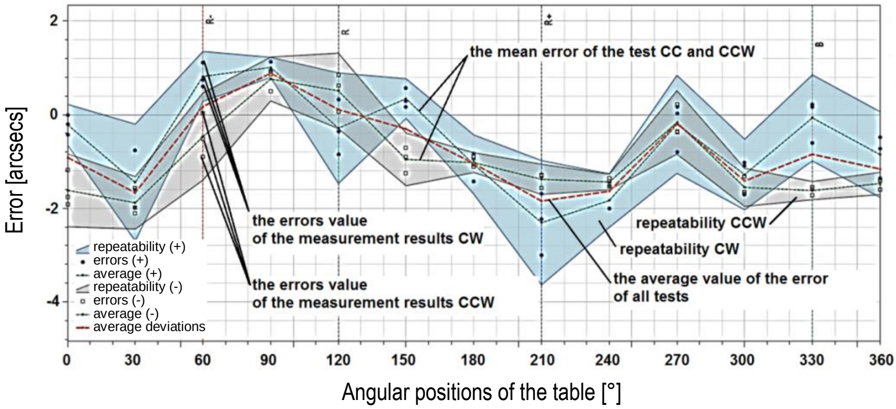

Fig. 22. Examples of the course of error value changes and angular positioning repeatability deviations

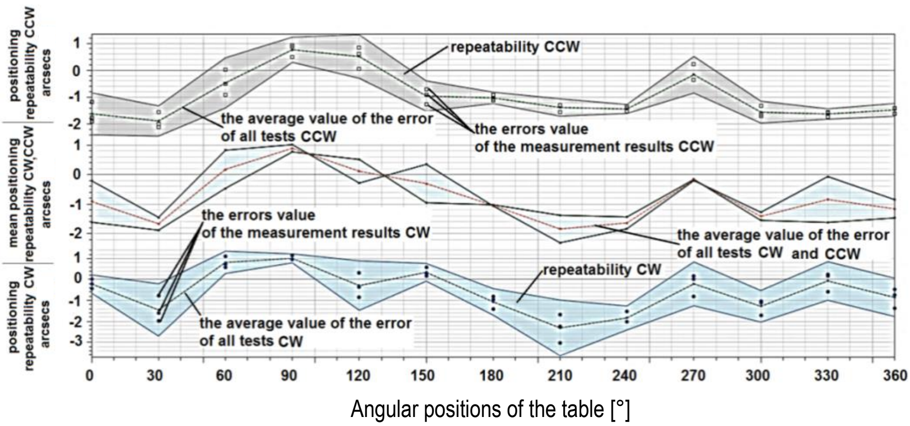

Fig. 23. Example values of errors and axis C angular positioning deviation with a specified rotation movement (CW, CCW)

Tab. 10 and 11 list detailed statistic data as well as the results for a triple table rotation of 360° in the direction of (CW) and (CCW). Tabs. 12 and 13 present selected errors observed during the measurement (Tests 1 and 2).

Tab. 10. Statistics of the results obtained from the accuracy and repeatability measurement of the C axis angular positioning (Test 1)

Statistics table – all errors in arc seconds																										
Target point number (i)	1		2		3		4		5		6		7		8		9		10		11		12		13	
Position (˚)	0		30		60		90		120		150		180		210		240		270		300		330		360	
Direction	-	+	-	+	-	+	-	+	-	+	-	+	-	+	-	+	-	+	-	+	-	+	-	+	-	+
Positioning deviation xij j=1	-1.2	0.0	-2.1	-0.8	0.0	0.7	0.9	1.1	0.8	0.3	-0.7	0.2	-1.1	-0.9	-0.3	-1.7	-1.4	-2.0	-0.4	-0.2	-1.7	-1.1	-15.0	0.2	-1.6	-0.5
j=2	-1.9	-0.2	-1.6	-2.0	-0.9	1.1	0.5	0.9	0.1	-0.4	-0.9	0.6	-1.1	-0.8	-1.3	-2.2	-1.5	-1.5	-0.4	0.0	-1.3	-1.0	-1.6	0.2	-1.0	-0.7
j=3	-1.8	-0.4	-2.0	-1.6	-0.5	0.6	0.9	0.9	0.6	-0.8	-1.3	0.3	-0.9	-1.4	-1.6	-3.0	-1.4	-2.0	0.2	-0.8	-1.7	-1.7	-1.7	-0.6	-1.4	-1.4
Mean directional deviation e	-1.6	-0.2	-1.9	-1.5	-0.5	0.8	0.8	1.0	0.5	-0.3	-1.0	0.3	-1.0	-1.1	-1.4	-2.3	-1.4	-1.8	-0.2	-0.2	-1.6	-1.3	-1.6	-0.1	-1.5	-0.9
Standard deviation si	0.4	0.2	0.3	0.6	0.5	0.3	0.2	0.1	0.4	0.6	0.3	0.2	0.1	0.3	0.2	0.7	0.1	0.3	0.3	0.5	0.2	0.4	0.1	0.5	0.1	0.5
2 x si	0.8	0.4	0.6	1.2	0.9	0.5	0.5	0.2	0.8	1.2	0.6	0.4	0.2	0.6	0.3	1.3	0.2	0.6	0.7	1.0	0.4	0.8	0.2	0.9	0.2	9.0
4 x si	1.6	0.9	1.1	2.5	1.9	1.1	0.9	0.4	1.6	2.4	1.1	0.8	0.4	1.3	0.6	2.7	0.3	1.1	1.4	2.1	0.8	1.5	0.4	1.8	0.5	1.8
Mean – 2si	-2.4	-0.6	-2.4	-2.7	-1.4	0.3	0.3	0.8	-0.3	-1.5	-1.5	-0.1	-1.2	-1.7	-1.7	-3.6	-1.6	-2.4	-0.8	-1.3	-2.0	-2.0	-1.8	-1.0	-1.7	-1.8
Mean + 2si	-0.8	0.2	-1.3	-0.2	0.5	1.4	1.2	1.2	1.3	0.9	-0.4	0.8	-0.8	-0.4	-1.1	-1.0	-1.3	-1.3	0.5	0.8	-1.1	-0.5	-1.4	0.9	-1.2	0.1
Returned value in the position reversal error Bi	1.4		0.4		1.3		0.2		-0.8		1.3		0.0		-0.9		-0.4		0.0		0.3		1.6		0.6	
Bidirectional positioning repeatability R	2.6		2.5		2.7		0.9		2.8		2.3		1.3		2.7		1.1		2.1		1.5		2.7		1.8	
Mean deviation	-0.9		-1.7		0.2		0.9		0.1		-0.3		-1.0		-1.8		1.6		-0.2		-1.4		-0.8		-1.2	

Tab. 11. Statistics of the results obtained from the accuracy and repeatability measurement of the C axis angular positioning (Test 2)

Statistics table – all errors in arc seconds																										
Target point number (i)	1		2		3		4		5		6		7		8		9		10		11		12		13	
Position (˚)	0		30		60		90		120		150		180		210		240		270		300		330		360	
Direction	-	+	-	+	-	+	-	+	-	+	-	+	-	+	-	+	-	+	-	+	-	+	-	+	-	+
Positioning deviation xij j=1	-1.4	0.0	-1.2	-0.6	-0.3	1.4	0.2	1.2	0.0	-1.2	-1.7	-0.4	-2.4	-1.5	-1.6	-2.2	-1.9	-1.9	-0.9	0.1	-1.1	-0.9	-1.9	0.4	-1.4	-0.8
j=2	-1.9	0.1	-1.2	-1.5	-0.1	0.4	0.3	0.2	-0.3	-1.5	-1.6	-0.8	-2.0	-1.7	-1.3	-2.5	-1.7	-2.3	-0.7	-0.7	-1.2	-1.2	-2.0	-0.4	-1.2	-0.7
j=3	-1.5	-0.5	-1.6	-1.2	-0.6	0.1	0.2	0.2	-0.5	-2.0	-2.3	-1.2	-1.9	-2.4	-1.9	-3.4	-1.9	-2.7	-0.8	-0.7	-1.4	-1.2	-2.1	-0.8	-1.3	-0.5
Mean directional deviation e	-1.6	-0.1	-1.3	-1.1	-0.3	0.6	0.3	0.5	-0.3	-1.6	-1.9	-0.8	-2.1	-1.9	-1.6	-2.7	-1.8	-2.3	-0.8	-0.4	-1.2	-1.1	-2.0	-0.3	-1.3	-0.6
Standard deviation si	0.3	0.3	0.2	0.5	0.2	0.7	0.0	0.5	0.3	0.4	0.4	0.4	0.3	0.4	0.3	0.6	0.1	0.4	0.1	0.5	0.2	0.2	0.1	0.6	0.1	0.1
2 x si	0.6	0.6	0.5	0.9	0.5	1.4	0.1	1.1	0.5	0.8	0.7	0.9	0.5	0.8	0.6	1.2	0.2	0.8	0.2	0.9	3.0	0.3	0.2	1.2	0.2	1.0
4 x si	1.2	1.3	0.9	1.8	1.0	2.8	0.2	2.2	1.1	1.6	1.5	1.8	1.1	1.7	1.2	2.4	0.3	1.7	0.4	1.8	0.6	0.7	0.4	2.4	0.4	0.3
Mean – 2si	-2.2	-0.8	-1.8	-2.1	-0.8	-0.8	0.2	-0.6	-0.8	-2.4	-2.6	-1.7	-2.6	-2.7	-2.2	-3.9	-2.0	-3.1	-1.0	-1.3	-1.5	-1.4	-2.2	-1.5	-1.5	-0.7
Mean + 2si	1.0	0.5	0.8	0.2	0.2	2.0	0.3	1.6	0.3	-0.7	-1.1	0.1	-1.6	-1.0	-1.0	-1.5	-1.7	-1.4	-0.6	0.5	-0.9	-0.7	-1.8	0.9	-1.1	-0.4
Returned value in the position reversal error Bi	1.5		0.2		0.9		0.3		-1.3		1.1		0.2		-1.1		-0.5		0.4		0.1		1.7		0.7	
Bidirectional positioning repeatability R	2.7		1.8		2.9		2.2		2.0		2.7		1.7		2.9		1.7		1.8		0.8		3.1		1.1	
Mean deviation	-0.9		-1.2		0.2		0.4		-0.9		-1.3		-2.0		-2.2		-2.1		-0.6		-1.1		-1.1		-0.9	

All the measurement results are presented in the form of a cyclometric function expressed in angular seconds *arcsecs*. The combined use of the XR20-W and a laser interferometer enables the arc measurement with an accuracy lower than ±1*arcsec* (equivalent to the displacement lower than 5μm on a 1m path).

Tab. 12. Analysis of the measurement results – an example (Test 1)					
Analysis functions					
Name	**(+) arcsecs**	**(-) arcsecs**	**(Bi-dir.) arcsecs**	**Name**	**Value (arcsecs)**
Accuracy (A)	5.0	3.8	5.0	Reversal (B)	1.6
Repeatability (R)	2.7	1.9	2.8	Mean reversal	0.4
Systematic deviation (E)	3.3	2.6	3.3	Mean deviation (M)	2.7

Tab. 13. Analysis of the measurement results – an example (Test 2)					
Analysis functions					
Name	**(+) arcsecs**	**(-) arcsecs**	**(Bi-dir.) arcsecs**	**Name**	**Value (arcsecs)**
Accuracy (A)	5.9	3.0	5.9	Reversal (B)	1.7
Repeatability (R)	2.8	1.5	3.1	Mean reversal	0.3
Systematic deviation (E)	3.3	2.4	3.3	Mean deviation (M)	2.5

Fig. 24 compares the C axis angular positioning accuracy and repeatability results obtained from all tests. As shown in Tabs. 13 and 14, the C axis angular positioning inaccuracy A ranges from 5 to 5.9*arcsecs* (a deviation of s=0.468*arcsec*). Other measured errors have even lower values. The rotary axis C positioning repeatability R and the systematic deviation E are, on the average, equal to 3*arcsecs*. The return error B ranges from 1.6 to 1.7*arcsecs* and the average return error is between 0.3 and 0.4*arcsecs*. The mean deviation M ranges from 2.5 to 2.7*arcsecs*.

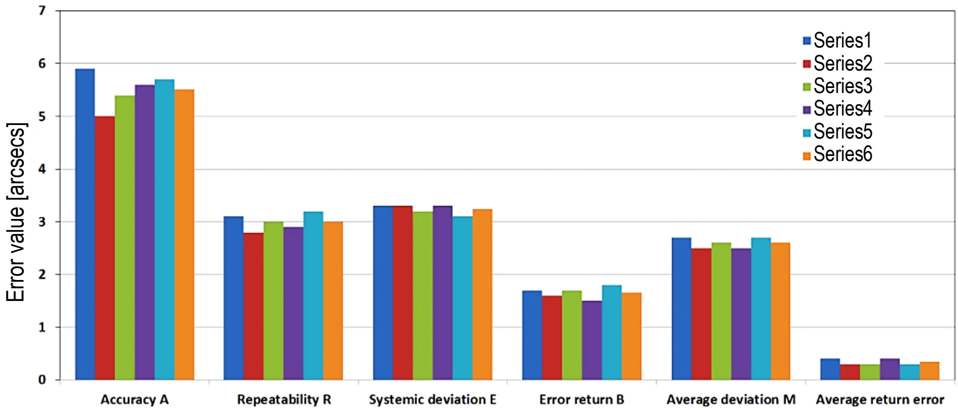

Fig. 24. Comparison of absolute errors and axis C positioning deviations in each measurement series

Fig. 25 shows results of the average positioning accuracy A obtained from all tests (6 trials) performed in the positive (CW) and negative (CCW) directions. They are presented as a function of the machine tool rotary table angle area of α=30°.

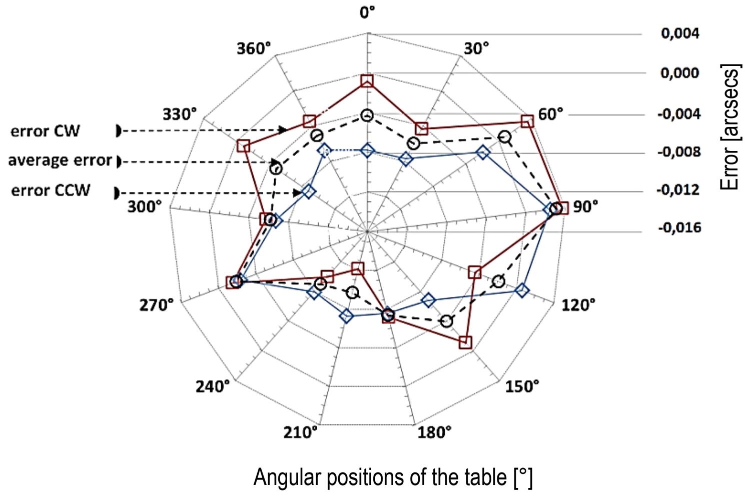

Fig. 25. Average positioning accuracy A in (CW) and (CCW) directions for DMU 65 monoBLOCK

Fig. 26 shows results of the unidirectional positioning deviation for feed motion in the positive (↑) and negative (↓) directions. The graph reveals that the deviation is the highest at 210° (negative value of the deviation is -0.022).

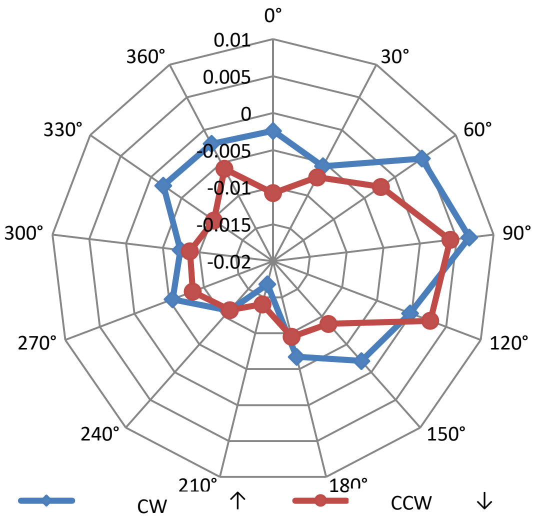

Fig. 26. Average unidirectional angular positioning deviations of the DMU 65 monoBLOCK

Fig. 27 shows a comparison of the average positioning accuracy and repeatability deviations obtained from all tests and repetitions in individual series.

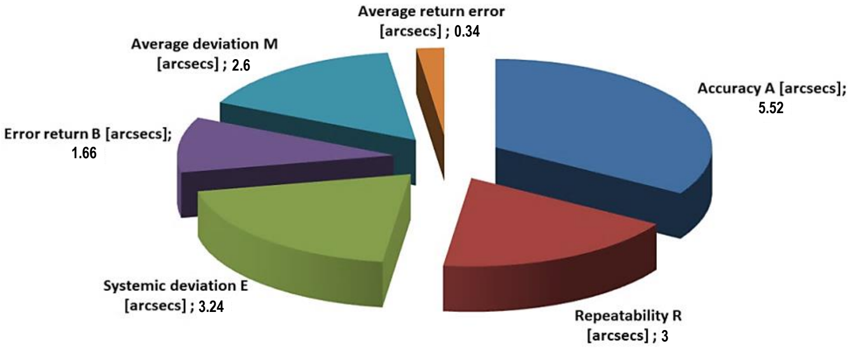

Fig. 27. Comparison of average positioning deviations obtained from the tests and repetitions in individual series

It can clearly be observed from Fig. 27 that the highest error values were reached by the positioning accuracy A, its average value being 5.52*arcsecs*. The average positioning repeatability R of the rotary axis C is equal to 3 *arcsecs*, and the average systematic deviation E is 3.24*arcsecs*. The average return error B is 1.66*arcsecs*, the average return value is 0.34*arcsecs* and the average value of mean deviation M is 2.6*arcsecs*.

Regular assessment of angular positioning accuracy and repeatability and other angular deviations of the tested machine tool axis enables the creation of a forecast model for testing machine tool geometric accuracy.

Assessment of the technical condition of CTX 310 eco lathe

Fig. 28 shows results of the average unidirectional positioning deviation for the feed motion from the positive (↑) and negative (↓) directions. The figure demonstrates that the deviation is the highest for at 240° (0.078*arcsecs*) and 100° (-0.070*arcsecs*).

The results demonstrate that the average axis C unidirectional positioning deviations of the lathe spindle $E\uparrow, E\downarrow$(for the feed motion from the positive (↑) and negative (↓) directions) reach very high values and thus exceed the permissible limit values specified in the ISO standard for this type of machines. The results clearly indicate an absolute need for compensation of the laser system registered errors, which can effectively increase the operating parameters of a given machine tool.

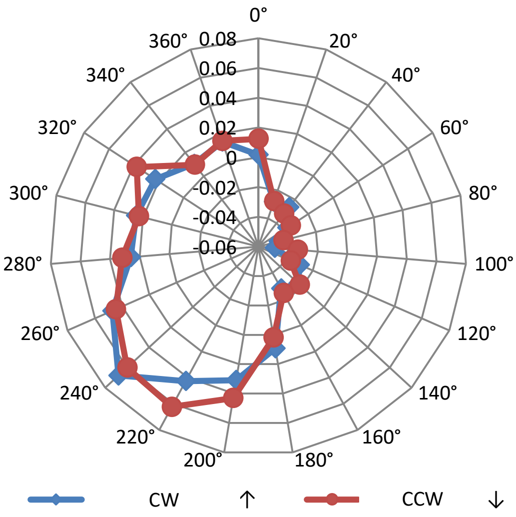

Fig. 28. Average angular positioning deviations $E\uparrow, E\downarrow$, of CTX 310 eco lathe

3.4. Summary and conclusions

Measurement and diagnostic methods for numerically controlled machines based on light wave interferometry nowadays play a leading role in CNC machine tool diagnostics. With non-contact measurements, it is possible to precisely determine both linear and angular position of machine tool movable parts while the use of laser system ensures a very high measurement accuracy. What is more, most of the modern CNC machine tools can compensate for linear and angular positioning errors of the axes. In effect, repeatable angular positioning errors can be compensated for. The prevention and minimisation of occurring errors lead to the improvement of machine technical condition, which has a direct impact on the quality of machining.

Based on all experimental results and their analysis, the following conclusions can be drawn:

1. Laser interferometer is presently the most accurate and universal measuring device used in CNC machine tool diagnostics. It enables the measurement of many geometric and kinematic parameters of the machine tool, thus allowing an effective compensation of identified errors.
2. The diagnostics of the linear axes of the tested lathes demonstrates that in most cases the accuracy and repeatability positioning errors and deviations as well as the axis returned value (A, A↑, A↓, R↑, R↓ and B) do not exceed the permissible tolerances specified in the standard. The permissible limit values were exceeded by the tested machining centres only in very few cases – especially in the Z axis, as shown in Figs. 17 and 19 and in Tab. 7.

3. The maximum values of linear positioning deviations for the DMC 635V ecoline machining centre were observed at extreme axis positions in all machine tool tests. To reduce the number of errors resulting from their local occurrence, it is recommended to use compensation or avoid machining in the workspace of the machine tool where the number of identified errors is higher.
4. For the analysed rotary C axis of the DMU65 monoBLOCK milling machine table, the maximum angular positioning deviations were achieved at the angular position of 210°. The angular positioning accuracy of the rotary axis is very high and remains at the average level of 6*arcsecs*. The angular positioning repeatability ranges from 1.5 to 3.1*arcsecs*. According to the ISO standards, the observed inaccuracies of the tested machine tool do not exceed the permissible values.
5. The deviations of angular positioning accuracy and repeatability obtained for the CTX eco lathe exceed the permissible values specified in the standard. As a result, the observed errors should be compensated or the lathe should be classified as suitable for producing parts with higher tolerances.
6. The results of angular positioning accuracy of this machine allow us to describe its technical condition as very good. The fact that the machine is not used for production but rather for didactic purposes and single production operations has an obvious impact on its condition.
7. The change of measurement axis during feed straightness testing (in all axes) requires the change of the laser optics. However, this solution is not very efficient and rather time-consuming. It requires multiple repetitions of all measurements (for each axis separately), while every change in laser position or optics requires the calibration of the whole system.
8. When selecting methods and measurement tools, the following factors should be taken into consideration: accuracy requirements for the machine tool, the cost of the machine, the time necessary for test completion, and the availability of the machine on the market. Regular and systematic diagnostic tests combined with potential adjustments (e.g., of control systems and drives) will ensure error minimisation and high accuracy of the machine tool.

The results obtained from the tests were collected in a database describing the service life history of the tested machine tool. They can be used to create forecast models of machine tool geometric accuracy. The creation of such models based on updated and recent information and their use in industrial practice will enable the implementation of proper planning of machine tool operation (maintenance) and the reduction and compensation of measured errors. This model will also serve as a classifier used for assigning a given machine tool to the production of parts of the required size and shape.

4. IDENTIFICATION OF ROTARY AXIS KINEMATIC CENTRE POSITION

The determination of machine tool errors usually requires long-term measurements and the use of many independent testing systems (for calibrating and inspecting machine tool condition or for performing static or dynamic measurements) [5–12]. It is worth noting that in terms of employed measuring instruments, most calibration data capture methods are static. Conventional diagnostic and calibration methods for five-axis machine tools, based on the use of an inspection measuring gauge of the machine tool and a calibration sphere (e.g. 3D quickSET or AxiSet™ Check-Up), only enable the static measurement in discrete positions defined in the machine measurement cycle [48]. Static measurement does not take into consideration the dynamics of the machine tool which is a complex, dynamic and mass-dissipative-elastic system [9, 10, 43, 48, 52]. Calibration is performed by entering into the machine tool control system (table of machine tool kinematics) values obtained from measurements, on the basis of which an algorithm in the control system measures the corrected set position by adding an adjustment to the nominal value of the position [50, 52]. One of the diagnostic systems dedicated to both static and dynamic measurements is R-Test measurement system (by IBS Precision Engineering). The most important metrological features and advantages of the R-test system include: 3D measurement of 5-axis machine tools, the possibility to run statistic measurements, the possibility to perform dynamic measurements, positioning measurement in three axes simultaneously, calibration of the rotary table position, axis straightness error measurement, calibration of the rotary table straightness, compensation by kinematic parameters, machine assessment according to ISO 10791-6, the possibility to perform FFT analysis, and user-friendliness [23–25, 32–35, 43, 48, 50, 52, 92, 104, 121].

4.1. Rotary axis kinematic centre positioning error

CNC machine tool diagnostics is one of the basic processes in the operation of these machines. It occurs in the course of machine use and during the whole period of its operation. The diagnostic and calibration systems for CNC machine tools make it possible to determine key static and dynamic parameters, control of their operational reliability and, at the same time, maintain their full performance capacity. The problem of static and dynamic assessment of CNC machine tool errors is widely discussed in the works [23–25, 32-35, 43, 48, 50, 52, 92, 104, 121]. Every numerically controlled machine tool is burdened with geometric and kinematic errors as well as errors resulting from thermal actions [13, 17, 53, 58, 89, 90, 91, 95, 118, 119, 125, 129]. Due to these errors, effective and highly accurate machining of parts is more difficult to ensure. The idea of compensating CNC machine tool spatial positioning errors in the aspect of machine geometric inaccuracy is presented in the works [22, 41, 72–75]. The errors cannot be fully eliminated, but they can considerably be reduced and their effects minimised. This is possible thanks to diagnostic measurements which enable error identification, calibration and compensation, as well as other equipment and software-related actions. The diagnostics is, therefore, a very important process affecting the machine's capacity to produce parts of high size and shape accuracy. Diagnostic and calibration systems of numerically controlled CNC machine tools enable the determination of key machine tool parameters and, at the same time, the control of the production process [70, 97, 111]. This, in effect, leads to reduced risk of production shortages and losses resulting from grave errors in machining and classification of machine tools with respect to their kinematic and geometric accuracy [51]. This assessment enables the schedule of works performed on machine tools. Every operated machine tool is burdened with many errors of a different nature (geometric, kinematic, thermal) [7, 26, 66, 68]. The assessment of machine tool errors is a relatively difficult task, given their occurrence in a 3D space. In fact, we deal here with volumetric error [65, 75]. This error requires the compensation of tool path relative to the workpiece due to machine geometric inaccuracies, which is of particular importance in multi-axis CNC machining [116].

Methodology and the diagnostic test

The work illustrates a diagnostic methodology for a five-axis vertical machining centre. DMG's numerically controlled machine tool DMU 65 MonoBlock equipped with a numerically controlled shape system from Siemens, Sinumeric 840 SL MD, was selected as the object of the research (Fig. 29).

The tests were performed with the use of a diagnostic and calibration measurement system (Fig. 29) consisting of the MT-Probe measuring head, the MT-Interface unit (MTI-0010), R-Test software (MTS-003) for recording measurement results, a 22 mm diameter master ball attached to a 75 mm pin (ball circularity error is lower than 0.5μm), aligning equipment and a magnetic mounting base. The MT-Probe measuring head is provided with 3 eddy current sensors (Fig. 29c) with a measuring range of 1mm and a resolution of 0.1μm. The extended uncertainty of the probe measurement is U1=0.6μm, if k=2. The probe sampling frequency is maintained constant at 6.5kHz. The head operation requires the use of the MT-Interface unit (MTI-0010), R-Test software (MTS-003) for recording measurement results, a master ball, an aligning device and a magnetic mounting base.

Tab. 14 gives the metrological specification of the T-Probe measurement head during the tests. The MT-Probe measurement head was attached at the spindle end, as shown in Fig. 29b (frame with a BT40 cone). The MT-Probe of the R-Test enables the measurement of position of the master calibration sphere centre attached at the pin in the magnetic mounting base. The calibration sphere and the base were mounted to the machine rotary table (Fig. 29b). During the measurements with the R-Test system, the 3D measurement head was in constant contact with the calibration sphere (Fig. 29d). Fig. 29d also shows that the eddy current sensors are positioned every 120° in relation to each other (view from the top) while in relation to the vertical head axis they are tilted at an angle of 45° (Fig. 29e).

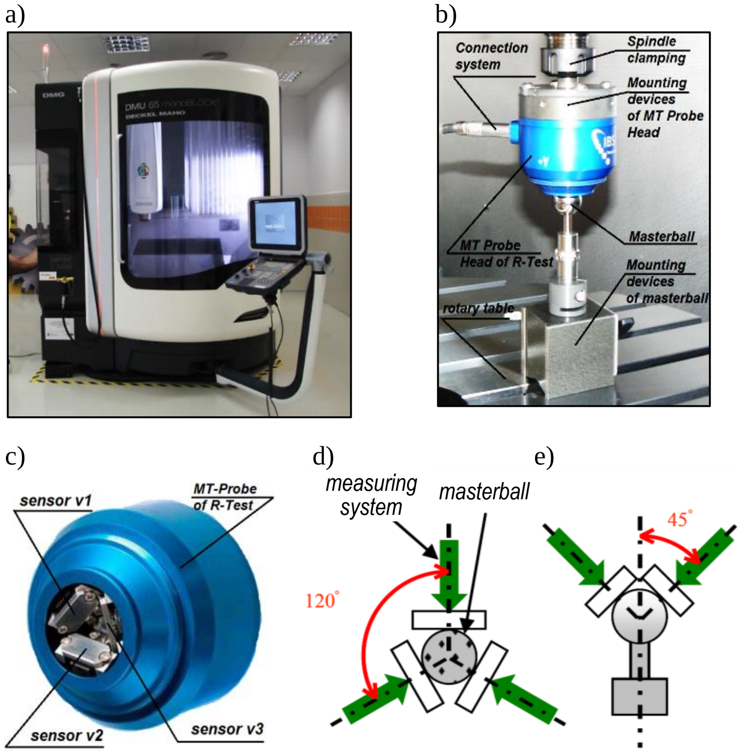

Fig. 29. Test stand: a) vertical 5-axis machining centre DMU 65 MonoBlock by DMG, b) R-Test measurement system attached to the machine tool, c) MT-Probe head and sensors, d) position of head sensors relative to each other in horizontal plane, e) schematic design of head sensors in vertical plane

For the tested machine tool with an integrated rotary tilting table, the linear and rotary axis errors interact. Fig. 30 shows positioning errors of the rotary C axis kinematic centre. The displacement of the kinematic centre of the rotary C axis (Fig. 30) is described as XOC, YOC, ZOC, and the rotation angles of individual numerically controlled axes are denoted as AOC, BOC, COC, where X, Y, Z are the numerically controlled linear axes in the initial position, A, B, C are the rotary axes, and C’ is a new position of the rotary C axis. During the static and dynamic measurements the rotary axis was located relative to the linear axes. The measurements were made in the XY plane of the CNC machine, with the constant axis position Z=const. During the dynamic measurements, the movement was performed in a constant way on three numerically controlled axes simultaneously (on two linear axes X, Y and on the rotary C axis of the machine table).

Tab. 14. Metrological specifications of the 3D MT-Probe system

3D MT-Probe measuring range	1mm
3D MT-Probe resolution	0.1μm
3D MT-Probe sampling rate	6.5kHz
3D MT-Probe measurement uncertainty	U1 = 0.6μm (k = 2)
Measuring head shaft (mounting) diameter	D = 16mm
3D MT-Probe dimensions	length: 56mm; diameter: 75mm; weight: 375grams

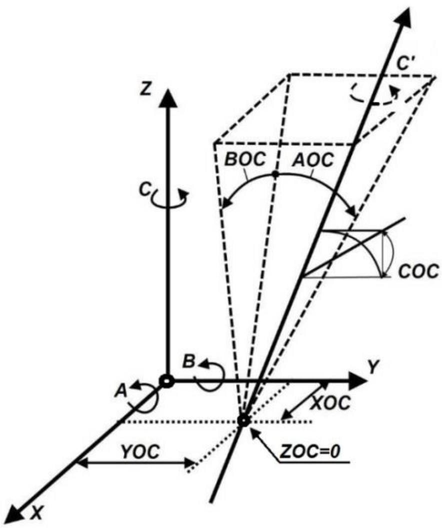

Fig. 30. Displacement of the rotary axis kinematic centre, where: X, Y, Z – numerically controlled linear axes and their initial position, A, B, C – rotary axes in their initial position, XOC, YOC, ZOC – rotary C axis kinematic centre displacement, AOC, BOC, COC – rotation angles of individual numerically controlled axes, C' – new position of the rotary C axis

During the static measurements, the motion was interrupted for approximately 4seconds after each step of a discrete angle value α (e.g. 30°) and the measurement was taken in the point. The MT-Probe measurement head of the R-Test system measures the actual 3D spatial position at the same time. The position of the calibration sphere is precisely specified in the space of the X, Y, Z coordinates. The differences between these displacements are considered to be inaccuracy positioning errors. The errors resulting from the machine kinematics as an effect of deviations during measurements are determined using specialist data acquisition software and then with the use of software for data analysis according to a specified algorithm. The applied R-Test software analyses measurement data and enables the determination of rotary axis kinematic centre position, rotary axis straightness error, FFT analysis in the direction of X, Y and Z axes, and provides a wide range of ways to present the results of measurements and analyses (linear and polar characteristics, axis and longitudinal displacements). Above all, the measurement results may be compared and compiled in one diagram (static and dynamic alike).

During the dynamic measurement, the rotary C axis of the machine tool was activated, whereas the linear axes followed its movement. The system communicated with the computer via USB 2.0. The measurement head for measuring the actual position of the sphere central point was attached to the CNC machine tool spindle and maintained stationary during the test, i.e., it did not perform rotational motion. Obtained results were shown on the screen via the dedicated software. The sampling frequency in the dynamic measurement was 6.5kHz. As a result, the measurement could be made on-line and the effect of the feed rate v_f on the accuracy of obtained results could be determined. This effect can be significant during tests. The dynamic measurements were made for the following values of feed rate v_f: 250mm/min, 800mm/min, 2500mm/min, 4000mm/min.

Based on the results, it was possible to determine the rotary C axis kinematic node centre displacements (offset errors) and straightness deviations (errors) of the axis.

Static measurement of the C axis

Static measurement of the rotary axis kinematic centre positioning error of a 5-axis CNC machine tool using the R-test system

The aim of the static measurement was to identify rotary axis kinematic node centre positioning errors (Fig. 31) for the 5-axis machine tool of a discreet angular positioning of the machine rotary table C_i, shown in Fig. 31a.

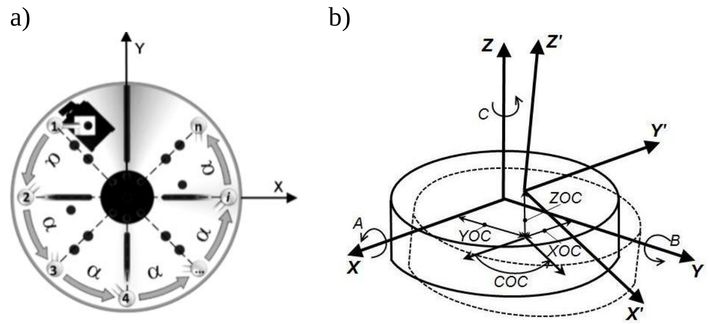

Fig. 31. Angular positioning of the machine tool table in static measurement (a) and a graphic interpretation of the measured errors (b); where 1, 2,..., i, i=12 – subsequent angular positions of the table during static measurement $i \cdot \alpha = C_i$ where α=30°), X, Y, Z, A, B, C – numerically controlled axes, XOC, YOC, ZOC – rotary axis kinematic centre positioning errors, AOC, BOC, COC – turning deviations of individual axes (axis straightness errors)

Tab. 15. Test conditions in static measurement

Angular discretisation of table rotation α, [°]	30°
Measurement time, t [s]	2s
Plane of table rotation	X–Y
Measurement errors	XOC, YOC, AOC, BOC
Number of tests series	5
Number of test repetitions	5

The following errors were measured: rotary axis kinematic centre position deviations in the X-Y plane (XOC, YOC) and squareness errors of individual axes (AOC, BOC) described in the X-Z and Y-Z planes, respectively. XOC stands for the C axis position error in X-direction, while YOC is the C axis error in Y-direction. AOC is the C axis straightness error in X-direction and BOC is the C axis straightness error in Y-direction. Two series of tests with 5 repetitions were performed. Each of the series provided data that enabled the assessment of repeatability. The estimates in the form of average error values and calibration sphere centre position deviations obtained from the static measurement in discrete positions were determined. The results are listed in Tab. 16 and shown in the figures. Fig. 32 shows the interface of the programme and the results of static measurements taken during table angular positioning.

Fig. 32 shows the programme interface as well as the results of static measurements performed during table angular positioning.

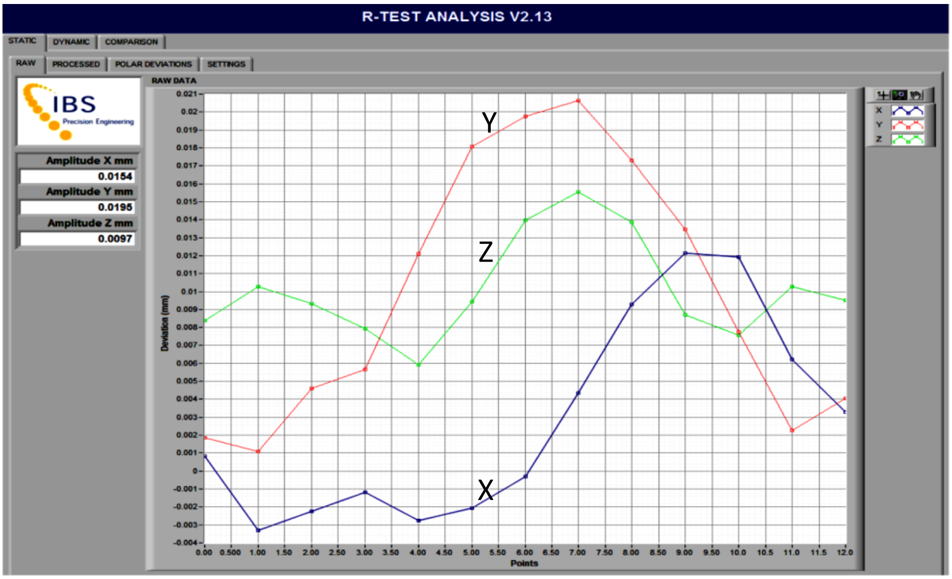

Fig. 32. Displacements of the calibration sphere centre point during discrete rotational motion in relation to the C axis, in relation to the measurement head sensors, during static measurement; abscissa points from 0 to 12 denote angular positions of the machine tool table C_i relative to the Z axis

Fig. 32 shows displacements of the centre point of the master ball in the course of a discrete rotational motion C in Z-direction versus measurement head sensors (static measurement). The curves marked in colour describe the numerically controlled machine tool axes X, Y, Z. Observed deviations are marked on the axis of ordinates and successive angular positions C_i of the machine tool table relative to the linear Z axis are marked with points from 0 to 12 on the abscissa. Angular points (i) are assigned angular positions according to i=0→ C_i=0°, i=1→ C_1=30°, i=2→ C_2=60°,…, i=12→ C_{12}=360°. The above-mentioned discretisation can be formulated with the following equation: C_i=i·30°, where i=1, 2, 3,….,12, and C_i is an angular position of the rotary table (expressed in angular degrees) in which the measurement was taken (Tab. 16).

Tab. 16. Discretisation of angular point positions in static R-test

	I												
	0	1	2	3	4	5	6	7	8	9	10	11	12
C_i	0°	30°	60°	90°	120°	150°	180°	210°	240°	270°	300°	330°	360°

Fig. 32 demonstrates that the displacements of the calibration sphere centre point (amplitudes in the full test range 0÷360°) are very low. The deviation in X-direction (amplitude, maximum displacement) is 15.4μm, in Y-direction – 19.5μm, and in Z-direction – 9.5μm. The low values of real deviations indicate high kinematic and geometric accuracy of the machine. The same measurement data were used to create a pie chart for the XY plane, as well as for the XZ and YZ planes. Obtained results are shown in the diagrams in Fig. 33. It can be observed that the rotary C axis kinematic centre position error in X-direction is XOC=3.8μm and in Y-direction – YOC=11.1μm. These values are most frequently used to change controller settings (offset error) and are considered essential for increasing positioning accuracy, and hence manufacturing accuracy. At the same time, the performed measurements and their analysis indicate that the C axis straightness error (linear Z axis) in relation to the A axis (linear X axis) is AOC=4.2μm while in relation to the B axis (linear Y axis) – BOC=1.1μm. Axis straightness error is determined by the method of least squares on the basis of data obtained from the measurements. The fitting of the line to the measurement results in the ZY plane is shown in the upper left-hand graph in Fig. 33, whereas that in the ZX plane in shown by the graph on the right (Fig. 33). For a perfect machine tool, values of XOC, YOC, AOC, BOC should be equal to zero (XOC=0μm, YOC=0μm, AOC=0μm, BOC=0μm).

The results indicate a small displacement of the rotary C axis kinematic centre of the tested CNC machine tool. To estimate repeatability, measurements were performed in two measurement series. The measurement results obtained from the two test series are listed in Tab. 17. The yellow-colour fields denote the highest displacement of the calibration sphere centre position as a function of rotation angle.

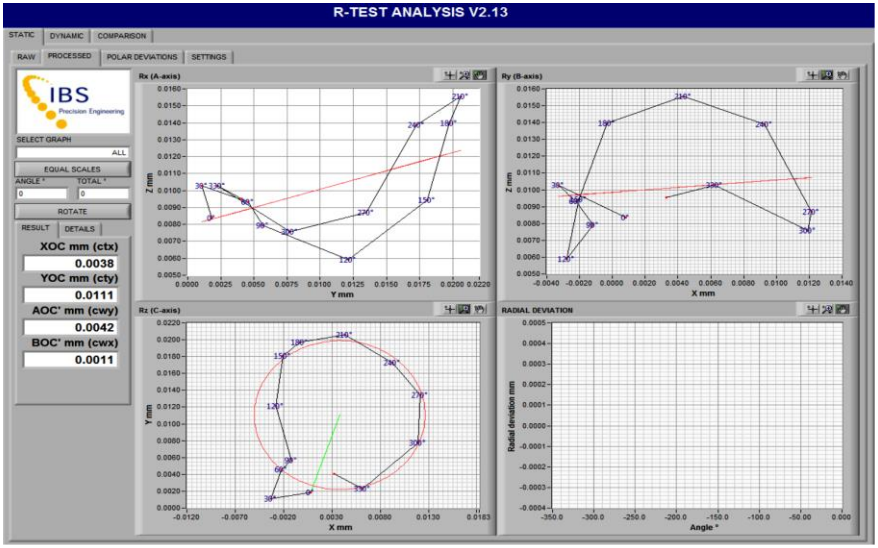

Fig. 33. Graphic presentation of static measurement results: fitting of the straight line determined by the least squares to the measurement data in the ZY (upper left-hand graph) and ZX (upper right-hand graph) planes; results shown against the perfect circle

Tab. 17. Static measurement results of calibration sphere position deviations as a function of machine tool table rotation angle n·α, determined with R-Test ; α=30°, n=1, 2 …12

	Average value, series 1	Average value, series 2	Average value, series 1	Average value, series 2	Average value, series 1	Average value, series 2
α	Axis **X** [mm]		Axis **Y** [mm]		Axis **Z** [mm]	
0°	0.0008	0.0026	0.0018	0.0015	0.0084	0.0079
30°	-0.0033	-0.0013	0.0011	0.0041	0.0103	0.0083
60°	-0.0022	-0.0010	0.0046	0.0069	0.0093	0.0077
90°	-0.0012	-0.0014	0.0057	0.0073	0.0079	0.0072
120°	-0.0028	-0.0031	0.0121	0.0103	0.0059	0.0081
150°	-0.0021	-0.0002	0.0181	0.0178	0.0094	0.0085
180°	-0.0003	0.0024	0.0197	**0.0211**	0.0140	0.0103
210°	0.0043	0.0054	**0.0206**	0.0199	**0.0156**	**0.0118**
240°	0.0093	0.0109	0.0173	0.0169	0.0139	0.0098
270°	**0.0121**	**0.0149**	0.0134	0.0123	0.0087	0.0043
300°	0.0119	0.0143	0.0077	0.0061	0.0076	0.0040
330°	0.0062	0.0097	0.0023	0.0034	0.0103	0.0042
360°	0.0033	0.0040	0.0041	0.0025	0.0095	0.0066

Fig. 34 shows the characteristics of calibration sphere centre position deviation relative to the test probe sensors as a function of table rotation angle of the C axis. The highest displacement in individual numerically controlled axes was identified as the amplitude value in the respective axes X, Y, Z. Average amplitude values from two measurement series presented in Fig. 34 show a high repeatability of the calibration sphere centre point deviations.

a) b)

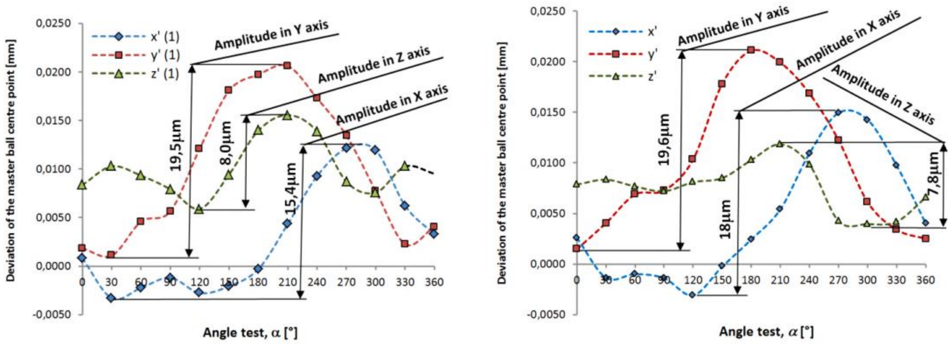

Fig. 34. Average values of the master ball centre point deviation as a function of machine tool table rotation angle: a) average value of the sphere centre position deviation in the X, Y, Z axes obtained from the first test series, b) average value of the sphere centre position deviation in the X, Y, Z axes obtained from the second test series

The highest amplitude values of the calibration sphere centre displacement relative to the 3D MT-Probe measurement head sensors were observed in the Y axis, in the first and second test series alike. The value of calibration sphere centre displacement amplitude is repeatable and remains within the range of 19.5–19.6μm (Fig. 34). In the X axis, the displacement of calibration sphere centre in relation to the 3D MT-Probe measurement head sensors is within the range of 15.4–18.0μm, whereas in the Z axis it ranges from 7.8–8.0μm. The values should be considered highly repetitive and accurate.

The results demonstrate that the displacement of the calibration sphere centre point in the Z-direction is 8μm for the first test series and 7.8μm for the second test series, respectively. It should be stressed that in the case of an ideal machine tool these values should be equal to zero; if different from zero, they indicate displacement of the table in the bearings in the Z-direction during rotation. The displacements affect the position of the rotary axis kinematic centre. The highest calibration sphere centre position deviation was observed in the Y-direction (Tab. 17). The maximum value of position change (deviation) was 20.6μm for the rotation angle of α=210° (test series 1) and 21.1μm at α=180° (test series 2). The X and Z axes have definitely lower deviation values, even by 75% for some values of the rotation angle α. In the X-direction, the maximum displacement of the calibration sphere centre was 12.1μm (test series 1) and 14.9μm (test series 2), respectively (Tab. 17). The maximum calibration sphere centre point displacement values obtained for the Z axis are similar to those obtained in the X direction. These values are 15.6μm (test series 1) and 11.8μm (test series 2), respectively (Tab. 17). A comparative analysis of the maximum values reveals that for the X and Z axes (for α angles of 180÷270°) the average maximum deviation values are 50% lower than those obtained for the Y axis.

Figs. 35÷37 show values of real deviations in the horizontal X-Y plane of the two test series (for the tested angle values) and the straightness errors of the X-Z and Y-Z axes. The values of obtained deviations were approximated with the equation of the straight line determined by the method of least squares (Figs. 36 and 37). Equations 23 and 24 are mathematical models of axis straightness error obtained from the test series 1 and 2.

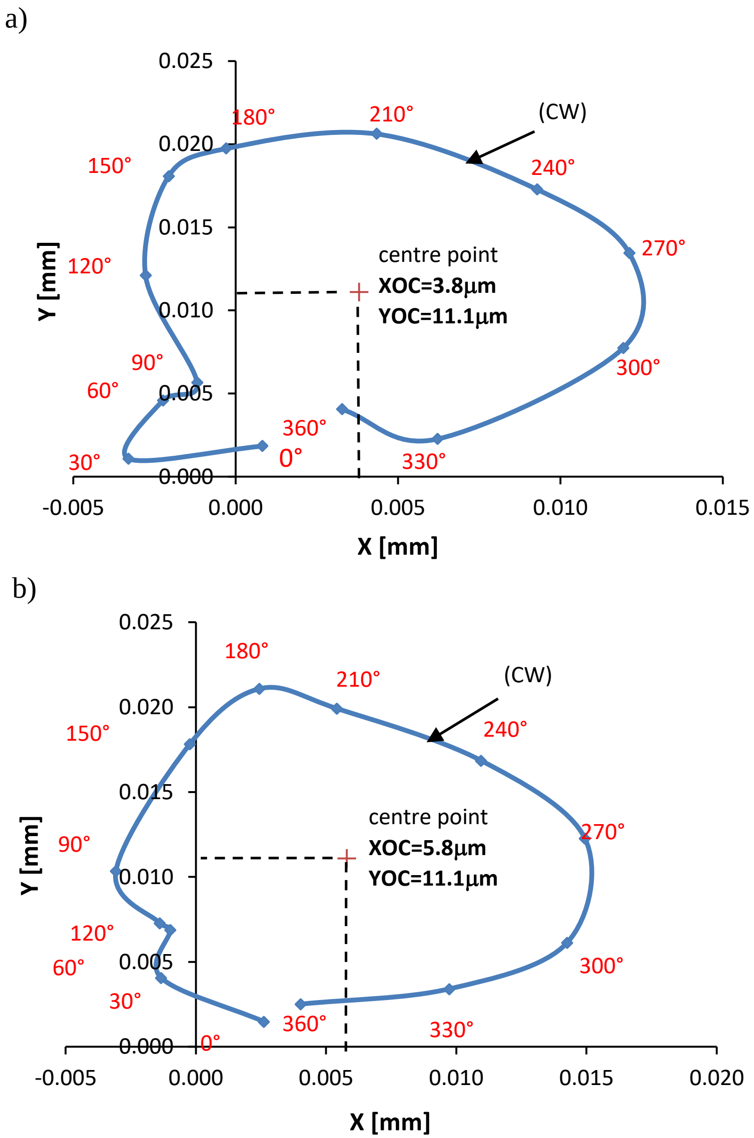

Fig. 35. Average real deviations in the horizontal plane for the tested rotation angles (0°÷360°): a) from the first measurement series, b) from the second measurement series

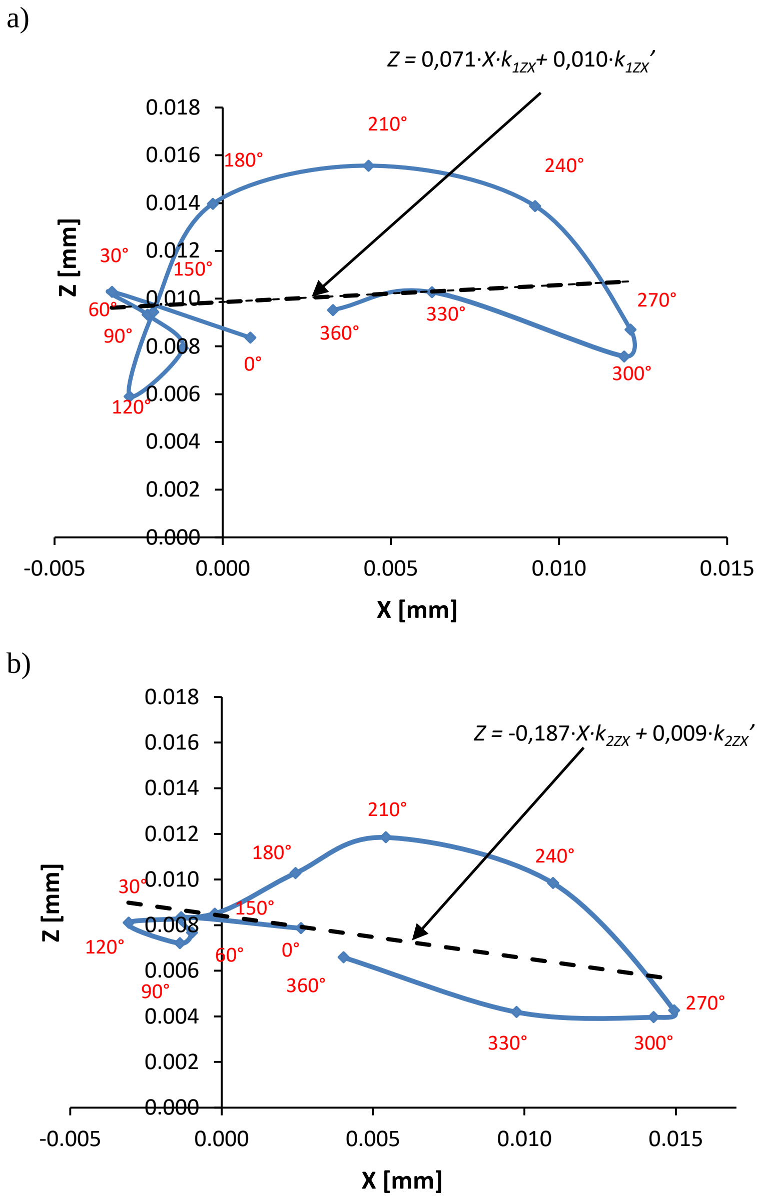

Fig. 36. Average axis squareness error in the vertical Z-X plane for tested rotation angles (0°÷360°): a) from the first measurement series, b) from the second measurement series

The straight line equation approximating the measurement results in the Z-X plane for the first measurement series (Fig. 36a) is expressed by Equation (23):

$$Z = 0.071 \cdot X \cdot k_{1ZX} + 0.010 \cdot k_{1ZX}' \tag{23}$$

where:
X – master ball centre position error in the X-direction [*mm*], k_{1ZX} – unit factor of X (k_{1ZX} =1mm/mm), k_{1ZX}' – unit factor of the expression free term (k_{1ZX}'=1mm).

Equation (24) describes master ball centre position deviations in the Z-X plane for the second measurement series (Fig. 36).

$$Z = -0.187 \cdot X \cdot k_{2ZX} + 0.009 \cdot k_{2ZX}' \tag{24}$$

where:
X – master ball centre position error in the X-direction [*mm*], k_{2ZX} – unit factor of X (k_{2ZX} =1mm/mm), k_{2ZX}' – unit factor of the expression free term (k_{2ZX}'=1mm).

Fig. 37 presents an approximation of the results of measurements in the horizontal plane Z-Y for the two measurement series.

For the measurement in the Z-Y plane, a straight line equation describing the observed results (Fig. 37a) is presented by Equation (25):

$$Z = 0.217 \cdot Y \cdot k_{1ZY} + 0.008 \cdot k_{1ZY}' \tag{25}$$

where:
Y – value of the calibrating sphere centre positioning error in the direction of the Y axis [mm], k_{1ZY} – variable unit factor Y (k_{1ZY} =1mm/mm), k_{1ZY}' – free equation unit factor (k_{1ZY}'=1mm).

Whereas for the second measurement (Fig. 37b) the equation approximating the results of the experimental measurement is described by the following equation (26):

$$Z = 0.218 \cdot Y \cdot k_{2ZY} + 0.005 \cdot k_{2ZY}' \tag{26}$$

where:
Y – value of the calibration sphere centre positioning error in the direction of the Y axis [mm], k_{2ZY} – variable unit factor Y (k_{2ZY}=1mm/mm), k_{2ZY}' – free equation unit factor (k_{2ZY}'=1mm).

The error values of the rotary axis kinematic node allocation were defied according to the algorithm implemented in the structure of the programme for the analysis of the measurement data. Tab. 18 presents the results of the calculations by R-Test Analysis V.2.13.

a)

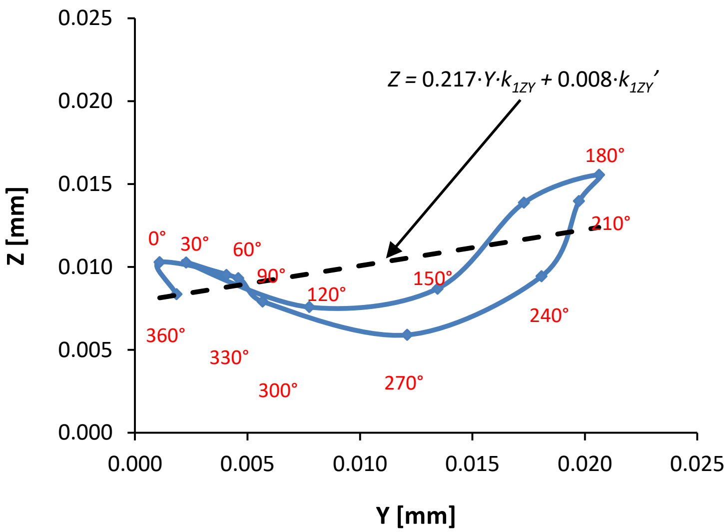

b)

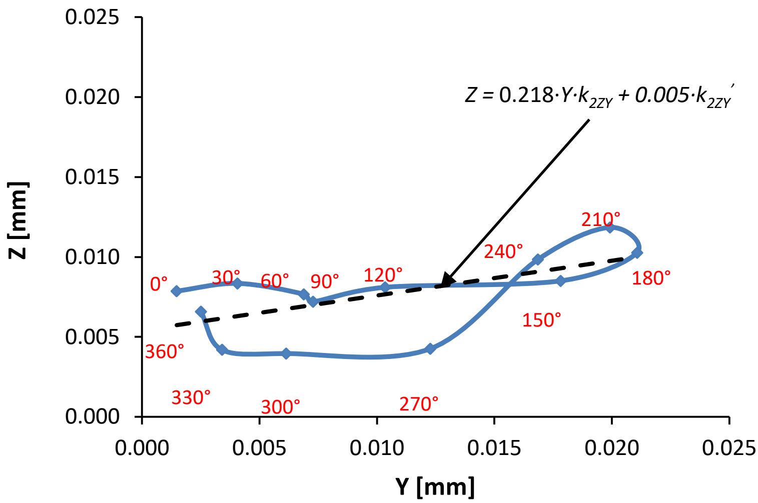

Fig. 37. Average value of axis squareness error in the vertical Z-Y plane for rotation angles (0÷360°): a) from the first measurement series, b) from the second measurement series

With the R-Test measurement system, the accuracy of 5-axis machine tools is determined with a high degree of accuracy. Measurement data from the two series are shown as polar plots (Fig. 35, i.e., this implies a coordinate transformation: the deviations are plotted in (rotating) workpiece coordinates instead of the machine's X, Y and Z coordinates). This static measurement can be executed in a manual or automatic capture mode. The static measurement results point to the following offset errors of the machine tool axis: XOC=3.8μm and YOC=11.1μm for the first measurement series and XOC=5.8μm, YOC=14.1μm for the second measurement series. This results indicate the machine tool axis errors: AOC=4.2μm, BOC=11.1μm for the first measurement series and AOC=6.8μm, BOC=15.2μm for the first measurement series. The errors in the machine's kinematic model present in the controller result in deviations calculated by the software module: allocation errors of the rotary axis and squareness errors of the rotary axis. By adjusting the machine's controller with these values, the machine's position is improved significantly in a short period of time. It is very important in manufacturing processes, especially after the collision and relocation of the CNC machine tool.

Tab. 18. Values of position and squareness errors

Name of error	Symbol of error	Error values [μm]	Nature of measurement
for 1st measurement series			
The error of the C-axis location in X	XOC	3.8	static measurement
The error of the C-axis location in Y	YOC	11.1	static measurement
The squareness error AOC of the C-axis	AOC	4.2	static measurement
The squareness error BOC of the C-axis	BOC	11.1	static measurement
for 2nd measurement series			
The error of the C-axis location in X	XOC	5.8	static measurement
The error of the C-axis location in Y	YOC	14.1	static measurement
The squareness error AOC of the C-axis	AOC	6.8	static measurement
The squareness error BOC of the C-axis	BOC	15.2	static measurement

The data listed in Tab. 18 allow a calibration of the rotary axis by entering the measured errors into the kinematics table in the machine tool control system. The diagnostics and calibration of the rotary axis enable the effective minimisation of machining errors in finished parts and, above all, the improvement of machine tool geometric accuracy. This task is extremely important in relation to the accuracy of simultaneous machining of geometrically complex objects on CNC machine tools. On the basis of the data, the control algorithm determines correct position of the preset target points resulting from the system control programme during realization of a specified path during machining. The use of estimated values during the calibration of the tested DMU65MonoBlock machine tool allows us to improve its geometric accuracy via quick correction of the rotary axis kinematic centre position errors and axis squareness errors.

Dynamic measurement of the C axis

Dynamic measurements were performed for various values of the feed rate v_f (250mm/min, 800mm/min, 2500mm/min, 4000mm/min). Measurement results were recorded during continuous rotational motion recorded with the measurement head sensors. Fig. 38 shows the centre point displacements of the calibration sphere performing continuous rotation C in the Z-direction relative to the measurement head sensors (dynamic measurement).

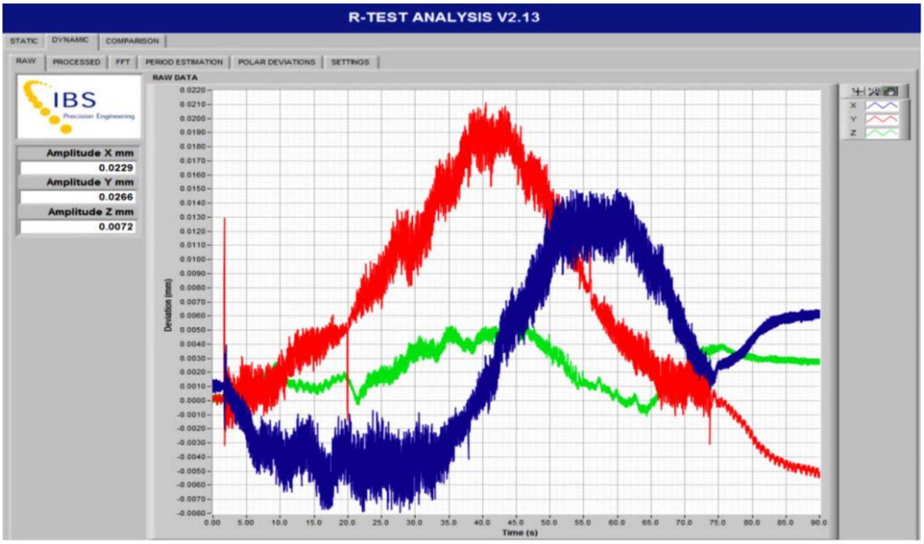

Fig. 38. Displacements of the centre point of the calibration sphere which performs constant rotation movement C in relation to the Z axis towards the measurement head sensors (dynamic measurement)

Fig. 39 shows selected dynamic measurement results. The fitting of the straight line (marked in red) determined by the method of least squares to the measurement data in the ZY plane is shown in the left-hand upper graph, whereas that in the ZX plane is shown in the right-hand upper graph in Fig. 39. The pie chart in Fig. 39 shows the results against the perfect circle in the XY plane.

Based on the results presented in Fig. 39 one can observe that the rotary C axis kinematic centre position error in the X-direction XOC is 3.8µm, whereas that in the Y-direction (YOC; offset errors) is 8.1µm. An analysis of the results (Fig. 39) also shows that the axis C squareness error (linear Z) in relation to the A axis (linear X) is AOC=2.9µm, whereas in relation to the B axis (linear Y) – BOC=0.5µm. Similarly to the case of static measurements, these values are usually used to change the controller settings and they are considered to be parameters responsible for increasing positioning accuracy. Figs. 40–42 show the real deviations in the horizontal X-Y plane and the squareness errors of the X-Z and Y-Z axes. Fig. 40 shows the variations in the real calibration sphere centre position deviations for the tested measurement angles in the horizontal X-Y plane, where v_f=2500mm/min. Fig. 40 clearly shows the displacement of the rotary axis kinematic centre in the horizontal X-Y plane.

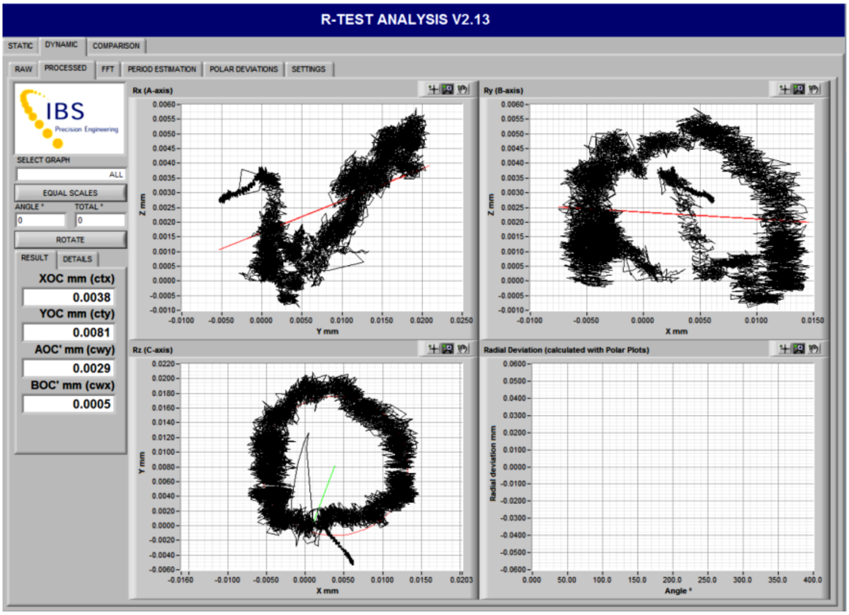

Fig. 39. Graphic representation of the dynamic measurement results: the fitting of the straight line determined via the least squares to the measurement results in the ZY plane (left-hand upper graph) and ZX (right-hand upper graph) is marked in red; results shown against the perfect circle

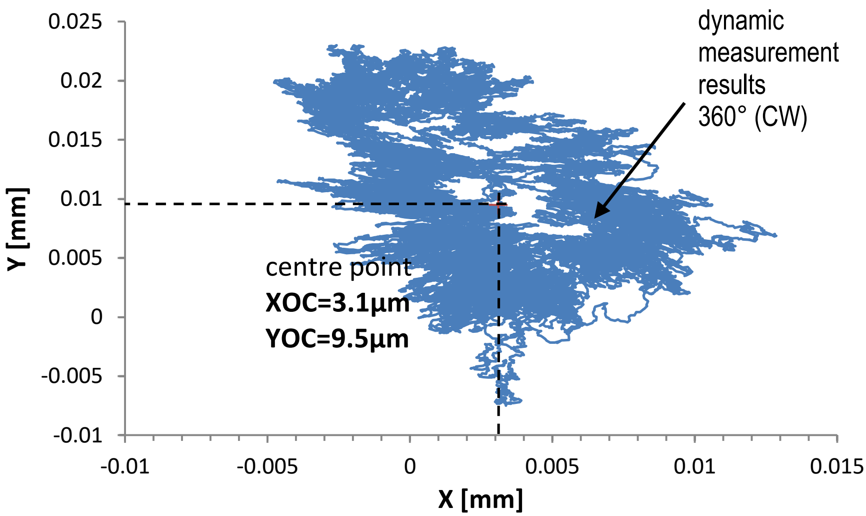

Fig. 40. Real values of calibration sphere position deviations for rotation angles in the horizontal X-Y plane, where v_f=2500mm/min

Fig. 41 shows selected results of the dynamic measurement, on the basis of which one can specify the Z axis squareness deviation in relation to the Y axis. The results of dynamic continuous measurement were approximated with a straight line equation. The following equation presents the results of dynamic continuous measurement results in the Z-Y plane for a selected measurement series, where v_f=2500mm/min (Fig. 41) (27):

$$Z_{Yd} = 0.1243 Y_d k_{2ZYd} + 0.0074 k_{2ZYd}' \tag{27}$$

where:
Y_d – value of the calibration sphere centre position error in the Y-direction [*mm*], k_{2ZYd} – unit factor of the variable X (k_{2ZYd} =1mm/mm), k_{2ZYd}' –unit factor of the equation free term (k_{2ZYd}'=1mm).

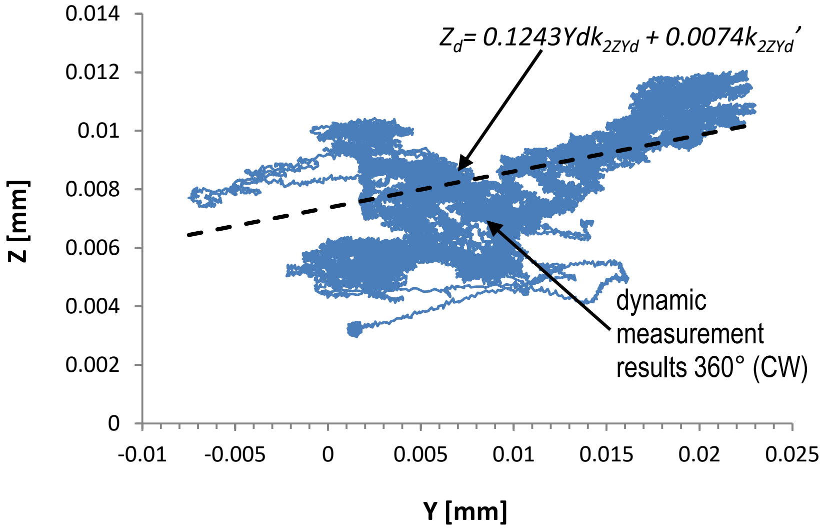

Fig. 41. Axis squareness error values as a function of rotation angle (0–360°) in the vertical Z-Y plane obtained from the dynamic measurement, where v_f=2500mm/min

Fig. 42 shows the dynamic measurement results of the Z axis squareness deviation in relation to the X axis. The straight line equation approximating measurement results in the Z-X plane for an example series of measurements, where v_f=2500mm/min is given in Equation (28):

$$Z_{Xd} = -0.1974 X_d k_{2ZXd} + 0.0088 k_{2ZXd}' \tag{28}$$

where:
X_d – value of the calibration sphere centre position error in the X-direction [*mm*], k_{2ZXd} – unit factor of the variable X (k_{2ZXd} =1mm/mm), k_{2ZXd}' – unit factor of the equation free term (k_{2ZXd}'=1mm).

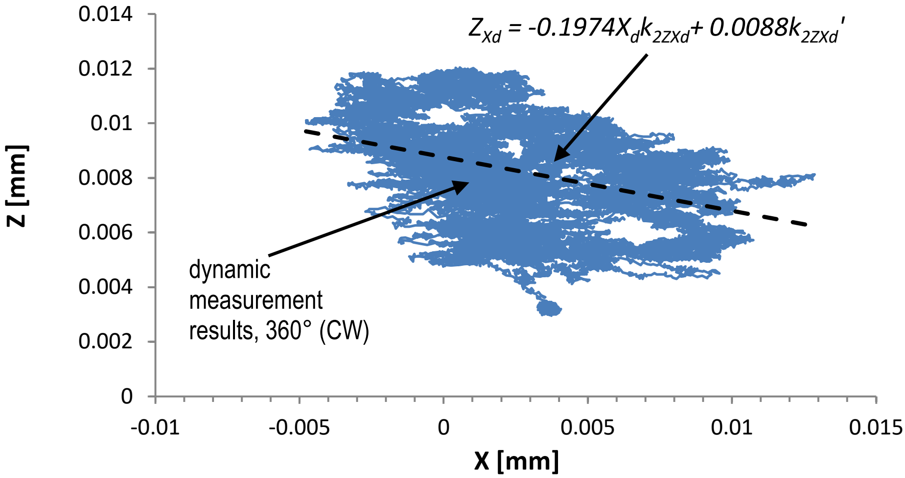

Fig. 42. Axis squareness error as a function of rotation angle (0–360°) in the vertical Z-X plane obtained from the dynamic measurement, where v_f=2500mm/min

Fig. 43 shows the dynamic measurement results of C axis kinematic centre position error in the X-direction (XOC) that in the Y-direction (YOC) (offset errors) as a function of feed rate v_f . The characteristics shown in Fig. 43 indicate a non-linear behaviour of errors as a function of feed rate v_f. The highest values of the rotary C axis kinematic centre position error were observed in the Y-direction (YOC) for the feed rates v_f=250mm/min (YOC=8.1μm) and v_f=2500mm/min (YOC=9.5μm). The lowest and comparable error values occur in the X-direction (XOC=2.8÷3.8μm) for all tested values of feed rate v_f and for other feed rates in the Y-direction (YOC=1÷1.1μm).

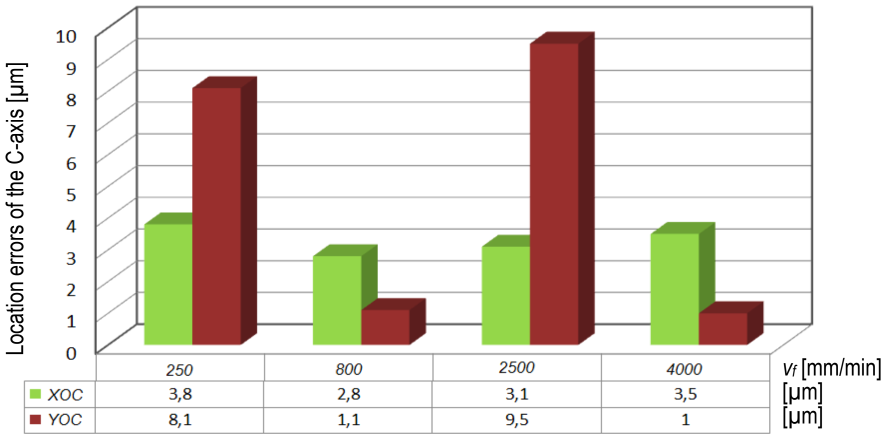

Fig. 43. Rotary C axis kinematic centre position errors in the X-direction (XOC) and Y-direction (YOC; offset errors) as a function of feed rate v_f (dynamic measurement)

Fig. 44 shows the axis squareness error AOC in relation to the A axis (linear X) and BOC in relation to the B axis (linear Y) as a function of feed rate v_f. Based on the obtained characteristics one may assume a non-linear dependence between the AOC and BOC errors and their feed rate v_f.

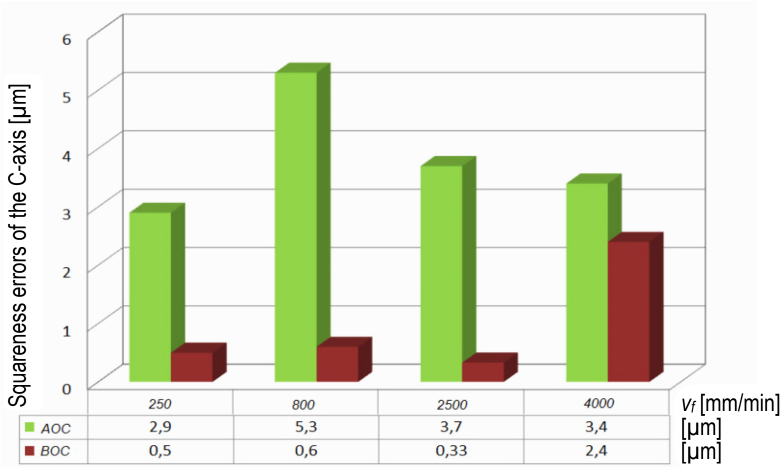

Fig. 44. Rotary C axis squareness errors in relation to the A axis (linear X; AOC) and to the B axis (linear Y; BOC) as a function of feed rate v_f

In the dynamic measurement, the axis squareness error is determined by the method of least squares. It is worth noting that the error is estimated on the basis of a far greater number of data obtained from dynamic measurements (6.5kHz) than in static measurement. Fig. 44 demonstrates that the squareness deviation of the C axis (linear Z) in relation to the X axis (AOC=2.9÷5.3µm) is significantly higher than in the case of the Y axis (BOC=0.5÷2.4µm). Like in the case of static measurement results, the ideal machine tool error values of XOC, YOC, AOC, BOC should be equal to zero (XOC=0µm, YOC=0µm, AOC=0µm, BOC=0µm). The results of the tests performed as a function of feed rate help determine the effect of the feed rate v_f of the on the displacement values in the diagnostic dynamic measurement.

The dynamic measurement results of centre point deviations of the calibration sphere in continuous rotation C in relation to the Z axis as a function of feed rate v_f in the X, Y, Z axes are shown in Fig. 45. The results reveal that there is a non-linear dependency between the entre point deviation of the calibration sphere in continuous rotation (C axis) in relation to the measurement head sensors. Equally, one can observed that the deviations (for different feed rates) are very low (deviations in the X-direction are within the range of 1.76÷2.29µm, in the Y-direction from 2.66 to 3.53µm, whereas in the Z-direction they range from 0.72 to 0.96µm. The low values of real deviations (displacements) confirm the machine's high kinematic and geometric accuracy.

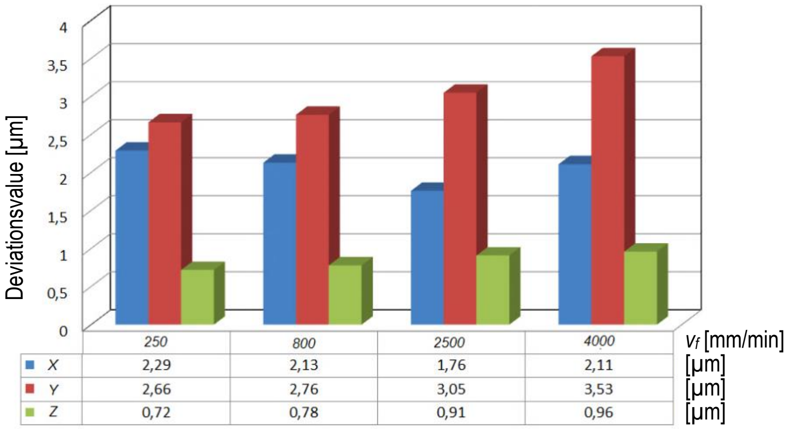

Fig. 45. Centre point deviations of the calibration sphere in continuous rotation C in the Z-direction relative to measurement head sensors as a function of feed rate v_f, in the X, Y, Z axes (dynamic measurement)

Fig. 46 compares the static measurement results and the average deviations and errors obtained from dynamic measurements. A comparison (Fig. 46) of average values of the tested errors and deviations (amplitudes) obtained from dynamic measurements with the static measurement results points to a similar and comparable level of machine tool inaccuracy. It should be noted that the dynamic measurement results show slightly higher deviations (amplitudes) in the X, Y, Z axes, which can be explained by the overlapping of machine kinematic errors and slightly lower values of XOC, YOC, AOC, BOC, which – in turn – confirms the high accuracy of measurements based on a large number of results.

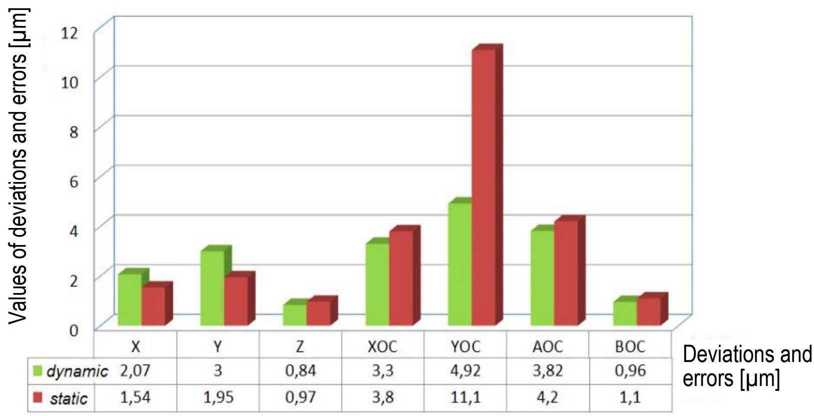

Fig. 46. Comparison of the analysed static measurement results and the average errors and deviations (amplitudes) obtained from the dynamic measurements

The diagnostics and calibration of numerically controlled machine tools is extremely important for proper and long-term operation of these machines. It helps maintain production capacity of CNC machine tools and control the reliability of their operation at the same time. This is of crucial importance, particularly in precise machining of critical parts. The diagnostics and calibration of numerically controlled machine tools is required after the collision or relocation of the machine tool. The use of the R-Test system for CNC machine tool diagnostics allows us to save time and reduce maintenance costs owing to automatic measurement and the possibility of performing measurements during calibration. The R-Test measurement system allows both static and dynamic measurements. This is an unquestionable advantage of the system.

The experimental tests conducted in the study enabled the assessment of the rotary C axis kinematic node position of the tested machine tool and squareness errors of the C axis (linear Z) in relation to the X and Y axes. In addition, they enable the determination of the effect of the feed rate v_f on results obtained with the R-Test diagnostic and calibration system. The results show a non-linear nature of the changes in the measured errors as a function of feed rate v_f. This non-linearity indicates that there is a need for precise dynamic measurements during each calibration of the machine tool under industrial conditions. The squareness deviation of the C axis (linear Z) in relation to the X axis is significantly higher (by three times approx.) than that of the Y axis. On the basis of a comparative analysis one can observe that higher deviations (amplitudes) in the X, Y, Z axes are associated with the dynamic measurement, which can be attributed to the overlapping of machine tool kinematic errors and lower position and axis squareness errors when compared to those obtained in the static measurement. This proves higher accuracy of the dynamic measurement (a large number of results on the basis of which these errors were determined).

The measurement and calibration of the machine tool with the R-Test device ensures a high geometric accuracy of the machine tool as well as quick correction of rotary axis kinematic centre position errors and axis squareness errors. The low values of both real deviations (displacements) in the X, Y, Z axes and determined errors confirm a high geometric and kinematic accuracy of the tested CNC machine tool. Measurement automation and the possibility of exporting data into the kinematics tables enables quick and easy calibration of a given machine tool.

4.2. Rotary axis kinematic centre coordinates assessment

The calibration of a 5-axis CNC machine tool with the use of 3D quickSET measurement system

Alignment and position control of the rotary axis is a crucial problem in machining with multi-axis numerically controlled machine tools [4–25]. In recent years there has been a significant increase in the use of multi-axis machines in industrial practice. This is due to the development of the aviation and automotive industries. The use of multi-axis machine tools and geometrically precise formation of finished products on these machines requires the determination of exact deviations of the rotary axis kinematic centre position relative to the machine tool linear axis. This ensures high machining accuracy on this type of machines. During the interpolation on 5-axis machine tools, the position of the rotary axis centres affects the machining conditions and especially the size and shape accuracy of geometrically complex surfaces on the workpiece [19, 51]. A lack of information or exact data concerning the "rotation points" (kinematic nodes) results in the fact that the CNC machine tool control system cannot reliably control relative positions of the tool and the workpiece during the movement of the rotary axes. This leads to significant errors in the machining of geometrically complex surfaces. The key to ensuring high precision of machining is to find the rotary axis centre position deviations in relation to the machine's linear axes [25, 32–35, 48, 50, 52].

As mentioned in Chapter 1.4, the 3D quickSET is one of the systems for quick and precise assessment of the machine tool kinematic node position [48]. The must be a point in the machine in relation to which the system is transformed during multi-axis machining. Until recently, with no 3D quickSET system, the process was performed by a serviceman who, with the use of sensors and measuring instruments, measured and manually set the required position of the rotary axis. The serviceman manually assigned the measurement values to the machine kinematic table. The tables are not usually available for an ordinary user of the machine, as a result of which the calibration of the machine tool rotary axis in operating conditions is more troublesome and requires service intervention. Another system for rotary axis calibration, R-Test, is described in Chapter 4.1.

The 3D quickSET test is based on the use of workpiece gauges attached to the machine spindle, nowadays a standard piece of equipment in most multi-axis machine tools. In effect, measurement results can be directly recorded in the machine tool kinematics table.

Only a properly calibrated inspection probe can be used in 3D quickset measurements to yield the desired effect.

The test performed with the 3D quickSET system manufactured by DMG (Fig. 47) requires defining a measurement cycle, DM_QSET 3D quickSET, implemented in the machine tool control system. The availability of the DM_QSET 3D quickset depends on the type of machine tool control system. The DM_QSET 3D quickset cycle is available in 5-axis machine tool control systems such as Siemens 840D, Heidenhain iTNC 530 and Heidenhain MillPlus. During the test, the test probe of the workpiece (after measuring and determining the calibration sphere centre) follows the system's calibration sphere. The calibration sphere is attached at the magnetic base and moves together with the rotary table (or spindle) during the test. The primary aim of the test with the use of the DMG 3D quickSET system is to determine the coordinates of the point in relation to which the machine control system calculates the physically set centre of the rotary axis. The process is performed so that the machine could perform the rotation cycle correctly and the workpiece dimensions were as accurate as possible. The physical setting of the rotary axis centre ensures high machining accuracy, especially in finish machining. The use of DMG 3D quickSET is hence justified in the machining of parts with narrow tolerances of size and shape, at frequent changes of machining profile (when using different materials, both in terms of their type and mechanical properties, e.g., hardness, surface layer properties), after spindle (tool) collision with the machine table (workpiece), after a long-term operation of the machine, in the machining of discontinuous surfaces (interrupted machining), after machine tool relocation, etc.

Fig. 47 shows the set up of DMG 3D quickSET (a) at the rotary table of DMU65 monoBLOCK. The object of the research, the five-axis machining centre DMU 65 MonoBlock, is equipped with a numerically controlled control system, Siemens Sinumeric 840 SL MD. This type of control enables the completion of the DM_QSET 3D quickSET measurement cycle. The completion of the DM_QSET 3D quickset cycle is based on selecting the workpiece cycle and defining its parameters. In effect, the 3D quickSET-a sphere is measured by a calibrated inspection probe, with rotation by a suitable test angle α (usually 90° or 180°) and determination of the rotary axis centre and recording it in the machine kinematics table. There is also a possibility to define other values of the calibration angle test. In the study, the calibration measurement of the A and C axes was performed assuming the angle test α had an interval of 15°. Given the kinematics potential, the A axis measurement was made within the range of -90° ÷ +90°, whereas that of the C axis was performed within the range of -180° ÷ +180°, clockwise (0° ÷ +90°, 0° ÷ +180°) and counter-clockwise (-90° ÷ 0°; -180° ÷ 0°), as shown in Tab. 19.

a) b)

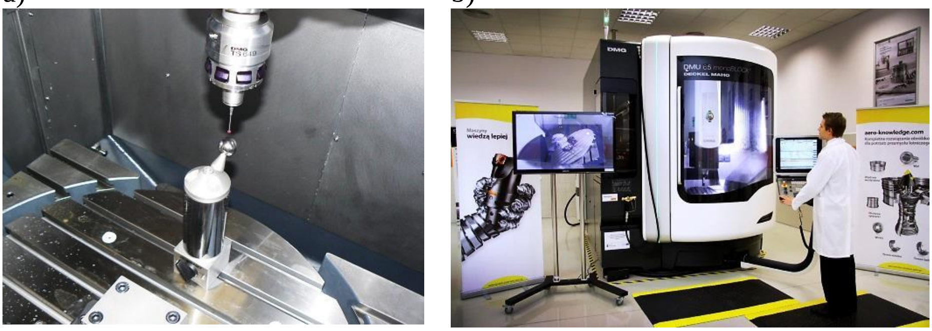

Fig. 47. Installation of DMG 3D quickSET (a) on the rotary table of DMU65 monoBLOCK machining centre (b)

The measurement programme (DM_QSET 3D quickSET, Fig. 48) was prepared according to the following procedure:

- define the 3D quickSET machine position at the machining table,
- attach the calibration sphere to the system body socket at an angle of 45°,
- place the 3D quickSET machine magnetic base in the machining table centre at a distance of 220mm from its axis (Fig. 47a),
- calibrate the machine tool measurement probe,
- select the DM_QSET 3D quickSET cycle from the machine numerically controlled system's catalogue structure (Figs. 48a, b),
- define the cycle parameters (a detailed description of the cycle parameters is given below in the present chapter; Fig. 48c),
  - a) define the type of measurement (rotary axis test),
  - b) determine the sphere diameter (25.0034mm),
  - c) determine the test angle α,
  - d) select the measurement method (0 – measurement only).

The measurement procedure:

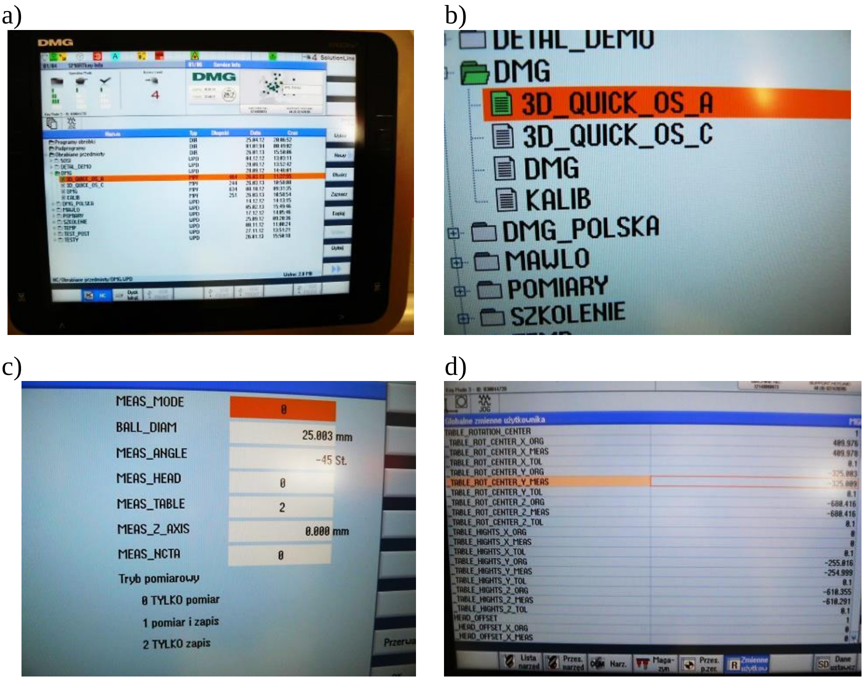

Fig. 48. DM_QSET 3D quickSET cycle interface: a) position in the control system catalogue structure, b) selection of DM_QSET 3D quickSET cycle, c) definition of cycle parameters, d) machine kinematics table with measurement results

Tab. 19. Angle values during the calibration test of CNC machine tool axes A and C																								
Values of angle α during the calibration test of A axis																								
-90°	-75°	-60°	-45°	-30°	-15°	0°	15°	30°	45°	60°	75°	90°												
Values of angle α during the calibration test of C axis																								
-180°	-165°	-150°	-135°	-120°	-105°	-90°	-75°	-60°	-45°	-30°	-15°	0°	15°	30°	45°	60°	90°	105°	120°	135°	150°	165°	180°	

For a correct definition of the DM_QSET 3D quickset cycle, it is necessary to define the following parameters: MEAS_MODE, BALL_DIAM, MEAS_ANGLE, MEAS_HEAD, MEAS_TABLE, MEAS_Z_AXIS, MEAS_Y_AXIS and MEAS_NCTA. Fig. 48c shows the values of defined parameters in an example measurement. The only variable cycle parameter was the measurement angle MEAS_ANGLE, its values α listed in Tab. 1.

The MEAS_MODE parameter defines the measurement method and requires entering the code symbols “0”, “1” or “2”. Code “0” means performing the measurement without recording obtained results in the kinematics table of the tested CNC machine tool. Code “1” means performing the measurement and recording obtained data in the machine tool kinematics table, as a result of which the previous machine kinematics is replaced with a new one based on obtained measurement results. Code “2” means data recording, i.e., the data is entered into the machine tool kinematics table, which results in replacing the previous kinematic parameters of the CNC machine tool. For the purpose of this study, code “0” was selected without recording obtained results. The BALL_DIAM cycle parameter defines a diameter of the 3D quickSET-a sphere. The value of the sphere diameter is given in millimetres and for the tested system it was 25.0034mm. In the data space of MEAS_ANGLE, the angle position α of the selected axes (+/-360°) is defined. Upon activating the dialogue window, one should enter the required angle α value in degrees (Tab. 19).

The MEAS_HEAD parameter is defined using code digits “0” or “1”. It is used for cutter head measurement. The entering of “0” in the data space means that the cutter head should not be measured, whereas code “1” means that the cutter head should be measured. Cutter head position vectors should always be determined from the spindle vertical position to the spindle horizontal position.

Another DM_QSET3D quickSET cycle parameter is MEAS_TABLE. By using code digits “0”, “1” or “2” in the data space of MEAS_TABLE we define the measurement of the rotary or rotary- tilting table. The selection of code “0” means that the table will not be measured. Code “1” means defining the measurement of the CNC machine tool rotary table centre. The entering of code “2” in the MEAS_TABLE data space stands for measuring the rotary table’s rotary axis (rotational vector). Code “2” can be used for machine tools with rotary tables.

The required value should be entered into the data space for the MEAS_Z_AXIS parameter only for a universal machining centre.

MEAS_Z_AXIS activates the measurement of rotary table height. MEAS_Z_AXIS is defined using code digits “0”, “1” or “>1”. Entering the “0” code means that the measurement of table height is inactive, whereas entering code “1” activates the measurement of table height. Code ”>1” starts the measurement of table height (as in the case of code “1”). However, it only measures extreme lengths.

The MEAS_Y_AXIS parameter is defined in a similar way to MEAS_Z_AXIS. This means that entering the “0” code for the MEAS_Y_AXIS parameter deactivates the measurement of table height, whereas entering code “1” activates the measurement of table height. Code “>1” starts the measurement of table height (like with code “1”); however, it only measures extreme lengths.

The last parameter of the DM_QSET 3D quickSET cycle is MEAS_NCTA. One should enter the code digit “0”, “1” or “2” in the data space for MEAS_NCTA. Entering the “0” code means that the division head will not be measured, whereas entering code “1”means that such measurement will be activated. Code “2” is active only for duoBlock machine tools and the portal gate, and defines positioning of the division head. The main problem in 3D quickSET measurements is the occurrence of thermal deflections of the measurement-calibration system, the measurement probe and the machine tool. The measurements should, therefore, be performed under thermally stable conditions.

On the basis of the experimental tests, it was possible to establish the characteristics of the calibration coordinates X_{zm}, Y_{zm} (measured) as a function of test angle α during calibration of the A and C axes of the tested machine tool. The tests led to estimating the coordinates entered into the machine kinematics table for discrete values of the calibration test angle α. The results indicate that the calibration accuracy depends not only on the degree of calibration accuracy of the test probe in 3D quickSET measurement, but also on the table rotation angle α during calibration of the rotary axes A and C.

Calibration of the A axis

Fig. 49 shows the variations in the measured value of the X_{zm} coordinate value as a function of measurement angle α during calibration of the numerically controlled rotary axis with the 3D quickSET device. The measurement results are compared with the original value of the X_{org} coordinate specified in the machine kinematics table.

Analysing the graph shown in Fig. 49 it can be observed that the X_{zm} coordinate reached the highest values for the measurement angles of α=+45°, α=-15°, α=-30° and α=-45°. The absolute error ΔX of the X_{zm} coordinate position as a function of measurement angle α is shown in Fig. 51. The absolute error value for the above mentioned angle positions α is the highest. One can also notice a relationship between the rotary axis centre coordinates and the measurement angle α. An analysis of the subsequent graphs (Figs. 49÷54) also shows that this relationship is non-linear. It is worth noting at this point that the repeatability of obtained measurement results for the constant value of measurement angle α remains within the range of 97÷99% for all performed tests with 10 repetitions.

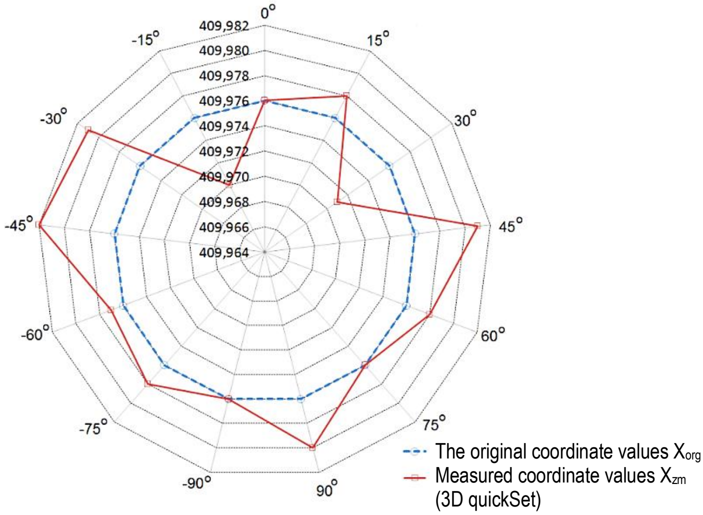

Fig. 49. Variations in the X_{zm} coordinate as a function of angle measurement α during calibration of the numerically controlled rotary A axis with 3D quickSET device, compared to the original coordinate value X_{zm} specified in machine kinematics table

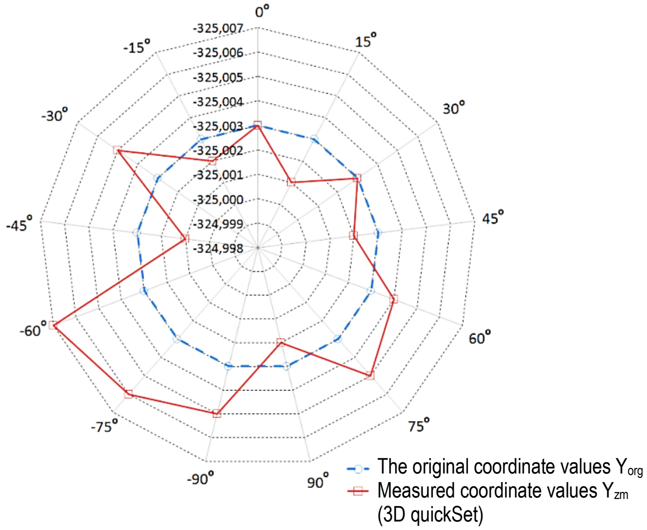

Fig. 50. Variations in the Y_{zm} coordinate a a function of measurement angle α during calibration of the numerically controlled rotary A axis with e 3D quickSET device, compared with the original coordinate value Y_{org} specified in the machine kinematics table

Fig. 50 shows the variations in the measured value of the Y_{zm} coordinate as a function of measurement angle α during calibration of the numerically controlled rotary A axis. Similarly to the case of the X_{zm} coordinate (Fig. 49), the measurement results are compared with the original values of the Y_{org} coordinate specified in the machine kinematics table. The highest values of the coordinate values were reached for α=-60° and α=-75°.

Figs. 51 and 52 show the absolute error values (ΔX, ΔY) of the X_{zm} and Y_{zm} axes. Fig. 51 shows the variations in the absolute error ΔX of the X_{zm} coordinate position as a function of measurement angle α during calibration of the numerically controlled rotary A axis with the 3D quickSET device.

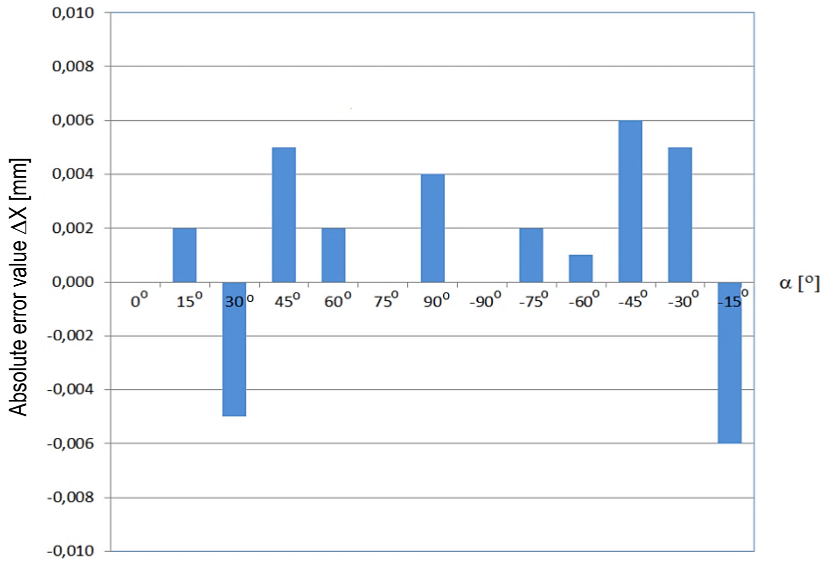

Fig. 51. Absolute error value ΔX of the X_{zm} coordinate position as a function of measurement angle α during calibration of the numerically controlled rotary A axis with 3D quickSET device

As shown in Fig. 52, the nature of variations in the absolute error ΔY of the Y_{zm} coordinate position as a function of measurement angle α during calibration of the numerically controlled rotary A axis is non-linear.

The characteristics (Figs. 51 and 52) clearly demonstrate that during calibration measurement of the A axis anti-clockwise rotation of the A axis (in relation to the X axis), the error values are higher than in the clockwise direction. The results also agree with the findings obtained with the R-test diagnostic system.

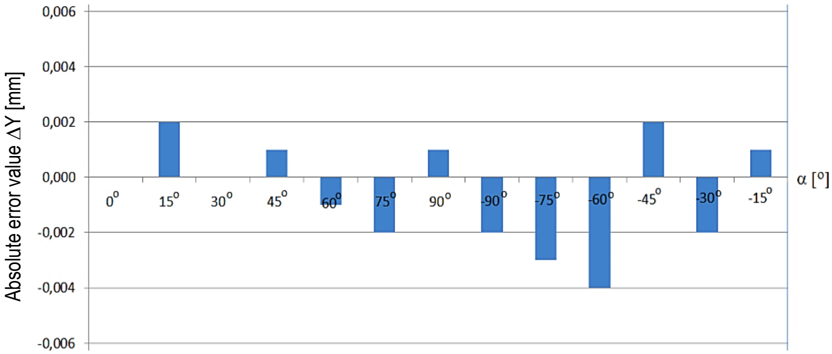

Fig. 52. Absolute error value ΔY of the Y_{zm} coordinate position as a function of measurement angle α during calibration of the numerically controlled rotary A axis with 3D quickSET device

Calibration of the C axis

Figs. 53 and 54 describe the nature of changes in values of the calibration coordinates (X_{zm}, Y_{zm}) during calibration of the numerically controlled machine tool axis C. Fig. 53 describes the nature of changes to the measured coordinate value X_{zm} as a function of measurement angle α during calibration of the numerically controlled rotary C axis with the 3D quickSET device. The results are compared to the original values X_{org} specified in the machine kinematics table.

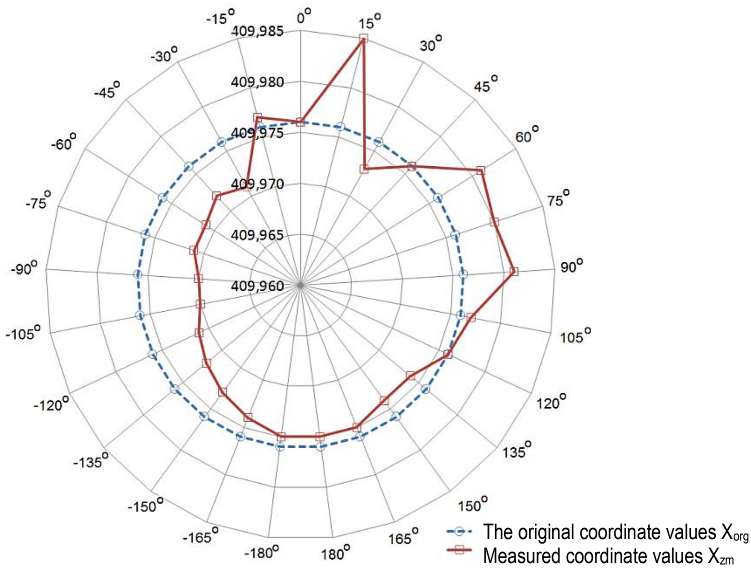

Fig. 53. Variations in the X_{zm} coordinate as a function of measurement angle α during calibration of the numerically controlled rotary C axis C with 3D quickSET device, compared with the original coordinate value X_{org} specified in the machine kinematics table

Fig. 54 shows variations in the Y_{zm} coordinate value as a function of measurement angle α during calibration of the numerically controlled rotary C axis with the 3D quickSET device, compared to the original values Y_{org} specified in the machine tool kinematics table.

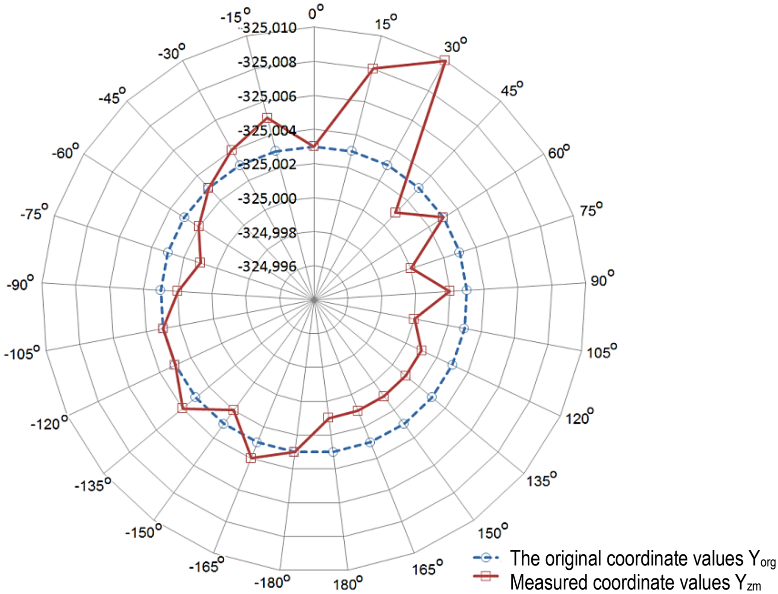

Fig. 54. Variations in the Y_{zm} coordinate as a function of measurement angle α during calibration of the numerically controlled rotary C axis with 3D quickSET device, compared with the original coordinate value Y_{org} value specified in the machine kinematics table

The values of the calibration coordinates X_{zm}, Y_{zm} given in Figs. 53 and 54 are the highest when α=-15°, 15°, 60°, 75°, 90° (for X_{zm}) and when α=15°, 30° (for Y_{zm}). For other angles, measured values are lower than those defined in the machine tool kinematics table. The shape of the curves points to the change in the rotary axis kinematic centre position, which is confirmed by the R-test results presented in Chapter 4.1.

Figs. 55 and 56 present absolute error values (ΔX, ΔY) of the calibration coordinates X_{zm} and Y_{zm} for the C axis. Fig. 55 shows the absolute error value ΔX of the X_{zm} coordinate position as a function of measurement angle α during calibration of the numerically controlled rotary C axis with the 3D quickSET device. Fig. 56 presents absolute error values ΔY of the Y_{zm} coordinate position as a function of measurement angle α during calibration of the numerically controlled rotary C axis with the 3D quickSET device.

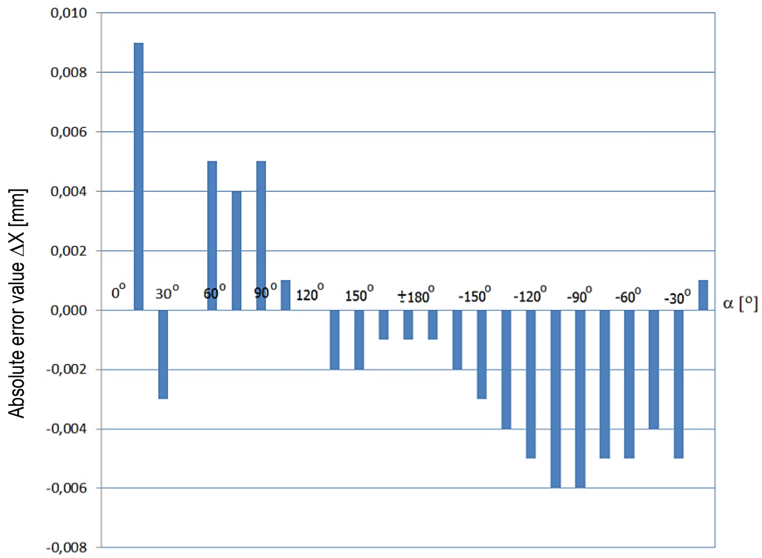

Fig. 55. Absolute error value ΔX of the X_{zm} coordinate position as a function of measurement angle α during calibration of the numerically controlled rotary C axis C with 3D quickSET device

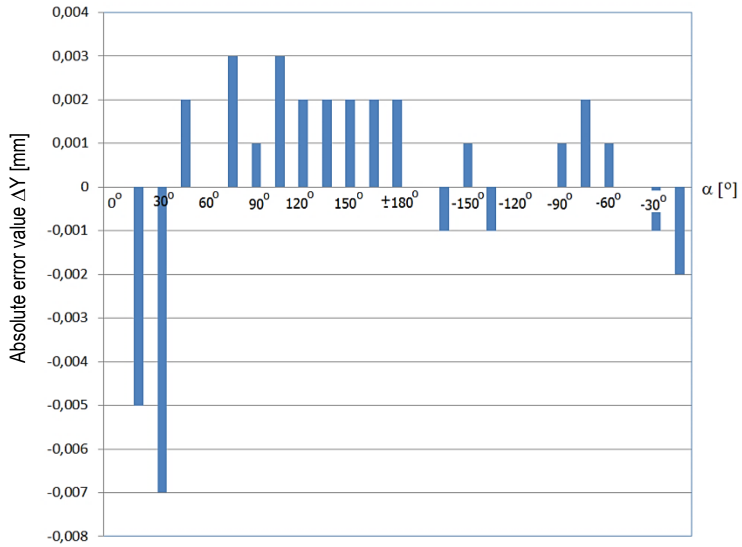

Fig. 56. Absolute error value ΔY of the Y_{zm} coordinate position as a function of measurement angle α during calibration of the numerically controlled rotary C axis with 3D quickSET device

The results demonstrate that the maximum values of absolute errors for particular calibration coordinates X_{zm}, Y_{zm} in C axis calibration are higher than those obtained from the A axis calibration. The maximum error values are within the range of 7÷9μm, but for the A axis, they are within the range of 4÷6μm. The results of rotary axis calibration with the R-test diagnostic system agree with the results obtained with the 3D quickSET system for the tested machine tool.

4.3. Summary and conclusions

The measurement and calibration of a machine tool using the 3D quickSET device ensure high kinematic accuracy of the machine tool and quick correction of kinematic errors. This is an extremely important task in machine operation, especially in terms of long-term operation, precise machining of parts or machine collision or relocation. The 3D quickSET system helps save time and minimise maintenance costs through automatic measurement. In an indirect way, this helps meet high quality requirements for finished parts and narrow tolerances for workpiece geometry. The detailed description of the test given in this study can also be a useful guide to the 3D quickset system. It helps the user to complete the test efficiently and, in this way, to improve the production accuracy of 5-axis machining. The experiments demonstrate that the calibration measurement results depend not only on the accuracy of calibration of the measurement probe used for the test, but also on the rotation angle α applied in calibration and the feed direction. The results confirm the non-linear nature of changes in the measured coordinates in a function of test angle α. This also demonstrates that the testing and calibration of a multi-axis machine tool using the 3D quickSET device should be proceeded by the investigation of the effect of the test angle α on measurement results. Optimised calibration data will help minimise the frequency of calibration tests, with an exception of events when machine tool calibration is necessary, e.g. after machine tool collision or relocation.

5. MACHINE TOOL DIAGNOSTCS WITH THE USE OF A TELESCOPIC KINEMATIC T BAR

The diagnostics of numerically controlled machine tools is one of the basic tasks in machine tool operation. Every machine tool is subject to wear with time in service. It should, therefore, be regularly tested, and its geometric condition should be diagnosed with specified frequency. Not only operated machines but also machines which are sold to buyers are subject to diagnostics. All machines are tested and assessed before it reaches the buyer. According to the information in Chapter 1.4, both contact and non-contact methods are used to this end. It often happens that some errors require the application of specialist research methods. The most widely used methods are interferometric, non-contact methods. A significant limitation of stationary interferometric methods in machine measurement is that the setting of interferometer optics is very time-consuming, especially in the case of machines with machining ranges of several metres. An unquestionable advantage of these methods is that they enable the measurement of the entire machining axis and provide information about errors over the entire feed range [8, 21, 30, 37, 40, 56, 59–61, 73, 88, 94, 105]. An alternative to laser system measurements are tests based on the use of a telescopic kinematic bar and circular tests specified in PN-ISO 230-4 standard. There is a number of measurement devices dedicated to circularity testing. One of the most popular is the Renishaw QC20 Ballbar device. Circularity deviation is the basic deviation affecting the size and shape accuracy of parts produced on CNC machine tools. The circularity deviation can be caused by geometric and kinematic errors of the machine tool, as well as incorrectly selected CNC machine tool drives or machine control and measurement system errors. The first step to reducing the circularity deviation is the restoring of squareness between the axes, adjustment of the drives and elimination of control interferences. The disadvantage of testing with the telescopic kinematic bar is the local character of this and the lack of possibility of direct assessment of positioning accuracy and repeatability.

5.1. Types of errors identified with a telescopic kinematic bar

Kinematic telescopic bar QC20 Ballbar allows to define machine tool's work The telescopic kinematic bar QC20 Ballbar enables the determination of machine tool work spaces with increased geometric deviations. The permissible deviations are specified in the standards for every type of geometric inaccuracy, and they pertain to the entire work space of the machine. The measurement and interpretation of machine errors are performed according to the guidelines specified in PN-ISO 230-4. The use of QC20 Ballbar testing enables the determination of errors and deviations which can be classified into three groups: clearances, geometric errors and dynamic errors connected with drive settings (Fig. 57). Following error compensation, a repeated test usually confirms the accuracy of machine operation.

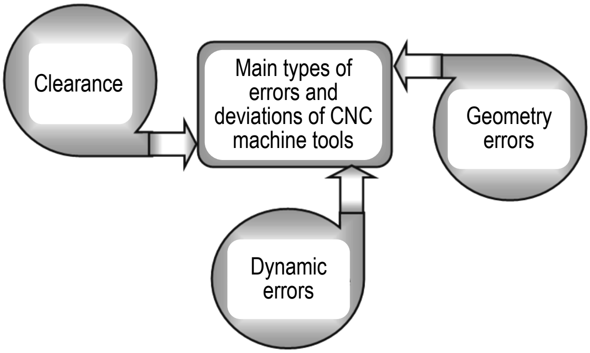

Fig. 57. Main types of errors and deviations of CNC machine tools

The most significant deviations identified in tests with the QC20 Ballbar device include circularity deviations, axis squareness deviations, temporary deviations and reversal spikes, reversal spikes in the measured axis and transversal clearance. Other errors identified by the QC20 Ballbar include squareness errors, cyclic errors, spiral errors, scale errors, servo mismatch, offset changes and radius changes. Most of the errors identified with the QC20 Ballbar are machine errors (M) and only some are of them are test errors (T). Tab. 20 presents the categories of errors occurring in diagnostic tests that can be identified with the Ballbar system. Taking into consideration the significance of particular errors and the potential of diagnostic software, only machine errors are described, excluding test errors and errors which cannot be analysed by the Ballbar system software. Other alternative measurement methods, e.g., return clearance, are far more time-consuming. The QC20 Ballbar system provides within minutes information about geometric and dynamic errors of the machine, the identification of which would be extremely time-consuming if classical methods were used.

Tab. 20. Machine errors (M) and test errors (T) identified with QC20 Ballbar

Machine tool errors – **M**	**Test error – T**
– cyclic error,	– discontinuity,
– servo mismatch,	– spiral error,
– reversal spikes,	– rotation,
– straightness,	– tri-lob,
– squareness,	– offset change,
– master-slave changeover,	– radius change.
– scaling error,	
– stick-slip,	
– backlash	
negative,	
positive,	
unequal,	
– lateral play,	
– machine vibration.	

The QC20 Ballbar system enables the assessment of circularity hysteresis and circular outline radius deviations determined during simultaneous movements in the two linear axes of the machine tool.

According to the PN-ISO 230-4 standard, circularity hysteresis is the maximum radius difference between two real outlines obtained on the machine tool in compliance with the programmed nominal outlines, one performed clockwise (CW,) and the other counter-clockwise (CCW) (Fig. 58).

a) b)

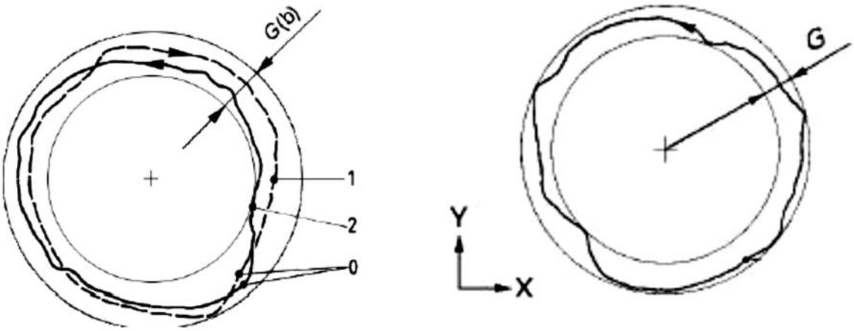

Fig. 58. Determination of circularity hysteresis G (a) and circularity deviation G (b): 0 – initial point, 1 – real clockwise outline, 2 – real anti- clockwise [133]

Circularity deviation is the minimal radius difference between two concentric circles with real outline, as shown in Fig. 59, which can be described as the maximum radius range including the circle determined by the methods of least squares.

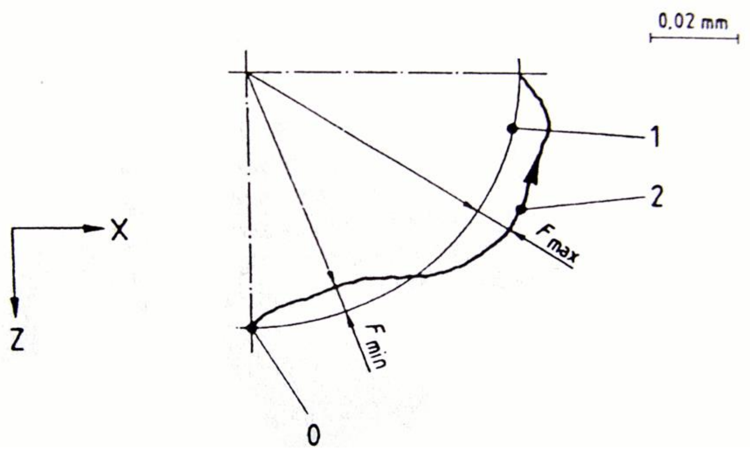

Fig. 59. Geometric interpretation of radius deviation *F*, 0 – initial point, 1 – nominal outline, 2 – real outline, F_{max} – maximum value of deviation, F_{min} – minimum value of deviation [133]

The radius deviation *F* is the difference between the real outline radii and the nominal outline radii when the centre of the outline is determined:

- by centring the measurement devices used in the machine tool,
- by centring analysis with the least squares, but only for full circles.

A positive deviation is measured from the centre of the circle, while a negative deviation is measured to the centre of the circle (Fig. 59). A radius deviation is determined taking the maximum value F_{max} and the minimal value F_{min}. Usually, individual errors have a complex effect on the real values of circularity outline. Geometric deviations of numerically controlled machine tools are determined in relation to the axis. Errors caused by numerical control and servomotors affecting circularity outlines are determined in relation to two linear axes. Circularity can refer to the sample shape or the shape of the path plotted by the moving part (parts). The circularity deviation can also result from incorrect selection of a CNC machine tool drive, as well as from errors of control and measurement systems. The basic action which should be taken to minimize the circularity deviation is to restore the squareness between the axes by adjusting the position of the guidebars and drives, and eliminating control interferences.

Impact of the linear positioning error (scaling error)

The group of geometric errors includes, among others, the positioning error. The positioning error has impact on circularity deviations. The circularity outline changes into an ellipse with its main diameter parallel to the X axis when the feed in relation to the X axis is longer, e.g., as a result of positioning errors or errors of the measurement rule scale. The influence of the linear shift in relation to the numerically controlled linear axes on the circularity outline is presented in Fig. 60. The interpolated clockwise (CW) and counter-clockwise (CCW) motion of the circle is marked in colour against a perfect test circle.

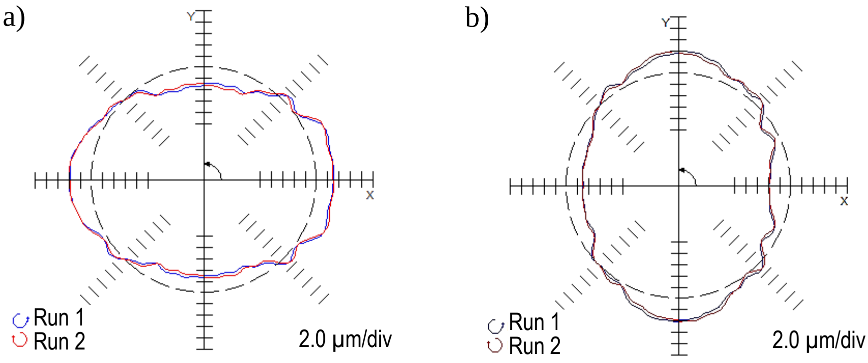

Fig. 60. Effect of the axis movement on the circularity outline: a) in relation to the X axis, b) in relation to the Y axis

The scaling error is defined in the literature according to the following equation (29) [31]:

$$\Delta R = \frac{a}{4} \times cos(2\theta) \tag{29}$$

where:
ΔR – deviation value of the nominal radius R, a – absolute error value, θ – angle of measurement in relation to the axis.

The positioning error can be caused by incorrect graduation in the measurement system (for a given feed, the axis displacement is either too small or too big), incorrectly selected or badly calibrated linear compensation parameters, uneven tenseness of the measurement rule, incorrect guidebar setting, over-heating or damage of the bolt in one of the machine tool axes.

Squareness deviation of the CNC machine tool axis

Squareness deviation of the CNC machine tool is one of the most important deviations identified by the QC20 Ballbar system (Fig. 61). The angle between two numerically controlled axes on a given measurement plane is the squareness error value. Unless the tested axes are perpendicular to each other, the angle between them is greater than 90˚ or smaller than 90°. If the angle between the two axes (calculated in their positive value) does not exceed 90°, then the squareness error takes negative values (Fig. 61a), but when the angle between the two axes (calculated in the positive direction) exceeds 90°, then the squareness error takes positive values (Fig. 61b). The occurrence of the squareness error results from incorrect position of the X and Y axis guidebars relative to each other, guidebar wear or their elastic or thermal deformations. Another reason for the occurrence of the squareness deviation can be an incorrect or inaccurate levelling of the machine tool table. However, results of the measurements performed in this study for different heights in the Z axis direction excluded this cause, which is confirmed by a repeatable nature of the error on every tested height.

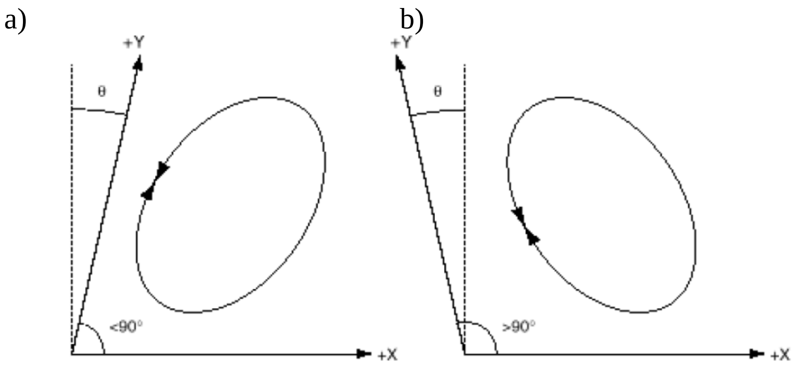

Fig. 61. Squareness deviation and its influence on the relative position of the machined surfaces: a) negative squareness error θ<90˚, b) positive squareness error θ>90˚ [12, 14]

The machine tool axis squareness error takes the zero value only when the axes on the tested plane are ideally perpendicular in relation to each other. A direct measure of the axis squareness error is the θ angle expressed in degrees and angular seconds. Another alternative unit to express the axis squareness error is μm/m, μm/mm, μm/ft. The selection is made via setting of the software parameters.

The graph showing the circularity outline obtained during the QC20 Ballbar test is oval in shape with the main axis positioned at an angle of 45° or 135° (Fig. 62). The graph deviation axis is identical for both directions of interpolation, in the clockwise and anti-clockwise directions. If there is a squareness error on the machine tool, the two machined surfaces are not perpendicular in relation to each other. Fig. 62 presents a situation when the angle is smaller than 90°. The lack of axis squareness adds to vital problems connected with deformation of cubic surfaces, both external and internal.

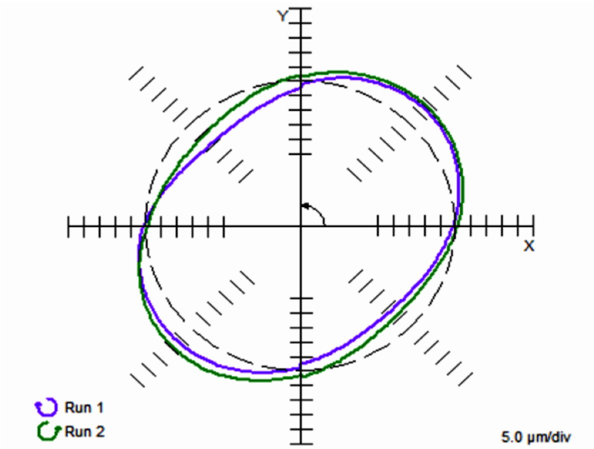

Fig. 62. Graphic representation of the squareness error identified in diagnostic test with the QC20 Ballbar system (Run1 – CW, Run2 – CCW)

The squareness deviation error is described in the literature with the following equation (30) [34]:

$$\Delta R = \frac{aR}{2} \times sin(2\theta) \tag{30}$$

where:

R – deviation of the nominal radius *R*, *a* – absolute error value, θ – angle of measurement in relation to the axis.

The axis squareness deviation can be local or may occur over the whole length of the axis, both in the horizontal (X-Y) and vertical (X-Z, Y-Z) planes. The occurrence of the squareness deviation results from badly positioned guidebars of the X and Y axes, guidebar wear or their elastic and thermal deformations. The squareness deviation can also be caused by incorrect or inaccurate levelling of the machine tool table. In the case of local axis squareness deviations, the way to prevent the machining errors resulting from the squareness deviation is to avoid machining in areas where the axis straightness deviation reaches high values. This, however, requires measurements of the entire work space of the machine tool as well as the identification and correct interpretation of the axis squareness error. If the straightness deviation occurs over the entire length of the axis, it is necessary to correct the guidebar settings or ultimately – with extensive guidebar wear or ineffective setting correction – the replacement of the guidebars. For a one-off assessment of the effect of the squareness error of the CNC machine tool axis, it is recommended to perform multiple testing in a number of points along the machine tool guidebars. In effect, one can determine whether the error is local or global (i.e., whether it occurs over the whole length of the guidebars). If the error is local (and only occurs at a certain point of the axis length), then one should try using the guidebar area where the impact of the squareness error is the lowest.

Impact of intermittent deviations

Intermittent deviations can be classified as geometric errors. Intermittent deviations lead to the occurrence of the cyclic error. Fig. 63 shows the changes in the outline due to the occurrence of an intermittent positioning error in the X direction. The error is described with the following equation (31) [34].

$$\Delta R = a \times cos\theta \times sin\left(\frac{2\pi R cos\theta}{p_x} - \varphi_x\right) \tag{31}$$

R – deviation value of the nominal radius *R*, *a* – absolute error value, θ – angle of measurement in relation to the axis, p_x – cyclic error pitch, φ_x – phase angle of the cyclic error.

a)

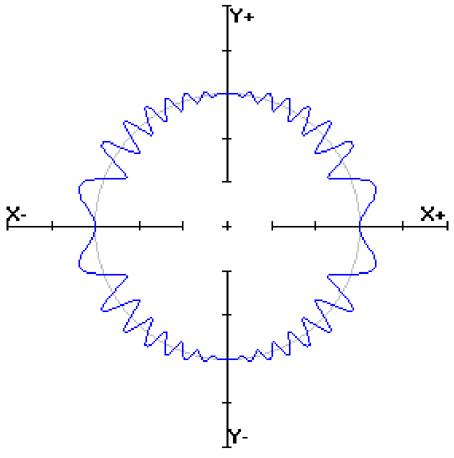

b)

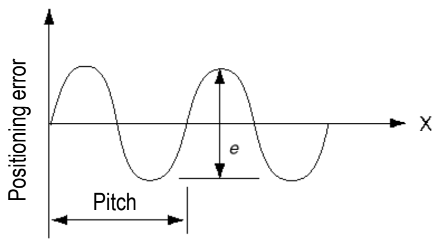

Fig. 63. Effect of the intermittent deviations in relation to the X axis where: e – positioning error amplitude: a) test result for the cyclic error, b) error positioning parameters

The cyclic error is a repeating error, and it is connected with machine tool design. It can result from the occurrence of clearance due to machine wear, e.g., on the guidebars. The main causes of the intermittent positioning error include: screw pitch error, damage of the screw thread or ball nut causing a sinusoidal axis displacement, non-centric mounting of the screw or encoder. The cyclic error does not depend of the sense of rotation if its cause relates to the screw axis. It can, however, depend on the feed rate.

Impact of the reversal spikes and their compensation

Reversal spikes are associated with backlash. In circular interpolation reversal spikes are shown in a pie chart as the pitch of the radius movement deviation to the outside or to the inside of the arc (Fig. 64). Reversal spikes result from clearances in the drive system of the machine tool or in the measurement system (clearance in the bolt nut joint, extensive gear wear, nut damage). Reversal spikes can also be caused by the clearance in the gear transmission of the drive system, guidebars, incorrect tension of the timing belt or insufficient stiffness of the systems.

Reversal spikes in the Y axis (Fig. 64a) can be described mathematically (32) in the following way [31]:

$$\Delta R = \pm\frac{\alpha}{2} \times sin\theta \tag{32}$$

where:
ΔR – radius deviation, α –absolute error value, θ – angle of measurement in relation to the axis.

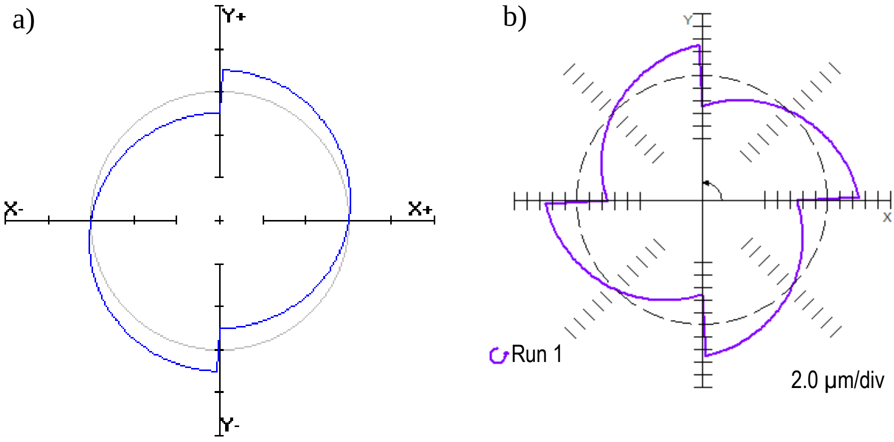

Fig. 64. Non-compensated reversal spikes:
a) only in the Y axis, b) simultaneously in the X and Y axes

If the reversal spikes occur in both servo-drives, then the nominal outline of circularity changes into four quarters of the circle with four different centres (Fig. 64b). The value of clearance can differ or can have different directions for the same axis. The pitch value presented in Fig. 64 does not usually depend on the set feed rate value of the machine tool. Positive reversal spikes have the form of short straight sections (planes) on the milling cutter trajectory in the machining with circular interpolation (Fig. 65). The correction reversal spikes via numerical control (to anticipate the change in screw rotation) needs some time. If the reaction of the servo drive is too slow, one can observe peak values of the reversal points (characteristic peaks). The peak values are the higher, the higher the mechanical clearance is or the slower the numerical control is (e.g., small increases in loop positioning, low amplification factor of the positioning regulator). In effect, there occurs an interruption to the movement during the change of feed drive direction in a particular axis (Y or X), as shown in Fig. 64.

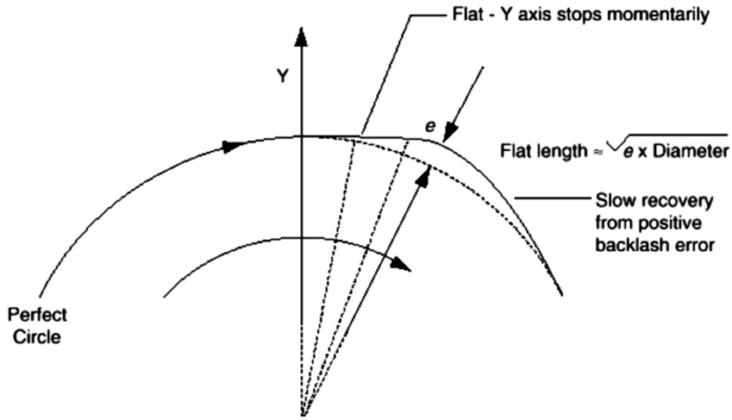

Fig. 65. Movement trajectory deformations during circular interpolation [133]

When the direction of movement is changes, then one of the axes starts it movement with delay due to clearance. To reduce reversal spikes, it is essential to delete the clearances in the drive (in the guidebars, screw, etc.) and measurement systems, to apply compensation directly in the machine tool control system, or, ultimately, to replace the damaged or worn elements in the machine tool.

Lateral play

The main reason for the occurrence of lateral play is machine tool guidebar defect, or non-parallel displacement of machine tool units in the guidebars during reversal spikes. An example of obtained graph for lateral play is shown in Fig. 66.

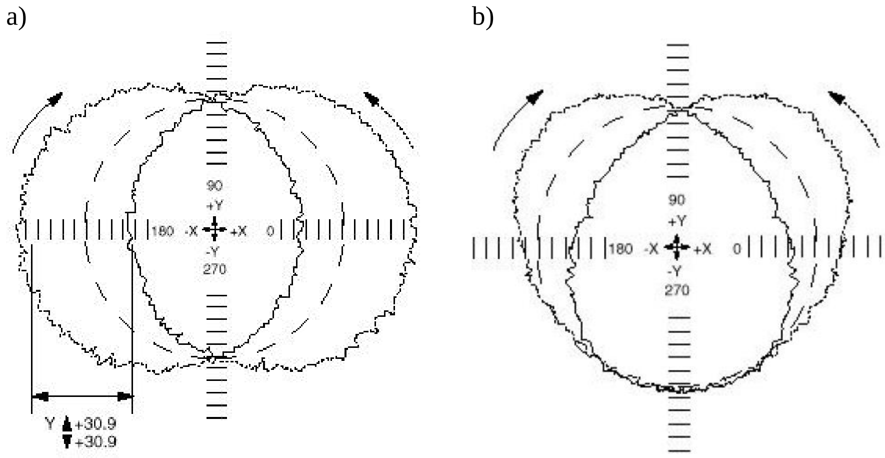

Fig. 66. Diagnostic graph showing the occurrence of lateral play:
a) regular, b) irregular [133]

Lateral play can have characteristics of regular or irregular clearance, as shown in Fig. 66.

Impact of reversal spikes

The symptom of reversal spikes is a temporary increase in the deviation value in a diagnostic test pie chart, as shown in Fig. 67. The height of the peaks usually depends on the set feed rate value. Reversal spikes primarily result from a too slow reaction of the servo drive to the signal from the control system during a movement direction change (crossing the axis in circular interpolation). A big delay in the movement caused by a too low position amplification factor k_v leads to a change to in the movement trajectory in relation to the set path. In effect, there occurs a small break between the unidirectional feed stoppage and the moment when the feed motion is started in the opposite direction. The time of servo drive response is not adequately selected to the value of backlash compensation, which lead to the stoppage in the axis feed at the moment of reversal-deletion of the backlash.

The reason behind the occurrence of this error can also be that the axis feed motion engines are assigned with incorrect torques, which results in the fact that they cannot level the effect of friction between the adjoining guidebar surfaces. A characteristic feature of reversal spikes is that, after some time following the crossing of the set position of the X axis by the Y axis, the engine of the Y axis performs a movement and the servo-drive eliminates the error in the axis. The effect of presence of reversal spikes in the machine tool is the occurrence of a short straight section (plane) in the trajectory of the tool movement during machining in the circular interpolation cycle and then a rapid reversal to the outline being machined, as shown in Fig. 68. Assuming that the length of the section *e* is equal to the peak height in the diagnostic graph generated by reversal spikes, one can determine the length of a straight section of the cutting trajectory as a square root of the ratio between the value of *e* and the set diameter of the cutting circle outline. Reversal spikes depend on the feed rate. Its effect can therefore be reduced by optimising the feed rate value.

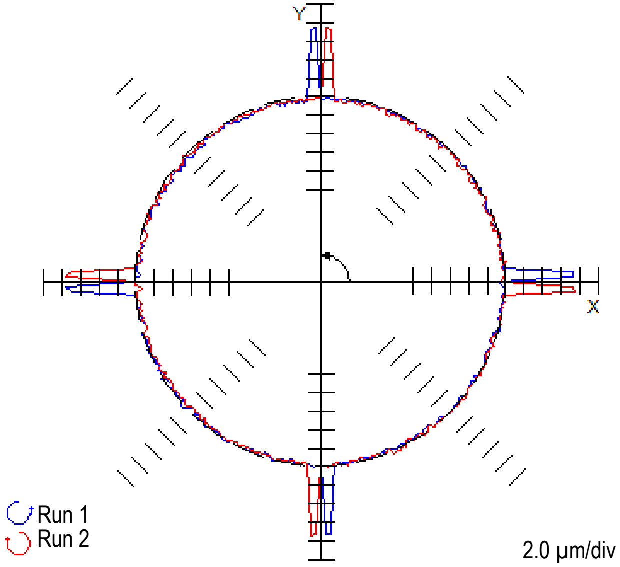

Fig. 67. Graphic illustration of reversal spikes

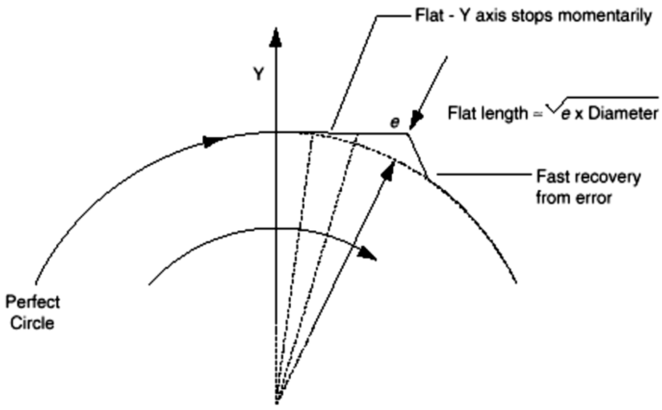

Fig. 68. Movement trajectory deformation in the case of reversal spikes [133]

Other reasons for the occurrence of reversal spikes include clearance in the drive system (clearance in the roller screw or gear) and incorrect work of the servo-drives. To reduce reversal spikes, it is essential to eliminate clearances in the drive and measurement systems. A long-lasting effect of reversal spike reduction can be brought about by correct setting of the amplification factors of the positioning regulator. Some CNC machine tool control systems allow for compensating reversal spikes.

Straightness error

The most frequent reason for the occurrence of the straightness error is local wear, deformation or damage of the machine tool guidebars. In Ballbar circularity testing one can encounter a case when the straightness error graph is a result of the presence of solid particles in the magnetic connectors or incorrect or unstable mounting of the Ballbar system. Therefore, the straightness error does not depend on the feed rate value. A typical graph illustrating the straightness error is similar to the shape defect known as angularity (Fig. 69).

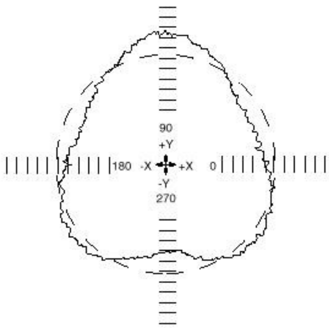

Fig. 69. Straightness error in the Ballbar roundness test [133]

5.2. Diagnostic test description

Diagnostic tests for measuring the circularity deviation can be performed by means of various tools. The research described in this work was conducted with the use of two telescopic kinematic bars, QC10Ballbar and QC20Ballbar. The QC10 (or QC20) Ballbar test requires the machine to perform circular interpolation (circular motion) in a selected plane for the set location and feed rate (Fig. 70). Between the spindle and the machine table there is attached a diagnostic probe (Ballbar), with a displacement converter which very precisely measures the circle radius for the whole range of interpolated motion of the machine.

a) b)

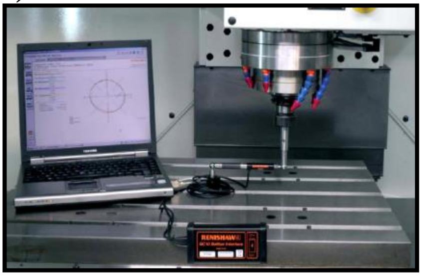

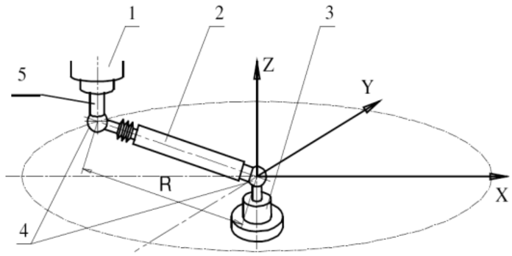

Fig. 70. The diagnostics measurement rule for CNC milling machines with a quick QC10 Ballbar test: a) general view, b) the principle of the test preparation; 1 – milling machine spindle, 2 – measurement converter (telescopic ball bar), 3 – magnetic centring base, 4 – ball tips, 5 – magnetic handle, R –nominal outline radius [55, 105]

The measurements were conducted on the following machine tools: a five-axis machining centre, HSC 105 linear (Figs. 71 a, c), equipped with a Heidenhain control system, a four-axis vertical milling centre, FV580A, equipped with a numerical control system by FANUC (Figs. 71 b, d) and CTX 310eco lathe with a control system by Heidenhain. The measurements were conducted at the temperature of 20°C. The thermal expansion factor for the machine tool was set equal to 11 μm/°C. A desk top computer QC10 meeting the equipment requirements was used to operate the software. Before commencing the diagnostic tests, additional activities were performed, including:

– the QC10 Ballbar device was connected to the desk top computer through a serial interface RS232,
– the X-Y measurement surface was selected,
– measurement points on the milling machine table were specified – 15 measurement points equally spaced in the Cartesian system (rectangular system) (Fig. 72),
– feed rate values for the machine tool table were selected as: v_f=500; 1000; 2000; 3000; 4000; 5000mm/min,
– gauge plunger radius values were selected (L=100, 150),
– the angle of measurement was set equal to 360°,
– the machine tool expansion factor was set equal to 11μm/°C and the temperature to 20°C,
– the programme performing the measurement motion was implemented into the CNC control system memory,
– the telescopic kinematic bar was calibrated,
– the telescopic kinematic bar was mounted on the milling machine table,

– the programme performing the measurement motion was started to begin the measurement procedure.

Fig. 71. Test stand: a) HSC 105 linear milling centre, b) FV580A milling centre, c) QC10Ballbar system mounted on the HSC 105 linear machine tool table, d) QC10Ballbar system mounted on the FV-580A machine tool table

The measurement points at the machine tool table were evenly spaced in a rectangular coordinate system. Measurements with different parameters of circular interpolation were performed in the points (different length of kinematic measurement, different feed rates). The distance of the "external" points from the table edge was 150mm. The spaces between the points in the X and Y axes were 60mm. 184 measurements were taken at fifteen measurement points located as shown in Fig. 72. Experimental tests were conducted using two lengths of the kinematic bar: 100mm and 150mm, as well as six different feed rates (v_f=500; 1000; 2000; 3000; 4000; 5000mm/min). During the measurements, no interferences from external factors were observed. The measurements were performed in compliance with both PN-ISO 230-4 and Renishaw's recommendations.

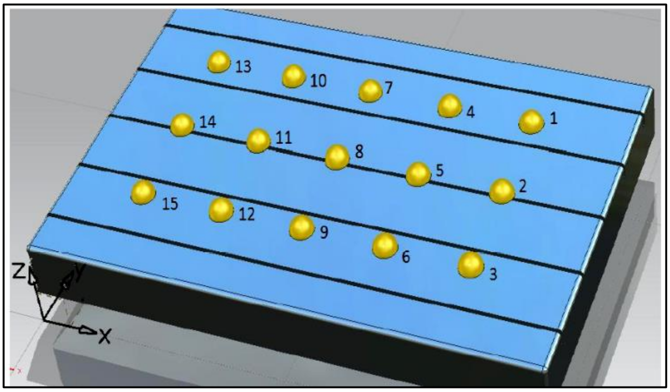

Fig. 72. Schematic of the machine tool table with marked measurement point

Additionally, the accuracy of the numerically controlled machine tool CTX 310eco by DMG was assessed (Fig. 73). The tests were performed with the telescopic kinematic Ballbar. Taking into consideration the machine work space, the radius of the interpolated circle was set equal to R=50mm.

Fig. 73. Test stand DMG CTX 310 eco lathe

Similarly to the case of milling machines, the tests were performed according to the PN-ISO 230-4 standard. The variable value during the test was the feed rate v_f. The value of feed rate was changed in the range from 500mm/min to 2000mm/min. Obtained results of individual errors are presented in the form of graphs. Fig. 74 shows the experimental test on the analysed CNC machine tool and the QC 20 Ballbar lathe set. The errors analysed in the testing of the CTX 310 eco lathe were as follows: axis squareness deviation, reversal spikes, reversal error.

a)

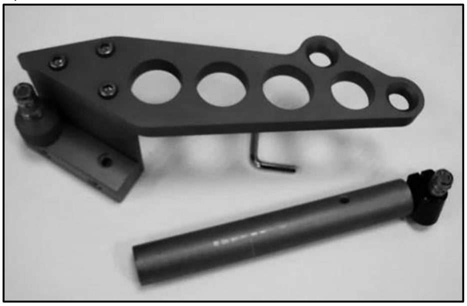

b)

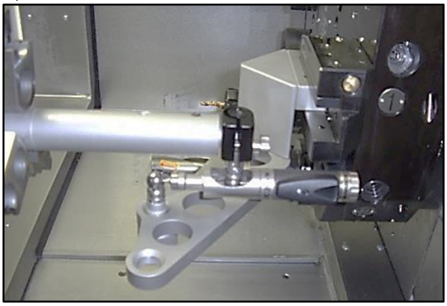

Fig. 74. Lathe set for CNC machine tool diagnostics: a) lathe handle and gauge plunger, b) experimental test performed with the testing system mounted on the lathe

5.3. Diagnostic measurement results and their analysis

Analysis of the experimental results of the FV580A milling centre for the measurement radius R=100 mm

As a result of conducted measurements for the measurement radius R=100mm, results of the CNC machine tool axis squareness deviation were obtained. The deviations are presented as a function of feed rate and measurement point position on the machine tool table (Fig. 75). The results demonstrate that the axis squareness deviation does not depend on the feed rate used in the roundness test. It was observed, however, that the higher the feed rate is, the higher the value of axis squareness deviations are. It was also noticed that in the measurement points 3, 6, 9, 12, 15 (Fig. 75) there are increased values of the machine tool axis squareness. The right hand upper corner of Fig. 75 shows a schematic design of the machine tool with marked measurement points.

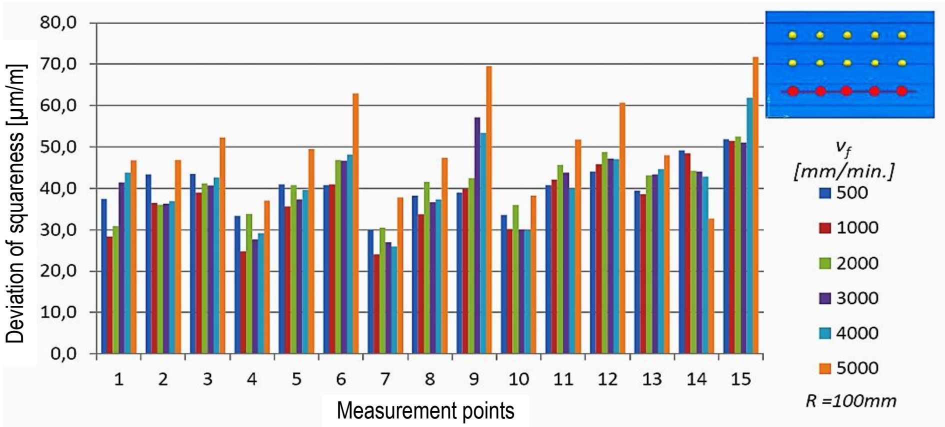

Fig. 75. Axis squareness deviations in fifteen points on the CNC machine table as a function of feed rate v_f, for R=100mm

From Fig. 75 it can be observed that the measurement points marked as 3, 6, 9, 12, 15 show increased values of the error and are located in one line corresponding to the X axis. This proves a local nature of the axis squareness deviation in the X-Y plane of the machine tool. The maximum squareness deviation is 71.8μm/m, whereas the minimum squareness deviation is 24.1μm/m. In almost all measurement points, the maximum squareness deviation values were obtained for the feed rate of v_f=5000mm/min.

Analysis of the experimental results of the FV580A milling centre for the measurement radius R=150mm

Fig. 76 shows the variations in the squareness deviation for the measurement radius R=150mm. A characteristic of these variations is the repetitive character of the maximum deviation values in the measurement points marked as 3, 6, 9, 12, 15. The points with increased squareness deviation values are marked in the figure in red colour. The reason for the occurrence of such variations can be local wear of the guidebars or incorrect machine tool table levelling. In most cases, the maximum values of squareness deviation were obtained for the feed rate of v_f=4000mm/min. The highest obtained value of squareness deviation is 57.6μm/m whereas the lowest is 30μm/m.

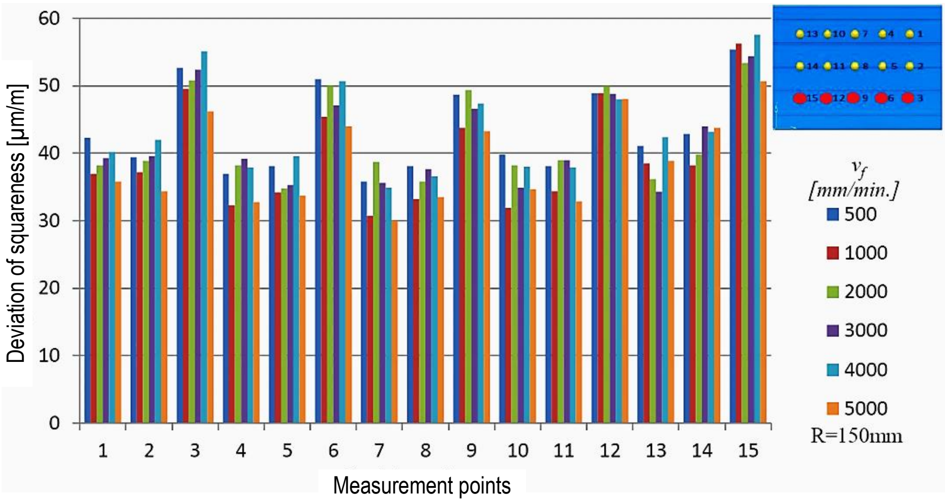

Fig. 76. Axis squareness deviations in fifteen points on the CNC machine tool table as a function of feed rate v_f, for R=150 mm

Results of the comparative tests for the FV580A and HSC 105 milling centres

For the purpose of comparison, the HSC 105 machine tool axis squareness was assessed, using identical measurement values. The measurement was conducted for a randomly selected measurement point marked as 7 in Fig. 72, as in the case of the FV580A milling centre. The roundness test was conducted for the measurement radius of R=150 mm, at three feed rates v_f (500, 1000, 2000mm/min). Obtained results are compared in the graph (Fig. 77). The values of squareness deviation for the FV580A machine tool and for the HSC 105 machine tool presented in the graph indicate a much higher geometric accuracy of the HSC 105 machine tool. It can be observed that the deviations of the FV580A machine tool take positive values and are more than two times higher than the squareness deviations of the HSC 105 machine tool. For the HSC 105 machine tool at the feed rate of v_f=500÷2000mm/min, a decrease in the squareness deviation values can be observed. The maximum axis squareness deviation (38.7μm/m) was obtained for the feed rate v_f=2000mm/min. The squareness deviation of the machine tool is caused by the lack of mutual squareness between the milled surfaces. This results from an incorrect setting of the X and Y axis guidebars relative to each other, wear of the guidebars or their elastic and thermal deformation. The reason for the high value of machine tool axis squareness deviation can also be extensive clearance. Another reason can be an incorrect or inaccurate levelling of the machine tool table. This reason, however, was eventually excluded, given the results of laser interferometer measurements. This assumption was later confirmed by a test performed on different heights in the direction of the Z axis, which clearly proves the repetitive nature of the error on every tested height.

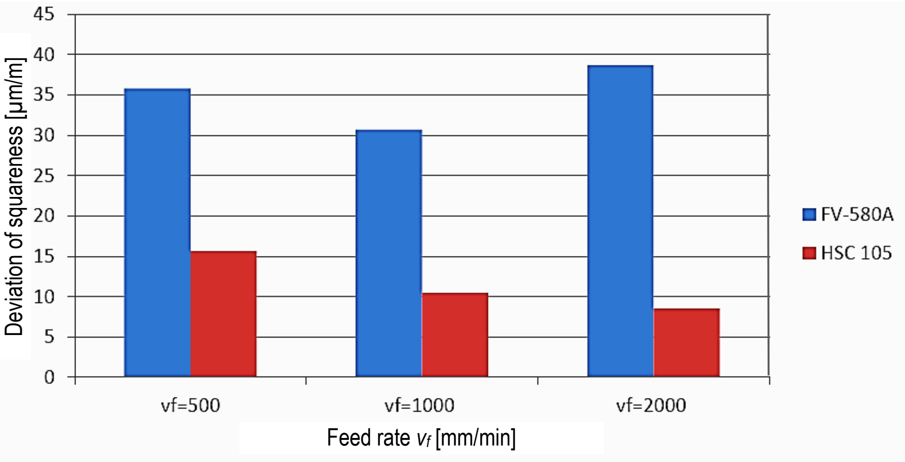

Fig. 77. Comparison of the axis squareness deviations of FV580A and HSC 105 linear in measurement point 7, for R=150 mm

On the basis of the conducted measurement, the local nature of the FV580A machining centre vertical axis straightness deviation was proved. To prevent the occurrence of machining errors resulting from the local axis squareness deviation, it is recommended to avoid machining the surfaces in the area of the machine work space where this error occurs. These are areas where the axis squareness deviation takes maximum values and in the points marked as 3, 6, 9, 12, 15.

Analysis of the axis squareness deviation results for the CTX 310 eco lathe

During the identification of axis squareness deviations, the diagnostic graph takes an oval shape ot the shape of a peanut, rotated askew at the angle of 45° or 135° (Figs. 61 and 62). The deviation axis in the graph is identical for both directions of the circular interpolation cycle, in the clockwise and anti-clockwise directions alike.

Fig. 78 presents the relationship between the squareness deviation and the feed rate v_f for the kinematic bar with R=50 mm. The lowest deviation value of -66.2µm/m was obtained for the feed rate of v_{f1}=500mm/min. The deviation values for other feed rates were respectively: for v_{f2} =1000mm/min the deviation value was -83.2µm/m, for v_{f3}=1500mm/min it was -78.4µm/m, whereas for the feed rate v_{f4}=2000mm/min the axis squareness deviation took the highest value and was -83.6µm/m. As the data presented in the graph (Fig. 78) demonstrate, the squareness deviation as a function of feed rate v_f is non-linear.

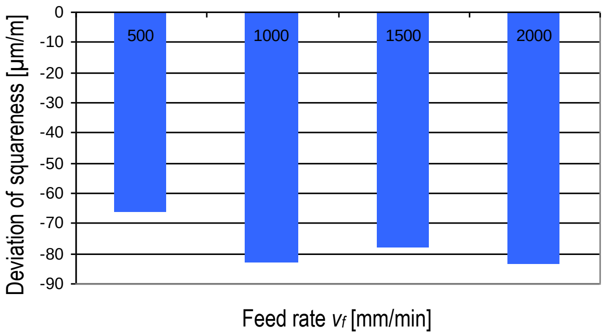

Fig. 78. Axis squareness deviations for the circle radius R=50 mm as a function of feed v_f

Like with the geometry and kinematics of milling centres, the squareness error of lathe design is caused by the deviation in the tested machine tool axis (X and Z) direction from the right angle of 90°. The axis squareness deviation can be local or can result from the lack of straightness of the machine tool guidebars over their entire length (usually due to collision or incorrect setting of the guidebars). However, with most lathes, the error is usually located near the machine tool spindle, where machining takes place. The location of the squareness error depends on the length of the workpiece. These areas are more prone to intensive wear and lateral play causing a local straightness deviation. The machine guidebars can also show deviations in the vertical plane (concavity, convexity or tilting), leading to a local straightness deviation. Moreover, the high degree of wear (causing increased in clearance during movement) implies the occurrence of straightness deviation.

One result of the lathe squareness error is the lack of squareness between the front surface and the workpiece. This leads to shape defects, primarily conicity, and if the error occurs more often and is local – to more complex shape defects of machined parts. Irrespectively of obtained results, the test should be repeated in several measurement points along the machine tool guidebars to establish whether the error is local or whether it occurs over the entire length of the guidebars. If the error is local, one should try to machine the workpiece in the area of the work space where the impact of the squareness deviation is the lowest, which – in the case of lathes – is more difficult, given the fixed position of the part attachment system. If the machine tool guidebars show the squareness error over the whole length, then, if feasible, one should run a correction of the guidebar settings, and if the guidebars are faulty, they should be replaced with new ones.

Reversal spike measurement

Reversal spikes in the numerical axes of the machine tool occur when the movement direction is changed. The main reason for the occurrence of this type of error is a too slow reaction of the servo-drive to the signal from the control system upon the direction change, as shown in Figs. 67 and 68. Fig. 79 presents the variations in reversal spikes in the CTX 310 eco lathe as a function of feed rate v_f. The reversal spikes were determined with the QC20Ballbar diagnostics system using the kinematic bar with the length of R=50mm.

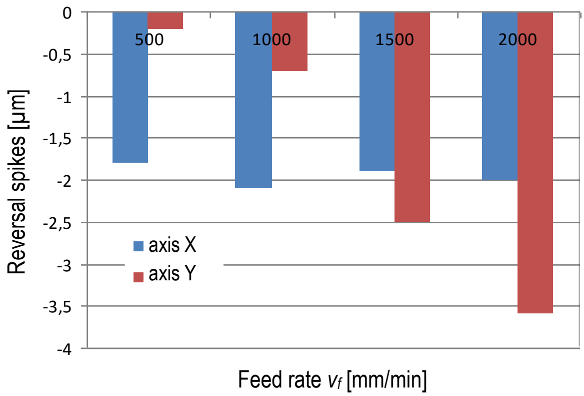

Fig. 79. Reversal spikes as a function of feed in the XZ plane of the CNC CTX 310 eco plane by DMG

The Z axis reversal spikes for the set feed rates are as follows: for v_{f1}=500mm/min, -0.2µm; for v_{f2}=1000mm/min, -0.7µm; for v_{f3}=1500mm/min, -2.5µm; for v_{f4}=2000mm/min, -3.7µm. On the basis of the data given in Fig. 79, one can claim that the decrease in the Z axis reversal spikes is almost directly proportional to the increase in feed rate. The values of the reversal spikes in the X axis are similar to ahave a sinusoidal pattern sinusoidal and are equal to: -1.8µm (for v_{f1}=500mm/min), -2.1µm (for v_{f2}=1000mm/min), -1.9µm (for v_{f3}=1500mm/min), -2.0µm (for v_{f4}=2000mm/min).

Analysis of the reversal spike results

Fig. 80 presents the relationship of reversal spikes as a function of feed rate. A detailed description of reversal spikes is given in Chapter 5.1.

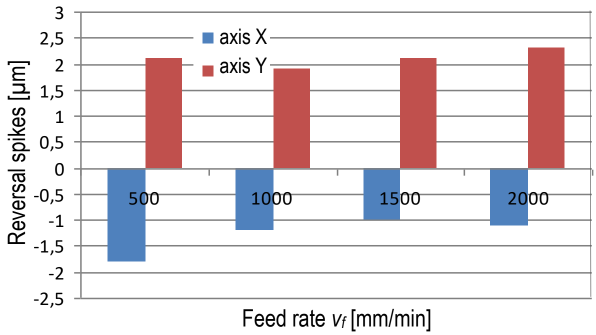

Fig. 80. Reversal spikes as a function of feed in the X-Y plane, for R=50mm and angle of 360°

The lowest value of reversal spikes in the X axis of-1µm is observed for v_{f3}=1500mm/min, whereas for the Z axis is obtained at v_{f2}=1000mm/min and equals 1.9µm. The highest reversal spikes for the Z axis can be observed for the feed rate of 2000mm/min, whereas for the X axis – for v_{f1}=500mm/min. The results are 2.3µm, -1.8µm, respectively. The error is especially visible in machine tools with an indirect measurement system. In order to remove the error, one should get rid of the cause, i.e., to delete clearances in the measurement or drive systems. It is also possible to compensate the reversal spikes directly in the machine tool control system, but this requires performing precise position accuracy measurements over the entire length of axis movement [14].

5.4. Prediction of the roundness and squareness deviations of the CNC machine tool axis

In practice, the use of immediate diagnostic measurements enables the assessment of machine condition and the taking of repair actions. Nevertheless, we cannot predict a future condition of the machine. It is often difficult to clearly state whether the machine tool meets the expected requirements. This may result from a limited number of performed diagnostic measurements due to savings of a non-productive time of machine operation. When running local tests, only a very small axis range in the work space is tested, which hampers a holistic and complex assessment of machine tool errors. As a result, the possibility of predicting CNC machine tool deviations and errors is of crucial importance. Forecast methods allow us to assess the machine condition beforehand, without running diagnostic tests.

The main objective of the tests was identification and quantitative assessment of selected CNC machine tool errors with the use of a telescopic ballbar as well as creation of a prognostic model for CNC machine tool axis roundness and squareness deviations. An attempt was made to forecast the machine tool geometric accuracy on the basis of time series based on measurements performed in a period of twelve quarters. The forecast methods applied in economy were used, including the simple moving average and weighted average as well as a simple model of exponential smoothing. A mathematical modification was made to the aforementioned methods, and forecasts were made based on the modified models. On the basis of obtained measurement and calculation results, final predictions concerning the machine tool axis roundness and squareness deviations were determined for the next forecast period. The forecasting process was performed in stages, taking into consideration the prepared time series.

The time series in relation to the diagnostic measurement results constitute the series of diagnostic observations, performed in equal periods of time, in a specified time frame. Fig. 81 shows a generalised form of the time series and its components.

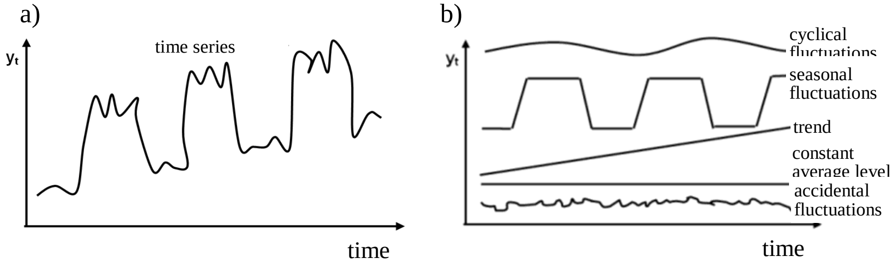

Fig. 81. General form of time series and its components: a) typical course of time series, b) time series components (random, seasonal, cyclic, trend fluctuations, fixed- average level)

Examples of time series are monthly, quarterly or yearly data of CNC machine tool errors and deviations, and they are generally provided by the diagnostic system for monitoring object condition. In the cases at hand, this object is a numerically controlled CNC machine tool and its geometric condition. Considering the time series in a context of machine and device diagnostics, one should consider the main trend and its interferences. The interferences can be assessed on the basis of average error value.

Considering the time series containing CNC machine tool errors and deviations, one can distinguish (Fig. 81b):

a) systematic component – occurs as a result of constant action of the fixed system of cause and effect, and has the form of:

– fixed (average) level of the variable – no development tendency, oscillation around a particular level,
– development tendency (trend) – long-term propensity for unidirectional changes (increase or decrease),
– intermittent component (periodical), e.g., cyclic variations – rhythmic long-term variations in a particular trend or fixed level of the variable, or seasonal variations (rhythmic variations with a cycle that does not exceed 1 year).

b) random component (random) – occurs as a result of random causes with different forces and directions.

In the time series model, the Y variable can only be expressed via the time variable or the past values or forecasts of the Y variable. Among the deviations and errors of the CNC machine tool which can serve as the forecast variable, one can distinguish roundness and squareness deviations, reversal error, reversal spikes or lateral play.

Characteristics of the Simple Moving Average

The method of simple moving average is based on a time series. Time series should be characterized by a fixed (average) level with random fluctuations. The simple moving average requires determining the variability factor of the time series v_z, providing information on the random fluctuation values. A low value of the variability factor of the tested variable v_z allows for the use of the aSimple moving average to construct a forecast for the next period/ quarter. The variability factor of the tested variable is determined from the following relation (33):

$$v_z = \frac{s}{\bar{y}} \cdot 100\% \tag{33}$$

where:
s – standard deviation of the tested variable y, $\bar{y}$ – arithmetic average of the tested variable value y (deviation).

Standard deviation necessary for determining the variable factor should be determined with the following relation (34):

$$s = \sqrt{\frac{1}{n-1}\sum_{t=1}^{n}\left(y_t - \bar{y}\right)^2} \tag{34}$$

Whereas the average arithmetic $\bar{y}$ of the tested variable y is calculated by the following equation (35):

$$\bar{y} = \frac{1}{n}\sum_{t=1}^{n} y_t \tag{35}$$

where:
n – the number of quarters, y_t – subsequent values of the tested variable y, "deviation" in particular quarters of the considered period.

Considering the changes in the variable value and assuming the height of the smoothing constant, one can observe a smaller impact of random fluctuations and slower reaction to the changes. The smoothing constant can be determined intuitively or on the basis of the lowest value of the average square prognosis error ex post s* or the average relative prognosis error ex post Ψ.

A forecast for the period/quarter t by the Simple Moving Average can be determined from the following relation (36):

$$y_t^* = \frac{1}{k}\sum_{i=t-k}^{t-1} y_i \tag{36}$$

where:
k – smoothing constant, y_i – subsequent values of the tested variable y in the particular quarters of a considered period of time t.

The forecast horizon is usually short, and because of that the method is used for making a short-term prognosis. The prognosis acceptability assessment is done on the basis of the average square prognosis error ex post s* (37).

$$s^* = \sqrt{\frac{1}{n-k}\sum_{i=k+1}^{n}(y_i - y_t^*)^2} \tag{37}$$

where:
k – smoothing constant, y_i – real value of a tested variable y in the period/ quarter t, y_t* – prognosis for a period/ quarter t.

Description of the Weighted Moving Average Method

Similarly to the simple moving average, the weighted moving average method is based on a time series. The basic assumption is that the time series of deviation change should be characteristic of a fixed (average) level with random fluctuations. The premise for using the method are high random fluctuations. This method takes into consideration the phenomenon of information dating (most recent information is of higher importance). The number of weight factors k is specified by the prognosis-maker, who retains some of their properties. The sum of the weight components w_i should always equal 1, whereas the successive weights should be higher (38) and (39):

$$w_1+w_2+\ldots+w_i+\ldots+w_k = 1 \qquad (38)$$

$$w_1<w_2<\ldots.<w_i<\ldots<w_k \qquad (39)$$

A disadvantage of the weighted average moving method is that while making a prognosis, not all variables but only k values are taken into account (previous data may also carry essential information). When k is high, it is essential to store a considerable amount of data. The average moving method makes prognosis in the following form (40):

$$y_t^* = \sum_{i=t-k}^{t-1} w_{i-t+k+1} \cdot y_i \qquad (40)$$

where:
k – smoothing constant, y_i – "deviation" of the tested variable y in the successive quarters of a considered time period t, w_i – weights given to particular observations.

The prognosis horizon is short, and hence the method is used for making short-period prognoses. This kind of prognosis is sufficient in relation to the predicted CNC machine tool error. The prognosis acceptability assessment is made on the basis of the average quarterly prognosis error ex post (s*) weighted with the following equation (37).

Measurement results and their analysis

Results of the experimental tests using the QC10 quick test provide data for making prognoses. For the sake of the analysis, the machine tool axis roundness and squareness deviations were selected. Tab. 21 lists the average values of roundness and squareness deviations of the CNC machine tool axes for the tests in particular quarters marked in the X-Y plane, performed in three successive years. The results were obtained successively on the basis of measurements made on the same numerically controlled CNC machine tool at regular time intervals.

Tab. 21. Average roundness and squareness deviations for the CNC machine tool axis for the tests in successive squares in the X-Y plane

		Arm length of telescopic kinematic bar: L=100mm, test angle: 360°											
		Year 1				Year 2				Year 3			
Deviation	Quarter	I	II	III	IV	I	II	III	IV	I	II	III	IV
Squareness deviation	µm/m	45	46	50.1	53.4	55.8	59	63.7	66	69	72	78	88
Roundness deviation	µm	15.1	16.8	18.2	18.7	19.7	19.9	20	21.3	22.1	23.1	25.1	27

The results of the tests were used to build a time series. On the basis of the prepared time series, a forecast method was selected. Taking into consideration the fact that it is easy to apply the test in practice, a modified simple moving average method is proposed. The modified model of simple moving average uses a prognosis in the following form (41):

$$y_t^{*} = \frac{1}{k}\sum_{i=t-k}^{t-1} y_i + (y_{t-1} - y_{t-k}) \tag{41}$$

where:
k – smoothing constant, y_i – subsequent values of the tested variable y, “deviation” in subsequent quarters of the considered period of time t, y_{t-1} –values of the tested variable, “deviation” in the period of time $t-1$, y_{t-k} –values of the tested variable, “deviation” in the period of time $t-k$

The classical model entails that the prognosis for a selected quarter is developed as a simple arithmetic value of deviations in three previous quarters ($t-1$, $t-2$, $t-3$). In the modified model of simple moving average (41), the prognosis is constructed as an arithmetic average of the deviation values from three previous quarters ($t-1$, $t-2$,$t-3$), adding the difference in the value of the first and the third (starting from the end) recorded result. The application of the aforementioned modified method for prognosis making allows us to use the classical method of simple moving average to predict variations in CNC machine tool errors showing a certain trend. The lack of the above mentioned modification leads to significant discrepancies between the expired prognoses and the real estimated value of deviations. For the purpose of comparison, assuming identical premises, the mathematical model for forecasting by the weighted moving average was modified too. The model assumes that the prognosis for the period/quarter *t* is made on the basis of an average value of the weighted variable predicted on the basis of *k* subsequent quarters. The values of the variable *k* from the last periods/quarters are multiplied by adequate weights, according to the rules presented in the previous chapter. In the modified mathematical model, the prognosis made by the weighted moving average method is extended to include the difference between the values of the first and the third (starting from the end) recorded result, according to the following relation (42):

$$y_t^{*} = \sum_{i=t-k}^{t-1} w_{i-t+k+1} \cdot y_i + (y_{t-1} - y_{t-k}) \tag{42}$$

where:
k – smoothing constant, y_i– subsequent values of tested variable y, “deviation” in subsequent quarters of the considered period of time t, w_i – values given to particular observations, y_{t-1} –values of the tested variable, “deviation” in the time period $t-1$, y_{t-k}– values of the tested variable, “deviation” in the time period $t-k$

Results of the performed stimulation demonstrate that the modified weighted average model can be used for making satisfactorily accurate forecasts based on time series with a trend. Three weight sets were taken into consideration in the conducted research: set 1 (0.1; 0.2; 0.7), set 2 (0.15; 0.25; 0.6), set 3 (0.2; 0.3; 0.5). Tab. 22 lists the results of CNC machine tool axis squareness deviation prognosis calculated by the simple moving average and weighted moving average with the use of the classical models, whereas Tab. 23 gives the results obtained with the modified models. Based on these results, one can observe that in the forecasts obtained using the extended model, the value of average square prognosis error ex post s* is nearly three times lower than in the forecasts made with the classical models. The lower values of prognosis error ex post s* point to higher better forecasting abilities of the models.

Tab. 22. CNC machine tool axis squareness deviations prognosed by simple moving average and weighted moving average using classical models

		Weight set k=3			s^* [µm/m]	y_t^* [µm/m]	prognosis
Weighted Moving Average	Weights I	0.10	0.20	0.70	**6.12**	**84.40**	
	Weights II	0.15	0.25	0.60	6.61	**83.10**	
	Weights III	0.20	0.30	0.50	7.11	**81.80**	
Simple Moving Average					8.08	**79.33**	

Tab. 23. CNC machine tool axis squareness deviations prognosed by simple moving average and weighted moving average using classical models

		Weight sets k=3			s^* [µm/m]	y_t^* [µm/m]	prognosis
Weighted Moving Average	Weights I	0.10	0.20	0.70	2.37	**100.4**	
	Weights II	0.15	0.25	0.60	2.24	**99.1**	
	Weights III	0.20	0.30	0.50	**2.22**	**97.8**	
Simple Moving Average					2.49	**95.33**	

As the results of numerical stimulations listed in Tabs. 22 and 23 demonstrate, the best forecasts of the axis squareness deviation were obtained for the modified model of weighted moving average with the set of weights (0.2; 0.3; 0.5), for which the prognosis is y^*=97.8µm/m and the ex post error is s^*=2.22µm/m.

The improved model accuracy led to a higher correlation between the expired forecasts and the experimental results. Fig. 82 shows a comparison of the CNC machine tool axis squareness deviations as a function of time and the forecasts made by the simple moving average method according to the classical model (Fig. 82a) and according to the modified model (Fig. 82b).

For the purpose of comparison, a numerical stimulation was performed, and the differences in the values of expired forecasts and axis squareness deviation forecasts for the I and IV quarter using the weighted average method were presented. Figs. 82c and d present the variations in to CNC machine tool axis squareness deviations versus time and the forecasts made using weighted moving average according to the classical (Fig. 82c) and the modified (Fig. 82d) models. According to data in the graphs presented in Fig. 82, the modified form of base equation for the weighted average method eliminates the discrepancies between the expired forecast and the results of the Ballbar test, and therefore can be used for making an accurate forecast for a given moment/ future time.

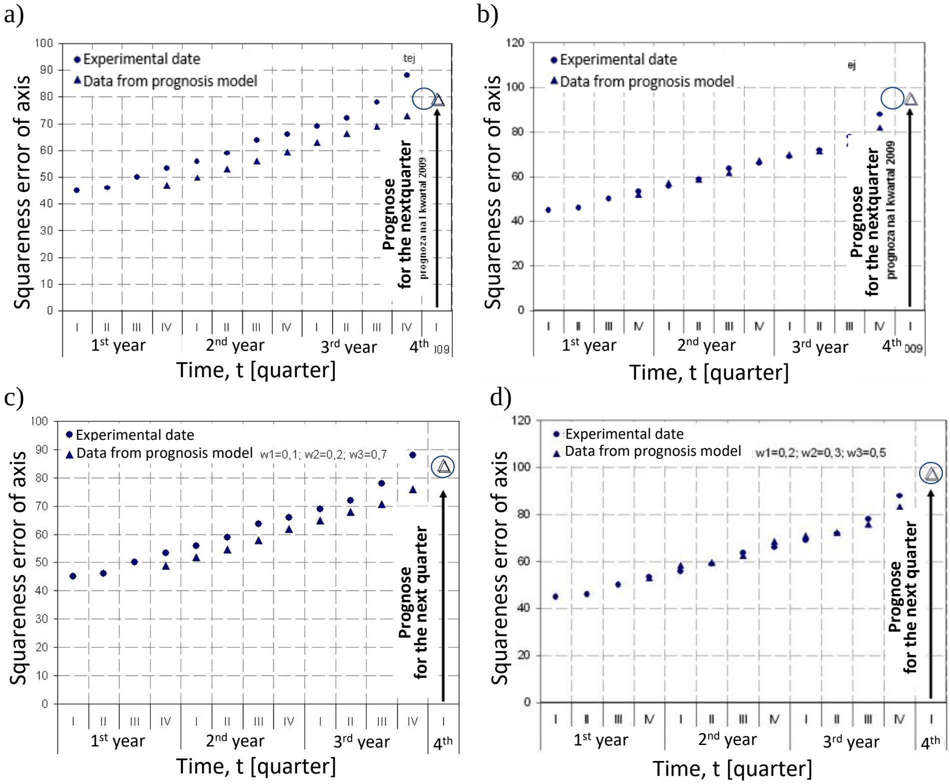

Fig. 82. CNC machine tool axis squareness deviations as a function of time and the prognosis by: a) simple moving average method according to the classical model, b) simple moving average according to the modified model, c) weighted moving average according to the classical model, d) weighted average according to the modified model

Tab. 24 presents the results of roundness deviation forecasts by the simple moving average and the weighted moving average using classical methods. As the data in Tab. 24 indicate, the values of prognosis error ex post s^* are within the range of 1.52÷2.07μm, which – compared to the results obtained with the modified models of simple moving average and weighted moving average – indicates that they are approx. 30% higher (Tab. 25). This demonstrates that the modification of mathematical models has contributed to the improvement of prognostic capabilities. The values of average square prognosis error ex post (s^*) decreased to a level within the range of 0.73÷0.96μm.

Tab. 24. Roundness deviations prognosed by simple moving average and weighted moving average using classical models

		Weight set k=3			s^* [µm]	y_t^* [µm]	prognosis
Weighted Moving Average	Weights I	0.1	0.20	0.70	**1.52**	**26.23**	⟵
	Weights II	0.15	0.25	0.60	1.65	**25.94**	
	Weights III	0.20	0.30	0.50	1.79	**25.65**	
Simple Moving Average					2.07	**25.06**	

The prognosis acceptability assessment for the roundness deviation on the basis of the ex post error s^* indicates that the final prognosis should be the one in which the value of roundness deviation is y_t^*=28.96µm, according to the modified simple moving average method. Fig. 83 shows the variations in roundness deviation as a function of time and the prognosis determined by the simple moving average, according to the classical (Fig. 83a) and the modified (Fig. 83b) models.

Tab. 25. Roundness deviations prognosed by simple moving average and weighted moving average using modified models

		Weight sets k=3			s^* [µm]	y_t^* [µm]	prognosis
Weighted Moving Average	Weight I	0.10	0.20	0.70	0.96	**30.13**	
	Weights II	0.15	0.25	0.60	0.87	**29.84**	
	Weights III	0.20	0.30	0.5	0.80	**29.55**	
Simple Moving Average					**0.73**	**28.96**	⟵

Looking at the comparison of the experimental values of roundness deviation and the corresponding expired prognoses, it can be noted that a far better fitting was obtained for the modified model (Fig. 83b).

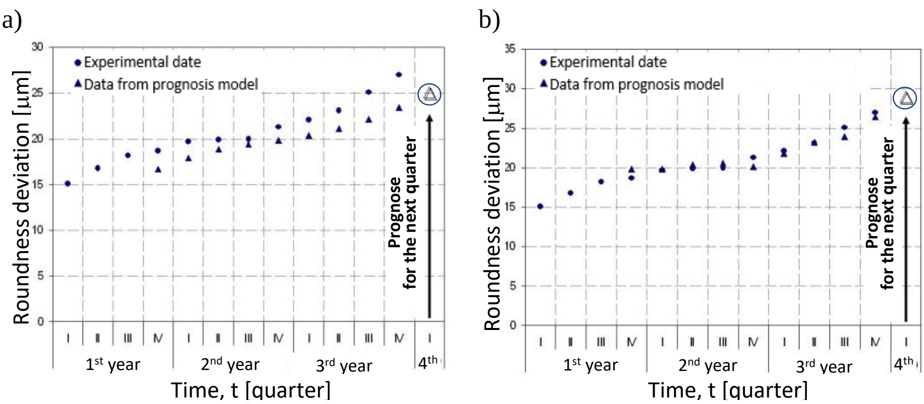

Fig. 83. Roundness deviation as a function of time and the prognosis determined by the simple moving average method a) using the classical model, b) using the modified model

The data presented in Fig. 83 were obtained from the prognostic process by the simple moving average method for the lowest prognosis error value ex post $s^*=0.73\mu m$ (Tab. 25) and the highest $s^*=2.07\mu m$ (Tab. 24).

Fig. 84 shows the variations in roundness deviation as a function of time and the prognosis made by the weighted moving average according to the classical (Fig. 84a) and the modified (Fig. 84b) models.

On the basis on the numerical stimulation results presented in Fig. 84 one can clearly claim that the degree of fitting of the modified model is higher than that of the classical model. On the basis of prognosis acceptability assessment performed in accordance with the average square prognosis error ex post s^*, it can be observed that the modified model enables the prediction of the CNC machine tool roundness deviation values with greater accuracy.

a) b)

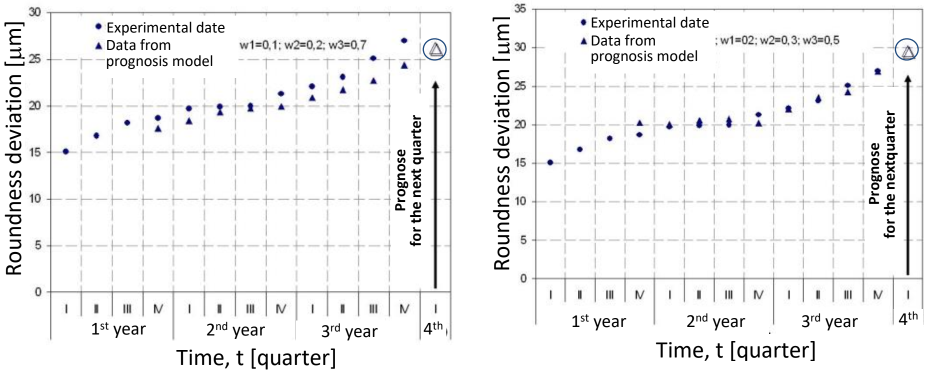

Fig. 84. Roundness deviations as a function of time and the prognosis determined by weighted moving average: a) according to the classical model, b) according to the modified model

The graphs (Fig. 84) present the prognosis results obtained by the weighted moving average, from the best (the lowest prognosis error value $s^*=0.80\mu m$) to the worst (the lowest prognosis error ex post $s^*=1.79\mu m$).

5.5. Summary and conclusions

The experimental results have demonstrated that machine tool errors identified with the telescopic kinetic bar have a local nature. The results reveal that in some measurement areas the deviations are significantly higher than in other locations. The measurement points in which the deviations are the highest are those marked as 3, 6, 9, 12, 15. The points are located in one line parallel to the X axis. Such positioning suggests the local nature of wear of the machine tool guidebars. An ad hoc remedy for reducing the impact of such a high axis squareness deviation on the machining results is to change the position of the handle in which the workpiece is mounted on the machine tool. Because the axis squareness deviation occurs in other measurement points as well, the only way to reduce it is to correct the guidebar settings or – should this not help – their replacement.

The comparison of errors identified for the FV-580A and HSC 105 machining centres has shown significant differences between the axis squareness deviations in the tested X-Y plane. The results point to higher wear of the FV-580A centre. This is reflected in the fact that the squareness deviation obtained for this machine is a twice as high as the values obtained for other tested machines. To ensure the required accuracy of movements and positioning precision, current repairs are not enough. It becomes vital to perform frequent systematic diagnostic testing combined with making adjustments, e.g., in control systems, drives, etc. In the case of the numerically controlled CTX 310 eco lathe, the key task is to determine and specify the main geometric errors that have the greatest impact on the size and shape accuracy of produced parts. Like in the case of milling machines, these errors include roundness deviations, axis squareness deviations, reversal errors and reversal spikes. Most of these errors depend on the rate of feed. The higher the feed rate is, the higher the deviation values become. However, in the tested case, for the three applied feed rates of v_{f1}=500mm/min, v_{f2}=1000mm/min, v_{f4}=2000mm/min, the roundnesscircularity deviations increased slightly and amounted to 11.1µm, 11.3µm and 11.6µm, respectively. For the feed rate v_{f3}=1500, there was a local increase in the deviation value to 13.6µm, which disturbed the linear nature of obtained results. The deviation from this trend may result from local errors in the measurement control systems of the machine tool. To minimise the negative impact of this deviation on the machine tool work, it is essential to reduce other errors and make sure that a relevant drive reduction is used and examine the machine for any interference to its control system. The experimental findings have also shown that the observed squareness deviation is non-linear as a function of feed rate v_f. To prevent this error from increasing, it is essential to inspect the condition of the guidebars and correct their settings. The study has also revealed that the increase in feed rate leads to the increase in reversal spikes in the Z-direction. The value of reversal spikes in the X axis remains unchanged. Reversal spikes in the X axis are non-linear, while in the Z axis they are close to linear. Reversal spikes can be caused by control system defects and considerable delay in the servo-drive reaction. Backlash does not depend on feed rate but can results from incorrect adjustment of the drive, e.g., incorrect clearances or clearances resulting from the wear of machine tool components.

An important area connected with reliable operation of CNC machines and devices is rational and scientifically proven prediction of machine tool future condition, in other words – forecasting of their condition. The possibility of forecasting machine tool errors poses a challenge for modern companies. It is widely known that performing experimental tests requires stopping the machine's work, which is often hardly feasible in industrial conditions. Excluding the machine from the production process and testing it over its entire work space lead to considerable economic losses. Prognostic models can significantly reduce these losses. The knowledge in the field of predicting machine future condition and prognostic models enables the prediction of machine condition and – with proper maintenance – reaching utilitarian goals. This work presented relatively simple prognostic methods that are easy to implement in any company. The indicated quarterly intervals of technical condition assessment are optimized and economically justified. The use of methods for predicting machine condition can lead to decreasing the number of diagnostic tests even by 50%, which, in consequence, may bring measurable utilitarian benefits.

Errors and deviations occurring in machine tools are a grave problem because they affect the machine tool operational accuracy, which – in turn – affects the quality and accuracy of products. If machine errors exceed acceptable values, specified as the set machining tolerances, the machine tool requires adjustment, repair or regeneration, and sometimes even replacement of old components.

6. MACHINE TOOL THERMOGRAPHIC DIAGNOSTICS

CNC metalworking machine tools heat up as a result of power loss in their area. This is due to the fact that in engines, servo drivers and electronic spindles almost the whole of energy coming from the electric network is transformed into work. One of the effects of this transformation is the generation of heat causing deformations of machine components. These deformations have a significant impact on the machine's technical condition, geometric errors, operation, and the accuracy of produced parts. The main effects of heat-induced deformation of machine tool components include the displacement of machine working systems relative to each other, the disturbance of control functions (predominantly, positioning accuracy), increased resistance to motion of machine components, and lower effectiveness of the machine [13, 53, 58, 87, 89–91, 95, 118, 119, 129]. A detailed analysis of thermal phenomena occurring in machine tools, a thorough balance of machine drive energy loss as well as a balance of machine tool-affecting heat waves provide a basis for the development of adequate diagnostic procedures during tests. This study presents an example approach to a thermographic analysis of technological machines. The proposed diagnostic procedures, including preparatory works, diagnostic assessment and conclusions, are of a universal nature. Therefore, they can be used for assessing the thermal state of almost any machine. The investigation of thermal phenomena occurring in machines (particularly, machine tools) during their operation has long been recognized useful for the assessment of machine work accuracy. An analysis of thermal images can be an important source of information about machine technical condition, production quality and the mounting of kinematic pairs constituting a thermal burden to the machine body, as well as a rich source of data about machine tool features affecting its practical application [13, 58, 87, 91, 129].

Due to the action of heat waves generated in the machine tool and carried away to the environment (transported by heat radiation and convection), there occurs a particular thermal state of the machine. The thermal state of the machine tool is described by the distributions of temperature on the surface of the machine body and other machine working subassemblies. As far as machine tools for metals are concerned, the internal sources of heat (resulting from power loss) include engines, bearing units, kinematic transmissions (idler, pulleys, etc.), clutches, kinematic pairs (guidebars, slides, etc.), pumps, electric and electronic systems. The external sources of heat include heat sources accompanying the machining process (cutting zone), other sources of heat located in the vicinity of the machine tool, radiation, etc. The temperature distribution describing the thermal state of a machine tool and its values depend on the location and efficiency of heat sources as well as the intensity rate of heat fluxes transferred to the environment. The balance of heat fluxes affecting the machine tool demonstrates that the main role in heat transfer is played by forced convection and convective heat transfer, emission and heat transfer to the surface. Given the uneven distribution of heat sources and their intensity, the degree of machine body heating is uneven too. Therefore, the thermal stability of a machine tool is also varied. It depends in equal measure on the heating of a machine tool but also on forced convection conditions, lubrication conditions, the emissivity of lacquers used for machine body protection, the way of connecting individual elements of the body, the occurrence of body wall ribbing and riser heads.

The location of heat sources in the machine tool and their effectiveness have a direct impact on heat deflections and hence on the size and shape accuracy of machined parts. A machine tool with high accuracy, i.e., with stable geometry, is particularly indispensable in finishing conditions, i.e., in the work conditions which are only slightly different from idle run. With this in mind, one may ignore the heat generated in the cutting zone, focusing instead on the heat sources located outside the machine tool body as well as on those located outside but affecting it through convection, radiation or induction. Most frequently these are components of the main and feed drive kinematic systems, including engines, bearings, gear and belt transmissions, clutches and brakes, as well as the components of hydraulic and pneumatic systems such as servomotors, pumps, glands, distributors, etc. The share of individual heat sources in the total energy balance varies depending on the type of heat source, its working conditions, and machine tool design [58, 91, 125]. For the selected kinematic structure of the lathe drive (Fig. 85), the sources of heat are located partly in the lathe spindle and the reducer under the headstock, as well as in the machine's belt transmission system and the engine system located outside the body. The energy balance determined for the afore-mentioned drive shows that spindle bearings have a large share in the total energy loss (47.3%). The share depends on the complexity of the drive kinematic structure and is usually higher than that in the modern variable speed drives of simple kinematic design. An important source of heat is the energy loss in electric engines (19.1%). In general, however, the engines are located outside the machine tool body, so only a small portion of the heat flux is transferred to them. The degree of energy loss in the engine depends on its mechanical and electric efficiency, which is a function of loading the engine with motion resistance in the drive and, possibly, of the cutting force.

A too high input power to the engine and, simultaneously, a higher temperature of work at constant motion resistance in the remaining part of the drive can be a sign of engine wiring failure, too small slot between the rotor and the stator (e.g., due to increased clearances in the bearings), or too high friction between rotor bearings.

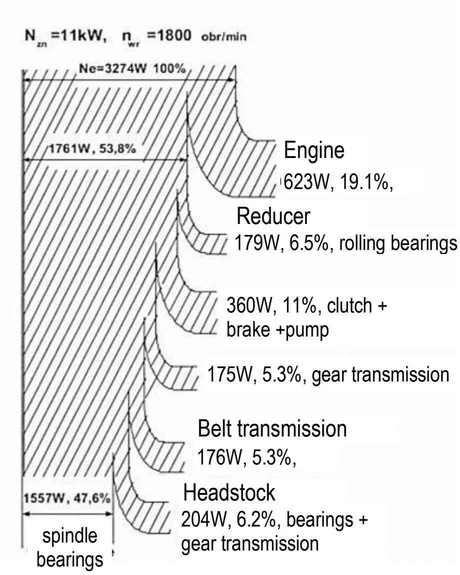

Fig. 85. Example balance of energy loss in the main lathe drive [91]

The range of rolling bearings used in machine tools is quite varied in terms of size, type and nature of load. In most bearings of machine tool kinematic systems, the dimensional changes resulting from the heating up of bearing node elements are too small to induce a negative clearance. Such bearings have a positive clearance and there is no internal load. If, however, the working temperature of the bearing is too high or the bearing design (e.g., angular bearing) requires a preload, then high internal loads can occur during their work, leading to high power loss. This happens primarily in spindle bearings which – due to spindle stiffness – are mounted with small clearances or preload. The thermal state of the spindle bearing nodes depends on a set of factors connected with:

- the type, size and work conditions of bearings, including lubrication factor, maintenance clearances, rotation velocities, load conditions,
- heat transfer conditions,
- elastic and thermal features of the node components,
- the size and shape of spindle system components.

Increased power losses in the bearings can result from a too high preload or the setting of too small clearances during machine mounting, inadequate oil viscosity, the mixing of oil with lubricant in the case of bearings lubricated with plastic lubricant, badly performed lubrication cycle, i.e., when the lubricant in newly lubricated bearings spreads unevenly, or a significant change of heat transfer conditions in the bearing node. Power losses in gear transmissions are, like in the case of bearings, the sum of hydro-dynamic and load losses. The load transmitted through the gear is the result of loading the drive with the cutting force, which hardly has any effect on the bearing load. Together with an increase in the cutting force, the losses in the gear transmissions rapidly increase, although the gears themselves are very efficient. On the other hand, the power losses in the shaft bearings where the gears are mounted do not depend on the power transmitted by the drive. In the idle run conditions, when the gear loads are only a result of the motion resistance of kinematic pairs, the dependence of the power loss on the load is practically non-existent. Taking this into consideration, the gears have a very small share in the power loss. Increased power losses in gears may result from too small clearances between the gear teeth, incorrect position of the shaft axes, chamfering of the shaft axes, too high roughness of the gear teeth surface, too high viscosity of the lubricating oil, or too extensive lubrication.

Machine tool speed boxes are often equipped with electromagnetic clutches and brakes. When the machine is switched on, the power losses in the clutch are a result of electric power absorbed by the winding. When the machine is switched off, they result from residual magnetism and friction between the plates wetted with oil. The degree of energy loss varies depending on the transmitted moment and the type of clutch. Apart from overload, increased power losses in the clutch may result from an insufficient axis clearance set during machine mounting, too extensive lubrication of the clutch or low quality of the plates.

6.1. Balance of heat sources in machine tools

The thermal state of a machine tool described with the temperature distribution on individual surfaces of its body results from complex interactions of heat fluxes transferred to the machine tool and carried away from it to the environment. Heat transfer in machine tools occurs via convection, radiation and induction. Fig. 86 shows the share of particular heat flux types and their potential variations. The selection of drive unit working conditions and heat transfer conditions depends on the power losses in heat sources located in the machine tool such as engines, bearings, clutches, belt transmissions and gears, kinematic friction pairs, electric and electronic elements, etc.

The distribution and effectiveness of heat fluxes and the heat flow rate intensity transmitted to the environment have a significant impact on the temperature and its distribution. The main factors of heat transfer are: forced convection (flux $Q_{\alpha W}$), free convection, (flux Q_{α}), thermal emission (flux Q_{λ}), heat transfer inside individual units (Q_{λ}) with particular heat capacity, and induction to the surface denoted as flux Q_k. The main sources of heat are power losses (Q_{SM}) resulting from engine work and the heating-up of the wiring, losses caused by mechanical transmission work, friction, e.g., in guidebar systems and bearing nodes, as well as elastic deflections. Other sources of heat include external effects such as the ambient temperature, the machine-affecting sunlight change or neighbouring heat sources. It is difficult to precisely estimate their effect, as individual heat flux depend on various factors and interrelated couplings. Free convection plays a major role primarily in the case units of considerable size or those heated up to a high temperature such as headstocks. In the case of surfaces with a high heating level, the heat flux transmitted to the surroundings in the form of radiation may be crucial. It is sometimes compared to the heat flux generated by free convection.

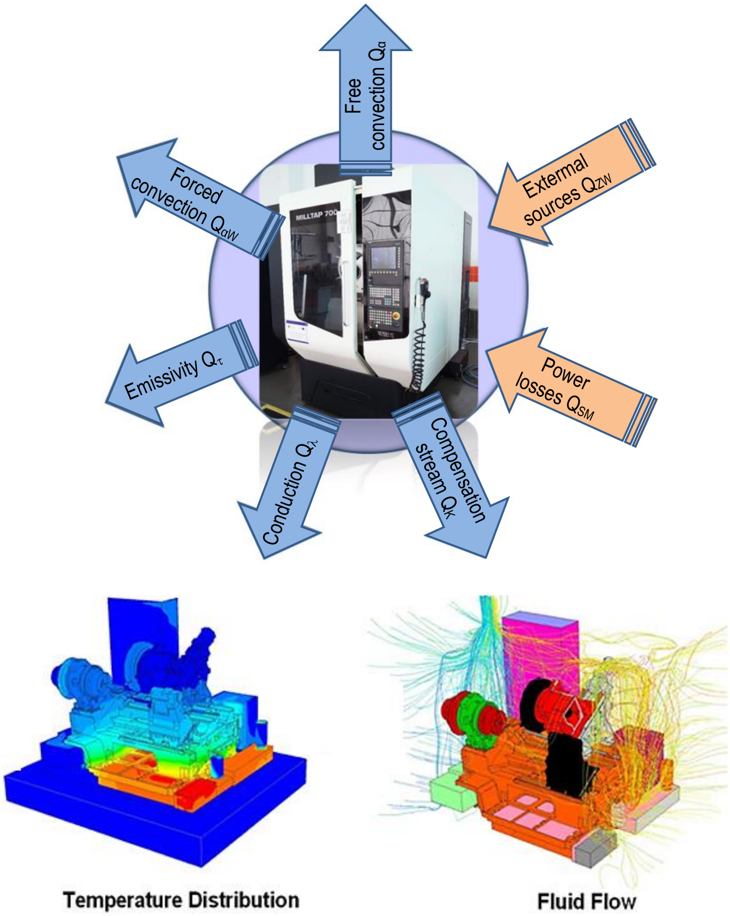

Fig. 86. Balance of heat fluxes affecting the machine tool [153]

Machine tool thermal state

The temperature distribution in the walls of the machine tool body and inside it results from the combined effects of all heat fluxes that are generated in the machine tool and transferred by means of convection, radiation and induction (Figs. 86 and 87). Moreover, the temperature distribution depends on the degree of heating and other factors such as:

- forced convection conditions,
- lubrication conditions,

– the way of connecting the machine bodies,
– emission factors of lacquers covering the machine body,
– the presence of riser heads and ribs on the external and internal walls of the machine body, etc.

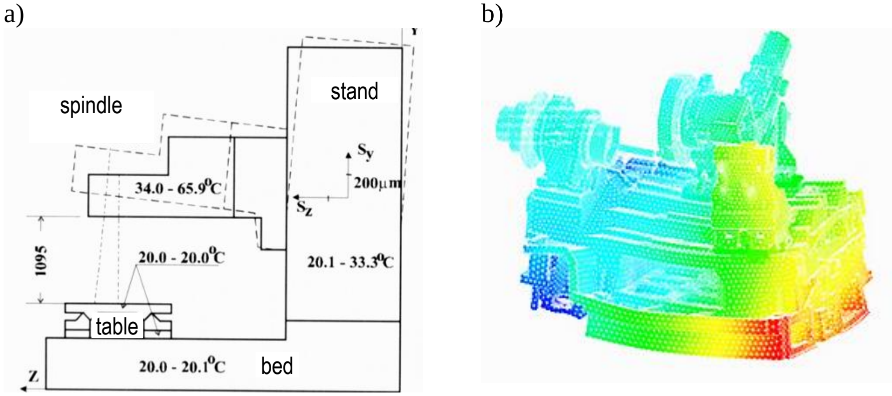

Fig. 87. Effects of heating up machine tool units: a) machine tool deformations, b) displacement model [91, 153]

Machine tool thermal stability may vary. The level of heating up the machine body varies to a high degree and is unequal. The highest temperature occurs in the spindle of the machine (Fig. 87), and the effect of temperature on the machine tool accuracy describing the displacement of the spindle axis in relation to the table depends on the machine tool design and its geometric dimensions. Even the smallest deformation of tall stands can lead to significant machine tool errors.

6.2. Design and technological methods for reducing machine tool thermal deflections

In machine tools, almost all energy supplied from the power network to the drive engines is exchanged into work resulting, among others, in the generation of heat. The essential components of the heat generated in the machine tool include:
– heat generated during current flow in the electric engine wiring,
– heat generated by the friction work of drive engines and transmissions, flow losses in hydraulic systems and others,
– heat generated in the machining process.

Due to different intensity rates and locations of heat sources as well as varying conditions of heat exchange with the environment by individual machine units, the basic components of the MHWT system (machine tool – holder – workpiece – tool) have different temperature values, which leads to thermal deformations impairing the machining accuracy. In addition, the temperature generated in the cutting zone has s significant, albeit indirect effect on the quality of machined surfaces. Measured temperatures are correlated with obtained surface parameters after machining, thermal deformations of the machine units, etc.

Among the above-mentioned heat components, the first two have the greatest impact on the deformation of the MHWT system, particularly in precise machining processes such as burnishing, coordinate drilling, and rolling. The heat generated in the machining process is emitted at the highest rate during roughing. However, elastic deformations of the MHWT system due to the action of the cutting force are much higher than thermal deformations, hence the latter can be ignored due to their secondary importance. Thermal deformations of the machine tool can be reduced via machine tool design by:

– reducing the amount of heat emitted in the vicinity of machine components and systems, the deformation of which has the greatest impact on machining accuracy,
– reducing variations in the temperature distribution, which can be done by artificial cooling of the heat sources or by heating up lower-temperature machine zones,
– using materials with low thermal expansion and thermal compensators.

Other methods for reducing the negative effect of thermal deformations on machining accuracy which can be employed by the machine tool user include:

– maintaining constant temperatures in rooms and protecting precise machine tools from exposure to local sunlight and hot air flows,
– avoiding production stoppages leading to machine cooling,
– maintaining a steady rhythm of flow production in machine tool lines,
– performing regular inspections and repairs to eliminate the sources of excessive heat emission.

6.3. Procedures for machine tool thermographic diagnostic testing

One may claim that the effectiveness of diagnostic tests depends to a high degree on the proper use of adequate diagnostic procedures. The literature and standards provide advice and guidelines concerning prognostic procedures. The procedures presented below were developed and discussed in works [13, 53, 87, 91, 129, 132, 146]. They primarily concern the problems such as:

– testing the value and direction of spindle axis displacement,
– testing thermal states of machine tools,
– testing the thermal stability of machine tools,
– testing the stiffness of spindle systems in varying thermal conditions,
– determining the emission capacity of machine components.

A starting point for developing a diagnostic procedure is to determine a “measurement path,” frequently on the basis of heuristic techniques determining a symptom model. The direct measures of technical condition assessment of mechanical objects (geometric dimensions of elements, geometry of kinematic pair cooperation, trajectory of working units) are determined as the features of the object's condition. It is known that the indirect measures of technical condition assessment reflecting the extent of wear processes and object operation quality are called symptoms, or measurable interchangeable values describing the technical condition. The symptoms (or thermal images, as they called in thermovision diagnostics) as the measures of diagnostic signals oriented at damage assessment, are determined on the basis of testing operating objects. According to the presented rules, one may apply specified procedures of diagnostic testing for selected cases. Every diagnostic procedure includes:

- preparatory works,
- diagnostic assessment,
- inference.

Determination of the value and direction of spindle axis displacement

Preparatory works

Preparatory works in the assessment of spindle axis displacement value and direction include:

- selection of general indicators of the thermal state for the front and back wall of the headstock body for a particular machine tool in order to assess the displacement of headstock slots in the vertical and horizontal positions with the highest displacement correlation factors,
- determination of the functional relationships between the selected thermal state indicators and the correct displacements of the axis bearing slots (e.g., linear function),
- determination of standard generalised values of the indicators for a particular machine tool design (on the basis of calculations or measurement of the correctly operating machine),
- determination of standard displacements, according to the developed functional relationship.

Diagnostic assessment

The diagnostic assessment of machine tool spindle axis value and displacement direction includes:

- capture of thermal images of the front and back wall of the machine body in a thermally stable state (e.g., after work time of t=120min if $n=n_{max}$),
- determination of general thermal indicators,
- comparison of the indicators with the values considered as standard.

Inference

A machine tool can be considered fault-free if, on the basis of the thermal images and discussed procedures, it is found that:

- the displacement of the slot axis on the front and back wall do not exceed the standard values (permissible limits),
- the direction of spindle chamfering is in line with the standard,
- the chamfering in the vertical and horizontal directions does not exceed the standard values (permissible limits).

Any deviations from the above-mentioned criteria indicate incorrect performance, mounting or operation of the machine. On the basis of machine tool design documentation, it is possible to explain why a given criterion is not satisfied.

Machine tool thermal state tests

Preparatory works

Preparatory works in the testing of machine tool thermal state include:

- selection of surfaces that are significant due to the location of heat sources in order to assess the degree of their heating,
- determination of the heating degree assessment indicator (e.g., the temperature in the vicinity of heat sources or average temperature).

Diagnostic assessment:

The diagnostic assessment of machine tool thermal state includes:

- capture of thermal images of selected surfaces in a thermally stable state (e.g., after the time of work t=120min, where $n=n_{max}$),
- several repetitions of the test.

Inference

Heat sources in machine tools are stable when the observed thermal states are repeatable (within the standard of e.g. 5%). A too high non-repeatability indicates incorrect operating conditions of the kinematic pairs or other heat sources. The causes of machine instability should be estimated on the basis of the design documentation of a particular machine tool.

Machine tool thermal stability tests

Preparatory works

Preparatory works in the thermal stability testing include:

- selection of thermal state indicators (e.g., average temperatures measured along the diagonals on the front and back wall of the headstock),
- determination of the work cycle of a machine tool (e.g., $n=n_{max}$ (20min), n=0 (10min), $n=n_{max}$ (20min), n=0 (10min), etc.),

– determination of the amplitude of changes in the selected indicators for a fault-free machine tool.

Diagnostic assessment

The diagnostic assessment of machine tool thermal stability includes:

– capture of thermal image at the end of every work cycle and every break cycle,
– determination of the amplitude of thermal state changes on the basis of the thermal images,
– comparison of the determined amplitude with the standard one.

Inference

Thermal stability is acceptable when the thermal state amplitude in the completed cycle does not exceed the standard amplitude. When the standard amplitude is exceeded, this points to incorrect operation of kinematic pairs or other sources of heat resulting from incorrect performance, mounting or operation of the machine tool.

Spindle unit stiffness assessment

Preparatory works

Preparatory works in stiffness assessment of machine tool spindle units include:

– selection of the spindle and frame heating indicators (e.g., average temperature of the front surface of the spindle end and average temperature of a surface fragment of the headstock front wall in the vicinity of a double-row bearing),
– determination of the difference between the temperature increase in the spindle and the selected fragment of the machine tool front wall with the correctly mounted bearing in a thermally stable state (e.g., after the time of work t=120min, where $n=n_{max}$).

Diagnostics assessment

The diagnostics assessment in machine tool thermal stability testing includes:

– capture of thermal images of a selected fragment of the front wall and the front of the spindle in a thermally stable state (e.g., after the time of work t=120min, where $n=n_{max}$),
– determination of heat indicators for the spindle and frame on the basis of the captured thermal images,
– comparison of obtained results with the standard difference.

Inference

The bearing is mounted correctly when the difference between the heat indicators of the spindle and the frame only slightly differs from the standard one. When the difference between the values of the spindle and frame heat indicators is bigger, this shows that the load carries only one row of rolling elements in the bearing, which, in effect, considerably reduces the stiffness of the spindle unit. When the difference is very high, this can indicate that the value of post-mounting clearance in the bearing is too low (provided that bearing lubrication was done correctly).

Machine element emissivity test

In diagnostic thermovision testing of technologic machines one can ignore the impact of atmospheric attenuation due to a small distance between the machine and the thermovision device. Prior to proceeding with the diagnostic thermovision tests, it is definitely recommended to determine the effective emissivity of all machine components. The use of table date can contribute to significant measurement errors [78–82].

6.4. Test stand and the diagnostic test

The aim of the research is a diagnostic assessment of selected CNC machine tools using a non-contact thermographic system. The thermal states of some machine tools and their thermal stability were assessed and the time of reaching the constant time value by a first-order inertial section was determined. The first-order inertial section describes the thermal changes in the tested object as a function of time. The objects of the research were three numerically controlled machine tools: CTX 310 ecoline CNC lathe, DMC 635 3-axis vertical machining centre and the DMU 65 monoBLOCK 5-axis machining centre (Fig. 88). All the tested machines are used for didactic and scientific purposes, and their general technical condition can be described as very good.

To determine the guidelines for testing, a thorough analysis of the scientific literature on diagnostic procedures was done. The groups of procedures described in the literature are determined for standard machine tools [53, 87, 91, 129, 132, 146]. Taking into consideration the technical capacity and user-friendliness, the procedures for diagnostics thermographic tests were tailored to the requirements for the tested CNC machine tools. Among them, the aforementioned procedures were selected including: machine element emissivity assessment, determination of the time constant, thermal states and thermal stability assessment. The tests were performed using the V20 thermovision camera. It is a laboratory camera equipped with a thermoelectrical cooling detector made of mercury cadmium telluride, produced by VIGO System S.A. It enables the measurement in three temperature ranges (range 1: 0–60ºC, range 2: 0–350ºC, range 3: 350–850ºC) with image geometric resolution of 240x240 points. The camera and the THERM-V20 software (for Windows) constitute a data capture and analysis system, which enables remote temperature measurements, complex analysis of obtained results and effective data management.

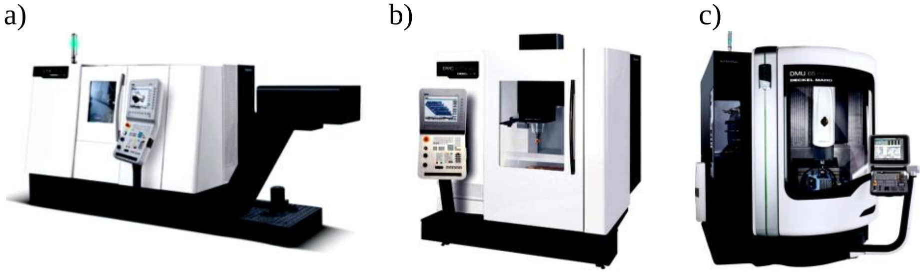

Fig. 88. Machine tool testing: a) 3-axis ecoline lathe CTX 310; b) vertical 3-axis ecoline machining centre DMC 635; c) vertical 5-axis machining centre DMU 65 monoBLOCK

Thanks to the system, detailed scanning parameters were determined, including the object emissivity ε, the ambient temperature T_{ot}, the distance from the object to the camera l, the number of measurements k and the time distance between the measurements Δt. The analysis of obtained results was facilitated thanks to the capabilities of the system allowing the definition of any area inside the thermograms (section, rectangular, point, ellipsis, polyline-limited area), the determination of minimum, maximum and average temperatures in the tested area, the measurement of temperature along the selected line marked in the thermogram, image filtering with digital filters: averaging, median, erosive, dilatant, and sharpening (Fig. 89).

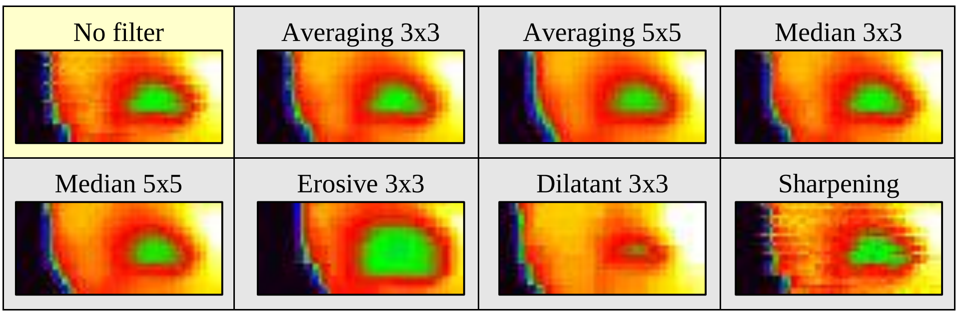

Fig. 89. Types of filters in THERM-V20

Selected results of digital filtration of the front end of the numerically controlled lathe spindle for particular types of filters are given in Figs. 90 and 91.

The measurements were performed in air-conditioned rooms at the ambient temperature of T_{ot}=20°C. The distance of the camera from the tested object was set to l=1.5m.

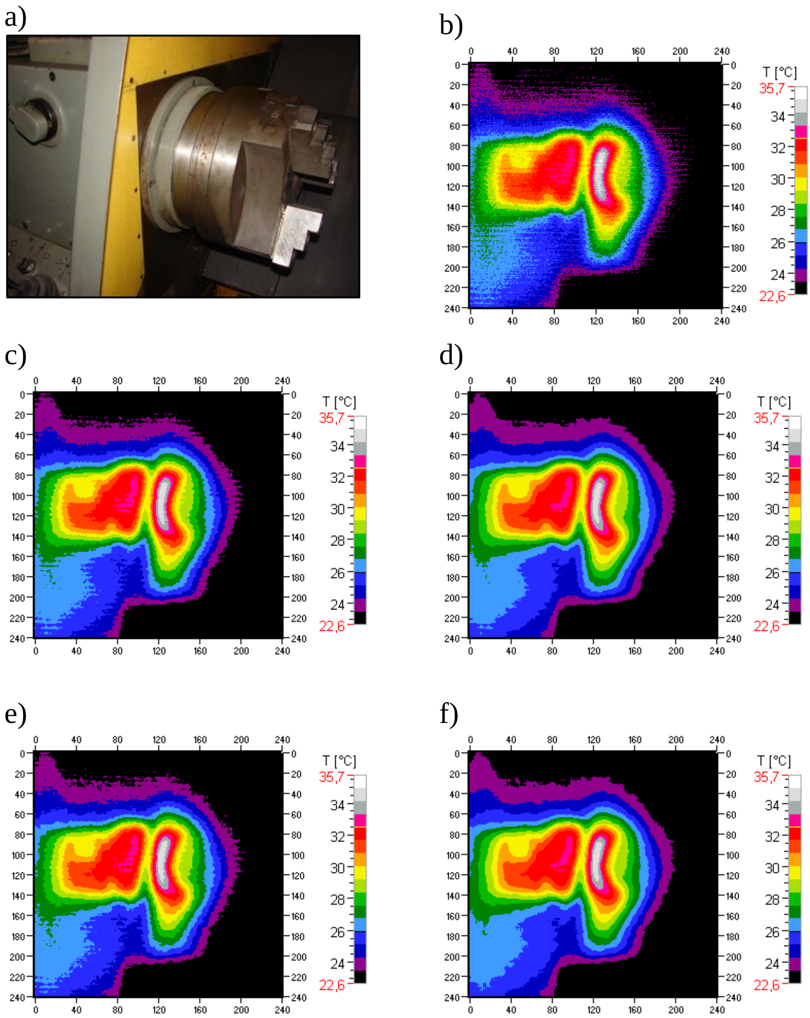

Fig. 90. Thermograms of the tested object after filtering with predefined filter machining: a) tested object, b) without digital filtration, c) after filtering with averaging filter of 3x3, d) after filtering with averaging filter of 5x5, e) after filtering with median filter of 3x3, f) after filtering with median filter of 5x5

The scope of the research involved capturing thermal images of selected surfaces during machine tool heating at the following set parameters:

- operation mode: idle run (conditions similar to finishing),
- rotational speed of the spindle: n=3500 rpm,
- thermal image capture time: t=120min,
- time distance between the measurements: Δt=2.5min.

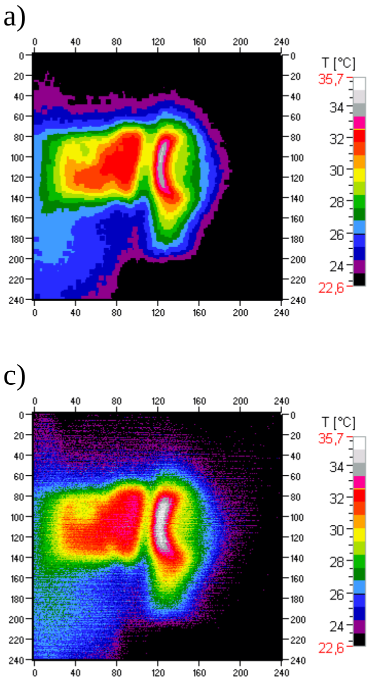

Fig. 91. Thermograms of the tested object after pre-defined filtering: a) after erosive filtering, b) after dilatant filtering, c) after intensifying filtering

6.5. Diagnostic measurement results and their analysis

Machine part element emissivity

Given the significant effect of the emissivity factor ε on measurement results, the best option is to determine its value for every surface of the tested machine tool. The emissivity ε of the key machine surfaces was determined in experimental tests. With this aim in mind, an indirect joining method was applied, using PT100 resistance temperature sensors attached to selected machine tool surfaces and a data recorder. The setting of the emissivity parameter ε in the THERMA programme environment of the V20 thermographic camera was changed such so as to maintain the same temperature in the thermogram and the data recorder alike. Ultra-red radiation suppression by the atmosphere was ignored due to atmosphere homogeneity and the lack of pollution, as well as the short distance between the camera lens and the tested object. The average value of emissivity for the tested surfaces was ε=0.96. The emissivity was determined for four different temperatures (20°C, 30°C, 40°C, 50°C).

Tested surfaces were selected according to the procedures established in the preparatory works. In each of the tested machine tools, the main tested area was the spindle bearing area (Fig. 92). Taking into consideration reflection caused by the metallic surface of the spindle and the handle, the surfaces were covered with a delustrant.

a) b) c)

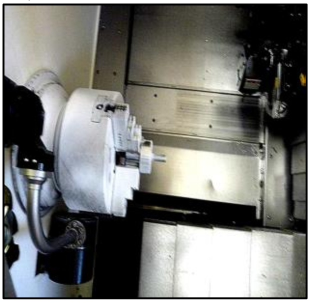

Fig. 92. Test stand and its preparation: a) CTX 310 Ecoline lathe spindle, b) DMC 635V machining centre spindle, c) DMU 65 monoBLOCK machining centre spindle

Determination of the time constant

The first step towards determining the time after which the machine tool reaches the thermally stable state was to select test surfaces in the vicinity of heat sources. The next step was to capture thermal images of the selected surfaces. An analysis of obtained thermograms showed that the highest heating intensity is located in the spindle bearing areas. Therefore, representative measurement points were selected in these areas. In order to compare the temperature increase in each of the areas, three points were selected for every machine tool. Examples of the thermograms with marked points are presented in Fig. 93.

After the capture of thermal images, results obtained from the thermograms were analysed. The results clearly demonstrate that the process of machine tool preheating has the characteristics of the first-order inertial element, expressed with the following equation (43):

$$h(t) = k(1 - e^{-\frac{t}{T}}) \cdot 1(t) \tag{43}$$

where:
k – system strengthening, $T=T_t$ – time constant, t – time.

Fig. 94 presents the method for determining the time constant T_t, as a tangent to the thermally unstable state in the initial moment until exceeding the stable value. Time constants T_t for particular machine tools determine the time after which the tested object reaches the thermally stable state. The measurements should be performed at constant rotational speed with a constant time step, e.g., every 2.5min.

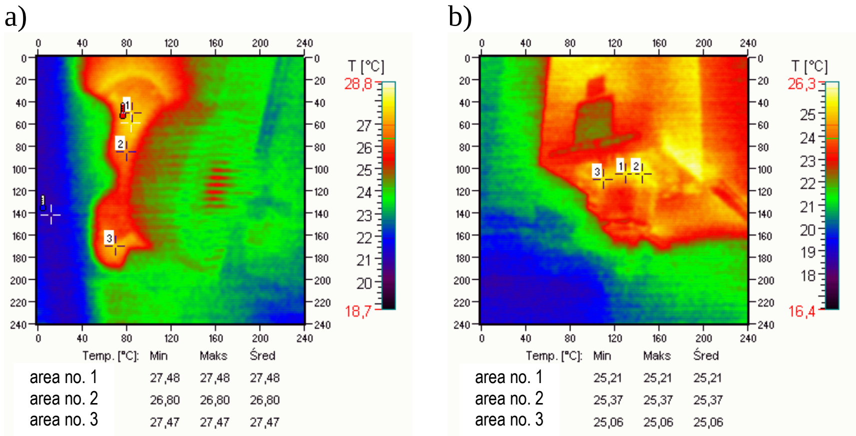

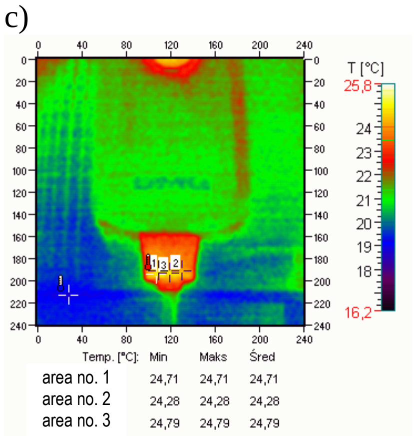

Fig. 93. Thermal images of the tested machine tools:
a) CTX 310 Ecoline lathe spindle,
b) DMC 635 V vertical machining spindle,
c) DMU 65 monoBLOCK machining centre spindle

Diagnostic assessment should be based on an analysis of temperature increases in the successive time units at a selected point in the thermograph. An example of variations in the temperature as a function of time obtained for the CTX 310 eco lathe is shown in Fig. 94. The measurement point should be located in the area of machine tool intensive heating. Based on the temperature as a function of time relationship presented in Fig. 94, time constants were determined, after which one can assume that the machine tool is in the thermally stable state.

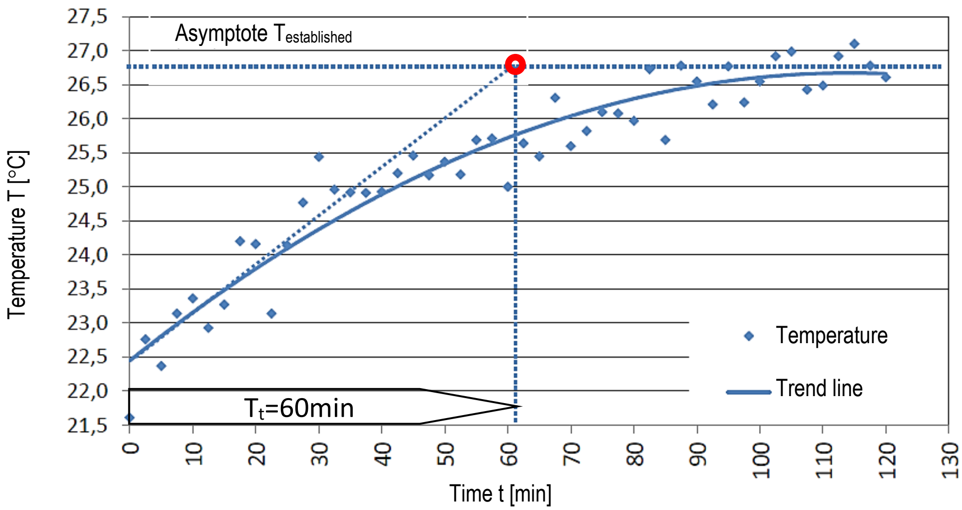

Fig. 94. Temperature versus time for the CTX 310 eco lathe

Fig. 95 shows an example of the temperature distribution T_{ij} as a function of time in the thermally stable state for selected measurement points in relation to the average temperatures. The data in Fig. 95 demonstrate that the time constant T_t is equal to T_t=60min.

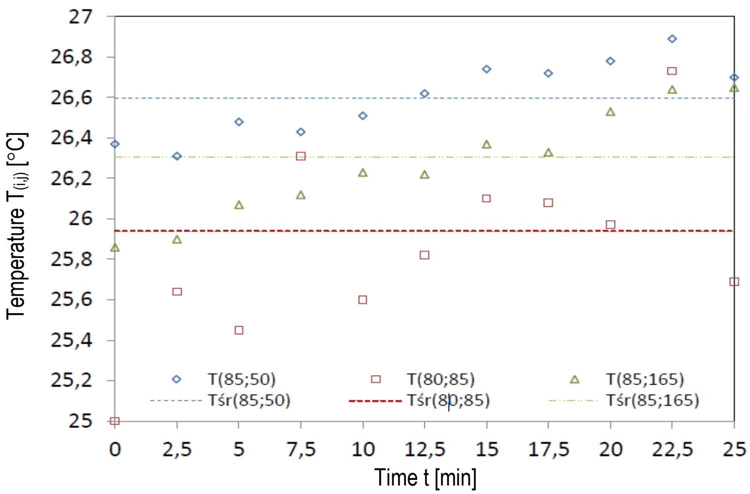

Fig. 95. Temperature distribution T_{ij} versus time t, in the stable thermal state (i.e., after the time T_t) for selected measurement points in relation to the average temperature (CTX 310 Ecoline late)

A comparison of time constants T_t for the tested CNC machine tools in relation to the time constant for the standard machine tool, T_{kl} , is presented in Fig. 96. As the data demonstrate, the lowest time constant was obtained for the DMU 65monoBLOCK 5-axis machining centre. The low value of time constant T_t for the standard machine tool results from an open design of this type of machines, i.e., the design has the minimum number of covers and protection for inhibiting heat transfer via radiation and convection.

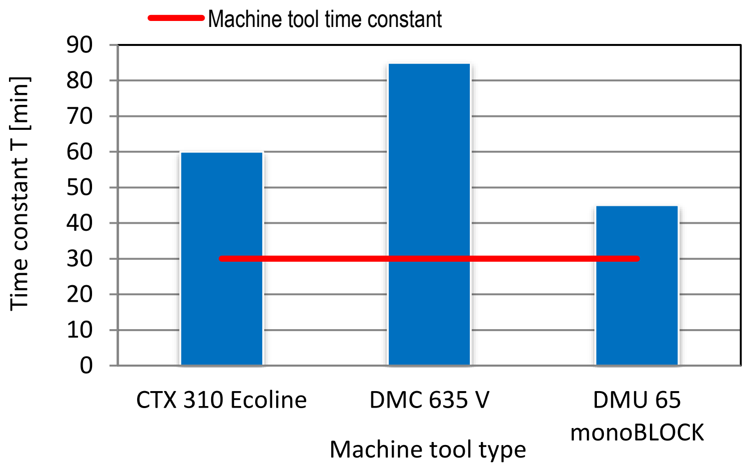

Fig. 96. Comparison of time constants T_t for the tested CNC machine tools in relation to a time constant of the classic machine tool T_{kl}

Machine tool thermal state assessment

Three stages were selected to assess the machine tool thermal states. The first one involved preparatory works to determine the machine areas significant for the assessment of their heating degree. The selection depended on the location of heat sources. It was also essential to select estimates serving as a basis for the assessment of heating degree. The next stage was the process of diagnostic assessment to capture thermal images of the selected surfaces. The image capture should be done in a stable thermal state obtained at specified rotational speed and after the specified time T (time constant of the first-order inertial element). Tab. 26 presents the results of temperature measurements in the selected measurement points for the stable thermal state of the CTX 310 eco lathe.

The measurements were repeated a number of times for the same stable conditions. The maximum value of the difference between the successive thermal states of the tested machine tools was assumed to be equal to 2%. As Tab. 26 demonstrates, for the states marked 1, 3, 4 as well as 9 and 10 the differences in the temperature exceed the assumed accepted value.

Tab. 26. Results of temperature measurements in selected points, in the stable thermal state for the CTX 310 eco lathe													
Sing.	t	T in points. (85;50)	The difference between the states in points. (85;50)	ΔT	|δT|	T in points (85;50)	The difference between the states in points. (80;85)	ΔT	|δT|	T in points. (85;165)	The difference between the states in points (85;165)	ΔT	|δT|
	[min]	[ºC]	[%]	[ºC]	[%]	[ºC]	[%]	[ºC]	[%]	[ºC]	[%]	[ºC]	[%]
heat. =>	60	26,37	-	-	-	25	-	-	-	25,86	-	-	-
1	2.5	26.31	0.23	0.29	1.09	25.64	**2.56**	0.3	1.16	25.9	0.15	0.41	1.56
2	5	26.48	0.65	0.12	0.45	25.45	0.74	0.49	1.89	26.07	0.66	0.24	0.91
3	7.5	26.43	0.19	0.17	0.64	26.31	**3.38**	0.37	1.43	26.12	0.19	0.19	0.72
4	10	26.51	0.30	0.09	0.34	25.6	**2.70**	0.34	1.31	26.23	0.42	0.08	0.3
5	12.5	26.62	0.41	0.02	0.08	25.82	0.86	0.12	0.46	26.22	0.04	0.09	0.34
6	15	26.74	0.45	0.14	0.53	26.1	1.08	0.16	0.62	26.37	0.57	0.06	0.23
7	17.5	26.72	0.07	0.12	0.45	26.08	0.08	0.14	0.54	26.33	0.15	0.02	0.08
8	20	26.78	0.22	0.18	0.68	25.97	0.42	0.03	0.12	26.53	0.76	0.22	0.84
9	22.5	26.89	0.41	0.29	1.09	26.73	**2.93**	0.79	3.05	26.64	0.41	0.33	1.25
10	25	26.7	0.71	0.1	0.38	25.69	**3.89**	0.25	0.96	26.65	0.04	0.34	1.29
Average		26.6	0.36	0.15	0.57	25.94	1.86	0.30	1.15	26.31	0.34	0.20	0.75
Standard deviation		0.187	0.202	0.09	0.32	0.462	1.369	0.22	0.85	0.271	0.262	0.13	0.51

Figs. 97÷99 show the successive thermograms of the spindle area with the temperature distribution that were obtained for the CTX 310 eco lathe (Fig. 97), the DMC 635 eco 3-axis machining centre (Fig. 98), and the DMU 65 monoBLOCK 5-axis machining centre (Fig. 99).

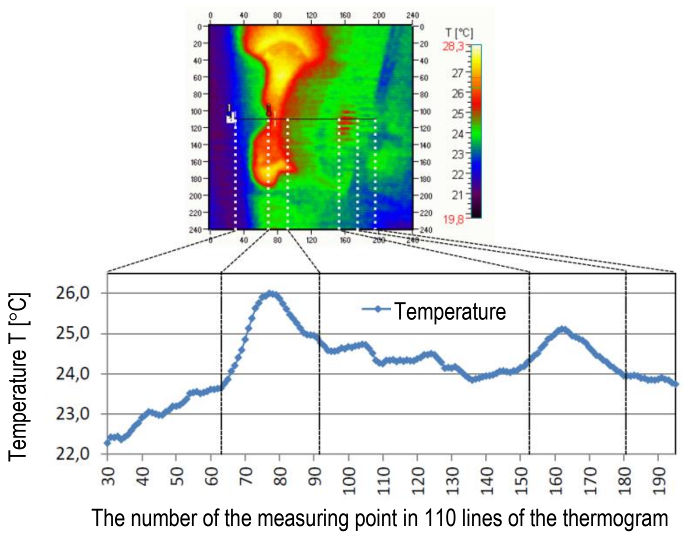

Fig. 97. Thermogram of the CTX 310 eco lathe spindle surface with temperature distribution in 110 lines of the thermogram

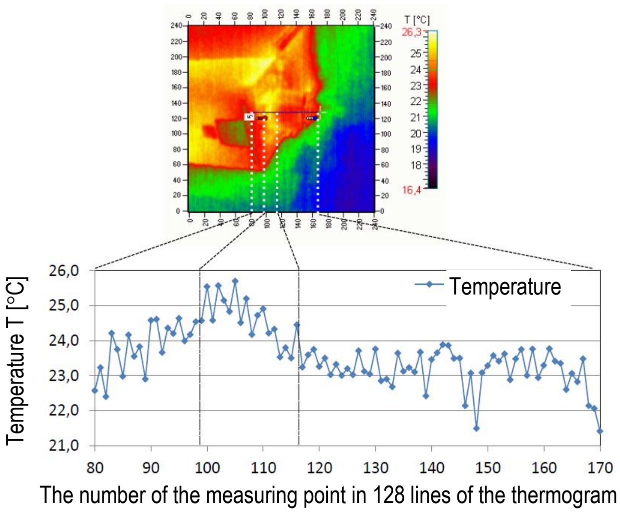

Fig. 98. Thermogram of DMC 635 eco machining centre spindle surface with the temperature distribution in 128 lines of the thermogram

The last stage of the tests as inference. The basis for considering a heat source as stable was the repeatability of the obtained thermal states. Taking into consideration the technical condition of the machine tools, the maximum value of differences between the successive thermal states was set at the level of 2%. The lack of repeatability means incorrect operating conditions of the kinematic pairs and the influence of other heat sources. The basis for the assessment of causes of the lack of heat source stability should be the machine design documentation.

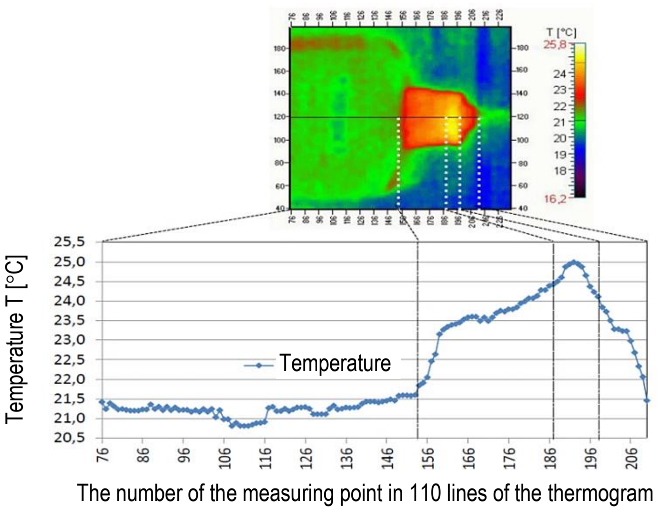

Fig. 99. DMU 65 Monobloc machining centre spindle area thermograph with temperature distribution in 110 lines of the thermogram

Fig. 100 shows a comparison of the standard average temperature deviations in the selected measurement points of the tested machine tool. The data shown in this figure demonstrates that the smallest difference in the average temperature in the selected points of the tested machine tools is characteristic of the DMC 635 eco 3-axis machining centre.

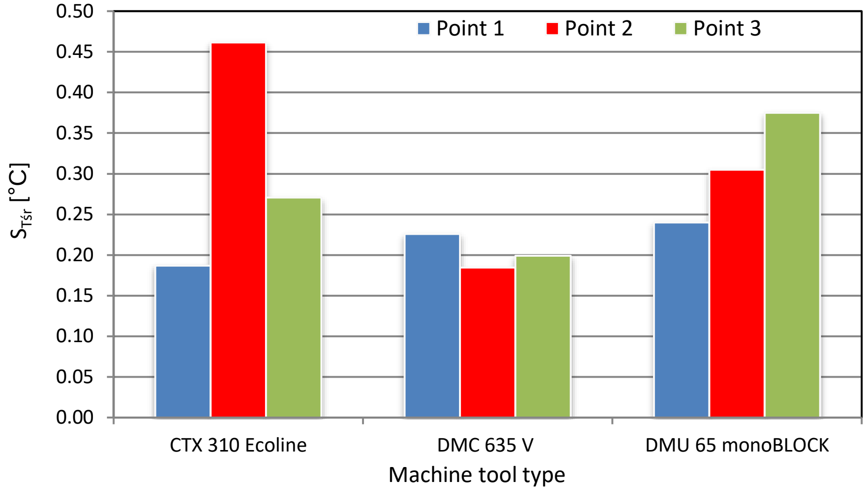

Fig. 100. Comparison of the standard average temperature deviation in selected points of the tested machine tool

Machine tool thermal stability assessment

The assessment of the machine tool thermal stability was divided into three parts. The first part involved preparatory works to select thermal state indicators, including the minimum, maximum and average values of the temperature. This part of the assessment also involved the setting of machine tool work cycle and the determination of the amplitude of changes in the selected indicators. The selection was made with respect to significant machine tool surfaces, as in the case of the previous procedures. The diagnostic assessment of thermal stability was based on capturing thermal images of the selected machine tool surfaces. Results were recorded at the end of every work cycle and break. Tab. 27 lists the temperature measurement results and the results of thermal state differences obtained from thermal stability measurements of the CTX 310 eco lathe in the selected measurement points, according to the work cycle specified in the preparatory part.

Tab. 27 proves the lack of thermal stability of the tested lathe in the initial period of temperature stabilisation. This is proved by the exceeded percentage difference in thermal state temperatures, both in the first (5.4%) and in the second (8.1%) test series. During the diagnostic assessment, the amplitudes of thermal state changes were also determined and compared with the standard amplitude.

The last stage of the tests involved the process of inference. Thermal stability was considered to be acceptable if the difference in thermal state changes does not exceed the standard amplitude. If this was not the case, it was inferred that the operating conditions of the kinematic pairs are inadequate, and the effect of other heat sources associated with incorrect machine design, mounting or operation is found to be significant. Fig. 101 presents a comparison of the determined percentage temperature changes between particular thermal states. These results pertain to the thermal stability tests of the selected machine tools. Fig. 102 presents a comparison of the average temperature values for machine tool stabilization in relation to the determined stabilisation temperature of the standard machine tool.

Tab. 27. Results of temperature measurements in selected points according to a determined work cycle for the CTX 310 eco lathe

Sing.	Spindle rotation n	Time	Temp. in point (85;50)	The difference between subsequent states	Temp. in point (80;85)	The difference between subsequent states	Temp. in point (85;165)	The difference between subsequent states
1	[rpm]	[min]	[ºC]	[%]	[ºC]	[%]	[ºC]	[%]
2	0	0	22.22		21.61		21.91	
Heating up the machine								
3	3500	10	23.33	5.00	23.36	**8.10**	22.96	4.79
4	0	15	23.27	0.26	23.27	0.39	22.89	0.30
5	3500	25	24.54	**5.46**	24.14	3.74	23.88	4.33
6	0	30	24.43	0.45	24.06	0.33	23.75	0.54
7	3500	40	25.59	4.75	24.93	3.62	24.91	4.88
8	0	45	25.51	0.31	24.81	0.48	24.81	0.40
9	3500	55	26.16	2.55	25.69	3.55	25.58	3.10
10	0	60	26.10	0.23	25.51	0.70	25.49	0.35
A determined thermal state								
11	3500	70	26,51	1,57	25,6	0.35	26.23	2.90
12	0	75	26.45	0.23	25.53	0.27	26.14	0.34
13	3500	85	26.70	0.95	25.69	0.63	26.65	1.95
14	0	90	26.61	0.34	25.58	0.43	26.52	0.49
15	3500	100	27.04	1.62	26.52	3.67	27.02	1.89
16	0	105	26.91	0.48	26.47	0.19	26.91	0.41
17	3500	115	27.12	0.78	26.82	1.32	27.3	1.45
18	0	120	27.03	0.33	26.61	0.78	27.21	0.33

The testing of heat phenomena intensity is also applicable to conventional machine tools. Examples of such tests can be found in the author's works [53, 129] and studies [13, 91]. The testing of thermal phenomena intensity in the operation of machines and technological devices is a source of valuable data enabling the assessment of their operational accuracy [13, 53, 91, 129]. An advantage of this type of testing is that the diagnosis can be performed under load in a non-contact way. Moreover, the number of areas detected with the thermovision system is higher than in the case of other methods (e.g., contact method) (Fig. 103). As a result, the quality of obtained data about thermodynamic phenomena, heat exchange or cooling condition is also improved.

a)

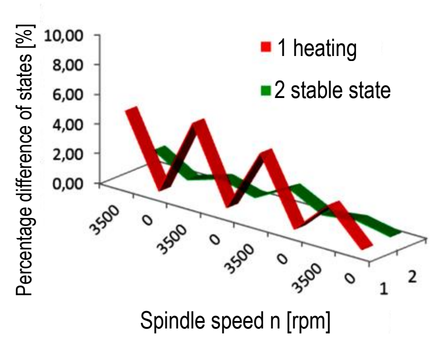

b)

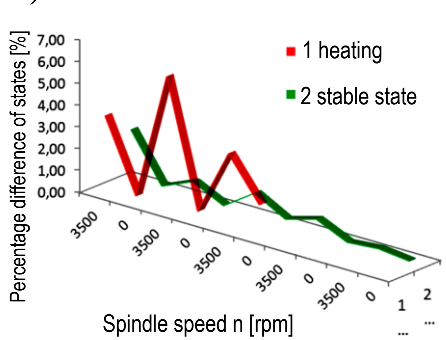

c)

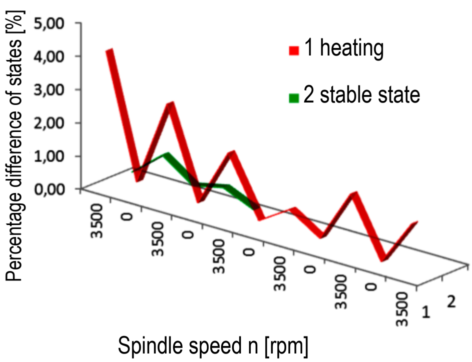

Fig. 101. An example recorded percentage heat change share between particular thermal states, during thermal stability test: a) CTX 310 eco lathes, b) 5-axis DMU 65 monoBLOCK machining centre, c) 3-axis DMC 635 eco machining centre

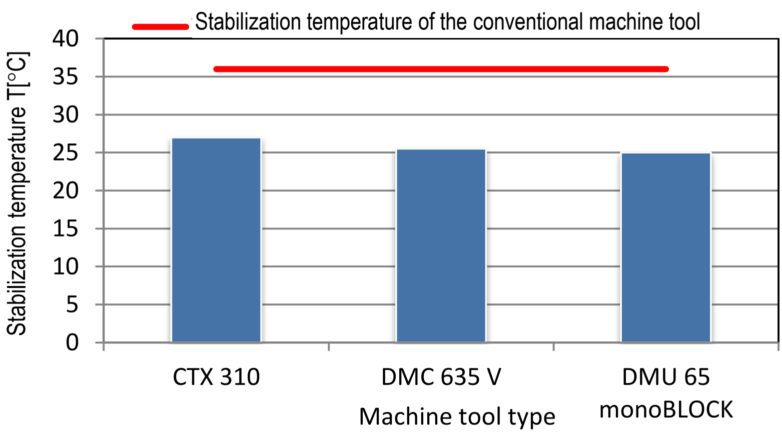

Fig. 102. Comparison of average stabilisation temperatures in CNC machine tools in relation to the example stabilisation temperatures of a classic machine tool

The impact of heat on the machine design results in deformations which can cause the impairment of control functions, the displacement of working units relative to each other, the excessive motion resistance of machine components, reduced efficiency of the machine, etc.

Results of the author's analyses demonstrate that the use of thermography leads to the early and precise detection of irregularities of machines and processes performed on these machines, heat loss assessment, the detection of damage correlated with the thermal state of the machine and the entire production lines (damage detection), increased machine operation safety thanks to quick and relatively accurate information about the occurrence of thermal changes due to damage progression, reduced losses in emergency states, reduced maintenance costs, elimination of operator information overload, increased information accuracy, support for the operator's decision in abnormal states and emergencies, diagnostics of machining machine tools for metals, monitoring of the machining process, etc., [13, 58, 129].

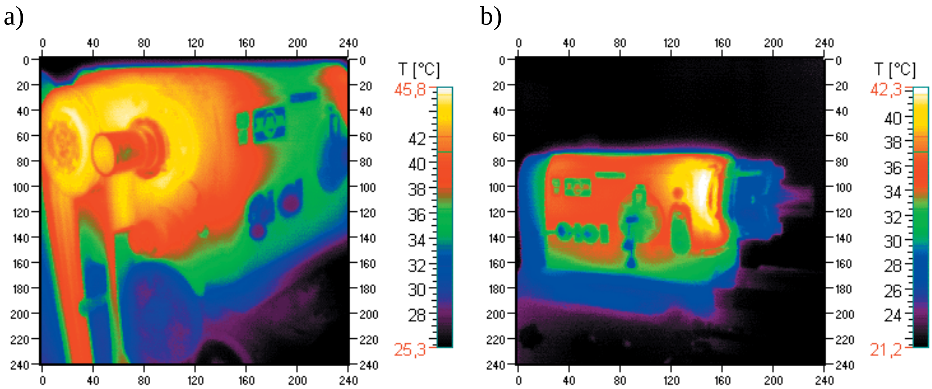

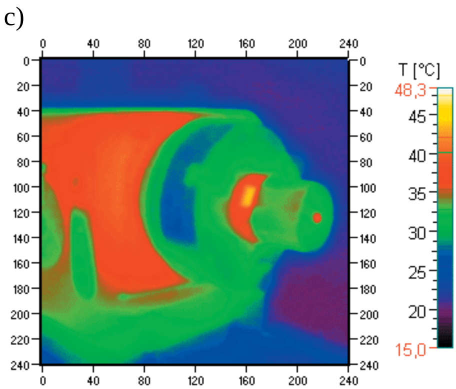

Fig. 103. Thermal images of the lathe: a) belt and bearing drive units, b) headstock unit, c) spindle bearing front end body (measurements were performed with a thermographic V20 camera from VigoSystem S.A.)

With long-lasting measurements, an ideal solution is to use a thermographic camera connected to a computer with an interface to capture data in a scheduled and automated way, without supervision on the part of the operator.

6.6. Summary and conclusions

The assessment of technological machine thermal state and its stability is one of the basic tasks concerning machining accuracy maximisation. The thermal state of a machine tool and its thermal stability can be a proof of the occurrence of damage processes in the machine kinematic nodes. The assessment of technological machine thermal state can be performed on the basis of an analysis of the temperature distribution in critical areas of the machine tool or on the basis of temperature increase dynamics analysis. The accuracy and reliability of machine tool thermal state assessment depends, among other things, on the measurement tools. The use of a non-contact thermography-based method increases the accuracy of obtained results and allows a full visualisation of temperature distribution on the tested surface. The use of a thermographic system for the thermal diagnostics of technological machines significantly reduces the necessity of using costly and time-consuming diagnostic procedures based on point measurements. The diagnostic symptoms in the form of thermograms obtained from the performed measurements serve as a basis for determining the current condition of the technological machine. They clearly indicate the location of heat sources in the machine tool. This allows an accurate identification of the areas where energy loss is the highest.

The analysis of all obtained results showed that in most cases, the maximum acceptable temperature is exceeded (max. 2%) by the DMU 65 monoBLOCK machining centre. This was observed both during machine preheating and in the stable thermal state of the machine. As for the CTX 310 eco lathe, the maximum acceptable temperature amplitude between the successive states was only exceeded during machine preheating. The highest difference was 8.10%. As for the DMC 635 eco machining centre, similarly to the thermal state assessment, no measurement results exceed the maximum acceptable temperature amplitude. The temperature amplitudes of DMC 635 eco are much lower than those observed for other tested machine tools. It can therefore be claimed that the DMC 635 eco machining centre has the highest thermal stability out of all tested machines. All in all, taking into consideration the fact that in all tested cased the maximum acceptable temperature amplitudes are exceeded to a very small extent and that it occurred mainly during machine preheating, all tested machine tools can be considered thermally stable.

Measurement results in the form of thermograms can serve for the diagnosis of the tested machine tool technical condition. Their accurate interpretation can help determine operating conditions, e.g., the time necessary for machine to reach a stable thermal state. The determination of the time constant helps determine the time after which the machine tool shows thermal stability. This time can be described as a period of time after which, with some probability, the parts produced on the machine will maintain their geometric repeatability (size and shape). The determination of the time constant helps maintain the steady rhythm of the production process connected with engaging particular machines into the production process in the right moment. A frequent use of thermally unstable machines may lead to size discrepancy of the products.

The assessment of heat source stability and thermal stability as well as of direction and displacement of the spindle axis enables the creation of a thermal history of the machine. Based on well-known standards, such history enables the identification of incorrect states resulting from power loss in critical friction pairs of the machine tool, electric engines, etc. The implementation of a technique for pattern recognition and limit state monitoring enables the effective prevention of wear progression, especially in the case of stochastic symptoms of machine tool failure or damage. Another way might be to implement thermovision for continuous monitoring of machine work.

The results of the thermovision tests for technologic machines can be a starting point for creating “a machine thermal history” saved in the form of thermograms constituting a properly organized “image” database. Thermograms for such database should be captured at all stages of “machine life” and which are considered by the designers and diagnosticians to be vital. The database created in this way can be used to assess the suitability for use or lack thereof of other machines of the same type and to precisely determine the time after which the machine should be repaired or replaced.

7. MONITORING OF CNC MACHINE TOOL SPINDLE ERRORS

Spindle is the critical component of every machine tool for metal. Spindles and electro-spindles in today's numerically controlled machine tools are complicated mechatronic systems of the main drive. Not only does their accuracy affect the quality of machined parts, it also has impact on the effectiveness of machining as well as the life and accuracy of a CNC machine tool. Bearing and spindle bearing mountings have a decisive effect on the accuracy of rotational axis position, the stabilisation of a rotating element (usually, the tool) and the transfer of cutting force. It should also be mentioned that the ultra-precise and high-speed spindles are among the most expensive parts of the CNC machine tool. Their control, diagnostics and proper maintenance are the key tasks in every industrial plant. To be effective, the diagnostics of spindles requires extremely accurate measurements. This study utilizes the method of spindle movement dynamics developed by Tlusty, specified in ISO 230-7:2006. It is a sampling method in real time using non-contact displacement sensors. The method enables the diagnostics of errors of transverse and longitudinal movements for any set rotational speed. Software-implemented dedicated algorithms enable the determination of parameters describing spindle accuracy, including:

- synchronous error motion,
- asynchronous error motion,
- total indicated run-out (TIR),
- total error motion,
- shift versus rpm,
- thermal drift.

Dynamic diagnostics of the machine tool spindle can be performed with spindle error analysers such as Precision Spindle Error Analyzer.

7.1. Factors contributing to spindle errors

A survey of the literature of the subject [39, 42, 57, 112, 117] reveals that machining accuracy depends not only on machine tool geometric accuracy but also spindle motion. Analysing the trends in machine tool design and machining, once can observe a tendency to increasing the cutting speed and the spindle rotational speed. Spindles, therefore, play a major role, especially in high-speed cutting (HSC). Static measurements (with immovable spindle or low rotational speed) are insufficient to determine spindle deviations due to the differences in spindle behaviour in dynamic and often unstable conditions (at very high rotational speed). The distributions of total synchronous and asynchronous errors and total indicated run-out (TIR) in high-speed conditions allow an indirect assessment of the bearing condition, clearances, insufficient stiffness or weight. CNC machine tool spindle errors, both longitudinal and radial, are shown in Fig. 104. The figure shows systematically the spindle position in relation to the spindle mounting and the theoretical spindle axis location in the vertical (longitudinal) direction (Fig. 104a) and in the radial direction (Fig. 104b).

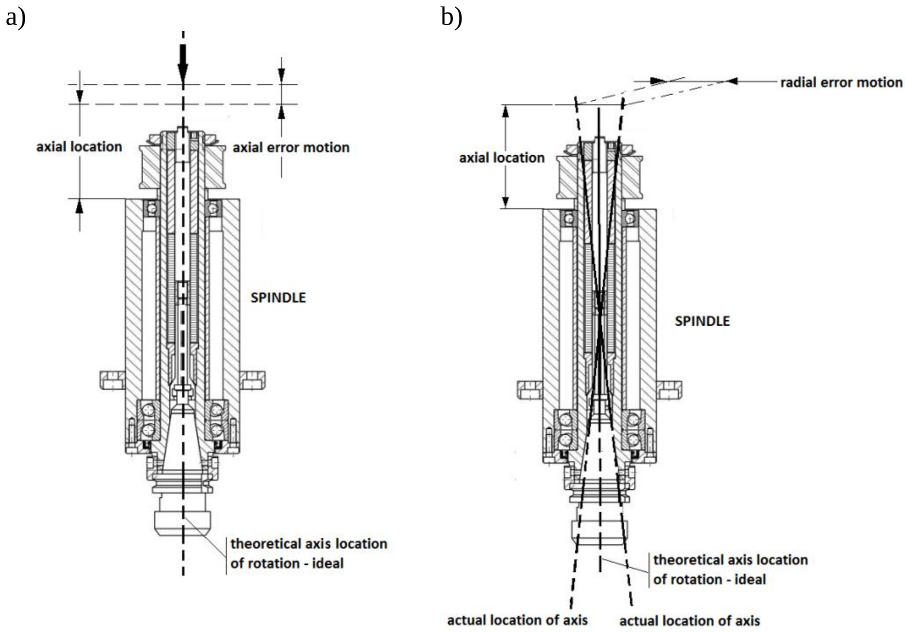

Fig. 104. CNC machine tool spindle motion errors: a) longitudinal, b) radial

Although machine tool spindle axis is a theoretical term, one can investigate its momentary angle position. At high rotational speeds, the momentary axis position depends on forces generated by the motion dynamics. The measurement of displacements is usually made at a point describing the position of the spindle head. For the ideal rotational axis position and measurement area roundness, the time diagrams show a sinusoid describing the measurement area eccentricity in relation to the axis of rotation. Any deviations of the sinusoid mean momentary changes in axis position. On the other hand, the changes in axis position have effect on machining results and machining errors.

7.2. Test methods and the experiment

The diagnostics of the tested CNC machine tool spindle was done the use of the Precision Spindle Error Analyzer, the components of which are shown in Fig. 105.

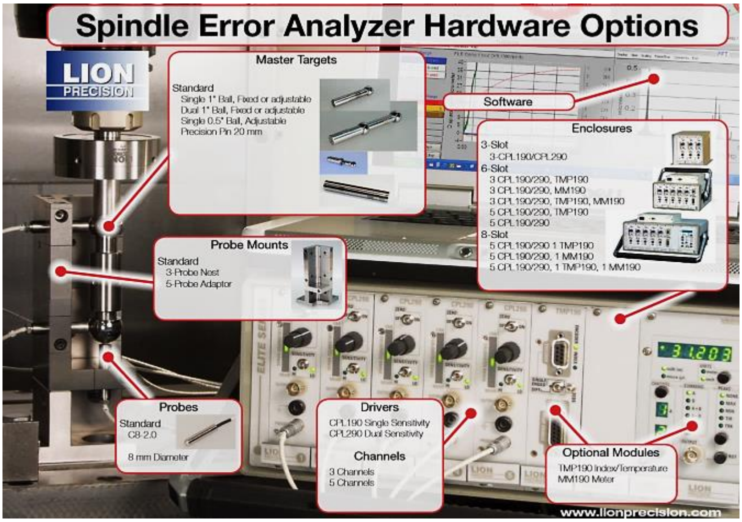

Fig. 105. Spindle error analyser set for the tests and the analysis of CNC machine tools erroneous motions [164]

a) b) c) d)

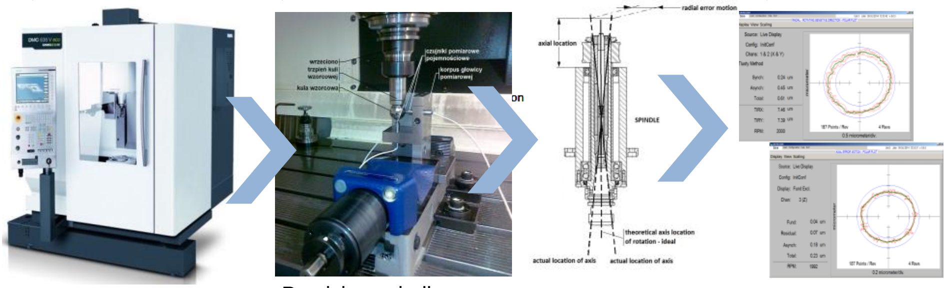

3-axis CNC machine tool

Precision spindle error analyzer probes and master ball on machine tool

Spindle of CNC machine tool

Data analyser with LionPrecision software

Fig. 106. Test stand: a) 3-axial CNC machine tool DMC 635 eco, b) set up of precision spindle error analyzer on machine tool, c) spindle, d) data analyzer

Measurements were performed in compliance with the guidelines specified in the latest edition of the ISO230-7 standard. The object of the analysis was the spindle of a 3-axis CNC milling centre, DMC 635 eco. Dynamic measurement of the rotary axis was performed. Fig. 106 shows a test stand for spindle accuracy measurements. The stand consisted of the following measurement modules:

- a measurement head consisting of three volumetric sensors (Fig. 107) located in the numerically controlled axes of the machine tool, X, Y and Z (CPL-290 driver, transmission sequence 15kHz, range 250µm, resolution 3.5nm (average square value). A five-sensor measurement head version of the system is also possible.

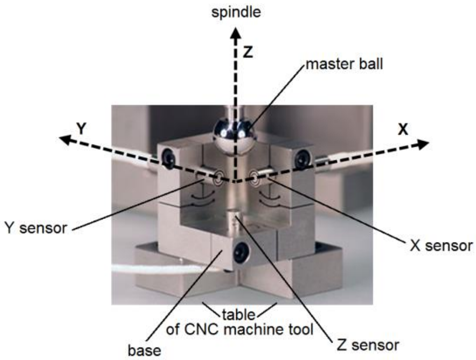

Fig. 107. Axis orientation of the precision spindle error analyser sensors [164]

– a data acquisition module from National Instruments, Lion Precision, using NI LabWindows™/CVI software and USB DAQ hardware to determine machine capability (Fig. 108),

Fig. 108. Data acquisition system DAQ [164]

– an analyser (Lion's Spindle Error Analyzer System) provided with a 3-sensor measurement system with Lion Precision software (Fig.109)

Fig. 109. Data analyser from Lion [164]

– a master ball of 25.4mm diameter (1 inch) with a deviation of <50nm, which reduces the non-roundness error of ball measurement area to negligible values.

The master ball was mounted in the tool holder, in the spindle head of the tested DMC 635 eco. Spindle motion was measured in three directions, X, Y, Z, using precise volumetric sensors placed in the shared, specially designed body with the base. The system was mounted to the machine table, creating a peculiar "measurement head." In the spindle with a vertical axis, radial and longitudinal errors are measured by the following sensors:

– sensor 1: radial movement errors in the X axis (in the horizontal plane),
– sensor 2: radial movement errors in the Y axis (in the horizontal plane),
– sensor 3: longitudinal movement errors in the Z axis (in the vertical plane).

The tests involved measuring spindle errors during idle run (i.e., when the machine is switched on and the motion axes are active, the spindle rotates without performing the cutting process). Proper measurements were preceded by initial measurements to assess the impact of master ball mounting accuracy in the spindle, the interaction between the head and the sensors, the presence of excessive vibration in the MHWT system generated by external and internal sources, electromagnetic field interferences or the presence of electric sources of errors, etc. Fig. 110 shows the variations in the signal in idle running as a function of time for the ranges of up to 50ms (Fig. 110a) and 2000ms (Fig. 110b).

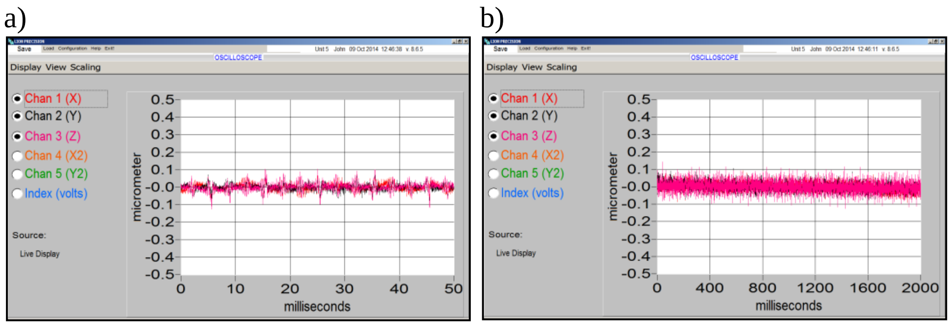

Fig. 110. Course of the signal from the sensors for the spindle measurement during idle running: a) 50ms, b) 2000ms

As can be seen in the figure, the signal stability is very high but its amplitude is lower than 0.1µm, which ensures high measurement accuracy and repeatability. The second stage of the tests involved a quasi-static measurement to assess the operation of the measurement system and all channels at a low rotational speed of the spindle. The measurement was performed for the spindle rotational speed set to 100 rpm.

As the variations in Fig. 111 demonstrate, the run-out in the idle run trial is lower than 3.5µm for all sensors, in a long period of time. This behaviour pattern is treated as stable.

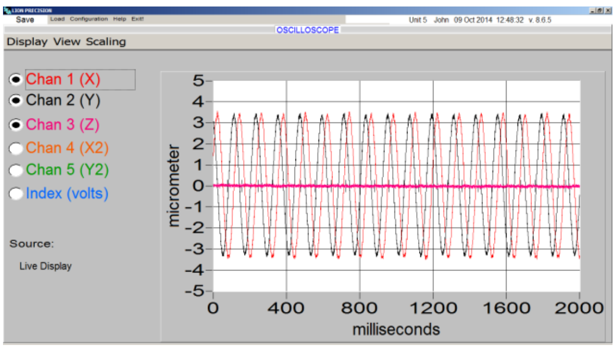

Fig. 111. Run-out recorded in the sample of idle running

7.3. Diagnostic measurement results and their analysis

Fig. 112 shows an interface of the system used in the experiment, presenting the results of radial (Fig. 112a) and longitudinal (Fig. 112b) errors of the spindle and digital indication of their values.

a) b)

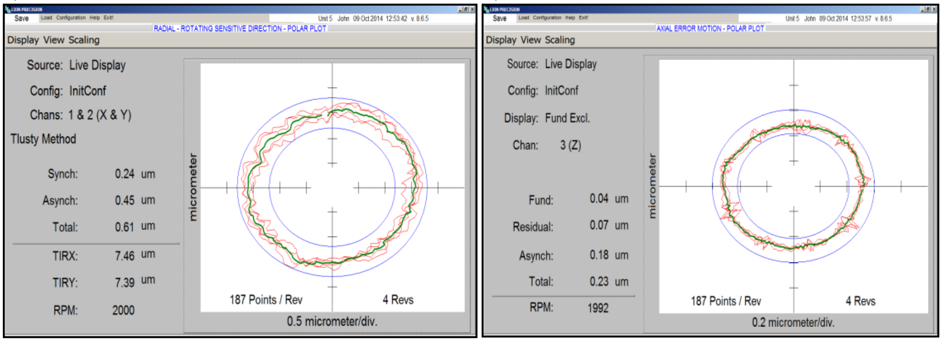

Fig. 112. Interface of the measurement system for spindle errors, with the measurement results for 2000rpm: a) spindle radial errors, b) spindle longitudinal errors

Fig. 112 shows examples of the momentary rotary axis position as a function of rotation angle for polar coordinates and the rotational speed set to 2000 rpm. The results were determined on the basis of four revolutions of the tested spindle. The proper tests were preceded by dividing the rotational speed range of the tested machine tool (0÷8000rpm) into eight sub-ranges including a speed increase to 1000rpm (Tab. 28). Following the system calibration, dynamic measurements were performed for different rotational speeds in the assumed sub-ranges, and obtained measurement results were analysed. The measurement was performed for 50% and 100% of the rotational speed in individual sub-ranges. Obtained measurement results in the established sub-ranges are listed in Tab. 28, where the maximum values of particular errors are framed.

Fig. 113 shows obtained results of the spindle radial errors in the horizontal plane (X-Y), for two spindle rotational speeds: 500rpm (Fig. 113a), 7000rpm (Fig. 113b).

Fig. 114 shows selected measurement results of spindle axis errors (axis Z) in relation to the horizontal plane (X-Y) obtained with the high-precision Spindle Error Analyzer (SEA), for selected spindle rotational speeds: 500rpm (Fig. 114a), 7000rpm (Fig. 114b).

a) b)

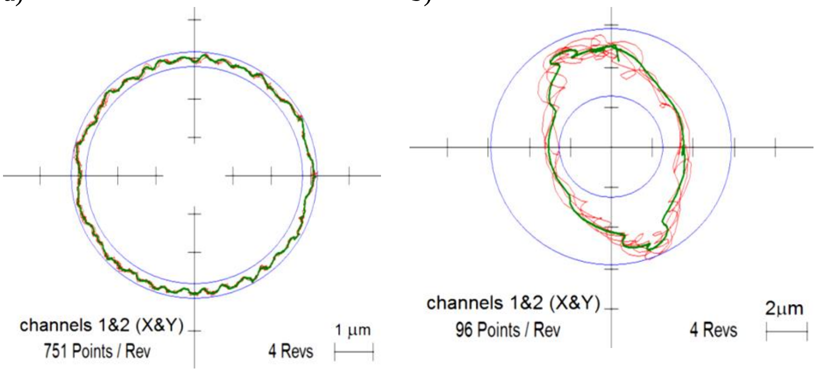

Fig. 113. Graphic presentation of the measurement results of spindle radial errors in the horizontal plane (X&Y) with spindle error analysing system (SEA), for select values of spindle rotational speed: a) at 500rpm, b) at 7000rpm

As the measurement results in Tab. 28 demonstrate, the highest values of TIR (total indicated run-out) are recorded for the rotational speed range of 4000÷5000rpm (4500rpm and 5000rpm), whereas other types of errors reach their maximum values for the rotational speed range of 7000÷8000rpm (7500rpm and 8000rpm). The TIR error is the total indicated run-out.

a) b)

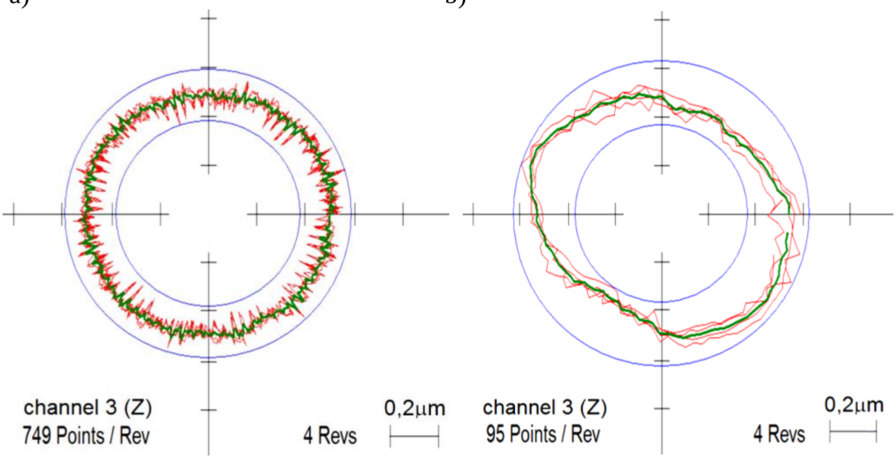

Fig. 114. Graphic presentation of longitudinal errors measurement results for a vertical spindle (Z) with spindle error analysing system (SEA), for select values of spindle rotational speed: a) at 500rpm, b) at 7000rpm

Table 28. Spindle motion errors of the 3-axis CNC-DMC 635 eco milling machine							
Error	Range of rpm	Value of error motion [µm]					
		for 50% rpm of range			for 100% rpm of range		
		Radial errors [µm]		Axial errors [µm]	Radial errors [µm]		Axial errors [µm]
		X	Y	Z	X	Y	Z
Total indicated run-out (TIR)	0000÷1000	7.14	7.08	x	7.14	7.32	x
	1000÷2000	7.43	7.12	x	7.76	7.39	x
	2000÷3000	7.57	7.29	x	7.75	7.07	x
	3000÷4000	8.14	7.30	x	8.01	7.47	x
	4000÷5000	8.49	7.60	x	8.29	7.80	x
	5000÷6000	8.21	7.56	x	6.60	7.32	x
	6000÷7000	5.65	6.92	x	4.07	7.23	x
	7000÷8000	2.73	6.70	x	3.60	7.33	x
Synchronous error motion	0000÷1000	0.26		x	0.41		x
	1000÷2000	0.30		x	0.24		x
	2000÷3000	0.52		x	0.39		x
	3000÷4000	0.81		x	0.68		x
	4000÷5000	0.66		x	0.88		x
	5000÷6000	1.30		x	1.27		x
	6000÷7000	1.85		x	2.37		x
	7000÷8000	2.77		x	3.08		x
Asynchronous error motion	0000÷1000	0.16		0.13	0.37		0.14
	1000÷2000	0.30		0.17	0.45		0.18
	2000÷3000	0.46		0.12	0.50		0.10
	3000÷4000	0.62		0.11	0.48		0.16
	4000÷5000	0.40		0.17	0.48		0.12
	5000÷6000	0.66		0.11	0.57		0.13
	6000÷7000	1.42		0.20	1.51		0.13
	7000÷8000	0.88		0.20	0.86		0.08
Fundamental error motion	0000÷1000	x		0.02	x		0.01
	1000÷2000	x		0.07	x		0.04
	2000÷3000	x		0.06	x		0.07
	3000÷4000	x		0.06	x		0.41
	4000÷5000	x		0.12	x		0.34
	5000÷6000	x		0.36	x		0.70
	6000÷7000	x		0.87	x		0.65
	7000÷8000	x		0.92	x		0.98
Residual error motion	0000÷1000	x		0.09	x		0.10
	1000÷2000	x		0.08	x		0.07
	2000÷3000	x		0.08	x		0.16
	3000÷4000	x		0.09	x		0.09
	4000÷5000	x		0.12	x		0.11
	5000÷6000	x		0.20	x		0.11
	6000÷7000	x		0.13	x		0.19
	7000÷8000	x		0.22	x		0.19
Total error motion	0000÷1000	0.38		0.22	0.55		027
	1000÷2000	0.61		0.22	0.61		0.23
	2000÷3000	0.78		0.23	0.87		0.19
	3000÷4000	1.08		0.21	0.91		0.57
	4000÷5000	0.93		0.34	1.15		0.45
	5000÷6000	1.65		0.52	1.64		0.75
	6000÷7000	2.35		1.00	3.34		0.79
	7000÷8000	3.14		1.08	3.36		1.11

TIR is the highest measured radial displacement in the direction of a displacement sensor. The TIR includes the measurement area eccentricity in relation to the measured spindle axis, geometric errors of the measurement area, axis errors in the measurement direction, dynamic displacements of the fast head resulting from imbalance, stiffness, dynamic properties (frequency of vibration), and measurement noise. Although the observed variations in spindle longitudinal and radial motion errors are not linear, the trend in these changes points to an increasing and non-linear nature of most of the analysed errors (excluding TIR). Fig. 115 shows the variations in maximum values of TIR in the X and Y axes.

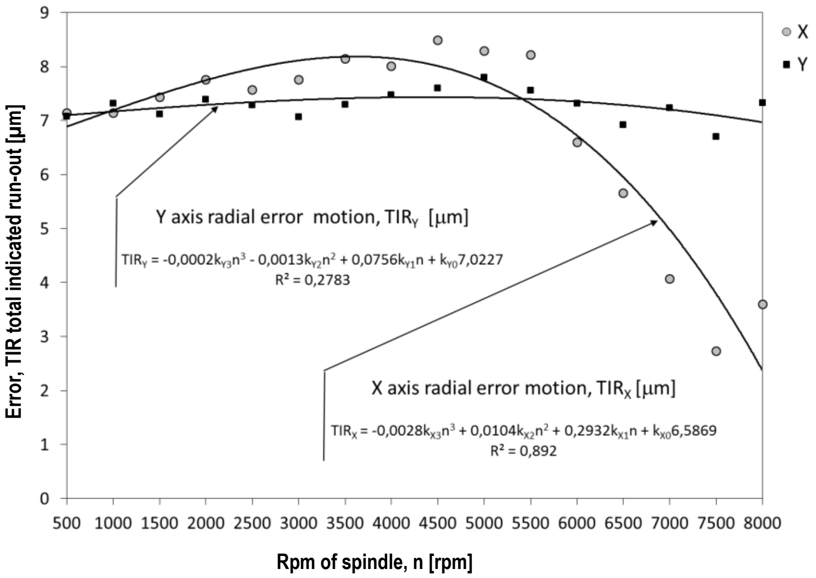

Fig. 115. Maximum variations in TIR in the X and Y axes

The total indicated run-out TIR of the tested spindle for the full rotational speed range (0÷8000rpm) is within the range of 2.79÷8.49μm, whereas the highest TIR value is obtained for the rotational speed of 5000rpm (Fig. 115). A low value of TIR points to small eccentricity of either the spindle holder or the axis of spindle rotation.

Another identified error associated with spindle motion is total error motion. The error is determined as the difference between the maximum deviation described with the maximum radius and the minimum deviation described with the minimum radius. Similarly to synchronous and asynchronous motion errors, the changes of total motion error (TEM) as a function of spindle rotational speed *n* are non-linear (Fig. 116). This error describes the maximum difference between the momentary deviations of spindle axis distance from the centre of coordinate system defined with Equation (44).

$$\sum_{i=1}^{N}[(x_i' - x_o)^2 + (y_i' - y_o)^2 - r_o^2] = min \quad (44)$$

where:
r_o – the circle radius corresponding to measurement area eccentricity, x_o, y_o, – circle centre coordinates, x'_i, y'_i – results of successive measurements (sensor indications calculated into µm).

The circle centre coordinates depend on the sensor settings. They determine the real centre of the coordinate system in relation to which measurement results are calculated.

Circle centre coordinates result from the sensor settings. They determine real centre of the coordinates system in relation to which the measurement results are calculated.

$$X = x' - x_o \quad (45)$$

$$Y = y' - y_0 \quad (46)$$

where:
x' – vector of sensor indication in the X axis, y' – vector of sensor indication in the Y axis, x_o –vector of spindle axis displacement in the X-direction, y_o –vector of spindle axis displacement in the Y-direction.

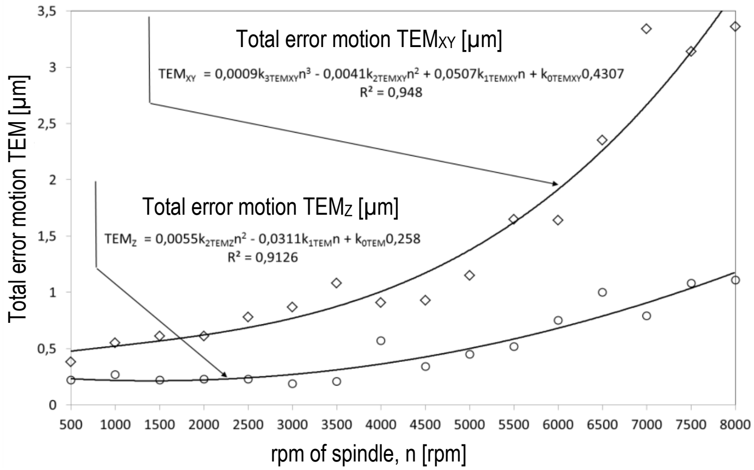

Fig. 116. Total error of radial motion TEM as a function of spindle rotational speed *n*

Based on sensor indications (x', y'), a circle reflecting to the average spindle axis motion is determined such that the sum square of point deviations from the circle is minimal (the so-called least square circle). Fig. 116 shows the variations in total (aggregate) motion error, defined as the total motion error indicated by the measurement system sensors (both in synchronous and asynchronous conditions).

Synchronous error motion is the component of the total error motion (TEM) and is associated with the ovality of machined surfaces (lack of roundness). If we calculate the average radius of every angular position, then a set of these values will be used to determine a synchronous (rotation-correlated) displacement of the spindle axis. Fig. 117 shows a graphic representation of synchronous and asynchronous errors.

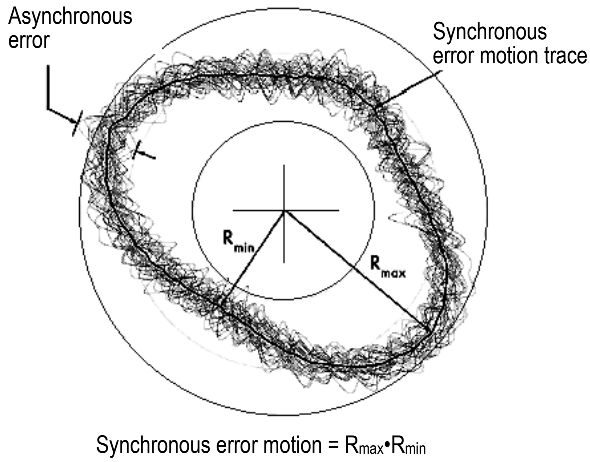

Fig. 117. Graphic interpretation of synchronous and asynchronous errors [136]

The difference between the radii of the circle inscribed and described on the average spindle axis distance from the centre of the system is defined as synchronous error motion. Should this error occur, it is necessary to identify and eliminate spindle errors resulting from bearing track circularity or bearing holder errors or the bearing holder setting error. If there are radial offsets on the longitudinal or radial error graphs, then the quality of machined surface is lower, which may be caused by bearing track damage. Synchronous error motion indicates incorrect reverse voltage of bearings or bearing holder setting error. This error leads to lower quality of machined surfaces. The data in Tab. 28 also demonstrates that the maximum synchronous error motion is within the range of 2.77÷3.08μm (for the rotational speed range of 7000÷8000rpm), whereas the maximum asynchronous error motion ranges from 0.20 to 1.51μm for the spindle rotational speed range of 6000÷7000rpm. Fig. 118 shows the variations in synchronous error motion (SE) as a function of spindle rotational speed *n*. The variations indicate a non-linear nature of the SE error as a function of spindle rotational speed. Low values of SE can point to slight errors of bearing mounting or to incorrect reverse voltage of bearings, while low values of ASE indicate the presence of relatively slight longitudinal or radial clearances as well as slight imbalance and insufficient stiffness.

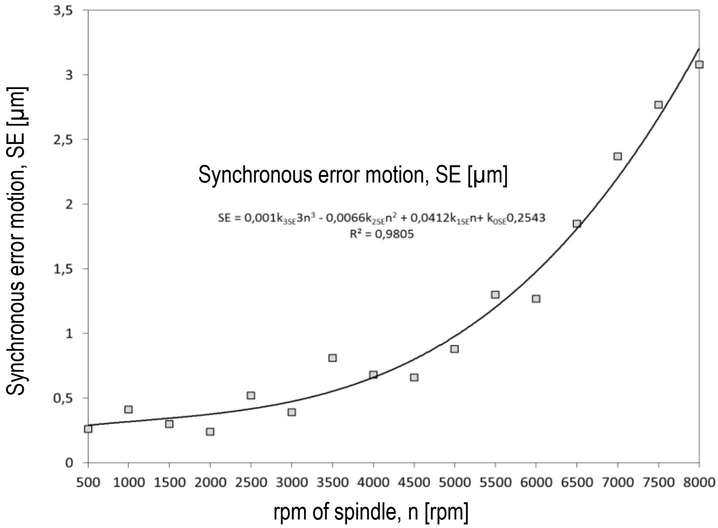

Fig. 118. Synchronous error motion SE versus spindle rotational speed *n*

Asynchronous error motion (ASE) is a component of the total error motion (TEM) and allows us to assess the repeatability of momentary axis positions. The error has a significant effect on the tool travel path and obtained contour of the machined surface (Fig. 119).

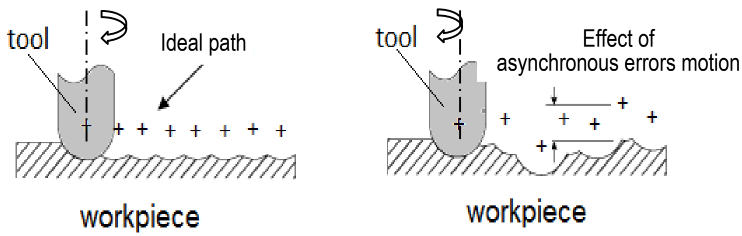

Fig. 119. Influence of ASE on tool track in machining

Fig. 119 demonstrates that, depending on it value, the asynchronous error motion has a significant impact on the surface solid geometry, its roughness and sinuosity. Fig. 120 shows the asynchronous error motion as a function of spindle rotational speed *n*. The asynchronous error motion is determined based on the number of rotations, and the result is averaged. If we calculate the maximum and minimum radial values for every angular position, we will obtain the maximum and minimum spindle axis deviations for every angular position.

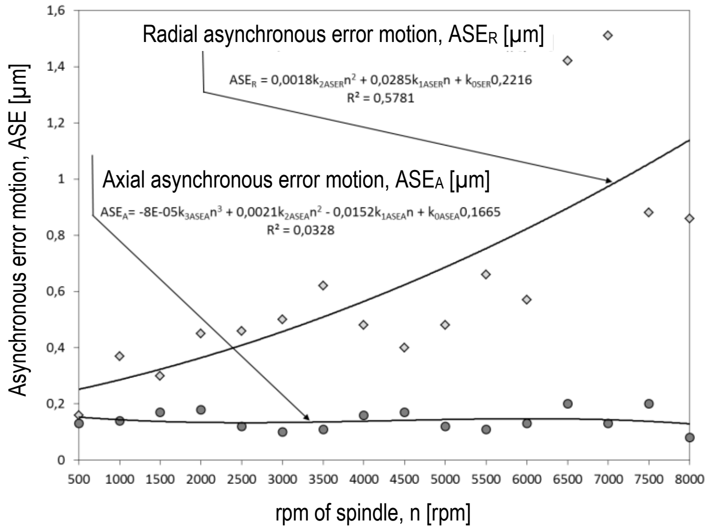

Fig. 120. Asynchronous error motion ASE as a function of spindle rotational speed *n*

This error can therefore be interpreted as the highest amplitude of transverse vibration of the rotary axis relative to the angular position. Asynchronous error motion is variable as a function of rotational speed.

Rotational speed variations

Obtained results of the experimental tests also allowed the determination of variations in the machine tool rotational speed. The measurements demonstrated a relatively high rotational speed stability of the tested spindle. Tab. 29 offers a comparison of the changes in spindle axis rotational speed for the tested sub-ranges.

Tab. 29. Tested rotational speed values of the rpm spindle in the tested sub-ranges for the three-axis CNC-DMC 635 eco milling machine

	Range of prm	Measured rpm	Measured rpm	Measured rpm	Measured rpm
		for 50% rpm of range		for 100% rpm of range	
Revolutions per minute rpm	0000÷1000	450	500	1001	999
	1000÷2000	1500	1503	2000	1992
	2000÷3000	2496	2492	3000	3006
	3000÷4000	3497	3497	4010	3990
	4000÷5000	4503	4492	5013	5000
	5000÷6000	5510	5496	5985	5970
	6000÷7000	6504	6504	7018	7055
	7000÷8000	7500	7481	8000	7973

The presented measurement results are compared with the programmed rotational speeds. On the basis of obtained results, the changes in absolute error Δrpm as a function of programmed spindle rotational speeds *n* are determined.

The variations in the Δrpm error as a function of spindle rotational speed is presented in Fig. 121. Obtained results show that the highest difference of rotational speed in relation to the programmed rotational speed amounts to 500rpm, determined on the basis of measurements with radial sensors X, Y.

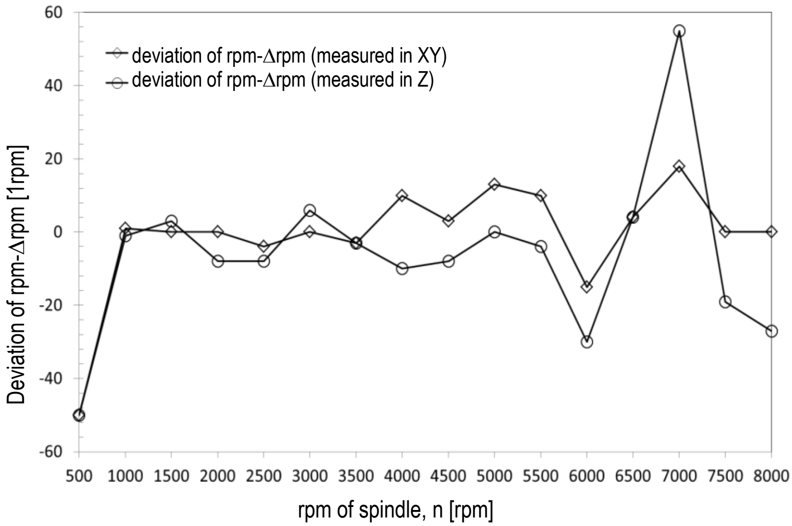

Fig. 121. Deviations of rpm as a function of spindle rotational speed *n*

The rotational speed difference for the above case is 50rpm, and it amounts to as much as 55rpm for the rotational speed of 7000rpm determined in the axial measurement. Other residual values of the spindle rotational speed range from 0 to 30rpm.

Shift vs rpm error

Fig. 122 shows relative spindle displacements (shift vs rpm) as a function of rotational speed *n* (rpm) in the X, Y, Z axes. As the data in the figure demonstrate, the relative displacement in the X-direction is lower than 0.33μm, in the Y-direction – below 0.49μm, and in the Z-direction of it is below 1.6μm. The test can also be used to assess real spindle bearing pre-load.

In this test, the measurement of spindle displacement in the X and Y directions and in the Z-direction is performed with increasing the spindle rotational speed in a very short time (Fig. 122). Since the spindle rotational speed leads to a higher mechanical load on the spindle unit (i.e., the change of centrifugal force and pre-load), this leads to the change of spindle relative position that describes the displacement as a function of rotations. Shift versus rpm is an axial displacement caused by a change in the rotational speed. It appears as axial shift (shift in the axis of rotation parallel to the Z reference axis), radial shift (shift in the axis of rotation perpendicular to the Z reference axis), tilt shift (shift in the axis of rotation relative to the Z reference axis) and face shift (combination of axial and tilt shifts in the axis of rotation measured at a specified location). For the tested range of rotational speed, the shift versus rpm error does not exceed the value of 1.6μm in the Z axis and 0.5μm in the X, Y axes.

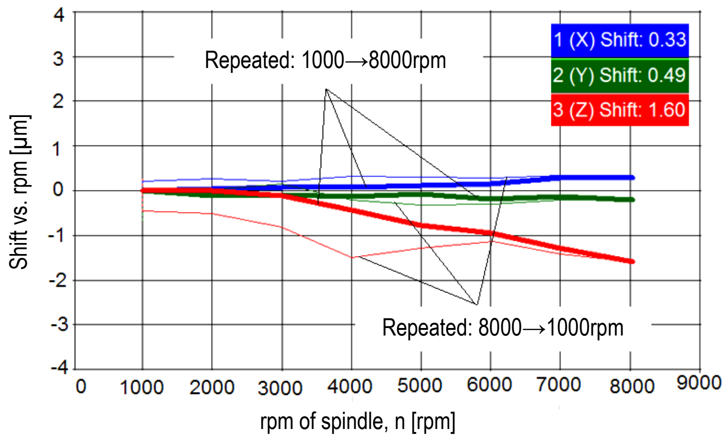

Fig. 122. Graphic presentation of the relative results of spindle displacements as a function of rotational speed (shift vs. rpm) obtained with precision spindle error analyser (SEA), in the range of 1000÷8000rpm [136]

Thermal drift

Thermal drift is determined as a function of time, according to the methodology described in ISO 230-3:2007. This error describes the displacement of the numerically controlled perpendicular axes X, Y, Z caused by an increase in the temperature of the rotating spindle as a function of time. Thermal drift testing is performed for long periods of time, e.g., 300min. Selected values of the spindle thermal drift obtained during 60 minutes of its operation are given in Fig. 123.

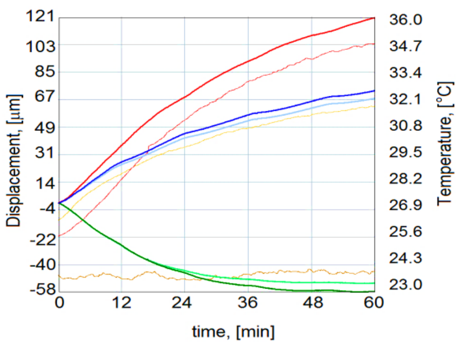

Fig. 123. Thermal drift of the CNC machine tool spindle [136]

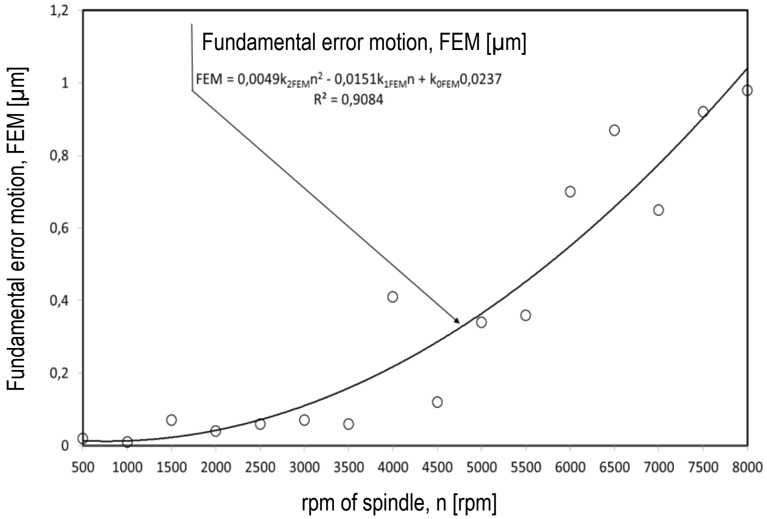

Fig. 124. Fundamental error motion versus spindle rotational speed *n*

Fig. 124 presents the variations in the fundamental error motion determined on the basis of one rotation and in the residual error motion determined as a function of spindle rotational speed. All errors determined in this study show non-linearity with changing the spindle rotational speed *n*.

Low values of the basic error motion, total error motion and residual error motion (Fig. 125) point to good technical condition of the tested spindle.

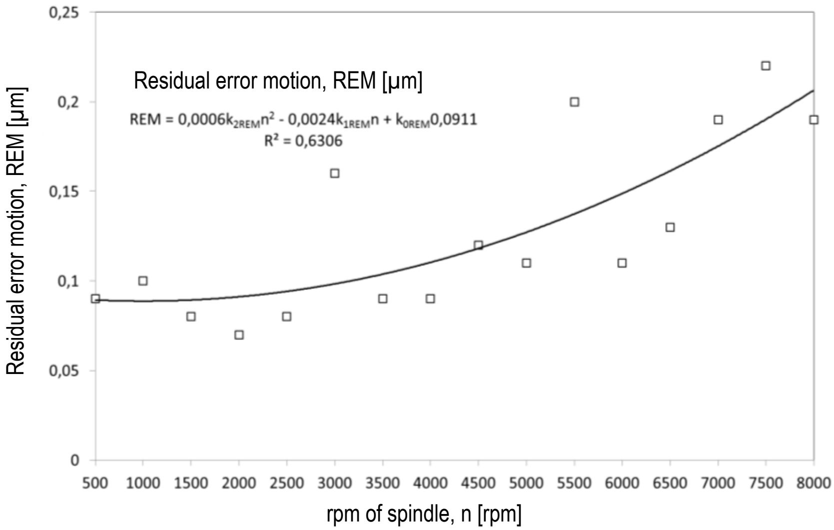

Fig. 125. Residual error motion versus spindle rotational speed *n*

7.4. Summary and conclusions

Early and effective diagnostics of numerically controlled machine tool spindles is critical for maintaining their continuous operational efficiency. According to the conducted study, without precise and effective methods and tools, the diagnostics process would be much more difficult. Modern technological machines are equipped with spindles of higher and higher rotational speed. Stable spindle work can be ensured by increasing both accuracy of bearings in the machine and stiffness of the headstock spindle. Spindle bearings have an impact on the accuracy of rotary axis position, the stabilisation of the rotated element, and the transfer of cutting force. To a high extent, they also affect total errors of the spindles they are part of. This accuracy depends more and more often on the rotational motion dynamics, not only on the geometric accuracy of the spindle. For this reason, the research on high-speed spindles should take into consideration the aspect of both geometric accuracy and motion dynamics. The innovative Precision Spindle Error Analyzer (SEA) used in the experiments can perform the above task. The main applications of this system include the monitoring of spindle technical condition in real time, potential spindle damage prediction, spindle damage detection, (mainly damage of bearings, etc.), the assessment of spindle condition in both experimental and acceptance tests, the verification of spindle technical condition after collision. This work described the potential and effectiveness of the tested system for the precise detection of errors (axial and radial) of machine tool spindle.

8. MONITORING OF FEED ACCURACY AND ROTATIONAL SPEED DEVIATIONS

Feed accuracy (more precisely: feed inaccuracy) and rotational speed deviations of a CNC machine tool (spindle, tool heads, rotary tables, etc.) are crucial parameters for finished part quality, machining tool life, and proper operation of the machine. A lack of stable rotations and constant programmed feed can cause vibrational excitation, surface unevenness, the change of chip form and shape, as well as imbalance of the machining process. It can therefore be claimed that variations in the rotational speed and feed values have a negative multi-faceted effect on the machining process. The PN-ISO 10791-6:2001 standard describes the testing condition for machining centres, and Part 6 of the standard specifies the conditions and methods for testing the accuracy of feeds, spindle rotational speeds and interpolations.

8.1. Errors of machine tool spindle kinematic parameters

The errors of set rotational speed are crucial for the assessment of machines and the type of machining requiring the synchronization of interpolation speeds. They can be associated with:

- angular errors of rotational synchronization in machining with counter spindle,
- errors of polygon machining due to integrated tool and workpiece motion,
- errors of contouring operations of the feed axis and C-axis spindle rotational motion, e.g., in drunken thread turning,
- errors of the feed axis interpolated motion trajectory, e.g. contour turning,
- errors of reversal and follow-up dynamics,
- contour duplication errors resulting from the lack of straightness and squareness, and scale differences and cyclic errors, the analysis of the effect of control unit regulators and their setting on the errors of set interpolated motion trajectory.

  The methods for measuring errors of set rotational speeds are used in the assessment of the effect of rotational speed errors on obtained shapes. This method is used for determining correctness indicators of spindle rotational motion:
- error of the average rotational speed of the spindle in set rotation mode. This error leads to shape defects of surfaces machined with integrated rotational motion methods. This error results from a follow-up error due to incorrect speed regulator settings or a gear reduction error due to axis positioning errors,
- error of rotational motion velocity evenness of the spindle in set rotation mode. This error leads to shape defects of surfaces machined by the

methods involving integrated rotational motion, as well as cause angular defects of the workpiece when machining is performed with a synchronized speed of two rotational axes. This type of error results from a radial run-out error of gear wheels in relation to the spindle axis or drive engine, incorrect tension of transmission belts or the lack of coaxiality between the rotation converter and the spindle axis,

- error of the set rotational speed of the spindle in angular positioning mode. This error leads to shape defects of surfaces machined by the methods involving integrated motion of feed and rotation axes. In terms of design, this error is caused by inaccurate precision of gear shift due to axial wheelbase errors and by a follow-up error resulting from too low speed regulator reinforcement or too high motion resistance,
- error of rotational motion speed evenness of the spindle in angular positioning mode leads to shape defects of surfaces machined by the methods involving integrated motion of feed and rotation axes. In terms of design, this type of error results from incorrect tension of a transmission belt, a radial run-out error of transmission wheels, a positioning error of rotation angle converter or variable motion resistance caused by incorrect initial tension of the bearing.

Given the possibility of concentrating operations on the CNC machine tool or even complete machining as well as the demand for higher efficiency, machining errors resulting from the accuracy of maintaining set technical motions (feed inaccuracy and speed deviations of rotational axes, heads and rotary tables of the CNC machine tool) are becoming a more and more serious design problem. These errors should be eliminated at the stage of machine tool design and mounting.

8.2. Diagnostic testing

Spindle rotational speed measurements

The scope of measurements included the determination of rotational speed deviations of the spindle in a vertical machining centre, FV580, for 50% and 100% of maximum rotational speed per every defined rotational speed range (Fig. 126). The tests were carried out in the clockwise CW (+) and anti-clockwise CCW (-) directions. A 5% threshold tolerance was assumed for both the rotational speed deviation and the feed accuracy. The diagnostic testing was performed according to the following procedure:

- preparatory works: setting the ranges of rotational speed and feed, defining the parameters of machine tool operation, starting the machine, etc.,
- diagnostic assessment: measurement of the rotational speeds n_z from the subranges in the clockwise CW and anti-clockwise CCW directions as a function of set rotational speed n (50% and 100% of maximum rotational speed for every defined rotational speed range), measurement

of the feed time t on a measuring length L and calculation of the feed rate (including run-in and run-out), calculation of average and standard deviations, result analysis,

– inference (comparison and assessment of obtained results).

Fig. 126. Tested vertical machining centre FV580a

The percentage value of the relative spindle rotational speed deviation Δn is determined with the following relation (47):

$$\Delta n = [(n_z - n_p) / n_p]\cdot 100\% \tag{47}$$

where:
Δn – relative rotational speed deviation [%], n_z – measured rotational speed [rpm], n_p – programmed rotational speed [rpm]

The measurement of rotational speeds n_z from the established sub-ranges was performed using a rotational speed laser meter, according the procedure illustrated in Fig. 127. In the measurements, the rotational speed deviation Δn was defined for both the clockwise CW direction, marked as Δn^+, and the anti-clockwise CCW direction, marked as Δn^-.

Average values of the measurement results and calculations from the test series are listed in Tab. 30.

The experimental results demonstrate that the average rotational speed deviation changes in the range from 0% to 0.39%. This also proves the fact that none of the tested rotational speeds, irrespective of the direction of motion, exceeds the tolerances defined in the standard. Fig. 128 shows the variations in the rotational speed deviations Δn^+ and Δn^-. The maximum value of rotational speed absolute error in the entire tested speed range does not exceed 2rpm. The standard deviation s_n was determined for both the results obtained from the CW clockwise tests, s_n^+, and CCW anti-clockwise tests, s_n^-. The results of deviation s are within the range of (0÷1.414)rpm. The results of these measurements are shown in Fig. 129.

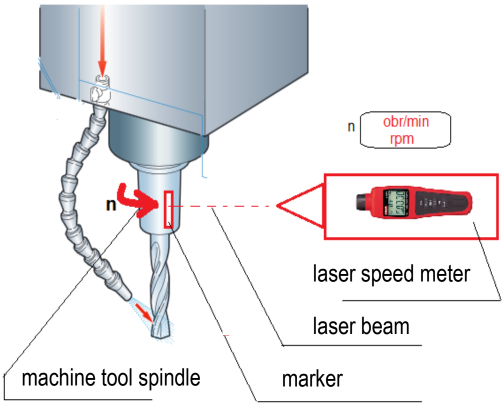

Fig. 127. Rotational speed measurement of of the CNC machine tool spindle

Tab. 30. Average values of rotational speed n during tests

Range of n_p [rpm]	**For 50% n [rpm] of range**						**For 100% n [rpm] of range**					
	Measured n_z^+ [rpm]			Measured n_z^- [rpm]			Measured n_z^+ [rpm]			Measured n_z^- [rpm]		
	n_z^+	Δn^+ [%]	s_n^+	n_z^-	Δn^- [%]	s_n^-	n_z^+	Δn^+ [%]	s_n^+	n_z^-	Δn^- [%]	s_n^-
0000÷1000	501.96	**0.392**	0.195	500.00	0.000	0.000	1001.40	0.140	0.134	1000.00	0.000	0.000
1000÷2000	1501.80	0.118	1.095	1500.00	0.000	0.000	2001.00	0.050	**1.414**	2000.00	0.000	0.000
2000÷3000	2500.20	0.008	1.095	2500.00	0.000	0.000	3000.80	0.026	1.095	3000.60	0.020	0.044
3000÷4000	3500.60	0.017	0.894	3500.00	0.000	0.000	4000.00	0.000	0.000	4000.00	0.000	0.000
4000÷5000	4499.00	0.020	0.000	4499.00	0.020	0.000	4999.20	0.016	0.447	4999.20	0.016	0.000
5000÷6000	5499.00	0.018	0.000	5499.00	0.018	0.000	5999.00	0.016	0.000	5999.20	0.013	0.447

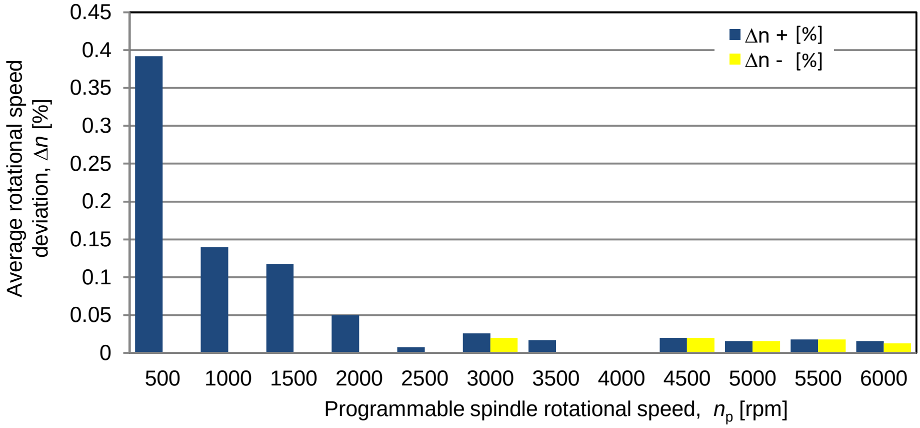

Fig. 128. Variations in the average percentage values of the spindle rotational speed Δn^+ and Δn^- as a function of programmed speed n_p

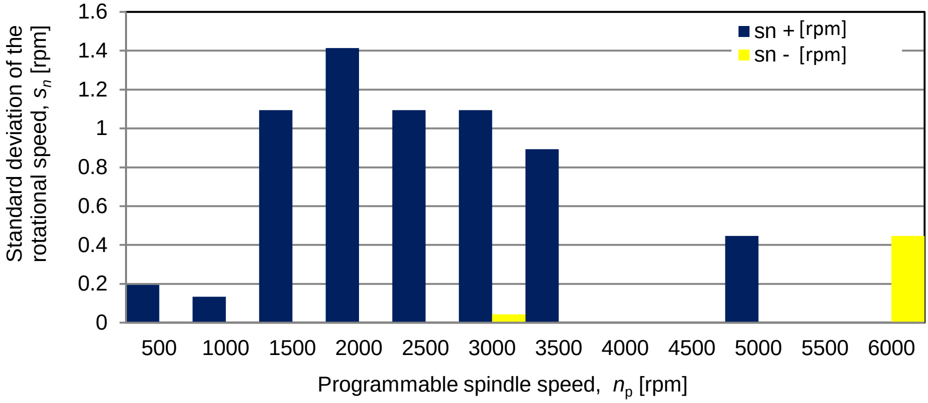

Fig. 129. Variations in the standard deviations s_n^+, s_n^- as a function of programmed speed n_p

Based on the data presented in Figs. 128 and 129, it can be assumed that with increasing the programmed spindle rotational speed n_p, the values of average percentage deviation change Δn^+ decrease. The highest variations in the rotational speed can be observed for low rotation values; however, after exceeding 2500rpm, the changes in rotational speed become stable at an average level below 0.026%. It can also be observed that there are no rotational speed deviations Δn^- in the anti-clockwise CCW direction. Small changes in the values of Δn^- can occur after exceeding 3000 rpm. The value of Δn^- is within the range of 0÷0.02%. The standard deviation determined in the anticlockwise CCW direction, s_n^-, is two times lower than the s_n^+ value obtained for the clockwise direction and amounts to 0.447rpm for the highest programmed speed n=6000rpm.

Feed accuracy tests

The present work undertakes to assess the feed accuracy in linear axes for the following feed rates: 100mm/min, 1000mm/min, maximum feed and fast line feed. Feed accuracy expressed as a relative percentage deviation is calculated from the following relation (48).

$$\Delta v_f = [(v_{fz} - v_{fp}) / v_{fp}] \cdot 100\% \qquad (48)$$

where:
Δv_f – relative percentage deviation of the feed rate [%], v_{fz} – measured feed rate [mm/min], v_{fp} – programmed feed rate [mm/min].

The feed v_{fz} was determined with an indirect method by measuring the time t necessary for the workpiece to pass through, using a time meter along the measuring length L. The measurement of feed rate v_{fz} in the tested axis (X,Y) was performed according to the schematic design shown in Fig. 130. The experiments took account of the run-in path L_d to stabilise the axis drive motion (drive engine run-up) and the run-out path L_w (axis drive engine), where the motion speed is variable (unstable). The values of L_d and L_w were set equal to 50mm (L_d=L_w=50mm). The measuring length L was set equal to 200mm. Obtained measurement and calculation results are listed in Tab. 31. The inferring process was conducted according to the PN-ISO 10791-6:2001 standard, with a 5% threshold tolerance for CNC machine tool feed accuracy. The results (and average values and standard deviation s_{vfz}) were compared for:

- feed deviations in the X axis (Δv_{fz}^{+}= f(v_{fp}) – for a motion in the X axis direction (+), Δv_{fz}^{-}= f(v_{fp}) – for a motion opposite to the X axis direction (-)),
- feed deviations in the Y axis (Δv_{fz}^{+}= f(v_{fp}) – for a motion in the Y axis direction (+), Δv_{fz}^{-}= f(v_{fp}) – for a motion opposite to the Y axis direction (-)),
- the standard deviation s_{vfz} as a function of motion s_{vfz}^{+}=f(v_{fp}) – in accordance with the direction of the axis (+), s_{vfz}^{-} =f(v_{fp}) – opposite to the direction of the axis (-)).

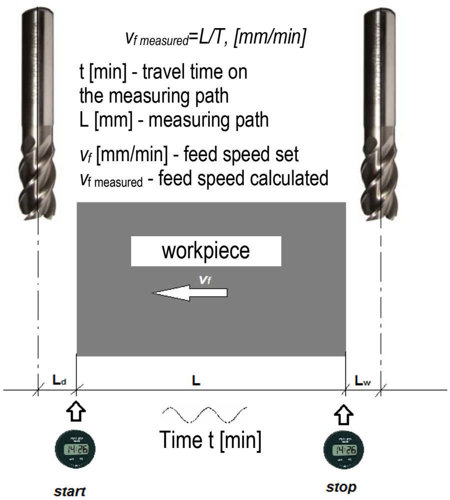

Fig. 130. Schematic design of the measurement of feed rate v_f in the tested axis

Fig. 131 illustrates the nature of variations in the feed velocity v_{fz} versus the programmed feed v_{fp} on the machine tool, in (+) and opposite to (-) to the X-axis direction. The variations shown in Fig. 131 reveal the presence of significant deviations of feed relative to the programmed feed of the machine tool. The higher the variations are, the higher the tested feed v_f. This observation is confirmed by the standard deviation given in Tab. 31, the value of which changes in a very wide range (0.8÷241mm/min). Fig. 132 shows the variations in feed rate v_{fz} versus machine tool programmed feed v_{fp}, in (+) and opposite to (-) to the Y-axis direction. The experimentally determined changes of the feed rate in the Y axis reveal that the feed deviations are far lower than the nominal values programmed on the machine tool, contrary to what was observed for the X axis. This is also demonstrated by the standard deviation values which change in the range (0.22÷54mm/min). Shown in Figs. 131 and 132, the results include the change of motion in the tested direction.

Fig. 133 shows the variations in the standard deviations s^+, s^- of the feed rate v_{fz} versus the machine tool's programmed feed v_{fp}, according to (+) and opposite to (-) to the sense of the tested axes X and Y. The graph shows that the increase in feed rate leads to a higher standard deviation expressing the scatter around the average value. For nearly all of the tested cases, the estimator s^+ is higher than the estimator s^-, irrespective of the tested axis (X, Y). Consequently, it can be claimed that the direction of motion has a decisive impact on the value of identified feed error.

Tab. 31. Accuracy results of the feed rate v_f

		For X axis				For Y axis			
		v_{fp} [mm/min]	v_{fz} [mm/min]	Δv_{fz} [%]	s_{vfz} [mm/min]	v_{fp} [mm/min]	v_{fz} [mm/min]	Δv_{fz} [%]	s_{vfz} [mm/min]
100	+	100	91.93	8.07		100	95.78	4.22	
		100	90.87	9.13	0.80	100	95.8	4.20	0.22
		100	90.35	9.65		100	95.4	4.60	
	-	100	91.91	8.09		100	95.7	4.30	
		100	90.61	9.39	0.65	100	94.93	5.07	0.38
		100	91.13	8.87		100	95.35	4.65	
1000	+	1000	980.00	2.00		1000	1044.26	-4.42	
		1000	965.10	3.49	29.46	1000	1061.60	-6.16	9.70
		1000	923.18	7.68		1000	1045.36	-4.53	
	-	1000	1044.26	-4.42		1000	1011.11	-1.11	
		1000	923.18	7.68	63.46	1000	998.65	0.13	8.32
		1000	950.74	4.92		1000	995.31	0.46	
v_h	+	2000	2116.39	-5.81		2000	2036.35	-1.81	
		2000	2539.28	-26.91	10.96	2000	2146.37	-7.31	55.02
		2000	2227.42	-11.37		2000	2089.34	-4.46	
	-	2000	2269.00	-13.45		2000	2127.9	-6.39	
		2000	2133.33	-6.66	94.09	2000	2169.23	-8.46	42.62
		2000	2088.23	-4.41		2000	2084.00	-4.20	
v_{max}	+	6000	6796.46	-13.27		6000	6195.32	-3.25	
		6000	6335.00	-5.58	231.29	6000	6220.65	-3.67	36.16
		6000	6593.60	-9.89		6000	6149.32	-2.48	
	-	6000	6987.00	-16.45		6000	6200.39	-3.33	
		6000	6545.23	-9.08	241.50	6000	6279.36	-4.65	54.00
		6000	6597.00	-9.95		6000	6303.69	-5.06	

v_{fp} – programmed value, v_{fz} – measured value, Δv_{fz} – feed deviation, s_{vf} – standard deviation, v_h – speed of quick idle run (if G0), v_{max} – maximum rate of the operational feed (if G1), G1 linear interpolation during operational motion (preparatory function), G0 – quick setting motion (preparatory function)

Fig. 133 also reveals that the scatter of the measured feed values in the X axis is even four times higher than in the case of the Y axis. This means that each of the axis must be measured separately, and the aggregate error of the machining process requires multifaceted analyses in a three-dimensional coordinate system.

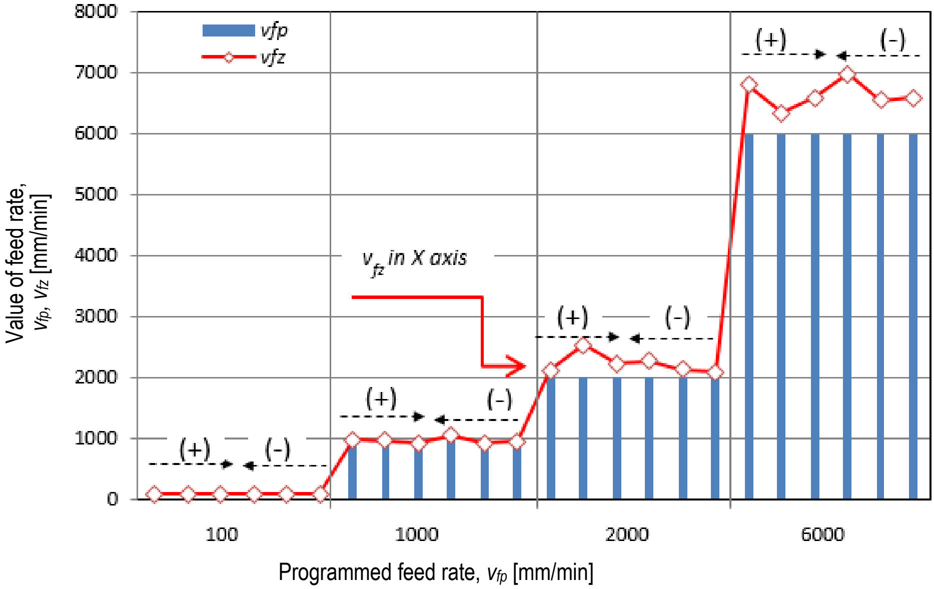

Fig. 131. Measured feed v_{fz} versus programmed feed rate v_{fp}, according to (+) and opposite to (-) the X axis

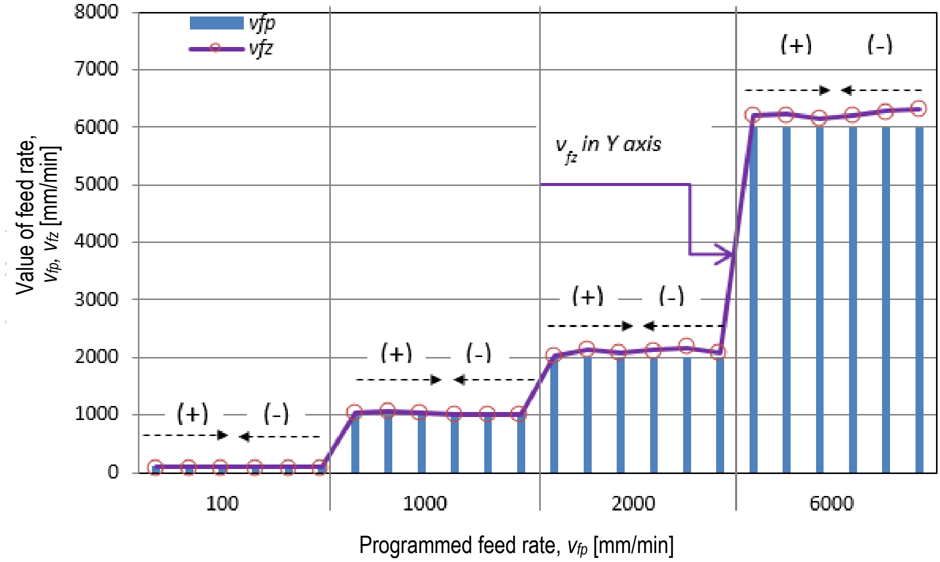

Fig. 132. Measured feed v_{fz} versus programmed feed rate v_{fp}, according to (+) and opposite to (-) the Y axis

The variations in the standard deviation s of the feed v_f as a function of programmed feed v_{fp} for the X axis can be described with power equation (49), whereas those in the Y-direction with Equation (50):

$$s = 0.0158\ v_{fp}^{2.988} \tag{49}$$

$$s = 0.0064\ v_{fp}^{2.977} \tag{50}$$

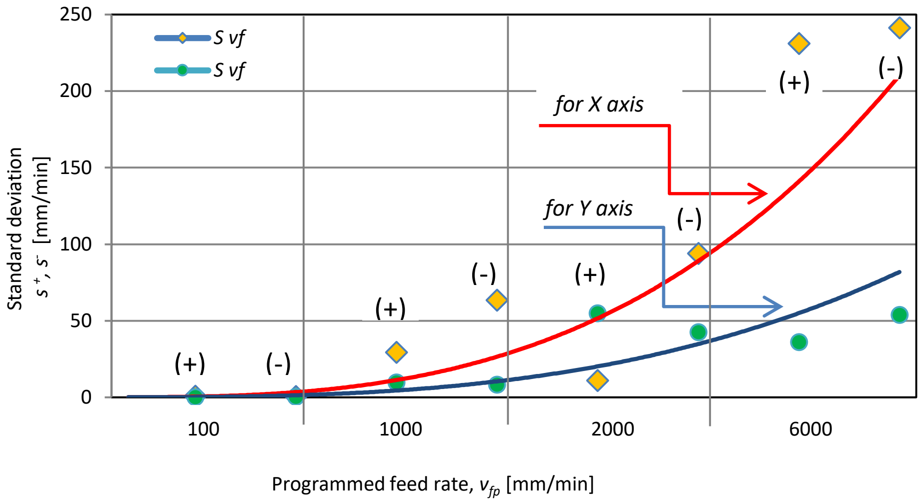

Fig. 133. Standard deviations s^+, s^- of feed rate v_{fz} versus programmed feed rate v_{fp}, in (+) and opposite to (-) the direction of the X and Y axes

Fig. 134 shows the percentage value change in the feed rate Δv_{fz} versus the programmed feed rate v_{fp}, in (+) and opposite to (-) to the direction of the X and Y axes. The feed rate percentage value Δv_{fz} as a function of programmed feed v_{fp} is described by linear equations: in the X-direction by Equation (51) and in the Y-direction by Equation (52):

$$\Delta v_{fz} = -1.1176 v_{fp} + 11.538 \tag{51}$$

$$\Delta v_{fz} = -0.4228 v_{fp} + 3.4626 \tag{52}$$

As the specifications given in Fig. 134 show, the speed increase changes the nature of feed error. The positive errors – for the feed of up to 1000mm/min, change their sign to negative for the feed rate of 2000÷6000mm/min. Different slopes of the curves described with Equations (51), (52) point to a varying intensity of error changes in individual axes.

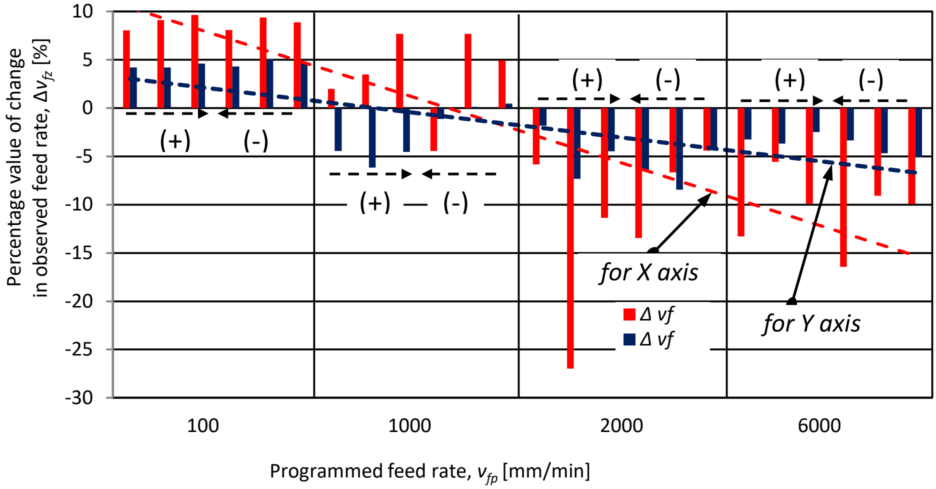

Fig. 134. Percentage value of change in Δv_{fz} versus programmed feed rate v_{fp}, according to (+) and opposite to (-) the X and Y axes

9. CNC MACHINE TOOL ACOUSTIC DIAGNOSTICS

Noise is one of the most burdensome environmental factors causing damage to the human organism, although the extent of the damage is difficult to estimate. Noise is also associate with a number of technological parameters describing the technical condition of a machine tool. Higher clearance, transmission wear and all negative geometric changes are caused by the change of signal acoustic emission level. Despite the use of various means of protection, the workplace requiring the operation of CNC machining centres for metals (lathes, milling machines, polishers and others) is always full of dangers caused by the impact of influence of noise. Many of these factors occur with time (operation) and there is no way to avoid them. This is mainly due to changes in the workplace environment, machine wear, failures and the ignorance of health and safety rules by the workers.

Noise is usually defined as sound which is unwanted and oppressive in some circumstances, sometimes it is simply harmful for the health of a CNC machine tool operator and his environment. Noise is connected with vibrations of particles in solids, liquids and gases. Taking into consideration its frequency, sound (vibrations) can be divided into three groups: infrasounds (<16(30) Hz), audible sounds (16÷20000Hz), ultrasounds (>20kHz). A long-time exposure to high sound frequencies may have a negative influence on the human being and his health. Ultrasounds as well as infrasounds have a negative impact on the human organs and tissues, nervous system, and – to a small degree on – hearing. The harmfulness and arduousness of noise depends on its strength, frequency, the nature of their change in time, the stability of their action and their inaudible component content as well as recipient features such as the state of health, age, psychological condition, individual sensitivity to sound. High sound levels cause irritability, and, in extreme cases, they may cause damage to hearing. Hearing protection is obligatory from 85dB (A). Noise emitted by machines is usually caused with the rotation or feed and rotation of elements. Noise and its frequency can be a quality measure of the machines and mechanical devices and may determine their selection and assessment of their technical condition.

9.1. Sources of noise in machine tools and noise reduction

The sources of noise in machine tools include: drive units, kinematic transmissions, pumps, clutches, swarf removal systems, rotating spindles, handles, tables, rotating covers and other working units of a machine tool. An important source of noise is the very physical process of machining, its kinematics (rotation, feed and rolling). The sources of sound constantly interact. Acoustic emissions are generated simultaneously by all sources during the operation of the technological machine. In some sense, this inhibits an analysis of obtained measurement results and often requires separating the sources of noise generated by particular units or separate parts. In order to determine noise emissions, one should check the running noise, its impact on the human body, noise generation in particular machine tool units for the assessment and possible improvement of their acoustic properties. Therefore, noise measurements are often conducted at special stations. The basic means by which the influence of noise can be prevented include: proper machine positioning and the use of protection covers, ensuring protection not only from injuries caused by chip and cooling liquid spillage but also providing a barrier against the spread of noise. As far as measurable factors are concerned, it is advised to run periodic inspection of the highest permissible noise concentration (NDS) and the highest permissible noise intensity (NDN). Creating a proper space around the machine tool has a considerable influence on the spread of noise in the room. The spaces between the machines should be of at least 0.75m, and there should be at least $2m^2$ of free floor space around each worker. If necessary, hearing protectors should be provided.

9.2. Machine tool noise measurement and the parameters describing acoustic energy

The methodology of machine tool noise diagnostics depends to a large extent on the aim of a study. Most frequently, it is performed in compliance with the ISO standards (Tabs. 2 and 3) specified for a wide range of machine tools of a given size and type. According to the presented standard, the methodology of noise parameter determination relates to their types. The standard specifies the level of acoustic power based on the measurement of noise strength according to relevant standards. One should use appropriate standards then.

Machine tool noise measurement

Most noise sources and their overlapping make it necessary to adopt a different approach to noise assessment. The approach depends on whether we want to determine the general condition of a machine, its silent-running or permissible impact of noise on the human hearing and the degree of nuisance for the human organism. One can distinguish:

a) inspection of the level of noise emitted by a machine tool in order to compare the noise emitted by the machine with the values defined in the standards for the machine tool and the guidelines,
b) inspection of the share in noise generation by particular units, components and parts for particular settings of the machine tool,
c) determination of the effect of machine tool noise on the human body and the environment,
d) inspection of machine tool silent-running,
e) acoustic diagnostics of the machine tool and error detection during operation and idle run.

The acoustic diagnostics of machine tool technical condition, especially of components such as shafts, bearings, transmissions of different type, clutches rotating spindles, handles, or tables, requires an analysis of acoustic amplitude and frequency spectrum in relation to the geometric and kinematic structure of the machine tool.

Parameters describing acoustic energy

Acoustic field energy is described with the following variables:

- acoustic force L_N,
- sound strength L_I,
- acoustic pressure L_p.

Acoustic force specifying the sound source is determined by the amount of acoustic energy emitted by the source in a time unit. Sound strength is defined as the amount of acoustic energy transmitted in the unit of time through the unit of surface. Acoustic pressure is the difference between the pressure at a given moment and the static centre pressure where the sound spreads. The determination of values in absolute units is inconvenient, given a very wide spread of measured values. Therefore, in acoustics, logarithms of the values are given in the tables or their tenth part called decibels (dB). A decibel is not a unit, but a method for presenting, some measurement results (a way of noise measurement). The relations describing the levels of acoustic strength L_N, acoustic pressure L_p and sound strength L_I are:

- acoustic force level dB $L_N = 10 \lg (N/N_o)$,
  where: N_o – is the reference force value, 10^{-12}W,
- the level of acoustic pressure dB $L_p = 20 \lg (p/p_o)$
  where: p_o is a value of the reference force, $2{*}10^{-5}$Pa,
- the level of sound strength dB $L_I = 10 \lg (I/I_o)$
  where: I_o is a value of the reference strength, 10^{-12}W/m^2.

The acoustic pressure level in the aerial centre is equal to the sound strength level. The permissible noise values in the work environment (NDN values) determined in relation to hearing protection are as follows:

- exposure to noise $L_{EX,8h}$ referred to an 8-hour work time should be lower than 85dB, and the daily exposure should not exceed $3.64 \cdot 10^3$Pa$^2 \cdot$s,
- in relation to the noise affecting the human body on particular days in an unequal way, the level of exposure should not exceed the value of dB in relation to the weekly work time ($L_{EX,W}$), and the weekly exposure should be lower than $18.2 \cdot 10^3$ Pa$^2 \cdot$s,
- the maximum sound level A (L_{Amax}) should be lower than 115dB,
- the peak sound moment C (L_{Cpeak}) should be lower than 135dB.

The threshold values for works involving exposure to noise or mechanic vibrations are as follows:

- the level of exposure to noise in relation to an 8-hour work time or the level of exposure to noise in relation to a week of work should not exceed 80dB,
- the peak level of sound C should be lower than 135dB.

The standard values presented above apply when other detailed regulations do not state otherwise, e.g., when they do not determine any lower values. In the case of juvenile workers, the permissible noise-exposure level in the workplace is $L_{EX,8h}$=80dB, whereas in the case of pregnant women it cannot exceed the value of $L_{EX,8h}$=65dB.

9.3. Exposure to noise in the workplace environment

According to data collected by the Central Statistical Office, almost 40% of workers (in Poland) work in harmful and arduous conditions exceeding the above-the-average noise-exposure level of 85 dB. According to the data, the most exposed are those workers who are employed in production plants producing metal and wooden items. Assuming that the basic noise sources in the workplace are machines, devices, technological processes, particular groups of noise sources can be specified:

- machine tools for metal – up to 104dB (e.g., polishers, automatic lathes, drills),
- machine tools for wood: slotting machines – up to 108dB, shapers – up to 101dB, milling machines – up to 101dB, circular saws – up to 99dB,
- energy sources: internal combustion engines – the maximum sound levels of the A sound – up to 125dB, compressors – up to 113dB,
- hand tools and pneumatic engines: polishers, pneumatic hammers, chisels – up to 134dB,
- ball mills – up to 120dB,
- vibrating sieve – up to 119dB,
- crushers – up to 119dB,
- grating shake-outs – up to 115dB,
- circular saws for metal – up to115dB,
- power hammers – up to 122dB,
- presses – up to 115dB,
- valves – up to 120dB,
- fans – up to 114dB,
- gantry cranes, conveyor systems, transfers, feeders – up to 112dB.

9.4. Noise measurement in the CNC milling centre and the results

The aim of conducted measurements was to determine the noise level emitted by the DMC 635 eco machining centre using a dedicated measurement system.

The measurements were performed in compliance with the well-established procedures for noise measurement in machine tools for metal, specified in PN-ISO 230-5: 2002 and PN-N-01307:1994. According to these standards, the basic values measured in each determined microphone for each section of work time or production cycle of the tested machine tool are:

L'_{pA} – averaged level of acoustic pressure, corrected with the frequency specification A, during the work of the tested machine tool,

L''_{pA} – averaged level of acoustic pressure, corrected with the frequency specification A, emitted by the background noise,

L_{pCpeak} – peak acoustic pressure level corrected with the frequency specification C.

The process of diagnostic assessment of the noise emitted by the tested machine tool was conducted according to a schedule which included:

- preparatory works (determining the number of measurement points and their positioning, machine commissioning, defining the parameters of machine tool work: idle run or work trial, etc.),
- the process of diagnostic assessment (performing measurements, determining environmental adjustments, calculations, result analysis),
- inferring (comparison and the assessment in comparison to the permissible value, permissible level value of exposure to noise which should not exceed 85dB).

The measurements were performed in the four microphone positions installed at a level of 1.55m with a tolerance of ±0.075m at a distance of 1m from the so-called reference cube surrounding the machine tool. The dimensions of the reference cube were 3x2.5x2.8m. These assumptions were in compliance with the standards, and described a case when the machine operator moves on a specified path in the vicinity of the tested machine tool. It was also assumed that the microphones would be placed at a distance of 0.2m with a tolerance of ±0.02m from the plane of symmetry of the operator's head. The level of acoustic pressure of the emissions should be noted as an acoustic pressure level of the tested machine tool. The place where the pressure value was measured should also be determined. The standard recommends that the time should not be shorter than 30s [134].

The measurement of acoustic emission of the tested machine tool was performed using a four-channel acoustic meter, Svantec 958, and four measurement microphones, Svantec SV22, with the Svantec SV12L preamplifier. The measurement station plan with four measurement points corresponding to the positioning of microphones is shown in Fig. 135. Acoustic emission measurements of the tested machine tool were performed in a room with the dimensions of 11.2x14.3x3.7m. The measurements were performed for a standard work cycle of the machine tool. A result analysis was conducted using the SvanPC++ application. The real measurement time was 60s.

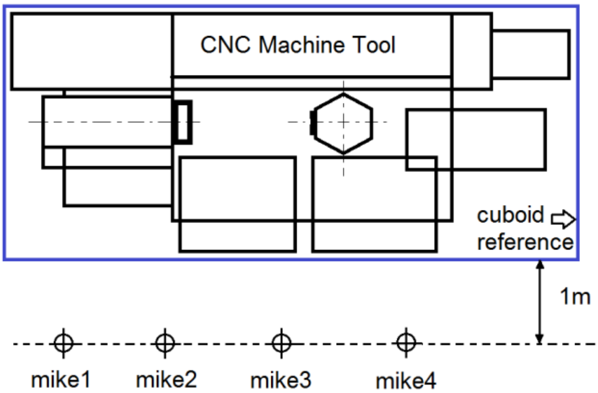

Fig. 135. Schematic design of the measurement station and arrangement of measurement points (microphones)

In order to determine the acoustic levels of pressure emitted by the machine tool, the measured levels of acoustic emission pressure levels L'_{pA} a correction was made to include the background noise and the so-called local environmental correction K_A, excluding the peak levels of acoustic pressure levels L_{pCpeak} for which any corrections are unacceptable. The level of acoustic pressure L_{pA} emitted by the machine tool is determined depending on the level of background noise, taking into consideration the following conditions:

a) for the differences ΔL_A between the measured emitted level of acoustic pressure L'_{pA} corrected by a frequency specification A of the machine tool in a specified position and the level of acoustic pressure L''_{pA} of the background noise corrected by a frequency specification A, higher than 10dB (15dB for the accuracy level 2), the level of emission acoustic pressure in this specified position was determined as (53):

$$L_{pA} = L'_{pA} - K_A \tag{53}$$

b) for the differences ΔL_A in a specified position from the range of 3dB÷10dB (15dB for the accuracy level 2), the level of emission acoustic level in this position was determined as (54):

$$L_{pA} = 10\lg\left[10^{0,1L'_{pA}} - 10^{0,1L''_{pA}}\right] - K_A \tag{54}$$

The correction taking into consideration the level of background noise was applied to every position where ΔL_A is within the range of 3dB÷10dB. If ΔL_A is higher than 6dB, the results correspond to the accuracy level of 2, otherwise the accuracy level of 3. If $\Delta L_A < 3$dB, then – according to the standard – the measurement is cancelled.

Local environmental correction K_A includes the influence of sound reflected and the level of emission acoustic pressure in a specified place of the tested machine tool. Taking into consideration the basic requirements, the environmental correction K_A should not exceed 7dB. As regards the survey method (accuracy level 3) presented in the work, the local environmental correction K_A was determined from the following relation (55) [134]:

$$K_A = 10\log\left[1 + 4(2\pi a^2 / A)\right] \tag{55}$$

where:
a – is the distance from a specified place to the nearest main source of sound of the tested machine tool [m], A – is an equivalent acoustic absorption of the room surface at the frequency of 1 kHz [m^2]

It should be stressed at this point that when the main source of sound is not precisely defined, the distance a should be accepted as the distance from the specified place to the nearest part of the tested machine tool. Value A of the equivalent acoustic absorption is determined with one of the two methods:

a) approximate method – according to which acoustic absorption A is determined with the following equation (56):

$$A = \alpha \cdot S_V \tag{56}$$

where:
α – is an average factor of acoustic absorption, given for values corrected with an A type frequency specification, S_V – is a total area limiting the measurement room (e.g., walls, ceiling, floor) [m^2]

b) reverberation method – where the acoustic absorption value of room surface A is determined by the measurement of reverberation time in a measurement room using broadband or impulse noise and the frequency correction A in the reception system. Value A expressed in square metres is determined from the Sabine's formula (57):

$$A = 0{,}16(V / T) \tag{57}$$

where:
V – is the measurement room volume [m^2], T – is the reverberation time of the measurement room [s]

Before the measurement of machine tool noise emission, the microphone calibration was done with the Svantec SV30A calibrator. The measurement of the background noise level L''_{pA} was performed in the first part of the experimental tests. The measurement results are listed in Tab. 32. The results prove that the average background noise level in the moment t=7s is L''_{pA}=32.76dB.

Tab. 32. Comparison of the results of background noise level measurement L''_{pA} corrected with type A frequency specification

Mik	Filter	Detector	Elapsed time [s]	Units	L''_{pA} [dB]
1	A	Fast	7	dB	32.58
2	A	Fast	7	dB	33.04
3	A	Fast	7	dB	32.86
4	A	Fast	7	dB	32.56
				Mean	32.76

Measurements were performed in three series during the work trial. The measurement results of momentary noise level recorded at the same time by subsequent microphones are presented in Fig. 136.

a)

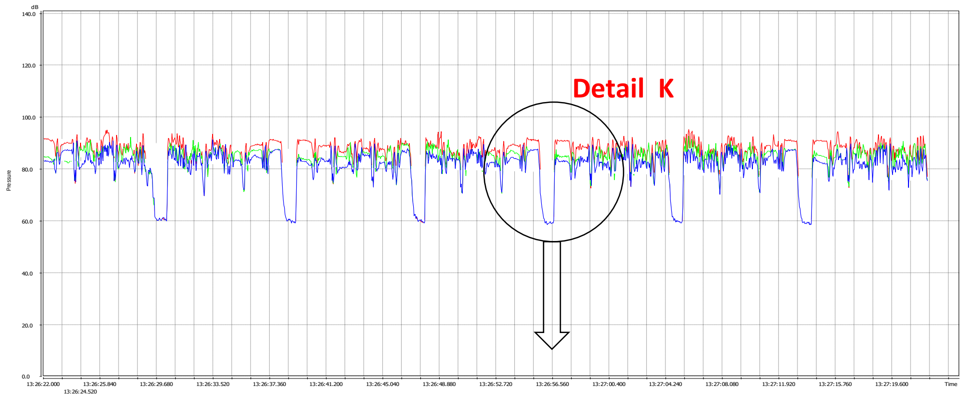

b)

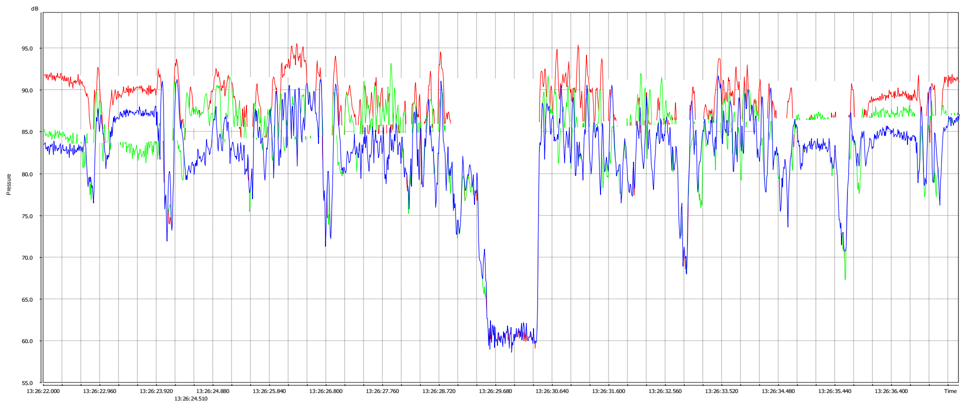

Fig. 136. Momentary values of acoustic pressure levels for 4 microphones recorded during the measurement: a) signal in the exposure time of 60 seconds, b) detail K

The first series of measurements investigated the impact of machining speed v_c from the range of 420-620m/min on the value of noise emitted by the machine tool. Other technological parameters: the feed and the depth of cut were maintained constant at f=0.2mm/blade and a_p=2mm, respectively. Obtained measurement results are compared in Tab. 33 and in Fig. 137. The maximum noise values were obtained from test 3 for the machining velocity of v_c=520m/min.

Tab. 33. Comparison of the results of noise emitted by the machine tool at variable machining velocity v_c

v_c [m/min]	L'_{pA} **[dB]**	L_{pCpeak} **[dB]**
420	59.68	92.29
470	79.2	94.15
520	**83.13**	**98.34**
570	80.33	97.82
620	81.71	97.94

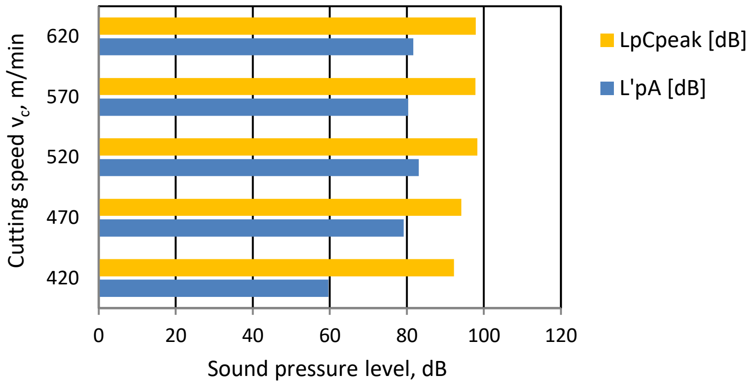

Fig. 137. Results of the first measurement series of noise emitted by the machine tool, for different values of machining velocity v_c

The second stage of measurements involved the determination of the effect of feed f on the value of noise emitted by the machine tool. The constant values of machining velocity (v_c=520mm/min) and the depth of cut (a_p=2mm) were assumed. The feed was changed within the range of f=0.1÷0.3mm/blade. The measurement results are compared in Tab. 34 and in Fig. 138. The maximum values of noise levels were recorded in test 5 for the highest tested feed value f=0.3mm/blade.

Tab. 34. Comparison of the results of measured noise emitted by the machine tool at variable feed

f **[mm/blade]**	L'_{pA} **[dB]**	L_{pCpeak} **[dB]**
0.10	78.28	95.7
0.15	79.89	96.11
0.20	83.13	98.34
0.25	83.74	99.78
0.30	**85.76**	**103.81**

In the third part of measurements, the machining velocity (v_c=520mm/min) and the feed (f=0.2mm/blade) were defined as constant values. The depth of cut in the range of a_p=1÷3mm remained variable. The measurement results are compared in Tab. 35 and in Fig. 139. The maximum values of noise levels were also obtained from test 5 for the maximum cutting depth a_p=3mm.

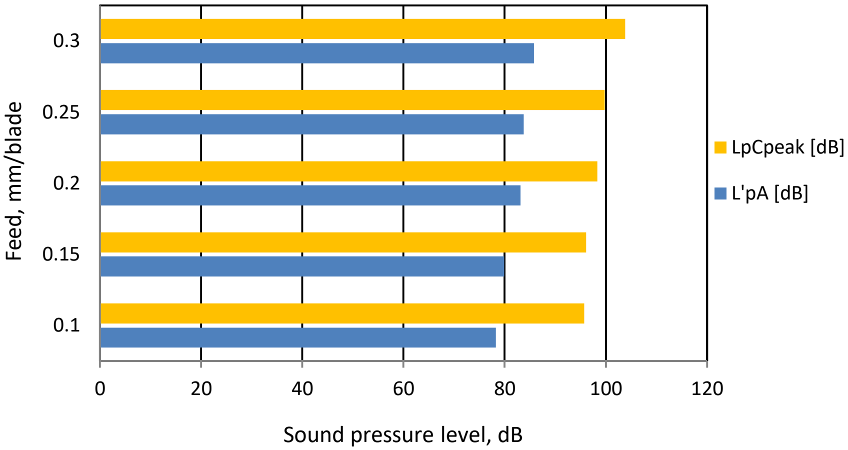

Fig. 138. Noise emitted by the machine tool as a function of feed *f*

The maximum average level of acoustic pressure L'_{pA} was recorded during the third stage of measurements (at v_c=520m/min, f=0.3mm/blade, a_p=3mm) and it amounted to L'_{pA}=88.33dB. In compliance with the standards, the result was treated as an averaged level of acoustic pressure of the tested machine tool.

Tab. 35. Comparison of the results of noise emitted by the machine tool at variable cutting depth a_p

***a*p [mm]**	**L'_{pA} [dB]**	**L_{pCpeak} [dB]**
1.00	80.36	99.50
1.50	81.50	98.20
2.00	85.76	103.81
2.50	86.51	102.03
3.00	**88.33**	**103.97**

In order to determine the local environmental correction K_A, the equivalent acoustic absorption *A* was measured by the reverberation method. To this end, an omnidirectional source of sound and a broadband noise generator were used. The measurement of room reverberation was performed with the use of a noise meter, Norsonic NOR140. The time of measurement room reverberation was set equal to T=1.83s. Hence, on the basis of Sabine's formula (57), the equivalent acoustic absorption *A* was estimated to be 51.8m^2 (for the measurement room volume of V=592.6m^3). Assuming that a=1m, the local environmental correction K_A for the measurement room determined on the basis of Equation (55) was 1.72dB.

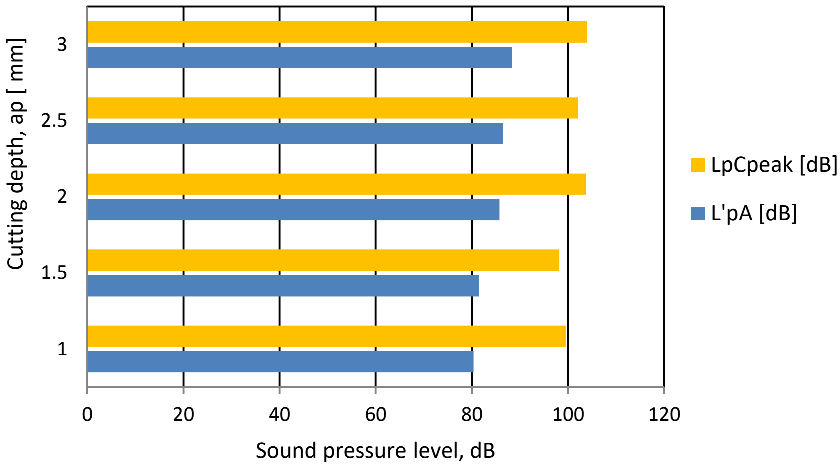

Fig. 139. Noise emitted by the machine tool as a function of cutting depth a_p

The difference ΔL_A between the measured level of acoustic pressure L'_{pA} corrected with the A frequency specification (emitted by the tested machine tool) and the level of acoustic pressure L''_{pA} of the background noise corrected by the A frequency specification during the measurements was higher than 10 dB. As a result, the level of acoustic emission level for the tested machine tool was determined on the basis of Equation (53). The value was 86.61dB. The maximum peak level for acoustic pressure was corrected with the type C frequency specification. In the third stage of measurements (with v_c=520m/min, f=0.3mm/blade, a_p=3mm), the corrected peak value of acoustic pressure was L_{pCpeak}=103.97dB. According to the standard, the above mentioned values of pressure levels were rounded to the closest total value. The final values of L_{pA}=87dB and L_{pCpeak}=104dB were accepted. Based on the conducted measurements of acoustic emission of the tested machine tool in the work trial, it can be observed that in some machining conditions (described with technological machining parameters) the noise emission standards in the workplace (85dB) are slightly exceeded. Taking into consideration the influence of noise on the human body, a long-term operation of the machine tool in such conditions requires the use of hearing protection devices. Data included in the noise parameter changes are the symptoms of machine tool damage, clearances, machine overload or incorrect work.

9.5. Noise sources identification by acoustic holography

Acoustic holography is relatively rarely used in the diagnostics and testing of machine tools. Given very few sources in the literature, it can be claimed that the technique based on searching for acoustic information, acoustic mapping by the holographic method and creating acoustic history of machine life is still being developed.

The scope of the research presented in the work involved the identification of noise sources in a wide range of frequency bands, acoustic mapping of the tested machine tools, the identification of dispersion directions and the value of acoustic pressure emitted during the spread of sound generated by the machine tool. The measurement of noise was performed for two numerically controlled machining machine tools with similar kinematic and geometric features. The research was performed by the acoustic holography method. Acoustic holography ensures the precise location of noise sources in the machine tool during its operation. It enables the determination of range of areas affected by noise. It also helps to reduce vibroacoustic noise and optimise its level. In addition, the method helps estimate the acoustic force and the composition of spectrum emitted by the machine tool. Thanks to acoustic holography one may create maps of acoustic pressure and vibration speed in measurement planes and those parallel to it.

The tests used a 56-channel signal analyser, Siemens LMS SCADAS Mobile (Fig. 140). The system is designed for very advanced measurements in both laboratory and field conditions. The sound (acoustic pressure) was measured with a holographic template for acoustic holography, TL-AHW.18.1 LMS Circuit Irregular Array, shown in Fig. 140a. The template consists of 56 measurement microphones, PCB 130E22. Every measurement channel connected to an individual microphone is calibrated. The measurements provide reliable sound amplitude values, whereas the recorded map provides a graphic presentation of obtained results.

Fig. 141 shows holograms illustrating the distribution of acoustic pressure and the identified noise-emitting sources in the 65 Mono Block 5-axis machining centre during idle run in a wide frequency band of 180÷7190Hz (Fig. 141a) and in a narrow frequency band range of 3580÷3920Hz (Fig. 141b).

a) b)

Fig. 140. Acoustic holography set-up used in machine tool tests: a) acoustic holography template TL-AHW.18.1 LMS Circuit Irregular Array with a set of 56 measurement microphones PCB 130E22, b) 56-channel sound analyser Siemens LMS Scadas Mobile equipped with dedicated acoustic holography software LMS HD Acoustics

The holograms identify the sources of noise emissions. They demonstrate that these sources are located in the vicinity of a machine door closing area. Bearing in mind that modern CNC machine tools are equipped with a built-in workspace, it should be expected that noise will be emitted through leaks on the path from the source to the recipient. According to the results obtained for different frequency bands, it turns out that the level of acoustic pressure during idle run is 45÷58dBA, and the acoustic pressure impact area is relatively limited and decreases with an increase in distance from the identified source.

a)

b)

Fig. 141. Holograms showing acoustic pressure areas and identified noise-emitting sources in the DMU 65 Mono Block five-axis machining centre during idle run in the band range of: a)180–7190 Hz, b) 3580–3920Hz

Fig. 142 shows a hologram illustrating the sources of noise in the DMU 65 Mono Block 5-axis machining centre during tests in a narrow frequency band ranging from 4600 Hz to 6100Hz (Fig. 142a) and in a very wide range of 180÷7190Hz (Fig. 142b).

a)

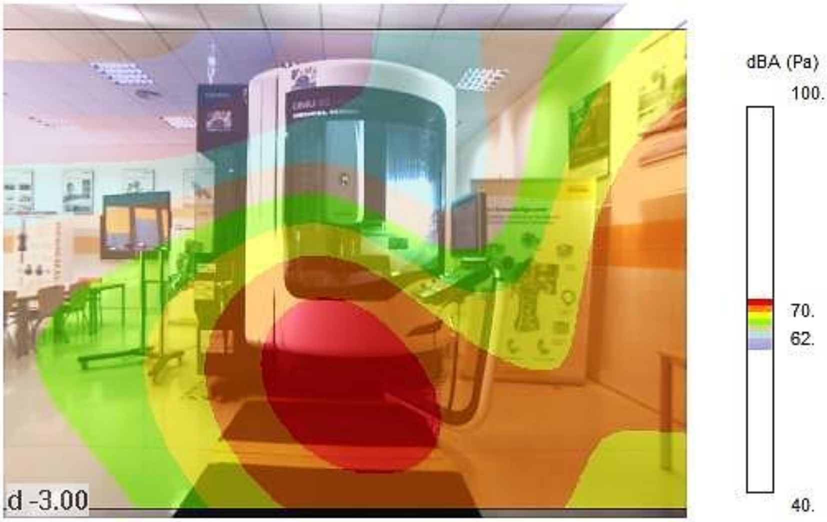

b)

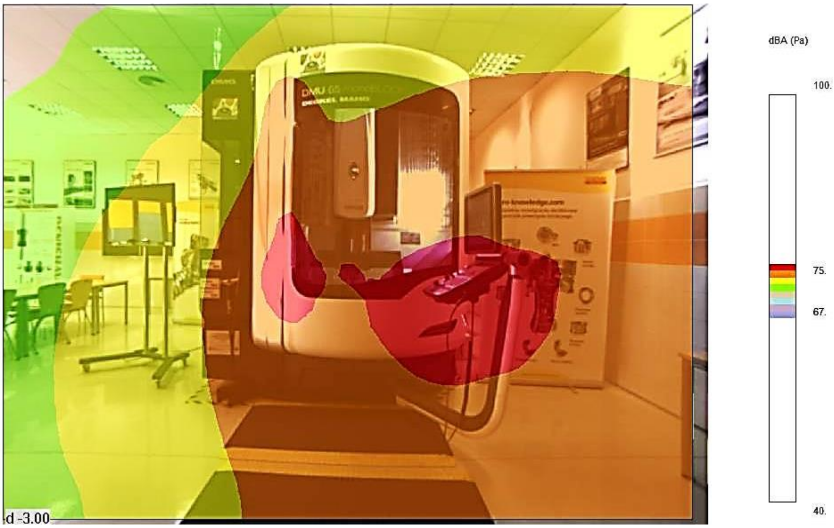

Fig. 142. Hologram showing the distribution of acoustic pressure and identified noise-generating sources in the DMU 65 Mono Block five-axis machining centre in the frequency band range: a) 4600–6100 Hz, b) 180–7190Hz

The presented holograms (Fig. 142) reveal that the noise-affected area increases significantly in relation to the idle run and includes the machine tool operator's stand. Given that the acoustic pressure near the machine operator's stand is high, it is hazardous for hearing and general health of the worker (in an eight-hour working day frame). The recorded acoustic pressure values are at the level of 75dB. The use of holography allows us to effectively identify the range of exposure to noise. Successive holographic measurements in defined time ranges enable the creation of an acoustic history of the machine service life, which – together with information about the machine tool technical condition – will enable the prediction of machine tool failure.

Figs. 143÷149 show the acoustic pressure dispersion holograms and the identified sources of generated noise in various frequency bands for the DMC 635 eco machining centre.

Fig. 143. Hologram showing acoustic pressure dispersion and identified noise-generating sources in DMC 635 eco machining centre in the band range of 930÷1210Hz

The figures clearly demonstrate that, depending on the frequency band, the noise is emitted by:

– main motion drive (Fig. 143 – within the range of 930÷1210Hz, Fig. 146 – 1840÷5280Hz, Fig. 149 – 2900÷2960Hz),
– power and control system (Fig. 145 – within the band range of 1640÷1820Hz, Fig. 146 – 1840÷5280Hz, Fig. 147 – 2630÷2710Hz), machine base (Fig. 144 – within the band range 1350÷1610Hz, Fig. 146 – 1840÷5280Hz),
– spindle end (Fig. 148 – within the band range of 2740÷2830Hz).

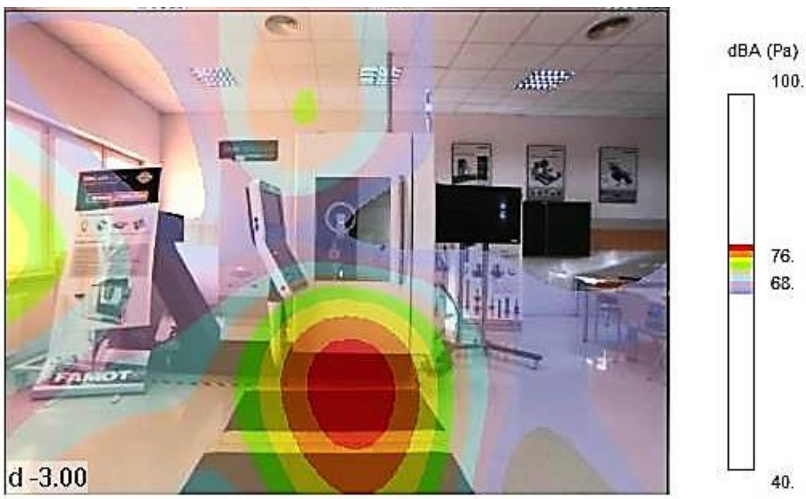

Fig. 144. Hologram showing acoustic pressure dispersion and identified noise-generating sources in DMC 635 eco machine centre in the band range of 1350÷1610Hz

Fig. 144 clearly shows that there is an area of sound reverberation from the walls, window panes, ceiling and floor, respectively, ranging from 1350÷1610Hz (Fig. 144), 1640÷1820Hz (Fig. 145), 2740÷2830Hz (Fig, 148) and 1840÷5280Hz (Fig. 146). The clearly noticeable reverberation effect leads to an higher negative impact on the operator's organism, especially during long-lasting exposure.

Fig. 145. Hologram showing acoustic pressure dispersion and identified noise-generating sources in DMC 635 eco machining centre in the range of 1640÷1820Hz

Fig. 146. Hologram showing acoustic pressure dispersion and identified noise-generating sources in DMC 635 eco machine tool in the band range of 1840÷5280Hz

As demonstrated above, depending on the frequency band range, all machine tool noise sources are shown together with reverberation.

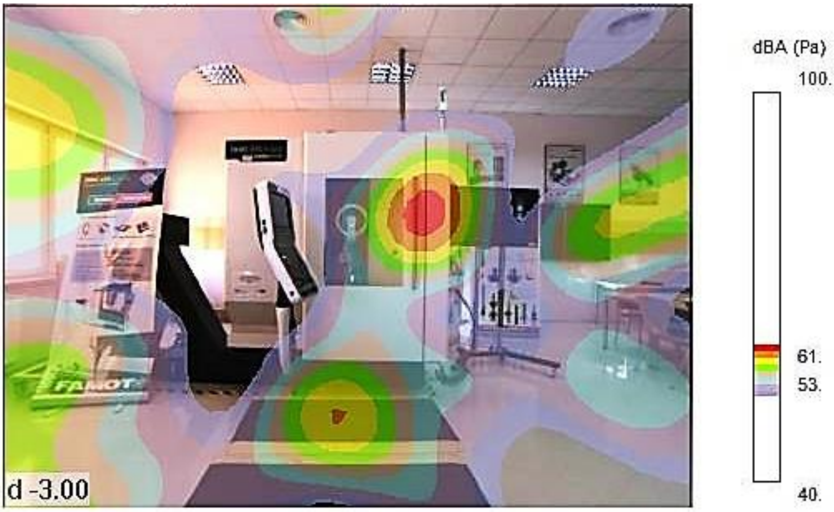

Fig. 147. Hologram showing acoustic pressure dispersion and identified noise-generating sources in DMC 635 eco machining centre in the range of 2630÷2710Hz

Fig. 148. Hologram showing acoustic pressure dispersion and identified noise-generating sources in the DMC 635 eco machining centre in the range of 2740÷2830Hz

Fig. 149. Hologram showing acoustic pressure dispersion and identified noise-generating sources in the DMC 635 eco machining centre in the range of 2900÷2960Hz

Fig. 150 shows the time course of noise in the range of 2740÷2830Hz for the DMC 635 eco machining centre and DMU 65 MonoBlock (Fig. 150b). Fig. 151 shows noise sonogram images obtained for the same frequency range as in the case of time. In Fig. 151 the areas of acoustic signal concentration are marked in colour and shown in the form of colourful stripes concentrated in the low frequency areas (0÷2000Hz).

a)

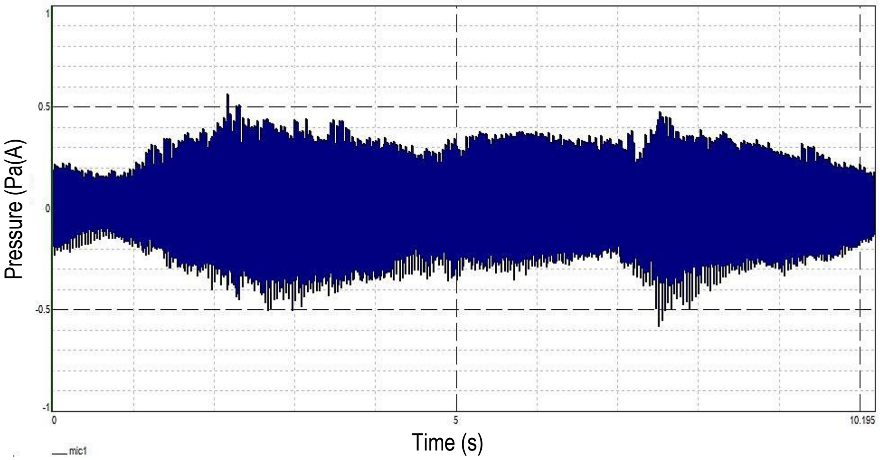

b)

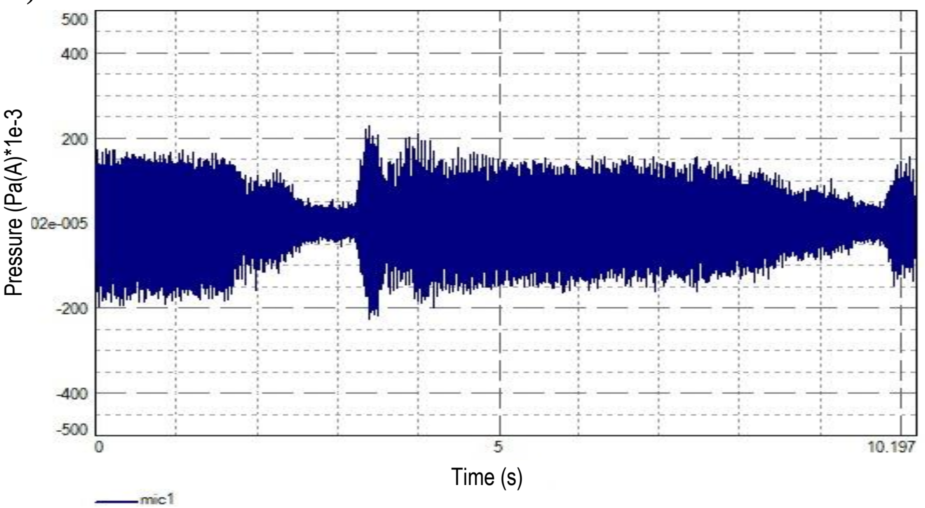

Fig. 150. Time-course of noise (in the range of 2740–2830Hz):
a) DMC 635 eco, b) DMU 65 MonoBlock

a)

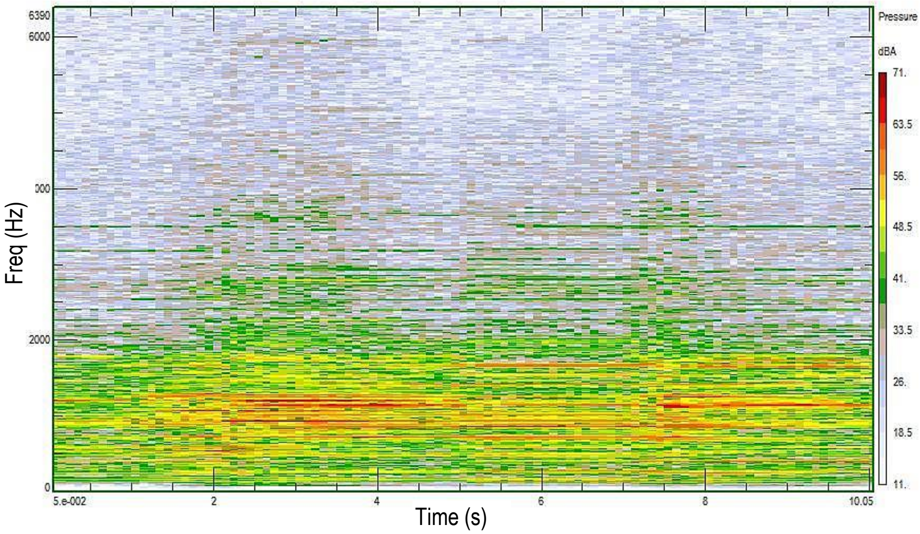

b)

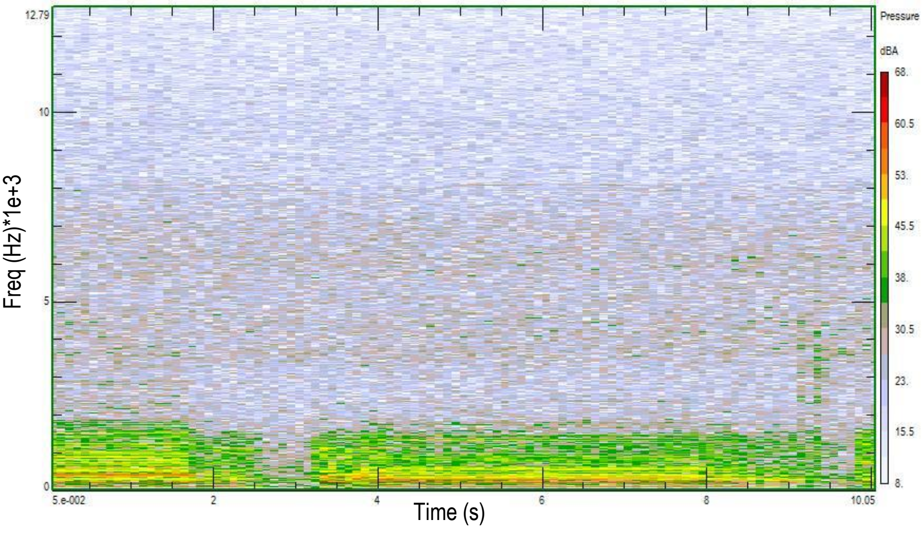

Fig. 151. Noise sonogram images (within the band range of 2740–2830 Hz):
a) DMC 635 eco, b) DMU 65 MonoBlock

Fig. 152 presents selected images of noise spectrum for the DMC 635 eco machining centre and DMU 65 MonoBlock.

a)

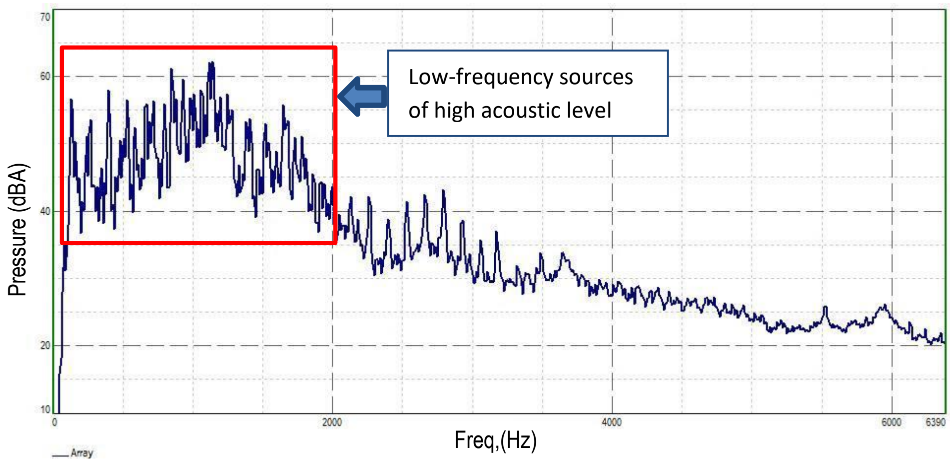

b)

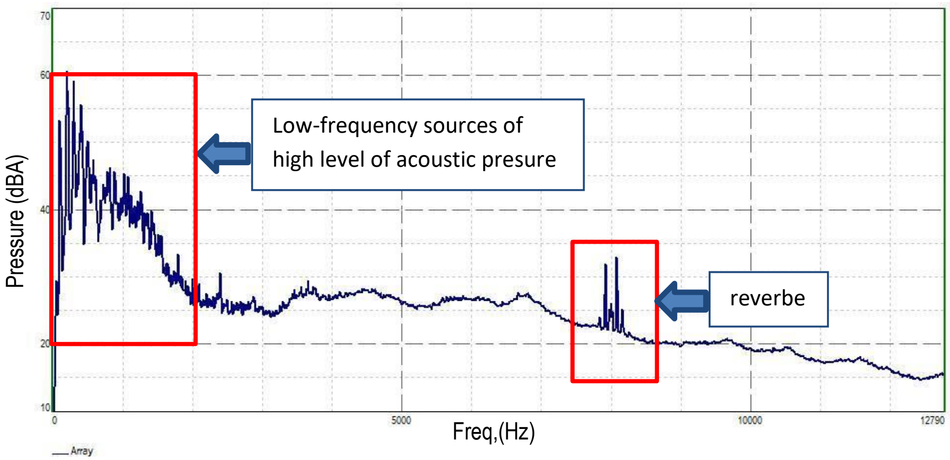

Fig. 152. Noise spectrum: a) DMC 635 eco,
b) DMU 65 MonoBlock

The noise spectrum as a frequency function shown in Fig. 152 reveals the presence of low-frequency sources (0–2000Hz) of high acoustic pressure levels. They can be caused by noise generated by the thin-walled design of the machine tool body or by auxiliary operations on the machine, e.g., tool replacement, probe removal, etc. The occurrence of high-frequency areas of noise with low levels of acoustic pressure is caused by noise reverberation.

10. SUMMARY AND CONCLUSIONS

Machine tool errors can be identified in many different ways and at different stages of service life of technical objects. In this work, production errors were analysed at the stage of machine design, production and – most of all – operation. They are identified using numerical, simulation, and experimental methods. Upon leaving a manufacturing plant, every machine tool receives a specific passport with its specified geometric and kinematic output accuracy. This output accuracy is usually identified with laser interferometers or roundness test using Ballbar diagnostics systems.

Error values for machine tools is determined by their utilization features and the capability of performing tasks which are required of them. The values of machine tools errors are also a determinant for taking a decision to eliminate a certain means of production. Identification of machine tools errors in an analytical way is a relatively difficult task and often mainly theoretical. There is no way to generalize and to move analytical models over to all machine tools, taking into consideration its design complexity, kinematic variety and the used materials and control systems, but most of all, the complex system of thermal and power interactions during exploitation (especially during multi-axial machining and the complex system of load in the axes). Therefore, machine tool error identification should be considered not only in static and dynamic conditions but also during idle running. Most of all, however, it should be tested during work trial in dynamic conditions. It turns out that the most effective, and, at the same time, an objective way to identify numerically controlled machine tools are methods of experimental identification. These are not sufficient methods in each and every case, however. All methods and research ways (specified in ISO standards) are methods of testing machine tools mainly in static, rather less frequently dynamic, conditions, but always performed during idle running. Such conditions do not fully reflect errors occurring during operation in dynamic conditions. It turns out that such tests are not sufficient for an objective assessment of machine tool inaccuracy. No effective and efficient method has yet been developed for machine tool error identification of machine tools under load during work trial. The truth is that the design of diagnostic tools and machines does not allow for that. Although the literature of the subject provides numerous examples of testing machine tools through trial with load, such ways have not found a wider industrial application and are only used for scientific and research purposes. As practical experience shows, the assessment of errors during work test is the only tool to effectively specify and influence machine tool results, even if via compensation of the identified error.

Significant advantages of this work include:

1. It is a comprehensive theoretical and practical study on the methods for machine tool diagnostic error identification, as well as on the ways and devices enabling effective error detection that are available on the European market.
2. The study provides a wide range of theoretical and practical information concerning diagnostic measurement by modern diagnostic tools, both linear and numerically-controlled rotary axes, including innovative systems for determining the kinematic centres of rotational axes in static and dynamic measurement conditions.
3. It offers an extensive description of experimental material in the form of kinematic and geometric errors enabling their prediction on the basis of specified equations.
4. It identifies crucial mathematical model parameters describing selected static and dynamic errors.
5. It proposes a concept of machine tool error prediction on the basis of time series.
6. The work proposes modified models of Simple Moving Average and Weighted Moving Average to make predictions verified by ex-post errors.
7. It determines values of the rotary axis coordinate system with 3D QuickSet and R-test systems.
8. It develops a way of visualising CNC machine tool rotary axis kinematic centre positioning in relation to linear axes and spindle motion errors by machine tool spindle analysis.
9. The study presents machine tool acoustic maps determined in various frequency ranges by the acoustic holography method used for identifying sound sources and reverberations.
10. It proposes the modification of machine tool thermal diagnosis procedures while determining thermal states and thermal stability.
11. It offers a concise and systematic compendium of static knowledge concerning experimental identification of machine tool errors, previously unavailable in the literature of the subject.

In his further work, the author will attempt to develop a system capable of identifying machine tool errors by dynamic measurements of machine tool operating condition and of storing the results in a data base. Then, based on developed prognosis algorithms, such system will generate predictions and provide emergency information if the set threshold (limit) values are exceeded.

Machine tool error analysis and the creation of an error development history are two extremely important tasks in industrial conditions. The knowledge of error values and the nature of their changes enables prolonging the service life of machine tools, for example via compensating and affecting their drive parameters. Moreover, such knowledge helps maintain the machine in constant operational readiness, take action connected with renovations and repairs, and predict the technical condition of machine tools with similar geometric and kinematic features.

Taking into consideration the scope of research undertaken in this work as well as the wide spectrum of discussed diagnostic methods, the analysis of obtained research results, the modelling and prediction of selected machine tool errors, one may claim that the objectives set by the author of this work have been met.

STRESZCZENIE

Przedstawiona praca jest kompendium wiedzy poświęconym analizie źródeł błędów obrabiarek CNC i skutkom ich oddziaływania. Jest kompleksowym studium teoretycznym i praktycznym dotyczącym metod diagnostycznych identyfikacji błędów obrabiarek (statycznych i dynamicznych, osi liniowych i obrotowych), sposobów i dostępnych na rynku europejskim urządzeń pozwalających na skuteczne ich wykrywanie. Rozpoznanie źródeł błędów dzięki monitorowaniu i diagnostyce jest niezwykle ważne do zoptymalizowania działań zapobiegawczych przed uszkodzeniem maszyny i wyeliminowaniem jej z procesu produkcyjnego.

Dynamiczne procesy mechaniczne zachodzące na obrabiarkach CNC dotyczą zamiany energii mechanicznej wytworzonej przez silniki elektryczne (lub inne) na pracę. Ponieważ przenoszenie energii wytwarzanej z silnia do zespołu roboczego obrabiarki CNC odbywa się za pośrednictwem fizycznych elementów wykonanych i zmontowanych z określoną dokładnością, stają się one źródłem błędów geometrycznych, które zmieniają się w funkcji czasu eksploatacji, głównie wskutek zużycia. Szczegółową analizę rodzajów błędów i ich charakterystykę zaprezentowano w rozdziale 1. W rozdziale 2 określono cel i zakres pracy. Skupiono się głównie na błędach pozycjonowania osi liniowych i obrotowych, którym poświecono rozdział 3 oraz rozdział 4, a także innych błędach geometrycznych, kinematycznych i termicznych. W rozdziale 5 omówiono błędy identyfikowane kinematycznym prętem teleskopowym. Wyniki tych prac wykorzystano do opracowania modeli prognostycznych identyfikacji błędów obrabiarek. Kolejnym rozważanym w pracy zagadnieniem są oddziaływania termiczne w obrabiarkach, którym poświęcono rozdział 6. Ich źródłem są głównie tarcie oraz odkształcenia sprężyste, zachodzące wskutek oddziaływań siłowych, bezwładnościowych i kinematycznych. Diagnostyka termograficzna obrabiarki daje podstawę do skutecznego minimalizowania odkształceń termicznych. Ważnym zagadnieniem zaprezentowanym w rozdziale 7 jest uwzględnienie błędnych ruchów wrzecion. W obrabiarkach sterowanych numerycznie realizowane są zaprogramowane ruchy opisane w założonym układzie współrzędnych. Precyzja realizacji opisanych w programie trajektorii zależy nie tylko od dokładności przemieszczeń w osiach sterowanych numerycznie ale także błędnych ruchów wrzecion. W pracy zawarto metody identyfikacji błędów wrzecion (synchronicznych, asynchronicznych, i innych), jak również omówiono metody identyfikacji położenia środków kinematycznych osi obrotowych wybranych obrabiarek (rozdział 8).

Rozdział 9 poświecono akustycznej diagnostyce obrabiarek. Generowane dźwięki mają różne źródła, natężenie i zakres oddziaływania. Z punktu widzenia bezpieczeństwa najbardziej niebezpieczny jest hałas i jego oddziaływanie na narządy słuchu operatora. Hałas jest również skorelowany z procesami

destrukcyjnymi zachodzącymi w maszynie. Jest wynikiem pogarszającego się stanu technicznego urządzenia, dlatego też niesie cenne informacje o zbliżającej się np. awarii. W pracy wyznaczono mapy akustyczne obrabiarek określonego typu, z wykorzystaniem holografii akustycznej. Zidentyfikowano źródła generowania hałasu w obrabiarkach oraz określono poziomy ciśnienia akustycznego generowanego przez obrabiarki.

Praca stanowi prezentację zwartego – syntetycznego i usystematyzowanego obszaru wiedzy, dotyczącego eksperymentalnej identyfikacji błędów obrabiarek, niedostępnego do tej pory w zbiorach bibliograficznych. Analiza błędów obrabiarek i tworzenie historii ich rozwoju jest niezwykle ważnym zadaniem w warunkach przemysłowych. Znajomość wartości błędów i charakteru ich zmian, umożliwia wydłużenie trwałości obrabiarek, między innymi dzięki możliwości kompensacji błędów i wpływaniu na parametry napędów. Pozwala to także na utrzymanie maszyn w ciągłej gotowości eksploatacyjnej i wyprzedzające działania związane z remontami i naprawami, a także prognozowanie stanów przyszłych dla określonej grupy obrabiarek o zbliżonych cechach geometryczno-kinematycznych.

BIBLIOGRAPHY

[1] Abderrahim M., Khamis A., Garrido S., Moreno L., *Accuracy and Calibration Issues of Industrial Manipulators*. Industrial Robotics – Programming, Simulation and Applications, Germany 2006.

[2] Alici G., Shirinzadeh B., *A systematic technique to estimate positioning errors for robot accuracy improvement using laser interferometry based sensing*. Mechanism and Machine Theory, 2005, 40, pp. 879–906.

[3] Angelidis A., Vosniakos G.Ch., *Prediction and Compensation of Relative Position Error along Industrial Robot End-Effector Paths*. International Journal of Precision Engineering and Manufacturing, 15/1, 2014, pp. 63–73.

[4] Bielenin M., *Laserowy układ do pomiarów przestrzennych*. Wyd. Politechnika Wrocławska, Wrocław 2009.

[5] Bohez E.L.J., *Compensating for systematic errors in 5-axis NC machining*. Computer Aided Design, 2002, 34, pp. 391–403.

[6] Bossoni S., *Geometric and Dynamic Evaluation and Optimization of Machining Centers*. Diss. ETH, 18382, 2009.

[7] Bringmann B., *Improving Geometric Calibration Methods for Multi-axes Machining Centers by Examining Error Interdependencies Effects*. Fortschritt-Berichte VDI 2/664, Dusseldorf 2007.

[8] Bringmann B., Knapp W., *Model-based 'Chase-the-Ball' Calibration of a 5-Axes Machining Center*. Annals of the CIRP 55(1), 2006, pp. 531–534.

[9] Bryan,J.B., *A simple method for testing measuring machines and machine tools*. Part 1: Precision Engineering, 1982, 4, 2: 61.

[10] Bryan J.B., *A simple method for testing measuring machines and machine tools*. Part 2: Precision Engineering, 1982, 4, 3: 125.

[11] Caban J., Iskra R., Józwik J., Kamieńska-Krzowska B., *Ocena stanu maszyny technologicznej CNC z zastosowaniem interferometrii laserowej*. Monografia pod red. J. Józwik i inni „Techniki wytwarzania w budowie maszyn – aktualne zagadnienia badawcze", LTN, Lublin 2007.

[12] Castroa H.F.F., Burdekinb M., *Calibration system based on a laser interferometer for kinematic accuracy assessment on machine tools*. In: Inter. Journal of Machine Tools & Manufacture, 2006, 46, pp. 89–97.

[13] Chajda J., Poloszyk S., Różański L., *Próba wykorzystania obrazów termalnych do oceny stanu technicznego maszyn technologicznych*. [w]: Pomiary Termowizyjne w praktyce, VIII Konferencja naukowo-techniczna „Metrologia w technikach wytwarzania maszyn" tom II, Politechnika Szczecińska, s. 463–470, Szczecin 1999.

[14] Chen J.S., Kou T.W., Chiou S.H., *Geometric error calibration of multi-axis machines using an auto-alignment laser interferometer*. In: Journal of the International Societies for Precision Engineering and Nanotechnology, 1999, 23, pp. 243–252.

[15] Conrad K.L., Shiakolas P.S., Yih T.C., *Robotic calibration issues: accuracy repeatability and calibration*. Proceedings of the 8th Mediterranean Conference on Control & Automation, Rio, Patras, Greece, 17–19 July 2000.

[16] Curran E., Phelan P., *Quick check error verification of coordinate measuring machines.* Journal of Materials Processing Technology, 2004, 155–156, pp. 1207–1213.

[17] Delbressine F.L.M., Florussen G.H.J., Schijvenaars L.A., Schellekens P.H.J., *Modelling thermomechanical behaviour of multi-axis machine tools*. Precision Engineering, 2006, 30, pp. 47–53.

[18] Du Z.C., Hong C.F.Lv., M. S., *Research or Error Moddeling end Identification of 3 Axis NC Machine Tools Based on Cross Grind Encored Measurement*. Journal of Physics, 2006, 48, pp. 91–100.

[19] Dugin A., Popov A., *Increasing the accuracy of the effect of processing materials and cutting tool wear on the ploughing force values*. In: Manufacturing Technology, 2013, 13, 2, pp. 169–173.

[20] Durica I., Kuric I., *Calibration and machine performance monitoring*. 9th International Conference Automation in Production Planning and Manufacturing, Published by Scientific and Technical Society at the University of Zilina, Slovakia 2008.

[21] Durica I., Kuric I., *Diagnostics of CNC machines with Renishaw equipment*. The international conference of the Carpathian Euro-Region specialists in industrial systems, 7th edition, 2012.

[22] Fan J.W., Guan J.L., Wang W.C., Luo Q., Zhang X.L., Wang L.Y., *A universal modeling method for enhancement the volumetric accuracy of CNC machine tools*. Journal of Materials Processing Technology, 2002, 129, 1–3, pp. 624–628.

[23] Florussen G.H.J., *Accuracy Analysis of Multi-axis Machines by 3D Length Measurements*. Technische Universiteit Eindhoven, Ponsen & Looijen bv., Wageningen 2002.

[24] Florussen G.H.J., Delbressine F.L.M., Molengraft M.J.G., Schellekens P.H.J., *Assessing geometrical errors of multi-axis machines by three-dimensional length measurements*. Measurement, Publisher Elsevier, 2001, 30, pp. 241–255.

[25] Florussen G.H.J., Spaan H.A.M., *Dynamic R-Test for rotary tables on 5-axes machine tools*. 5th CIRP Conference on High Performance Cutting 2012. Proceedia CIRP 1, 2012, Available on-line at www.sciencedirect.com, pp. 536–539.

[26] Gondek L., *Analiza dokładności geometrycznej manipulatorów robotów przemysłowych*. Politechnika Krakowska, Seria mechanika, Kraków 2006.

[27] Gong C., Yuan J., Ni J., *Nongeometric Error Identification and Compensation for Robotic System by Inverse Calibration*. International Journal of Machine Tools and Manufacture, 2012, 40, 14, pp. 2119–2137.

[28] Greenway B., *Robot accuracy. Industrial Robot*. An International Journal, 2000, 27, 4, pp. 257–265.

[29] Ha In-Chul, *Kinematic parameter calibration method for industrial robot manipulator using the relative position*. Journal of Mechanical Science and Technology, 2008, 22.

[30] Honczarenko J., Kwaśniewicz J., *Nowe systemy pomiarowe do sprawdzania obrabiarek CNC,* Mechanik, Agenda wydawnicza SIMP, 2008, 12, s. 1012–1016.

[31] Honczarenko J., *Roboty przemysłowe. Budowa i zastosowanie*. WNT, Warszawa 2010.

[32] Hong C., Ibaraki S., Oyama Ch., *Graphical presentation of error motions of rotary axes on a five-axis machine tool by static R-Test with separating the influence of squareness errors of linear axes*. International Journal of Machine Tools & Manufacture, 2012, 59, pp. 24–33.

[33] Ibaraki S.,Iritani T., Matsushita T., *Calibration of location errors of rotary axes on five-axis machine tools by on-the-machine measurement using a touch-trigger probe*. International Journal of Machine Tools and Manufacture, 2012, 58, pp. 44–56.

[34] Ibaraki S., Iritani T., Matsushita T., *Error map construction for rotary axes on five-axis machine tools by on-the-machine measurement using a touch-trigger probe*. International Journal of Machine Tools and Manufacture, 2013, 68, pp. 21–29.

[35] Ibaraki S., Oyama Ch., Otsubo H., *Construction of an error map of rotary axes on a five-axis machining center by static R-test*. International Journal of Machine Tools & Manufacture, 2011, 51, 3, pp. 190–200.

[36] Iwasawa K., Iwama A., Mitsui K., *Development of a measuring method for several types of programmed tool paths for NC machine tools using a laser displacement interferometer and a rotary encoder*. Precision Engineering, 2004, 28, 4, pp. 399–408.

[37] Jastrzębski R., Kowalski T., Osówniak P., Szepke A., *Wyznaczanie dokładności urządzeń technologicznych methodą interpolacji kołowej,* Technologia i Automatyzacja Montażu, 2010, 2, s. 14–21.

[38] Jastrzębski R., Krajewski G., *Methody diagnostyki błędów precyzyjnych stołów obrotowych w obrabiarkach CNC*. XIV Krajowa i V Międzynarodowa Konferencja Naukowo-Techniczna „Metrologia w Technikach Wytwarzania", Pułtusk, 11–14 września 2011.

[39] Jemielniak K., *Analiza błędnych ruchów wrzecion szybkoobrotowych*. Archiwum Technologii Maszyn i Automatyzacji, Politechnika Warszawska, 24/2, Warszawa 2004.

[40] Józwik J., *Ocena odchyłki prostopadłości osi obrabiarki sterowanej numerycznie z wykorzystaniem systemu diagnostycznego QC10 Ballbar*. Postępy Nauki i Techniki, 2010, 4, s. 91–102.

[41] Józwik J., Byszewski M., *Badanie dokładności positioning osi obrotowych wieloosiowych obrabiarek CNC oraz błędów wolumetrycznych*. Mechanik, 2015, 3, s. 144–149.

[42] Józwik J., Byszewski M., *Badanie dokładności ruchów osi wirującej wrzeciona oraz położenia środków osi obrotowych obrabiarek CNC*. Mechanik, 2015, 3, s. 150–155

[43] Józwik J., Ceclan V., Grozav S.D., Kuric I., *Diagnostics of CNC machine tool with R-Test system*. Academic Journal of Manufacturing Engineering, 2014, 12, 1, pp. 52–57.

[44] Józwik J., Czwarnowski M., *Angular positioning accuracy of rotary table and repeatability of five-axis machining centre DMU 65 MonoBlock*. Advances in Science and Technology Research Journal, 2015, 9, 28, pp. 89–95.

[45] Józwik J., Kuric I., *Non-contact diagnostic systems of CNC machine tools*. Published by Scientific and Technical Society at the University of Zilina, 2013.

[46] Józwik J., Kuric I., Saga M., Lonkwic P., *Diagnostics of CNC Machine Tools in Manufacturing Process with Laser Interferometer Technology*. Manufacturing Technology, 2014, 14, 1, pp. 23–30.

[47] Józwik J., Kuric I., Semotiuk L., *Laser Interferometer Diagnostics of CNC Machine Tools*. Communications, 2014, 3A, pp. 167–173.

[48] Józwik J., Kuric I., Grozav S., Ceclan V., *Calibration of 5 axis CNC machine tool with 3D quickSET measurement system*. Academic Journal of Manufacturing Engineering, 2014, 1, 12, pp. 20–25.

[49] Józwik J., Kuric I., Král J.sr, Král J. jr, Spišák E., *Wybrane rozwiązania konstrukcyjne frezarek i centrów obróbczych sterowanych numerycznie*. Postępy Nauki i Techniki, 2012, 13, s. 101–116.

[50] Józwik J., Kuric I., Grozav S.D., Ceclan V., *R-TEST dynamic measurement of 5-axis CNC machining centre rotary axis kinematic centre error*. By: Popescu, D. Conference: International Conference on Production Research – Regional Conference Africa, Europe and the Middle East (ICPR-AEM), 3rd International Conference on Quality and Innovation in Engineering and Management (QIEM) Location: Cluj Napoca, ROMANIA Date: 01–05 JUL 2014, 2014, pp. 278–283.

[51] Józwik J., Lipski J., *Błędy obróbki skrawaniem i ich prognozowanie z wykorzystaniem sztucznych sieci neuronowych*. Politechnika Lubelska, 219, Lublin 2014.

[52] Józwik J., Lonkwic P., Sága M., Kuric I., *R-test static measurement of the 5-axis CNC machining centre rotary axis kinematic centre error*. Manufacturing Technology: Journal for Science, Research and Production, 2014, 14, 2, pp. 186–193.

[53] Józwik J., Madej R., Wójcik R., *Ocena stanu cieplnego wrzeciennika tokarki uniwersalnej*. [W]: Postęp w technikach wytwarzania i konstrukcji maszyn, Lubelskie Towarzystwo Naukowe, s. 139–144, Lublin 2005.

[54] Józwik J., Ostrowski D., Wieczorek M., Czwarnowski M., *Evaluation of accuracy and positioning repeatability of an industrial robot*. Advanced technologies in designing, engineering and manufacturing: research problems, 2015, pp. 146–156.

[55] Józwik J., Pieśko P., Krajewski G., *Evaluation of QC10 Ballbar diagnostics method for CNC machine*. Maintenance and Reliability, 2010, 3, 47, pp. 10–20.

[56] Józwik J., Semotiuk L., Kuric I., *Diagnostic of CNC Lathe with QC 20 Ballbar system*. Advances in Science and Technology Research Journal, 2015, 9, 28, pp. 96–102.

[57] Józwik J., *Diagnostics of CNC machine tools spindle errors*. Mechanik, 2015, 2, s. 197–210.

[58] Józwik J., *Wybrane zastosowania pomiarów termograficznych w obróbce skrawaniem*. Pomiary Automatyka Robotyka, 2009, 2, s. 756–762.

[59] Józwik, J., *Ocena odchyłki prostopadłości osi obrabiarki sterowanej numerycznie z wykorzystaniem systemu diagnostycznego QC10 Ballbar*. Advances in Science and Technology Research Journal, 2010, 4, pp. 91–102.

[60] Józwik J., Krajewski G., Jacniacka E., Pieśko P., Włodarczyk, M., *Prognozowanie dokładności obrabiarki CNC na podstawie szeregu czasowego*. *Cz. 1. Wybrane urządzenia diagnostyczne obrabiarek CNC.* 10th International Conference „Automation in Production Planning and Manufacturing", Published by Scientific and Technical Society at the University of Zilina, Zilina 4–6.05.2009, Slovakia 2009.

[61] Józwik J., Krajewski G., Jacniacka E., Pieśko P., Włodarczyk M., *Prognozowanie dokładności obrabiarki CNC na podstawie szeregu czasowego*. *cz. 2. Prognozowanie odchyłki okrągłości i prostopadłości osi obrabiarki CNC.* 10th International Conference „Automation in Production Planning and Manufacturing", Published by Scientific and Technical Society at the University of Zilina, Zilina 4–6.05.2009, Slovakia 2009.

[62] Jywe W.Y, Hsu T.H, Liu C.H., *Non-bar, an optical calibration system for five-axis CNC machine tools*. Original Research Article. International Journal of Machine Tools and Manufacture, 2012, 59, pp. 16–20.

[63] Kakino Y., Ihara Y., Shinohara A., *Accuracy Inspection of NC Machine Tools by Double Ball Bar Method*, Hasnser Verlag Publishers, 1993.

[64] Kiersztyn M., Wolszczak P., Płaska S., *Automatyczna kontrola positioning robota w elastycznym gnieździe wytwarzania z zastosowaniem technik wizyjnych*. Mechanik, 2014, 8–9, s. 281–290.

[65] Khim Seng, Tan and Chin Keong i inn., *Modelling the volumetric errors in calibration of five-axis CNC machine*. Proceedings if the International Multi Conference of Engineers and Computer Scientist, 2010.

[66] Kuric I., Ďurica I., Madud M., *Accuracy monitoring and calibartion of CNC machines*. Scientific Bulletin, Serie C, XXIII, Fascicle: Mechanics, Tribology, Machine Manufacturing Technology, 2009, pp. 113–118.

[67] Kuric I., Józwik J., Tofil A., *Quality of CNC machine tools and monitoring of their accuracy*. 8th Research/expert conference with international participations – Quality 2013, Neum, B&H, 2013.

[68] Kuric I., Kosinar M., *Geometric Errors in CNC Machine Tools*, 2012.

[69] Lei W.T., Sung M.P., Liu W.L., Chuang Y.C., *Double ballbar test for the rotary axiss of five-axis CNC machine tools*. International Journal of Machine Tools and Manufacture, 2007, 47, 2, pp. 273–285.

[70] Lipski J., *Diagnostyka procesów wytwarzania*. Politechnika Lubelska, Lublin 2013.

[71] Madura H., Minkina W., *Budowa, parametry i zastosowania kamer termowizyjnych*. [W]: Pomiary Termowizyjne w praktyce, Agenda Wydawnicza PAK, s. 27–37, Warszawa 2004.

[72] Majda P., *Relation between kinematic straightness errors and angular errors of machine tool*. Advances in Manufacturing Science and Technology, 2012, 36, 1, pp. 47–53.

[73] Majda P., *The influence of geometric errors compensation of a CNC machine tool on the accuracy of movement with circular interpolation*. Advances in Manufacturing Science and Technology, 2012, 36, 2, pp. 59–67.

[74] Majda P., *Pomiary i kompensacja błędów geometrycznych obrabiarek CNC*. Inżynieria Maszyn, 2011, 16, 1–2, s. 126–134.

[75] Majda P., *Modelowanie i eksperymentalna ocena dokładności przestrzennego positioning zespołow posuwowych obrabiarek sterowanych numerycznie*. Wyd. Przedsiębiorstwo Produkcyjno-Handlowe ZAPOL Dmochowski, Sobczyk, Szczecin 2012.

[76] Mayer K., Pexa M., Pavlů J., *Impact of technical diagnostics interval on machinery maintenance*. In: Manufacturing Technology, 2012, 12, 12, pp. 42–46.

[77] Miko E., Maj P., *Badanie dokładności positioning pionowego centrum obróbkowego*. PAK, 2012, 56, 1, pp. 63–65.

[78] Minkina W., Dudzik S., *Termografia w podczerwieni – błędy i niepewności*. Pomiary Automatyka Kontrola, 2009, 55, 11, s. 868–873.

[79] Minkina W., Madura H., *Podstawy teoretyczne pomiarów termowizyjnych*. [W]: Pomiary Termowizyjne w praktyce, Agenda Wydawnicza PAK, s. 10–26, Warszawa 2004.

[80] Minkina W., Rutkowski P., Wild W., *Podstawy pomiarów termowizyjnych – część I – Istota termowizji i historia jej rozwoju*. Pomiary Automatyka Kontrola, 2000, 1, s. 7–10.

[81] Minkina W., Rutkowski P., Wild W., *Podstawy pomiarów termowizyjnych – część II – Współczesne rozwiązania systemów termowizyjnych, błędy* methody. Pomiary Automatyka Kontrola, 2000, 1, s. 11–14.

[82] Minkina W., *Pomiary termowizyjne – przyrządy i methody*. Wydawnictwo Politechniki Częstochowskiej, Częstochowa 2004.

[83] Morek R., *Pomiary bezstykowe*. STAL Metale & Nowe Technologie, 2012, 5–6, s. 136–138.

[84] Muditha Dassanayake K.M., Tajima K., Cui CH., Tsutsumi M., *A New Device for Accuracy Measurements of Multi-axis NC Machines*. The Second TSME International Conference on Mechanical Engineering, Krabi, Thailand, 19–21 October 2011.

[85] Nakazawa H., Ito K., *Measurement system of contouring accuracy on NC Machine Tools*. Bull. Japan Soc. Prec. Eng., 1978, 12, 4, 189.

[86] Nubiola A., Bonev I., *Absolute calibration of an ABB IRB 1600 robot using a laser tracker*. Robotics and Computer – Integrated Manufacturing, 2013, 29, pp. 236–245.

[87] Orzechowski T., *Technika pomiarów termowizyjnych w diagnostyce maszyn*. Pomiary Automatyka Kontrola, 2002, 4, s. 18–20.

[88] Pahk H.J., Kim Y.S., Moon J.H., *A new technique for volumetric error assessment of CNC machine tools incorporating ball bar measurement and 3D volumetric error model*. International Journal of Machine Tools and Manufacture, 1997, 37, 11, pp. 1583–1596.

[89] Pahk H., Lee S.W., *Thermal Error Measurement and Real Time Compensation System for the CNC, Machine Tools Incorporating the Spindle Thermal Error and the Feed Axis Thermal Error*. International Journal of Advanced Manufacturing Technology, 8, 2002.

[90] Pieczonka Ł., Szwed M., Uhl T., *Termograficzne methody detekcji uszkodzeń*. Pomiary Automatyka Kontrola, 2009, 55, 9, pp. 699–702.

[91] Poloszyk S., Różański L., *Termowizyjna diagnostyka maszyn technologicznych*. Pomiary Automatyka Kontrola, 2000, 1, s. 15–18.

[92] Postlethwaite S.R., Ford D.G., Morton D., *Dynamic calibration of CNC machine tools*. International Journal of Machine Tools and Manufacture, 1997; 37, 3, pp. 287–294.

[93] Ptaszyński W., *Badanie dokładności obrabiarek*. Laboratorium Badania Maszyn CNC, Politechnika Poznańska, Instytut Technologii Mechanicznej, Poznań 2005.

[94] Qiu H., Nishitani H., Kubo A., Yamamoto J., HirakawaI., *Examinations on Motion Accuracy Evaluation Based on the Ball Bar Test for a Machining Center*; Bulletin of the Faculty of Engineering Kyushu Sangyo University, 2003, 40, pp. 11–18.

[95] Różański L., Poloszyk S., *Zastosowanie termowizji w diagnostyce maszyn*. [W]: Pomiary Termowizyjne w praktyce, Agenda Wydawnicza PAK, s. 75–83, Warszawa 2004.

[96] Rżysko T., *Nowe systemy pomiarowe do stosowania na tokarkach CNC*. Mechanik, 2001, 10, 74:665.

[97] Schwenke H., KnappW., Haitjema H., Weckenmann A., Schmitte R., Delbressine F., *Geometric error measurement and compensation of machines – An update*. CIRP Annals – Manufacturing Technology, 2008, 57, 2, pp. 660–675.

[98] Shiakolas P.S., Conrad K.L., Yih T.C., *On the accuracy, repeatability, and degree of influence of kinematics parameters for industrial robots*. International Journal of Modelling and Simulation, 2002, 22, 3.

[99] Shirinzadeh B., Teoh P.L., *Laser interferometry-based guidance methodology for high precision positioning of mechanisms and robots*. Robotics and Computer-Integrated Manufacturing, 2010, 26, pp. 74–82.

[100] Shirinzadeh B., *Laser-interfe $v_f$rometry based tracking for dynamic measurements*. Industrial Robot: An International Journal, 1998, 25, 1, pp. 35–41.

[101] Slamani M., Joubair A., Bonev I., *A comparative evaluation of three industrial robots using three reference measuring techniques*, Industrial Robot: An International Journal, 2015, 42, 6, pp. 572–585.

[102] Slamani M., Nubiola A., Bonev I., *Assessment of the positioning performance of an industrial robot*. Industrial robot: An International Journal, 2012, 39, 1, pp. 57–68.

[103] Ślązak Ł., Magdziak M., *Nowoczesne systemy pomiaru przedmiotów na obrabiarkach NC*. Mechanik, 2007; 5–6, 81, s. 483–489.

[104] Spaan H.A.M., Florussen G.H.J., *Determining the 5-axes machine tool contouring performance with dynamic R-test measurements*. Proceedings of the 12th Euspen International Conference – Stockholm – June 2012.

[105] Staniek R., *Badanie dokładności obrabiarek zybkim testem QC10 (Ballbar)*. Praca niepublikowana, Poznań 2005.

[106] Swevers J., Verdonck W., De Schutter J., *Dynamic model identification for industrial robots*. IEEE Control Systems Magazine, October 2007.

[107] Szafarczyk M., Chrzanowski J., *Nowa koncepcja sprawdzania dokładności maszyn NC*. Materiały konferencyjne „Automatyzacja – Nowości i Perspektywy”, s. 405–413, Warszawa 2005.

[108] Szafarczyk M., *Urządzenie do sprawdzania dokładności obrabiarek 5-osiowych*. Mechanik, 2005, 4, 79:268.

[109] Szkodny T., *Dynamika robotów przemysłowych*. Wydawnictwo Politechniki Śląskiej, Gliwice 2013.

[110] Szkodny T., *Kinematyka robotów przemysłowych*. Wydawnictwo Politechniki Śląskiej, Gliwice 2013.

[111] Sztendel S., Pislaru C., Longstaff A.P., Fletcher S., Myers A., *Five-Axis Machine Tool Condition Monitoring Using dSPACE Real-Time System*. Journal of Physics: Conference Series 364, 25th International Congress on Condition Monitoring and Diagnostic Engineering, 2012.

[112] Kowalski T., Jastrzębski R., *Methody oceny dokładności technologicznej precyzyjnych tokarek CNC*. Inżynieria Maszyn, 2012, 17, 2.

[113] Turek P., Kwaśny W., Jędrzejewski J., *Zaawansowane methody identyfikacji błędów obrabiarek*. Inżynieria Maszyn, Publisher: Wrocławska Rada FSNT NOT, 2010, 5, 1–2, s. 8–37.

[114] Uhlmann E., Hohwieler E., Geisert C., *Monitoring of Slowly Progressing Deterioration of CNC-Machine Axes*. 2nd I'PROMS Virtual International Conference, 3–14 July 2006, Intelligent Production Machines and Systems, 2006

[115] Veldhuis S.C., Elbestawi M.A., *A Strategy for the Compensation of Errors in Five-Axis Machining*. CIRP Annals – Manufacturing Technology, 1995, 44, 1, pp. 373–377.

[116] Weikert S, Knapp W., *R-test: A New Device for Accuracy Measurements on Five Axis Machine Tools*. Annals of the CIRP, 2004, 53, 1, pp. 429–432.

[117] Wu L.S., Yang Y., Zhou D.S., *Dynamic Measurement Technology of the Spindle Motion Error of High Speed Spindle*. Aviation Precision Manufacturing Technology, 2008, 44, 4, pp. 26–29.

[118] Wesołowski M., Niedbała R., Kucharski D., *Wiarygodność termograficznych technik pomiaru temperatury*. Przegląd Elektrotechniczny, 2009, 12, s. 208–211.

[119] Więcek B., De Mey G., *Termowizja podczerwieni: Podstawy i zastosowania*. Wydawnictwo PAK, Warszawa 2011.

[120] Wiśniewski M., *Propozycja methody pomiaru dokładności i powtarzalności positioning robotów przemysłowych w warunkach przemysłowych*. Technologia i Automatyzacja Montażu, 2014, 3, s. 39–43.

[121] Woźniak A., Byszewski M., Jankowski M., Krajewski G., *Spatial Characteristics of the Triggering Force of Touch Probes for CNC Machine Tools*. 2nd International Conference on Virtual Machining Process Technology, McMaster University, 2013, Hamilton, Ontario, Canada, 13–17 May 2013.

[122] Wypysiński R., *Zastosowanie niezależnego układu współrzędnych do badania dokładności maszyn NC*. XII Konferencja Naukowo-Techniczna Automation, 2008, Pomiary Automatyka Robotyka, Warszawa 2008.

[123] Wypysiński R., *Vector Bar for accuracy testing of NC lathes*, IV International Conference on Machining and Measurement of Sculptured Surfaces, A/2/MMSS06, 2006.

[124] Wypysiński R., *Wektorowa methoda sprawdzania maszyn NC na przykładzie tokarek*. XI Konferencja Naukowo-Techniczna Automation, Pomiary Automatyka Robotyka, Warszawa 2007.

[125] Wyżgolik R., Budzan S., *Wybrane zagadnienia pomiarów termowizyjnych*. Pomiary Automatyka Kontrola, 2011, 57, 10, s. 1256–1259.

[126] Young K., Pickin C.G., *Accuracy assessment of the modern industrial robot*. Industrial robot: An International Journal, 2000, 39, 6, pp. 427–436.

[127] Zhao Xuesen, Sun Tao, Yan Yongda, Hu Zhenjiang, Dong Shen, *A new rotational error measurement method for precision spindle based on the registration analysis of motion topography*. The 10th International Symposium of Measurement Technology and Intelligent Instruments, June 29–July 2, 2011.

[128] Zhenhua W., Hui X., Guodong Ch., Rongchuan S., Sun L., *A distance error based industrial robot kinematic calibration method*. Industrial Robot: An International Journal, 2014, 41, 5, pp. 439–446.

[129] Ziółkowski G., Madej R., Józwik J., *Proceedury termograficznych badań diagnostycznych tokarki uniwersalnej*. [W]: Postęp w technikach wytwarzania i konstrukcji maszyn, Lubelskie Towarzystwo Naukowe, s. 123–134, Lublin 2005.

Standards

[130] PN-ISO 230-1:1988 Regulations regarding machine tools tests. Part 1: Geometric accuracy of machine tools operating without load or in finishing machining conditions.

[131] PN-ISO 230-2:1999 Regulations regarding machine tools tests. Part 2: Determining the numerically controlled axis positioning accuracy and repeatability.

[132] PN-ISO 230-3 Regulations regarding machine tools tests. Part 3: Determining the thermal states.

[133] PN-ISO 230-4:1999 Regulations regarding machine tools tests. Part 4: Roundness tests for numerically controlled machine tools.

[134] PN-ISO 230-5:2002 Regulations regarding machine tools tests. Part 5: Determining noise emission.

[135] PN-ISO 230-6:2002 Regulations regarding machine tools tests. Part 6: Diagonal displacement Test.

[136] PN-ISO 230-7:2006 Regulations regarding machine tools tests. Part 7: Test code for machine tools - Part 7: Geometric accuracy of axes of rotation.

[137] PN-ISO 10791-1:2000 Machining centres test conditions. Part 1: Checking geometric accuracy of machine tools equipped with a horizontal spindle (with horizontal axis Z) and replaceable heads.

[138] PN-ISO 10791-2 Machining centres test conditions. Part 2: Geometric tests for machines with vertical spindle or universal heads with vertical primary rotary axis (vertical Z-axis).

[139] PN-ISO 10791-3:2001 Machining centres test conditions. Part 3: Checking the geometric accuracy of machine tools with spindle index heads or positioned in a continuous way (with a vertical axis Z).

[140] PN-ISO 10791-4:2001 Machining centres test conditions. Part 4: Positioning accuracy and repeatability in linear and rotary axes.

[141] PN-ISO 10791-5:2000 Machining centres test conditions. Part 5: Positioning accuracy and repeatability of stillages used for attaching machined objects.

[142] PN-ISO 10791-6:2001 Machining centres test conditions. Part 6: the accuracy of feed motion, rotational velocities of the spindle and interpolation.

[143] PN-ISO 10791-7:2000 Machining centres test conditions. Part 7: Accuracy of a machined sample object.

[144] PN-ISO 10791-8:2001 Machining centres test conditions. Part 8: The assessment of contours in three coordinate planes.

[145] PN-ISO 10791-9 Machining centres test conditions. Part 9: The assessment of Times when the tools and stillages should be replaced.

[146] PN-ISO 10791-10 Machining centres test conditions. Part 10: thermal Interferences test.

[147] PN-ISO 10791-11 Machining centres test conditions. Part 11: Accoustic emission test.

[148] PN-ISO 10791-12 Machining centres test conditions. Part 12. Vibration level test.

[149] PN-EN ISO 8373:2001 Industrial Robots- therminology.

[150] ISO 9283 Manipulating industrial robots. Performance criteria and related test methods.

Internet Web Sites

[151] http://en.dmgmori.com/ (13.13.2017).

[152] http://etalon-ag.com/ (11.11.2017).

[153] http://www.dtlab.com/pages/analysis.php/ (11.11.2017).

[154] http://www.instrumenty-pomiarowe.pl/interferometr%20pomiarowy.html (28.03.2016).

[155] http://www.lasertex.com.pl/ (11.11.2018).

[156] http://www.renishaw.pl/pl/1030.aspx (11.11.2017).

[157] http://www.renishaw.pl/pl/1030.aspx (13.13.2017).

[158] http://www.robotraders.co.uk/sites/default/files/styles/uc_product_full/public/HP20_196x400_0.png (24.07.2018).

[159] www.fidia.com/english/acc_eng_fr.htm (27.07.2018).

[160] http://blog-uk.faro.com/wp-content/uploads/2010/07/reflection.jpg (03.07.2018).

[161] http://www.renishaw.com.pl/media/img/gen/14a56d9a79894ae594a9efc66b3cbb78.jpg (06.07.2018).

[162] http://www.robotraders.co.uk/sites/default/files/styles/uc_product_full/public/HP20_196x400_0.png (24.07.2018).

[163] http://www.motoman.pl/index.php?eID=tx_nawsecuredl&u=0&file=uploads/tx_catalogrobot/Flyer_Robot_HP20D_HP20F_E_06.2014_12.pdf&t=143783 4084&hash=d889ed1aec7fc916901dcc89e0f97afd38271737 (24.07.2018).

[164] http://www.ibspe.com/category/machine-tool-inspection-and-analyzer-solutions.htm (27.07.2018).

[165] http://www.renishaw.com.pl/media/img/gen/e498ad7c92c34554b072572b394c43a1.jpg (27.07.2018).

[166] http://resources.renishaw.com/download.aspx?lang=gen&data=12262&btn=1 (27.07.2018).

[167] http://www.renishaw.com/media/img/gen/7e6985108b68445a81ee33211063012f.jpg (27.07.2018).

[168] http://renishaw.com.pl/pl/stan-techniczny-i-testowanie--8276 (27.07.2018).

[169] http://www.renishaw.com.pl/pl/system-qc20-w-ballbar--11075 (27.07.2018).

[170] http://www.newport.com/Motion-Basics-and standards/140230/1033/content.aspx (27.07.2018).

Technical documentation

[171] LSP30 laser system technical documentation.

[172] Podręcznik użytkownika Interferometr Laserowy LSP-30-3D. Wrocław 2009, Rev, 1.0.2.

[173] Interferometr LSP30 – podręcznik użytkownika, www.lasertex.eu, (z dn. 28/02/2016r.).

[174] Machine tool and control systems documentation.

[175] Quick-start guide. H-5642-8501-02-A. Renishaw plc. 2010–2011.

[176] Renishaw Ballbar. Help.

[177] Renishaw brochure, Issued 1211 L-9920-0101-03-A.

Glossary

50mm zerodur	50mm zerodur
add a ballbar	dodaj przyrząd Ballbar
adjust	dostosuj
all reports	raporty
all specs	ustawienia
all specs & reports	raporty i ustawienia
axes	osie
backlash	luz poosiowy
ballbar details	typ przyrządu Ballbar
ballbar diagnostics	diagnostyka za pomocą przyrządu Ballbar
ballbar must be calibrated	przyrząd Ballbar musi zostać skalibrowany
both cw and ccw simulated	symulowane (cw i ccw)
calculated feedrate	obliczony posuw
calibrated length (mm)	długość skalibrowana (mm)
calibration date	data kalibracji
calibrator	kalibrator
capture	zbieranie danych
ccw	ccw (przeciwnie do ruchu wskazówek zegara)
ccw and simulated ccw	ccw oraz symulowane ccw
ccw only	ccw tylko
calibration interval	czas pomiędzy kalibracjami
centre offset	błąd centrowania
certificate number	numer certifikatu
circular deviation	odchyłka kołowości
circular hysteresis	histereza kołowości
circularity	odchyłka kołowości
com port conflict	konflikt portów com
configuration mode	konfiguracja zestawu
cw	cw (zgodnie z ruchem wskazówek zegara)
cw and ccw	cw oraz ccw
cw and simulated cw	cw oraz symulowane cw
cw only	cw tylko
cyclic error	błąd cykliczny
cyclic pitch	błąd skoku
date	data
delete	usuń
div	podziałka
dynamic ballbar	test dynamiczny Ballbar
end angle	kąt zakończenia
error	błąd
error of fit	brak dopasowania
excellent	wzorowy

expansion coefficient	współczynnik rozszerzalności cieplnej
failed to initialise ballbar	niepowodzenie uruchomienia przyrządu Ballbar
fair	dostateczny
feed	posuw
fit	dopasowanie
good	dobry
independent	niezależny
independent circularity	niezależna odchyłka okrągłości
instrument	instrument
last calibrated	data ostatniej kalibracji
lateral play (slop)	luz poprzeczny
location	położenie
machine	obrabiarka
machine id	numer obrabiarki
machine type	typ obrabiarki
magnitude	wielkość
maintain ballbars	zarządzanie przyrządami Ballbar
maintain calibrators	zarządzanie kalibratorami
manufacturer	producent
maximum deviation	największa odchyłka
minimum deviation	najmniejsza odchyłka
model	model
nc program id	nazwa programu NC
nominal	nominalny
nominal length (mm)	długość nominalna (mm)
non roundness	odchyłka okrągłości
operator	operator
other	inny
other details	inne szczegóły
overshoot	rozbieg
overshoot angle	kąt rozbiegu
pitch	skok
plane under test	płaszczyzna testu
please select the communications port that you would like to use for your ballbar	proszę wybrać port, do którego będzie podłączony przyrząd Ballbar
poor	złej jakości
pre-test comment	komentarz przed testem
quick check	szybki test
quick check mode	tryb szybkiego testu
radial deviation	odchyłka promieniowa
radius	promień
ranking	znaczenie
rename	zmiana oznaczeń
renishaw ballbar diagnostics	diagnostyka za pomocą przyrządu Ballbar Renishaw
reversal spikes	błąd nawrotu

review results	przegląd wyników testów
rotate	obróć
rtb files	pliki rtb
run 1	przebieg 1
run 2	przebieg 2
run a ballbar test	wykonaj test za pomocą przyrządu Ballbar

Jerzy Józwik is a staff member of the Faculty of Mechanical Engineering at the Lublin University of Technology (since 1998) and of the State Higher Professional Education School in Chełm (since 2007), where he holds the positions of Deputy Director at the Institute of Technical Studies and Aviation and Head of Engineering Studies Centre (since 2012). He is a member of Lublin Scientific Society (LTN) and the Polish Society of Engineers and Mechanics, the Polish Society of Production Management and the Polish Welding Society where, since 2015, he has held the position of Chairman of the Scientific and Technical Section of the Polish Welding Society, Lublin Branch. In 2011 he was honoured with the Bronze Cross of Merit from the President of the Republic of Poland. He graduated from the Faculty of Mechanical Engineering of the Lublin University of Technology in Mechanics and Machine Design with a specialization in Machine Technology and Macromolecular Material Processing. He is the author of over 150 reviewed papers and scientific publications, two monographs (2014, 2016), the editor of one monograph (2009) and a co-editor of two monographs (2005, 2007). He authored two patents, two utility models and three patent applications (2012, 2014, 2015). A supervisor of engineering diplomas and master theses as well as an auxiliary supervisor of doctoral dissertations. He worked with the Maintenance Plant of Energetyka Warszawa and the private enterprise WEZAN. For years, he has been a holder of welding qualifications in electric and gas welding as well as oxygen cutting. He is the author of various expert opinions concerning innovations for industry. He holds certificates related to the operation of machines and numerically controlled devices, CNC machine tools, robots, cutters, tool setting system operation, CNC machine tool diagnostic systems, microscopes, and optical tools utilized in reverse engineering and research (ATOS, PONTOS, ARAMIS, TRITOP). He also holds certificates in computer thermography as well as monitoring and parameter recording in GMAW and GTAW welding by LORCH devices, welding process automation, welding monitoring by the SAW method and modern solutions used in industrial production of pressure equipment. He completed and taught many courses and trainings financed by the European Union. He is also a member of various scientific committees and scientific conference organizing committees, both domestically and internationally (Poland, Czech Republic, Slovakia). He is also a member of scientific committees and a reviewer for scientific magazines as well as a reviewer and member of the jury in a Polish national competition for Best Master Thesis organized by Sandvik Coromant in Poland. For many years he was a tutor of the Scientific Circle of Students of Production Engineering Fundamentals at the Lublin University of Technology (2003–2009). He is a member of the Defence Commission for the Diploma Theses in Mechanics and Machine Design at the Lublin University of Technology. A dean representative and member of the Committee for the Academic Education Quality, Health and Safety Committee, he is also the Faculty's Social Labour Inspector (2005–2010). Actively engaged in the Erasmus and Ceepus programmes both at the Lublin University of Technology and the State Higher Professional Education School in Chełm, he has been awarded by the Rectors of the Lublin University of Technology and the State Higher Professional Education School in Chełm.